Understanding the Intermolecular Interaction and Structural Organization in Some Imidazolium and Pyrrolidinium-based Ionic Liquids: Implications in Biological and Electrochemical Applications

by

AMITA MAHAPATRA

CHEM11201804011

National Institute of Science Education and ResearchBhubaneswar, Odisha

A thesis submitted to the

Board of Studies in Chemical SciencesIn partial fulfilment of requirements for the degree of

DOCTOR OF PHILOSOPHY

of

HOMI BHABHA NATIONAL INSTITUTE

January, 2024

Homi Bhabha National Institute

Recommendations of the Viva Voce Committee

As members of the Viva Voce Committee, we certify that we have read the dissertation prepared by Ms. Amita Mahapatra entitled "***Understanding the Intermolecular Interaction and Structural Organization in Some Imidazolium and Pyrrolidinium-based Ionic Liquids: Implications in Biological and Electrochemical Applications***" and recommend that it may be accepted as fulfilling the thesis requirement for the award of Degreeof Doctor of Philosophy.

Chairman – (Name: Prof. Alagar Srinivasan) Date: 10.04.24

Guide / Convener – (Name: Dr. Moloy Sarkar) Date: 10.04.24

Co-guide –

Examiner – (Name: Prof. Satyen Saha) 10.04.2024

Member 1 – (Name: Dr. Sharnappa Nadaboenna) Date: 10.04.2024

Member 2 – (Name: Dr. Arindam Ghosh) Date: 10/04/2024

Member 3 – (Name: Dr. Yatendra Singh Chaudhary) Date: 10.04.24

Final approval and acceptance of this thesis is contingent upon the candidate's submission of the final thesis copies to HBNI. I/We hereby certify that I/we have read this thesis prepared under my/our direction and recommend that it may be accepted as fulfilling the thesis requirement.

Date: 10.04.24
Place: Jatni Campus, NISER, Bhubaneswar

Signature
Co-guide (if any)

Signature
Guide

STATEMENT BY AUTHOR

This dissertation has been submitted in partial fulfilment of requirements for an advanced degree at Homi Bhabha National Institute (HBNI) and is deposited in the library to be made available to borrowers under rules of the HBNI. Brief quotations from this dissertation are allowable without special permission, provided that accurate acknowledgement of source is made. Requests for permission for extended quotation from or reproduction of this manuscript in whole or in part may be granted by the Competent Authority of HBNI when in his or her judgment the proposed use of the material is in the interests of scholarship. In all other instances, however, permission must be obtained from the author.

Amita Mahapatra

DECLARATION

I, hereby declare that the investigation presented in the thesis has been carried out by me. The work is original and has not been submitted earlier as a whole or in part for a degree/diploma at this or any other Institution / University.

Amita Mahapatra

DEDICATION

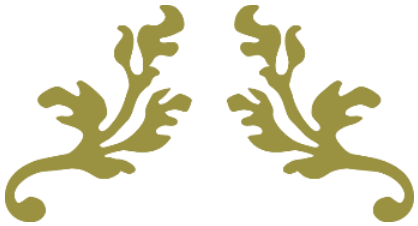

I dedicate this thesis to my beloved family.

To My Beloved Parents

Your unconditional love has been the source of my strength.

To My Precious Siblings

Your constant encouragement has been the driving force behind my achievements.

I am grateful for the love and inspiration you have infused into every aspect of my life.

ACKNOWLEDGEMENT

I would like to express my sincere gratitude to my supervisor Dr. Moloy Sarkar for his invaluable guidance for the successful completion of this thesis work. His constant support both at professional and personal aspects throughout this Ph. D journey is deeply appreciated. His mentorship, encouragement and meaningful advices have significantly contributed to my personal and professional growth.

I would like to thank Prof. Hirendra Nath Ghosh, Prof. Sudhakar Panda (Former Director, NISER) and Prof. T.K. Chandrasekhar (Founder Director, NISER) for establishing well-equipped research facilities in NISER. I would thank Dr. Pranay Swain, (Dean of academic affairs, NISER) for understanding and supporting in various academic issues. I would also like to thank my thesis committee members: Prof. Alagar Srinivasan, Dr. Arindam Ghosh, Dr. Sharanappa Nembenna, and Dr. Yatendra Singh Chaudhary, for their valuable suggestions during my Ph.D. tenure. I also like to acknowledge my course instructor Dr. Upakarasamy Louderaj, Dr. A. Srinivasan, Dr. Himanshu Sekhar Biswal for their useful discussion with me during my course work. I acknowledge present (Dr. Sharanappa Nembenna) and former (Dr. Himansu S. Biswal, and Dr. Alagar Srinivasan) Chairpersons (SCS) during my research tenure in NISER. I am also thankful to all other faculty members, scientific officers (Dr. Arun Sir and Dr. Priyanka Madam) and the non-teaching staffs of our SCS department for providing a healthy environment. I am grateful to NISER, Bhubaneswar, for providing suitable infrastructure for research. I am also thankful to Council of Scientific and Industrial Research (CSIR) for the financial assistance.

I wish to convey my warm and sincere thanks to both my present and former lab members for making this journey enjoyable and memorable. My heartfelt thanks to Dr. Somanath Banerjee, Dr. Lakkoji Satish and Dr. Muhaiminul Islam for their valuable advices and constructive comments to carry out good research work. I am forever thankful to Dr. Manjari Chakaraborty and Dr. Naupada Preeyanka for their untiring help and support both in personal and professional level. The warmth and care that Manjari dee has bestowed upon me, will forever hold a special place in my heart and memory. I express my heartfelt thanks to Dr. Sahadev Barik for his persistent help throughout this thesis work. I also owe a deep sense of gratitude for his calm response in the face of my continuous queries and disturbances. The friendship with Amit and Debabrata will forever be cherished by me. The fun, sharing, and caring we had will be eternally memorable. Amit's timely lessons by

exemplifying Mahabharat will be greatly appreciated. Additionally, I am very much thankful to Joyoti who has made me believe in myself. I would also like to express a special token of thanks to my beloved juniors Subhakant, Rashmita, Yashaswini, Jyoti, Joyoti, and Aditi for loading the end of my Ph.D. journey with a lot of fun and happiness. I will also acknowledge the contribution of M.Sc. students Dinesh, Ramya Aman, Biswa, Aditya, Nilesh and Aradhana in this journey.

My Ph.D journey outside the lab has been truly pleasant and delightful because of Prajna, Priyanka. The sharing and caring we had throughout the years will forever hold a special place in my heart. I also extend my deepest gratitude to my friends Tanmayee, Niroja, Chinmayee, Chutki, Sinu for their timely support. Additionally, I would also like to thank Kasturi dee, Malaya, Unmesh, Aneeya bhai for valuable scientific discussions.

I owe deep gratitude to all my respected mentors especially Kailash Sir, Babi Sir and Raju Dadei for believing in me. Their constant encouragement during my academic period will be greatly acknowledged. I would also like to thank my extended family members Dadei, Dethei, Mamu, Mai, my cousin brother and sisters for their individual contribution and support.

Finally, I am extremely grateful to my mother, Mrs. Sabita Mahapatra, whose unconditional love and inspiration have made me the person who I am. I am very much grateful to my father Mr. Naba Kishore Mahapatra who has always taught me to be patient and has made me believe in hardwork. His love and care for me will remain forever indebted. Last but certainly not least, I am very much thankful to Nana, Chulbuli and Banty for their indubitable support and encouragement throughout this period. I am immensely grateful for the unwavering love, affection, and support of beloved family member, without which the smooth progression of my Ph.D. journey would have been unimaginable.

Above all I offer my soul and Prayers to Lord Shiva for providing me with lot of blessings and with a heavenly family.

Amita Mahapatra

List of Publications

1. [#]**Mahapatra, A**.; Chakraborty, M.; Barik, S.; Sarkar, M.; Comparison between Pyrrolidinium-based and Imidazolium-based Di-cationic Ionic Liquids: Intermolecular Interaction, Structural Organization, and Solute Dynamics. *Physical Chemistry Chemical Physics* ***2021***, 23, 21029-21041.

2. [#]**Mahapatra, A**.; Barik, S.; Chakraborty, M.; Lakkoji, S.; Sarkar, M.; Assessing the Suitability of a Dicationic Ionic Liquid as a Stabilizing Material for the Storage of DNA in Aqueous Medium. *Langmuir* ***2022***, 125, 47, 13015–13026.

3. [#]**Mahapatra, A**.; Samantara A., Barik, S.; Sahoo, M.; Behera, JN; Sarkar, M.; Insight into the Structure and Transport Properties of Pyrrolidinium-based Geminal Dicationic-Organic Ionic Crystals: Unravelling the Role of Alkyl-Chain Length. *Soft Matter*, ***2023***, 19, 3510–3518

4. [#]**Mahapatra, A**.; Ghosh, J.; Barik, S.; Parida. S.; Sarkar, M.; Understanding the Influence of Ethylene Glycol on the Microscopic Behavior of Imidazolium-based Monocationic and Dicationic Ionic Liquid. *Chemical Physics Impact,* **2023,** 7, 100331.

5. [#]**Mahapatra, A**.; Chowdhury. U.D.; Barik, S.; Parida. S; Bhargava, B. L.; Sarkar, M.; Deciphering the Role of Anions of Ionic Liquids in Modulating the Structure and Stability of ct-DNA in Aqueous Solutions. *Langmuir* **2023**, 39, 48, 17318–17332.

6. Barik, S.; Chakraborty, M.; **Mahapatra, A**.; Sarkar, M.; Choline Chloride and Ethylene Glycol Based Deep Eutectic Solvent (DES) versus Hydroxyl Functionalized Room Temperature Ionic Liquids (RTILs): Assessing the Differences in the Microscopic Behaviour between DES and RTILs. *Physical Chemistry Chemical Physics* ***2022***, 24, 7093-7106.

7. Barik, S.; Preeyanka, N.; Chakraborty, M.; **Mahapatra, A**.; Sarkar, M.; Temperature-dependent Ultrafast Solvation Dynamics of Choline Chloride-based Deep Eutectic Solvent (DES) and Hydroxyl Functionalized Room Temperature Ionic Liquids (RTILs): Exploring the Difference in Solvent Response between DES and RTILs. *Journal of Molecular Liquid* ***2022***, 367, 120545.

8. Barik, S.; **Mahapatra, A**.; Jena, D.; Sarkar, M.; Assessing the Impact of Increase in the Number of Hydroxyl Groups on the Microscopic Behaviors of Ammonium-based Room Temperature Ionic Liquids: A Combine Fluorescence Up-conversion, Fluorescence Correlation and NMR Spectroscopic Study. *Journal of Photochemistry & Photobiology, A*, ***2022*** 437, 114505

9. Chakraborty, M.; Barik, S.; **Mahapatra, A**.; Sarkar, M.; Effect of Lithium-Ion on the Structural Organization of Monocationic and Dicationic Ionic Liquids. *Journal of Physical Chemistry B* ***2021***, 125, 47, 13015–13026.

10. Chakraborty, M.; Barik, S.; **Mahapatra, A**.; Sarkar, M.; Binary mixtures of Ionic Liquids: Ideal, Non-ideal, or Quasi-ideal? *Journal of Chemical Physics* 154, ***2021***, 224507.

11. Majhi, D.; Chakraborty, M.; Barik, S.; **Mahapatra, A**.; Sarkar, M.; Understanding the Microscopic Structural Organization of Neat Ammonium Based Ionic Liquids through Resonance Energy Transfer (RET) Studies. *Chemical Physics Impact,* ***2021***, 3, 100034.

12. Barik, S.; **Mahapatra, A**.; Preeyanka, N.; Sarkar, M.; Assessing the Impact of Choline Chloride and Benzyltrimethylammonium Chloride-Based Deep Eutectic Solvents on the Structure and Conformational Dynamics of Bovine Serum Albumin: A Combined Steady-State, Time-Resolved Fluorescence and Fluorescence Correlation Spectroscopic Study. *Physical Chemistry Chemical Physics* ***2023****, 25, 20093-20108.*

a. Manuscript under prepartion

13. [#]**Mahapatra, A**.; Barik, S.; Parida.S.; Sarkar, M.; Probing Lithium-ion Driven Microenvironment Change in Pyrrolidinium-based Mono-cationic and Di-cationic Ionic Liquid. (Manuscript under preparation)

14. Parida. S.; **Mahapatra, A**.; Sarkar, M.; Enhanced Dissolution Behavior of Cellulose in Imidazolium-based Di-cationic Ionic Liquid. (Manuscript under preparation)

 # pertaining to thesis

CONFERENCE/SYMPOSIUM

1. Presented a flask talk in Trombay Internal Symposium on Radiation and Photochemistry 2022 (**TSRP-2022**) held at Training School Hostel, Anushakti Nagar, Mumbai, India via virtual meet during January 12-15, 2022.
2. Participated online and presented a POSTER in the international conference on ‘‘Aggregation-Induced Emission from Fundamental to Applications’’ (**ICAIEFA2022**) organised by department of chemistry, BITS Pilani (Goa Campus) during 16th to 18th December.
3. Participated and presented an oral presentation in 14th National Symposium on Radiation and Photochemistry (**NSRP-2021**) held at Indian Institute of Technology, Gandhinagar, Gandhinagar, India via virtual meet during June 25-56,2021.

Contents

SYNOPSIS

Ionic liquids (ILs) are a fascinating class of materials composed entirely of ions and exhibit properties reminiscent of molten salts as well as molecular liquids under ambient conditions. However, one of the unique characteristics that sets ionic liquids apart from both traditional organic solvents and inorganic salts is their complex micro-heterogeneous nature. Although their intriguing macroscopic characteristics, such as high viscosity, low vapour pressure, and exceptional thermal stability, have driven their widespread use in numerous scientific disciplines, the kinship between the microscopic structure and macroscopic physical attributes is not well understood. To bridge this knowledge gap, the present thesis focuses on understanding the intermolecular interactions and structural organization of some selected mono-cationic and di-cationic ionic liquids by exploiting several spectroscopic techniques and computer simulation studies. Specifically, steady-state and time-resolved fluorescence, fluorescence-correlation spectroscopy (FCS), and nuclear magnetic resonance (NMR) techniques have been employed to carry out the investigations. Moreover, the present thesis also makes an attempt to comprehend how the microscopic structural feature of ILs can impact the electrochemical and biological applications.

Organization of thesis: The present thesis has been divided into six chapters. A brief description of the contents of different chapters of the thesis is provided below.

Chapter 1: Introduction

Chapter 1 provides a comprehensive overview of ionic liquids (ILs) and their significance in various fields of science and technology. It starts with a broad introduction to ILs and their unique properties, followed by outlining of a historical perspective on the discovery and development of ILs. Subsequently, a brief discussion regarding the progress in

realizing the intricate correlation between the structure and physicochemical properties of various classes or categories of ionic liquids ILs has been provided. Additionally, the applications of different classes of ILs in the domains of chemistry, biology, and materials science have also been highlighted in this section. Moreover, this chapter also provides a thorough discussion on the nano-structural organization of ILs and the intricate solvent dynamics by highlighting some recent literature reports. This section also discusses relevant photophysical processes such as excitation wavelength-dependent emission behavior and rotational relaxation dynamics of some suitable solutes in ILs and translational diffusion dynamics of ILs etc., which are often used to demonstrate the existence of nano-structural organization in ILs in detail. Finally, based on the current challenges in the field of ILs, the objective of this thesis has been outlined

Chapter 2: Instrumentation and Methods

This chapter provides the fundamental principles of various experimental techniques that have been employed for various measurements both at single molecular and ensemble-average levels in the current thesis work. Different spectroscopic techniques, such as absorption spectroscopy, steady-state and time-resolved fluorescence emission spectroscopy, have been discussed briefly in this chapter. More specifically, the fundamental working principle of time-correlated single photon counting (TCSPC) and fluorescence correlation spectroscopic (FCS) technique have been discussed in detail. Additionally, measurements of the self-diffusion coefficient through pulsed-field-gradient NMR (PFG-NMR) techniques have also been provided. Apart from this, various methodologies that are commonly used to obtain the fluorescence decay parameters, rotational relaxation parameters, and their analysis by employing hydrodynamic and quasi-hydrodynamic theories and translational diffusion time have been described. The error limits corresponding to different experimental parameters are provided at the end of this chapter.

Chapter 3: Difference in the behavior of Imidazolium-based and Imidazolium-based Di-cationic Ionic Liquids: Intermolecular Interaction, Structural Organization and Solute Dynamics

In recent times, dicationic ionic liquids (DILs) have gained considerable interest owing to their superior physicochemical attributes when compared to monocation-based IL (MIL) systems. Despite the widespread use of DILs in diverse areas of chemistry, comprehensive investigations into their microscopic structure and dynamics are still in their preliminary stage. Notably, much of the research conducted in this area has focused on imidazolium-based DILs. [1-5]This signifies the need for more comprehensive investigation on other type of DILs. In this context, both imidazolium and pyrrolidinium cations-based ILs share nearly similar physicochemical properties such as viscosity, density etc. However, their distinct structural characteristics, particularly the planar and non-planar nature of imidazolium and pyrrolidinium cation, may result in subtle variations in the interactions between cations and anions which may ultimately influence their microstructure and dynamic properties.

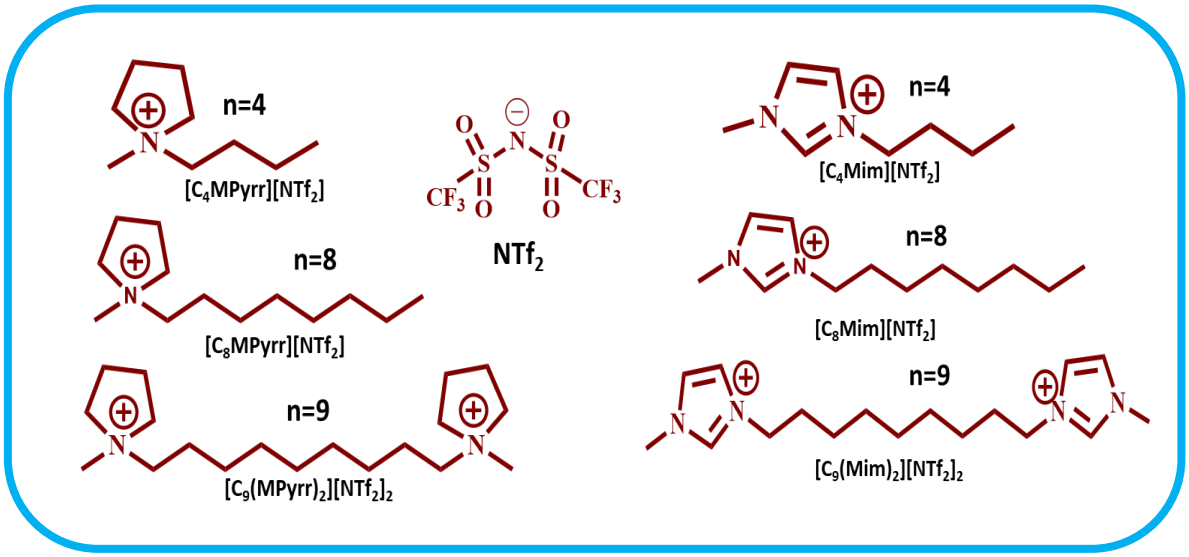

Scheme 1. Chemical structure of the ILs used in this study

In view of this, the current chapter aims to understand the difference in the behavior of imidazolium and pyrrolidinium-based dicationic ionic liquids (DILs) in terms of

intermolecular interactions, microscopic structure, and dynamics. For this purpose, a set of imidazolium and pyrrolidinium-based DIL and MIL, as shown in Scheme 1, are systematically investigated by exploiting combined steady-state and time-resolved fluorescence (TRFA), electron paramagnetic resonance (EPR) and NMR spectroscopic techniques. Steady-state fluorescence and EPR studies have provided an idea about the micro-polarity of selected ILs. TRFA studies involve monitoring the rotational relaxation dynamics of two suitable-chosen probes, perylene and 8-methoxypyrene-1,3,6-trisulfonate (MPTS) in the chosen IL systems. The experimentally obtained rotational relaxation data and analysis of the data through Stoke-Einstein-Deby (SED) hydrodynamic theory have helped us to understand the differential structural organization of imidazolium and pyrrolidinium-based DIL. The outcomes of all of these studies have depicted that the microscopic structural organizations in imidazolium and pyrrolidinium-based DILs are different from each other and their respective mono-cationic counterparts.

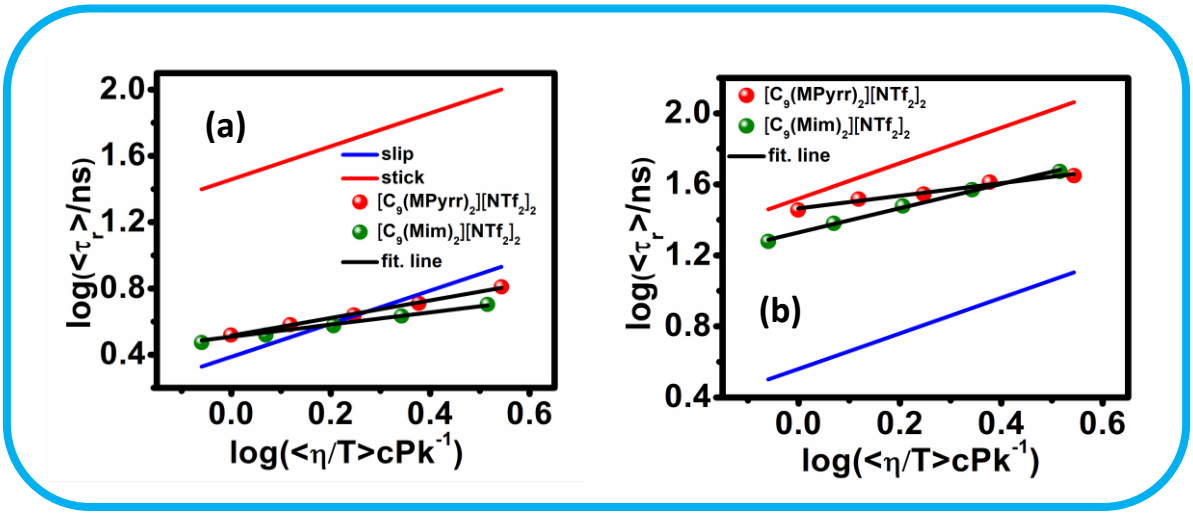

Figure 1. SED analysis (a) for perylene and (b) MPTS shows the difference in the variation of rotational relaxation time (τ_r) of both the probe with (η/T) in imidazolium and pyrrolidinium-based DIL. The red (stick) and blue (slip) solid line represents theoretically predicted (τ_r) and the solid spheres are the experimental data points.

Chapter 4a: Understanding the Influence of Ethylene Glycol on the Microscopic Behavior of Imidazolium-based Mono-cationic and Di-cationic Ionic Liquids

Having understood the microscopic structural organization of DILs in Chapter 3, we next have made an attempt to understand the microscopic behavior and intricate dynamics of some imidazolium-based DIL and MIL in the presence of a molecular solvent.

Due to the presence of polar and nonpolar domains within the IL structure, ILs play a significant role in the dissolution of complex molecules and also in ion transport. However, the high viscosity of ILs always limits their ability to mix and interact properly with the complex molecule. However, the introduction of a trace amount of co-solvent can facilitate the dissolution process by reducing the viscosity of the medium.[6-9] However, it is essential to note here that the addition of molecular solvents can also impact the microscopic structure within ILs. Hence, acquiring a comprehensive understanding of how the introduction of co-solvents influences the relevant microscopic properties in ILs represents a worthwhile objective to pursue. Therefore, with an aim to understand the structural organization and various intermolecular interactions that prevail in DIL-molecular solvent mixtures, a DIL 1,8-bis(3-methylimidazolium-1-yl) octane bis(trifluoromethanesulfonyl) imide $[C_8(Mim)_2][NTf_2]_2$ and a MIL 1-methyl-3-octyl-imidazolium bis(trifluoromethanesulfonyl) imide $[C_8(Mim)][NTf_2]$ have been synthesized and are investigated in the absence and presence of various mole fraction of ethylene glycol (EG). Rotational diffusion of two selected probes, 9-phenyl anthracene (9-PA) and Rhodhamine R110 (R110) have been carried out by employing TRFA studies to monitor the apolar and polar domain within the MIL and DIL separately in the absence and presence of EG. Furthermore, NMR studies have also been carried out to shed more light on the intermolecular interaction at the molecular level. Analysis of the data has shown that while the addition of EG induces an appreciable change in the domain structure of both MIL and DIL, the changes are observed to be

prominent in the case of MIL as compared to that in the DIL. The outcomes of this study have enhanced our knowledge on understanding the behavior of both MIL and DIL in the presence of an organic solvent.

Table 1. The rotational relaxation time (τ_r) of probe molecules in MILs and DILs monitored under iso-viscous condition. The variation in (τ_r) shows the influence of EG on the domain structure of ILs.

$[C_8(Mim)][NTf_2]$ η=34cP	τ_r (9-PA)	τ_r (R110)	$[C_8(Mim)_2][NTf_2]_2$ η=165cP	τ_r (9-PA)	τ_r (R110)
X=0	1.5	9.9	X=0	3.3	18.0
X=0.2	1.7	8.6	X=0.2	3.0	15.7
X=0.4	1.9	7.1	X=0.4	2.8	13.3
X=0.6	2.3	5.9	X=0.6	2.5	13.0

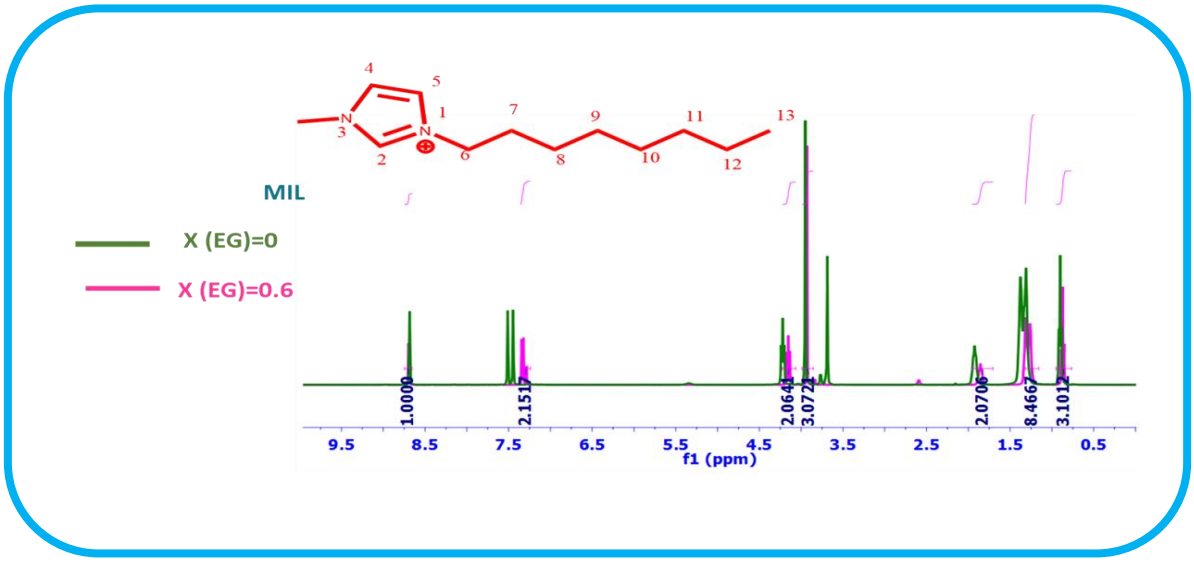

Figure 2. ^{1}H NMR spectrum of MIL in absence and presence of EG. The figure shows an upfield shift of the C (4,5)-proton and C (6,7)-proton after addition of 0.6 EG to the MIL.

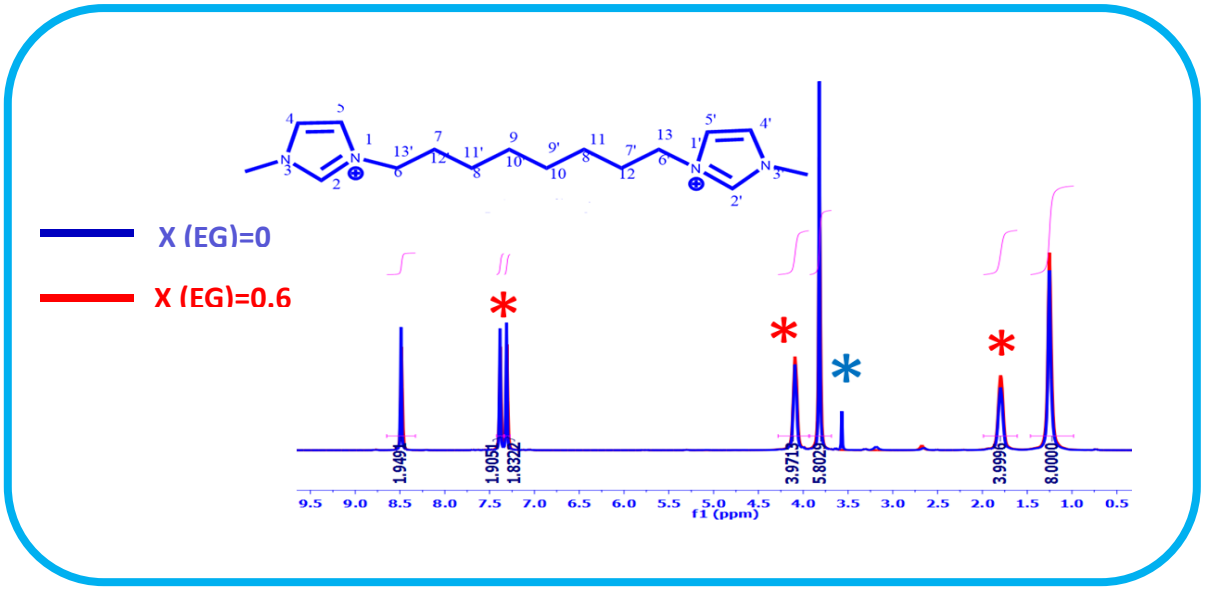

Figure 3. ^{1}H NMR spectrum of MIL in absence and presence of EG. The figure shows no shift in the signal due C (4,5)-proton and C (6,7)-proton after addition of 0.6 EG to the DIL.

Chapter 4b. Probing Lithium-Ion Driven Micro-Environment Changes in Pyrrolidinium-Based Mono-cationic and Di-cationic Ionic Liquid

Lithium salts dissolved in ionic liquids (ILs) are interesting alternatives to the commonly used electrolytes for Li-ion batteries. Owing to the higher thermal and electrochemical stability of pyrrolidine-based ILs they are widely used as electrolytic media for Lithium-ion batteries.[10-12] However, it is also equally essential to understand how Li^+ ions influence the structural organization of ILs in a microscopic scale. Therefore, in this chapter, the structural organization and diffusion dynamics of pyrrolidinium-based monocatonic ILs (MIL) and dicationic ILs (DIL) containing the similar alkyl units (8-9 alkyl unit) have been studied in the absence and presence of lithium salt by employing TRFA, PFG-NMR, and FCS studies. The findings of these studies have revealed that the coordination of Li^+ ions with the anions of both MILs and DILs triggers a change in the structural arrangement of the nonpolar regions of the concerned media. Interestingly, our results have also indicated that the introduction of Li^+ ions induce a significantly more pronounced perturbation in the nano structural organization of MILs as compared to its impact on DILs.

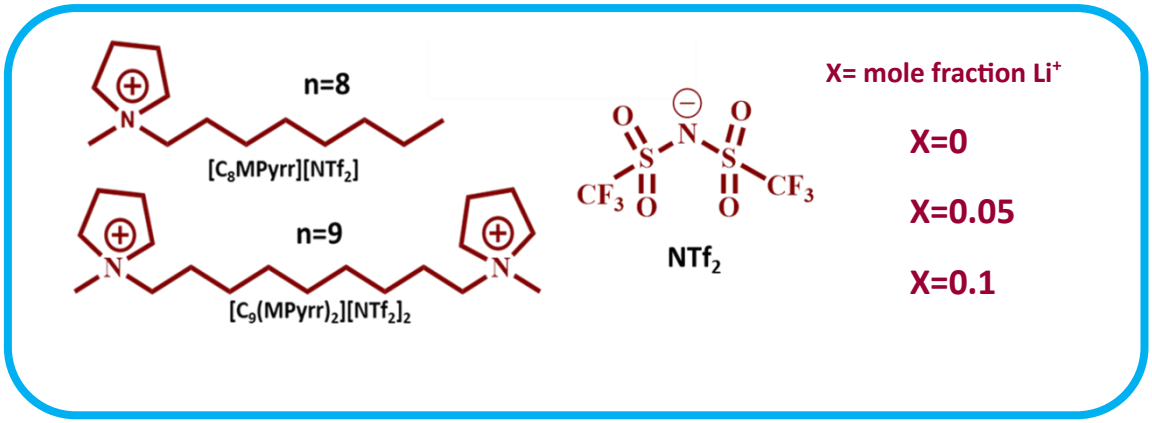

Scheme 2. Chemical structure of ILs and used in this study.

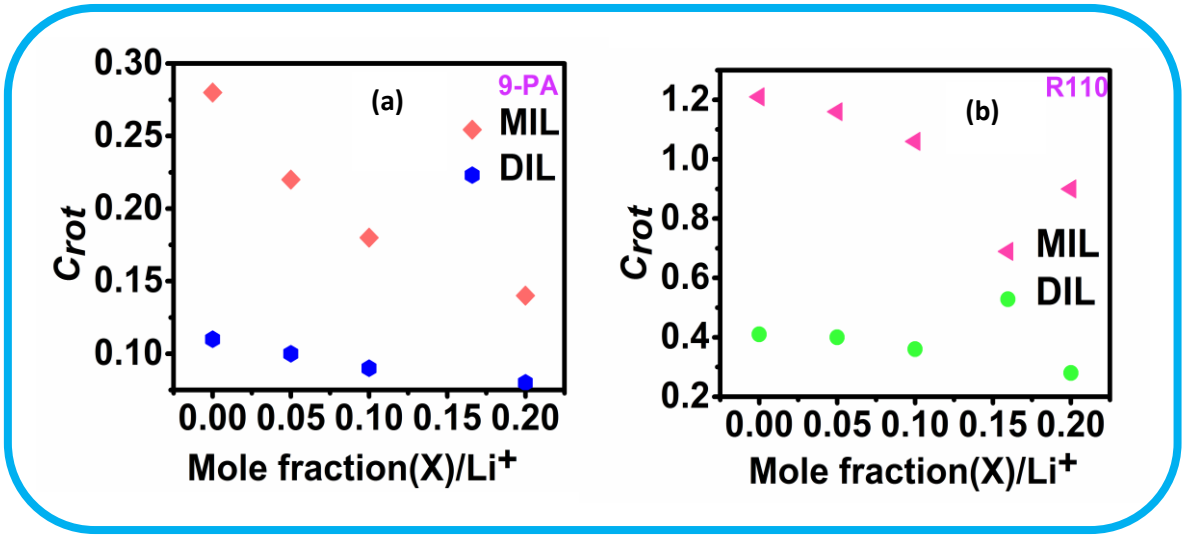

Figure 4. Variation of friction coefficient (C_{rot}) of probe molecules (a) 9-PA and (b) R110 with MIL and DIL with addition of Li^+ ions

Chapter 5a: Assessing the Suitability of a Di-cationic Ionic Liquid as a Stabilising Material for Storage of *ct*-DNA in Aqueous Medium

In recent times, the quest for a suitable alternative storage media which can ensure long term preservation of DNA in its native form has become a worthwhile objective to the scientific community to pursue. Recently, several researchers have acknowledged the use of ILs and more specifically, MILs in DNA technology.[13-15] The unique microenvironment provided by

adjustable hydrophilic and hydrophobic properties of MILs have been useful in many nucleic acid-based applications such as extraction, solubilization and stabilization of *ct*-DNA in aqueous medium. However, the perspective of DILs, which are shown to be more versatile than MILs, towards nucleic-acid-based applications have not been explored yet. As DILs possess a different structural backbone from MILs; the presence of two cationic head groups is expected to induce extra stabilization due to dication-DNA interaction. For this purpose, in this chapter, the potential of a pyrrolidinium-based DIL in stabilizing *ct*-DNA has been investigated by following DNA-DIL interaction. Additionally, in order to understand the fundamental aspects of DNA-DIL interaction in a comprehensive manner, studies are also done by employing structurally similar MILs. The investigations have been carried out both at ensemble-average and single molecular levels by using various spectroscopic techniques. The molecular docking study has also been performed to throw more light into our experimental observations. The combined steady-state and time-resolved fluorescence, FCS, and circular dichroism (CD) measurements have demonstrated that DILs can effectively be used as a better storage media for *ct*-DNA as compared to MILs. Investigations have also shown that the extra electrostatic interaction between the cationic head group of DIL as well as the structural feature of DIL are primarily responsible for providing better stabilization to *ct*-DNA, retaining its native structure in aqueous medium.

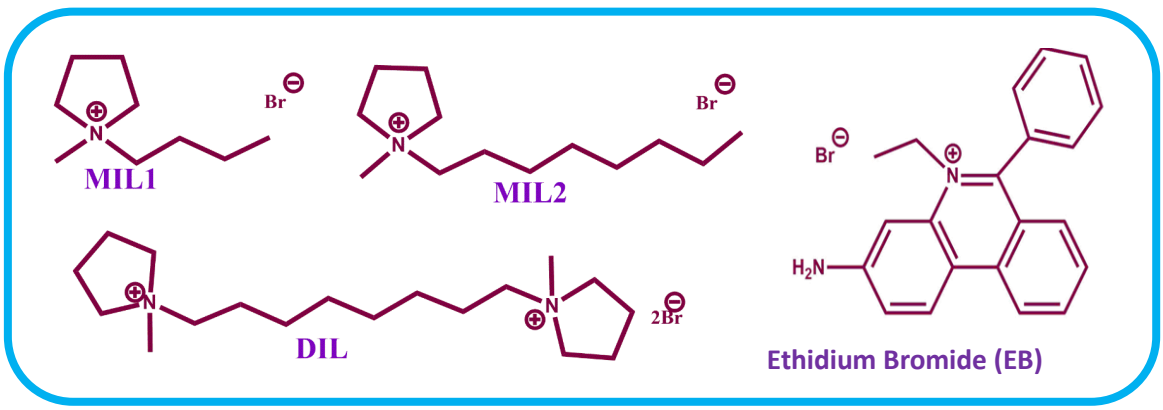

Scheme 3. Chemical structure of ILs and probe molecules used in this study.

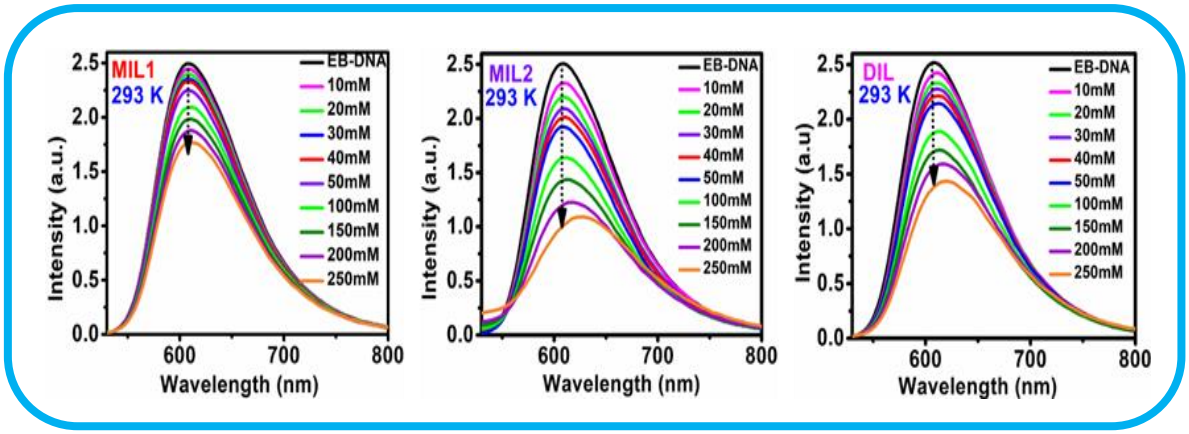

Figure 4. Variation of fluorescence intensity of EB-DNA complex with gradual addition of ILs.

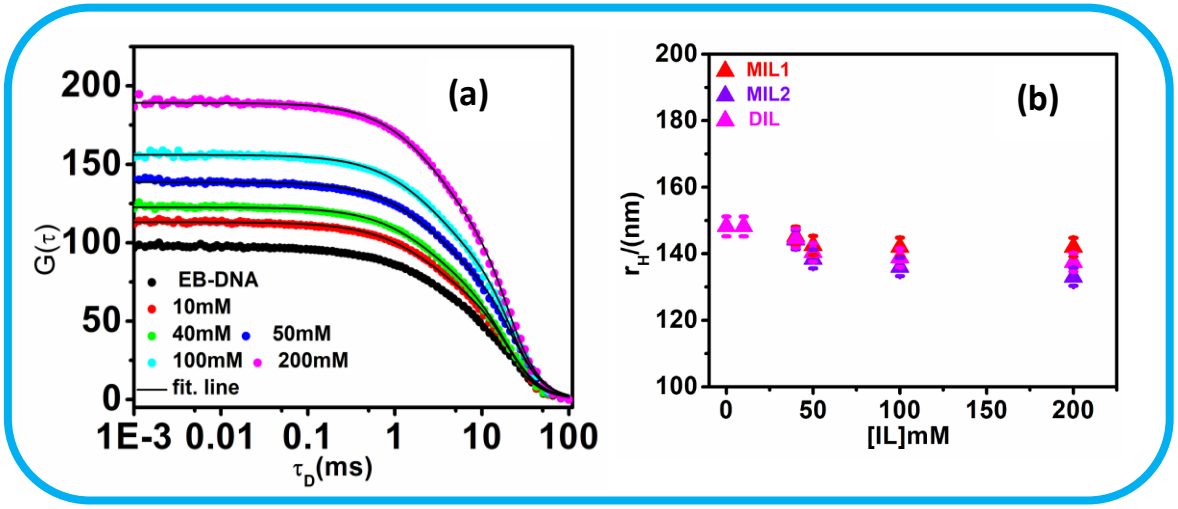

Figure 5. (a) FCS traces in presence of MIL1 (b) variation of hydrodynamic radius (HDR) of ct-DNA in presence of IL using FCS studies. This shows that the HDR of *ct*-DNA changes in MIL2 in a greater extent than DIL indicating better conformational stability of *ct*-DNA in presence of DIL.

Chapter 5b: The Synergistic Impact of Cations and Anions in Ionic Liquids in Modulating the Structure and Stability of *ct*-DNA in Aqueous Medium

As discussed in Chapter 5a, ILs are utilized as a potential tool in the realm of nucleic-acid stabilization and preservation in aqueous solution, and in this context, the cationic components of ILs are always believed to play an important role. The cations in ILs are shown to preferentially interact with the phosphate backbone of DNA, thereby stabilizing the double helical structure. Indeed, in the majority of research studies that are focused on DNA-IL interactions, a significant emphasis has often been placed on understanding the role of cationic moiety of ILs.[16-18] The importance of IL anions in the said event has often been overlooked. This is possibly due to lower binding affinities of IL anions for the DNA backbone. However, ILs are known to display structural transitions from ion pairs to distinct ions based on their hydration characteristics, and these free ions and associated ion pairs are considered to exhibit different behavior during the interaction event with the biomolecules.

Considering the above fact, the current chapter has tried to investigate and understand the structure and stability of *ct*-DNA in a series of imidazolium-based ILs comprising of different anions spanning the Hofmeister series. The ILs that are examined in this work include 1-ethyl-3-methylimidazolium chloride (EmimCl), 1-ethyl-3-methylimidazolium bromide (EmimBr), 1-ethyl-3-methylimidazolium nitrate ($EmimNO_3$), 1-ethyl-3-methylimidazolium acetate (EmimAc), 1-ethyl-3-methylimidazolium hydrogen sulfate ($EmimHSO_4$), and 1-ethyl-3-methylimidazolium tetrafluoroborate ($EmimBF_4$). The selection of IL anions is based on their solubility in buffer solutions and their different hydration properties. The binding characteristics and thermodynamics of IL-DNA interaction have been investigated using various spectroscopic techniques such as UV-Vis absorption spectroscopy, steady-state, and time-resolved fluorescence spectroscopy. Furthermore, the conformational stability of *ct*-DNA is evaluated using circular dichroism

(CD) spectroscopy. MD simulation study has also been employed to shed more light on the experimental observations. Quite interestingly, the findings of this study also underscore the significance of consideration of both the cation and anion of ILs in understanding the overall DNA-IL interaction event. Among the selected ILs, Emim Cl and Emim Br are observed to stabilize the *ct*-DNA structure in a better manner.

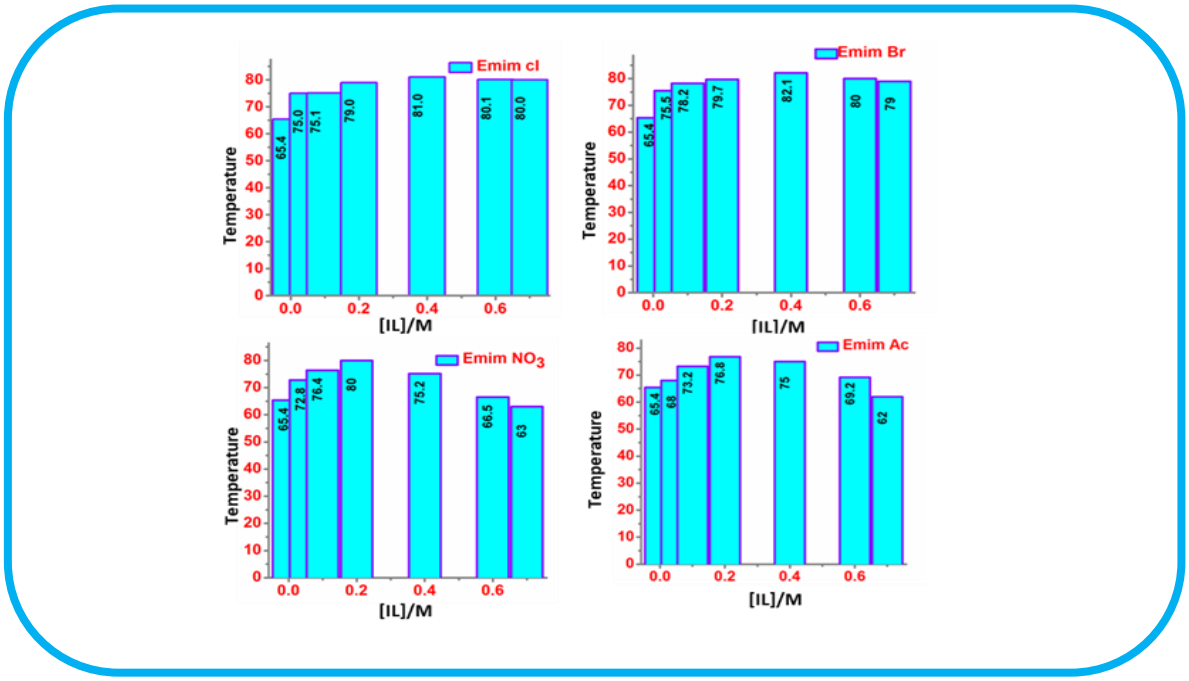

Figure 6. Variation of melting point of *ct*-DNA in absence and presence of varying concentration of different anion-based ILs.

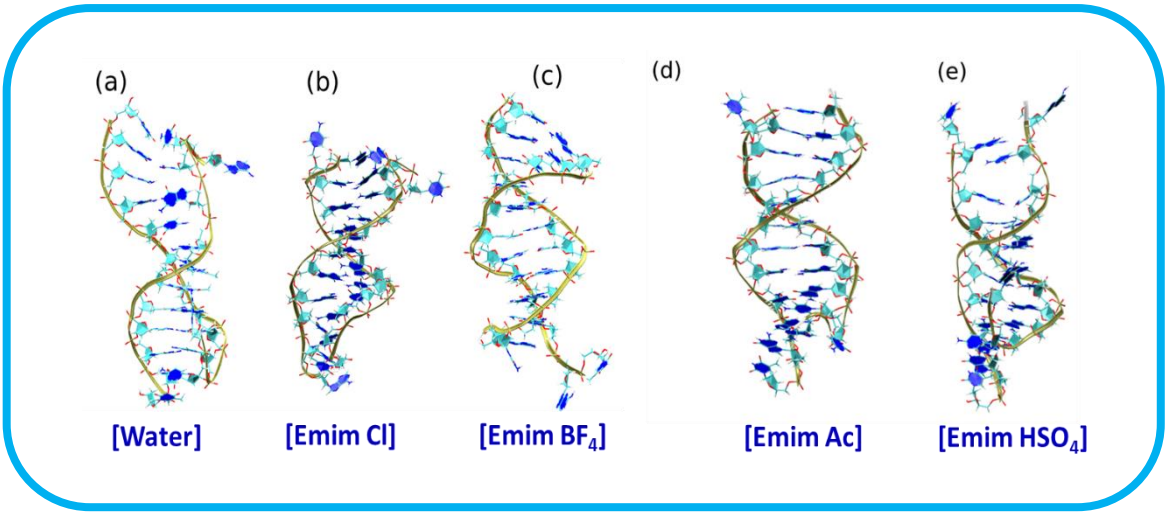

Figure 7. Analysis over a 200 ns simulation reveals the disrupted base stacking and disorganized Watson-Crick hydrogen bonding, particularly prominent with HSO_4^- anions, causing the collapse of inter-helical hydrogen bonding.

Chapter 6: Insight into the Structure and Transport Properties of Pyrrolidinium-based Geminal Di-cationic-Organic Ionic Crystals: Unravelling the Role of Alkyl-Chain Length

In recent times, the majority of the research works on ILs are devoted to the study of structure, properties and application of ionic liquids in their liquid state. However, studies on organic ionic crystals (OICs), which are solid-state analogues of RTILs, are rather limited. Interestingly, these organic ionic crystals have shown great promise to replace liquid-based electrolytes in energy-related applications such as in dye-sensitized solar cell, Li-ion batteries etc.[19-21] OICs are a kind of crystalline compound consisting of anions and cations whose properties are different from those of conventional crystals. The microstructure with three-dimensional ionic channels in this kind of ionic crystal are responsible for their excellent electrochemical properties. Interestingly, these systems also show comparable conductivity and diffusion efficiency like a usually employed liquid-based electrolyte. More importantly, these OIC-based electrolytes are exempted from the leakage problem that are

commonly associated with the liquid-based electrolyte. While some OICs based on MILs as well as DILs have been synthesized and have been used as electrolyte matrices for various electrochemical devices, the design and development of OIC-based electrolyte with high thermal stability and high conductivity has remained as a formidable challenge.

This chapter aims to provide comprehensive information on the correlation between structure and electrochemical properties of pyrrolidinium-based germinal OICs. To fulfil this objective, a series of geminal di-cationic Organic Ionic Crystals (OICs), based on C_3-, C_6-, C_8- and C_9-alkyl bridged bis-(methylpyrrolidinium)bromide are synthesized, and the structural features, thermal properties and phase behaviors of as-synthesized OICs have been investigated. Additionally, a number of electro-analytical techniques have been employed to assess their suitability as an efficient electrolyte composite (OIC: I_2: TBAI) for all-solid-state dye-sensitized solar cells (DSSC). The structural analysis has revealed that along with excellent thermal stability and well-defined surface morphology, OICs exhibit a well-ordered three-dimensional network of cations and anions that can serve as a conducting channel for the diffusion of iodide ions. Electrochemical investigations have shown that OICs with an intermediate length of alkyl bridge (C_6- and C_8-alkyl bridged) show better electrolytic performance than that are based on OICs with a relatively shorter (C_3-) or longer (C_9-) alkyl-bridged OICs. A careful analysis of the data has also demonstrated that the length of the alkyl bridge chain plays a significant role in determining the structural organization, morphology, and, eventually, the ionic conductivity of OICs.

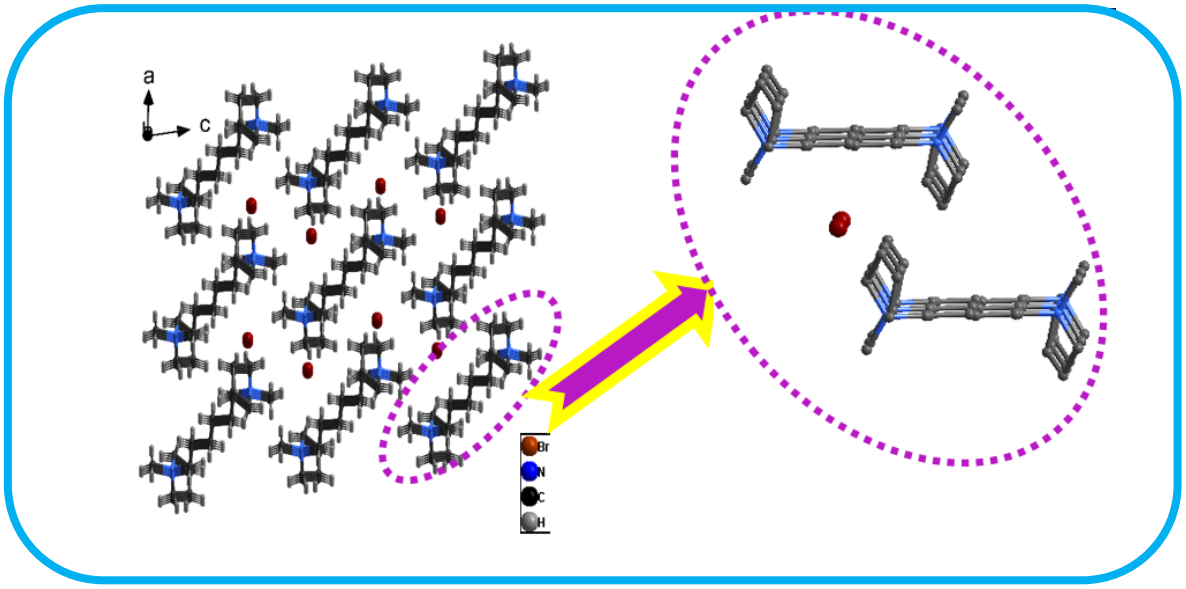

Figure 8. Three-dimensional crystal packing diagram of HMPYBr crystal showing existence of three-dimensional ion conducting channel that facilitate the ion conduction in the lattice.

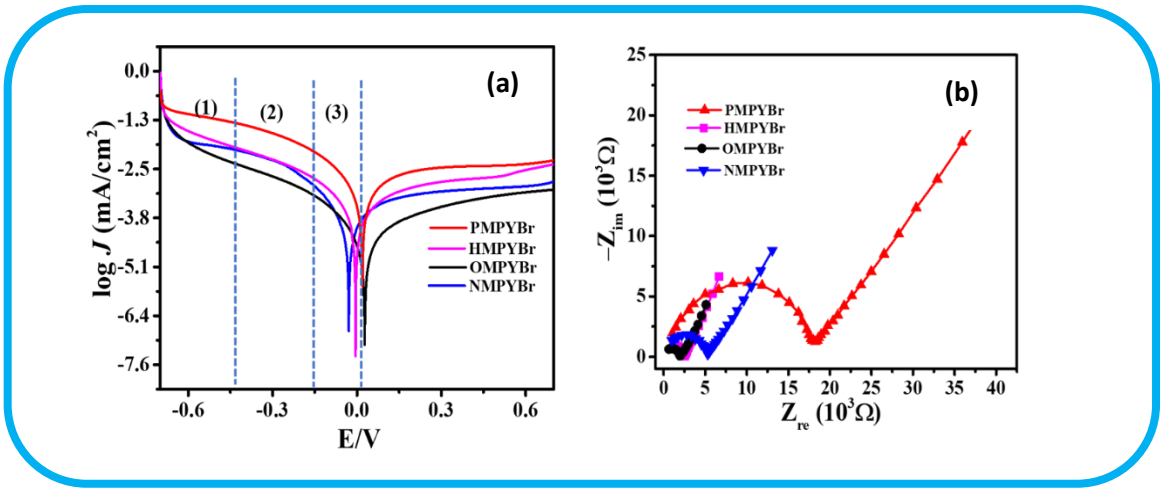

Figure 9. (a) Tafel polarization plots shows the exchange current density increases with increase with the length of the alkyl bridge (3 to 8) in OICs and decreases further with increase in chain length further (b) The Nyquist plots shows the variation of resistance of OIC-based electrolyte composites.

REFERENCES

1. Hallett, J. P.; Welton, T. Room-temperature ionic liquids: solvents for synthesis and catalysis. *Chemical Reviews* **2011**, *111*, 3508-3576.
2. Pârvulescu, V. I.; Hardacre, C. Catalysis in ionic liquids. *Chemical Reviews* **2007**, *107*, 2615–2665.
3. Wang, H.; Gurau, G.; Rogers, R. D. Ionic liquid processing of cellulose. *Chemical Society Reviews* **2012**, *41*, 1519–1537.
4. Y. Shimizu, Y. Ohte , Y. Yamamura , S. Tsuzuki and K. Saito , *The Journal of Physical Chemistry B*, 2012, **116** , 5406 —5413.
5. Tsuzuki, S.; Matsumoto, H.; Shinodaa, W.; Mikamia, M. Effects of conformational flexibility of alkyl chains of cations on diffusion of ions in ionic liquids. *Physical Chemistry Chemical Physics* **2011**, *13*, 5987–5993.
6. Yamada, H.; Miyachi, Y.; Takeoka, Y.; Rikukawa, M.; Yoshizawa-Fujita, M. Pyrrolidinium-based organic ionic plastic crystals: Relationship between side chain length and properties. *Electrochemical Acta* **2019**, *303*, 293-298.
7. Gorrasi, G.; Bugatti, V.; Milone, C.; Mastronardo, E.; Piperopoulos, E.; Iemmo, L.; Di Bartolomeo, A. Effect of temperature and morphology on the electrical properties of PET/conductive nanofillers composites. *Composites Part B: Engineering* **2018**, *135*, 149-154.
8. Prabhu, S. R.; Dutt,G.; Rotational diffusion of organic solutes in 1-methyl-3-octylimidazolium tetrafluoroborate–diethylene glycol mixtures: influence of organic solvent on the organized structure of the ionic liquid, *The Journal of Physical Chemistry B* **2014**, 118, 5562-5569.
9. Yaghini, N.; Abdurrokhman, I.; Hasani, M.; Martinelli, A. Transport properties and intermolecular interactions in binary mixtures based on the protic ionic liquid ethylimidazolium triflate and ethylene glycol, *Physical Chemistry Chemical Physics* **2018**, 20, 22980-22986.
10. Huang, Q.; Lourenco, T. C.; Costa, L. T.; Zhang, Y.; Maginn, E. D.; Gurkan, B. Solvation Structure and Dynamics of Li+ in Ternary Ionic Liquid– Lithium Salt Electrolytes. *The Journal of Physical Chemistry B* **2019**, *123*, 516– 527.
11. Ray, P.; Vogl, T.; Balducci, A.; Kirchner, B. Structural Investigations on Lithium-Doped Protic and Aprotic Ionic Liquids. *The Journal of Physical Chemistry B* **2017**, *121*, 5279– 5292.
12. Lawler, C.; Fayer, M. D. The Influence of Lithium Cations on Dynamics and Structure of Room Temperature Ionic Liquids. *The Journal of Physical Chemistry B* **2013**, *117*, 9768– 9774.
13. Samanta, D.; Iscen, A.; Laramy, C. R.; Ebrahimi, S. B.; Bujold, K. E.; Schatz, G. C.; Mirkin, C. A. Multivalent Cation-Induced Actuation of DNA-Mediated Colloidal Super lattices. *Journal of the American Chemical Soc*iety ***2019***, 141,19973−19977.
14. Grueso, E.; Cerrillos, C.; Hidalgo, J.; Lopez-Cornejo, P. Compaction and Decompaction of DNA Induced by the Cationic Surfactant CTAB. *Langmuir* **2012**, 28, 10968−10979.

15. Benedetto, A.; Ballone, P. Room Temperature Ionic Liquids Meet Biomolecules: A Microscopic View of Structure and Dynamics. *ACS Sustainable Chemistry & Engineering* **2016**,4, 392−412
16. Shukla, S. K.; Mikkola, J.-P., Use of Ionic Liquids in Protein and DNA Chemistry. *Frontiers in Chemistry* **2020**, *8*, 598662.
17. Wang, X.; Liu, M.; Ding, X., Guanidinium Hydrophobic Magnetic Ionic Liquid-Based Dispersive Droplet Extraction for the Selective Extraction of DNA. *Langmuir* **2021**, *37*, 11665-11675.
18. Xuan, S.; Meng, Z.; Wu, X.; Wong, J.-R.; Devi, G.; Yeow, E. K. L.; Shao, F., Efficient DNA-Mediated Electron Transport in Ionic Liquids. *ACS Sustainable Chemistry & Engineering* **2016**, *4*, 6703-6711.
19. Han, L.; Wang, Y. F.; Zeng, J. H. Effective Solid Electrolyte Based on Benzothiazolium for Dye-Sensitized Solar Cells. *ACS Applied Material & Interfaces* **2014**, *6*, 22088-22095.
20. Cao-Cen, H.; Zhao, J.; Qiu, L.; Xu, D.; Li, Q.; Chen, X.; Yan, F. High performance all-solid-state dye-sensitized solar cells based on cyanobiphenyl-functionalized imidazolium-type ionic crystals. *Journal of Material Chemistry* **2012**, *22*, 12842-12850.
21. Gorrasi, G.; Bugatti, V.; Milone, C.; Mastronardo, E.; Piperopoulos, E.; Iemmo, L.; Di Bartolomeo, A. Effect of temperature and morphology on the electrical properties of PET/conductive nanofillers composites. *Composites Part B: Engineering* **2018**, *135*, 149-154.

List of Schemes

List of Figures

List of Tables

Acronyms	
ILs	Ionic liquids
RTILs	Room temperature ionic liquids
MILs	Monocationic ionic liquids
DILs	Dicationic ionic liquids
EG	Ethylene Glycol
C153	Coumarin 153
MPTS	Sodium (8-methoxypyrene-1,3,6- sulfonate)
TEMPO	(2,2,6,6-Tetramethylpiperidin-1-yl)oxyl
REE	Red edge effect
T_m	Melting temperature
η	Viscosity
ρ	Density
a_N/G	Hyperfine splitting constant in Gauss
E_T**(30)**	Electronic transition energy of Reichardt's dye
EPR	Electron Paramagnetic resonance
UV	Ultra-Violet
TCSPC	Time-Correlated Single Photon Counting
PMT	Photo multiplier tube
CFD	Constant fraction discriminator
TAC	Time-to-amplitude converter
PGA	Programmable gain amplifier
ADC	Analog-to-digital converter
WD	Window discriminator
MCA	Multichannel analyzer
MCP	Microchannel plate
IRF	Instrument response function
FLUPs	Fluorescence Upconversion Spectroscopy
ϕ_f	Fluorescence quantum yield
k_{nr}	Non-radiative rate constant
k_r	Radiative rate constant
r_f	Fluorescence lifetime

Chapter 1

Introduction

Introduction

Abstract

This chapter provides a comprehensive overview of ionic liquids (ILs) and their significance across various scientific and technological domains. It commences with a broad introduction to ILs and their distinctive properties, followed by a historical synopsis of the discovery and evolution of these liquids. The subsequent section briefly delves into advancements in understanding the intricate relationship between the structure and physicochemical properties of different categories of ILs. Furthermore, the applications of diverse classes of ILs in chemistry, biology, and materials science are emphasized. Moreover, this chapter also provides a thorough discussion of the nano-structural organization of ILs and their intricate dynamics by highlighting some recent literature reports. This section also discusses relevant photophysical processes such as excitation wavelength-dependent emission behavior and rotational relaxation dynamics of some suitable solutes in ILs and translational diffusion dynamics of ILs, etc., which are often used to demonstrate the existence of nano-structural organization in ILs in detail. Finally, the chapter outlines the objectives of this thesis in response to the current challenges within the field of ILs.

CHAPTER 1

1.1.Introduction to Ionic Liquid

In the dynamic landscape of scientific exploration and industrial advancements, the prominence of ionic liquids (ILs) has steadily risen over recent decades. This captivating class of substances has not only become a subject of intense investigations among researchers but has also found compelling applications across various industries, capturing the interest of professionals and experts throughout the field [1-5]The unique ability to serve both as solvents and materials for diverse applications has led to a profound shift in their relevance within the field of modern chemistry. They represent a category of molten salts that primarily consist of relatively larger, asymmetrical organic cations paired with smaller inorganic or organic anions, all of which have melting points below 100°C.[2-3] Within the realm of ILs, the cations are typically organic groups, including but not limited to ammonium, imidazolium, pyrrolidinium, and pyridinium, whereas the anions encompass both organic and inorganic types, such as chloride, bromide, tetrafluoroborate, and hexafluorophosphate.[6] The bulky cations in ILs often have relatively low charge densities due to their extended molecular structures and the delocalization of charge. The low charge density and diffused charges result in less effective packing of ions, leading to the formation of viscous liquid materials under ambient conditions.[7] More interestingly, it has also been observed that this liquid material exhibits very negligible vapour pressure.[8] This attribute has positioned them as potential replacements for traditional organic solvents.[9] But in recent times, the utilization of ILs has experienced a notable shift, reaching beyond their traditional role as solvents.[10-11] Researchers have shown their effectiveness as solid-state electrolytes, as well as gas capture and storage materials.[12-17] These attributes have made them useful for the development of various energy storage systems. Moreover, ILs have also found their utility in drug delivery systems and preservation of biomolecules like protein and nucleic acids demonstrating their potential in developing new pharmaceutical

formulations.[18-20] Beyond the comprehensive exploration of macroscopic attributes and pertinent applications discussed earlier, the scientific community has increasingly turned its focus to another exciting feature of ILs, i.e., the presence of microheterogeneity within their liquid structure.[21-24]Advanced experimental and theoretical techniques have revealed the existence of distinct regions or domains within these systems. The discovery of microheterogeneity has introduced a new layer of understanding to the behaviour of ILs in various applications. These regions, often referred to as microdomains, exhibit varying compositions and interactions among the constituent ions. Since, the macroscopic behaviours of ILs are intricately related to their microscopic structures, they play a profound role in shaping the overall behaviour of ILs.[25-26]Therefore, understanding the behaviour of ILs at a microscopic level and also comprehend how the inter-constituent interactions and the resulting structural organisations of ILs are related to their microscopic behaviour has become an essential pursuit in the current-day research. This research endeavour is expected to unveil novel perspectives by enhancing our understanding of ILs and pave pathways for potentially ground-breaking applications in the times ahead.

The journey of ionic liquids began in the early 20th century, with their first synthesis of an ionic salt, ethyl ammonium nitrate (EAN), in 1914, by Paul Walden.[27] However, their potential remained largely unexploited for decades. It was during the latter half of the 20th century that researchers began to recognize their unique properties and versatile applications. In fact, Hurley and Wier, in 1959, provided more explicit insights into the potential advantages of ILs by introducing organic chloroaluminates synthesized from aluminium compounds and alkyl-pyridinium chloride salts and these chloroaluminates are considered as the first generation of ILs.[28] Notably, both pyridinium and imidazolium-based chloroaluminates were observed to have a susceptibility to react with water. Interestingly, in 1990, Mike Zaworotko proposed a method to synthesize ILs that remained

stable in the presence of water. [29]This led to the development of the second generation of ILs, featuring anions like nitrate (NO_3^-), tertrafluoroborate (BF_4^-), hexafluorophosphate (PF_6^-) and subsequently, the third generation of ILs emerged, incorporating perfluorinated anions such as bis(trifluoromethylsulfonyl)imide (NTf_2^-), tris(pentafluoroethyl) trifluorophosphate (FAP), and diverse organic cations such as imidazolium, pyridinium, pyrrolidinium, ammonium, phosphonium, others as depicted in Scheme 1.1[30].

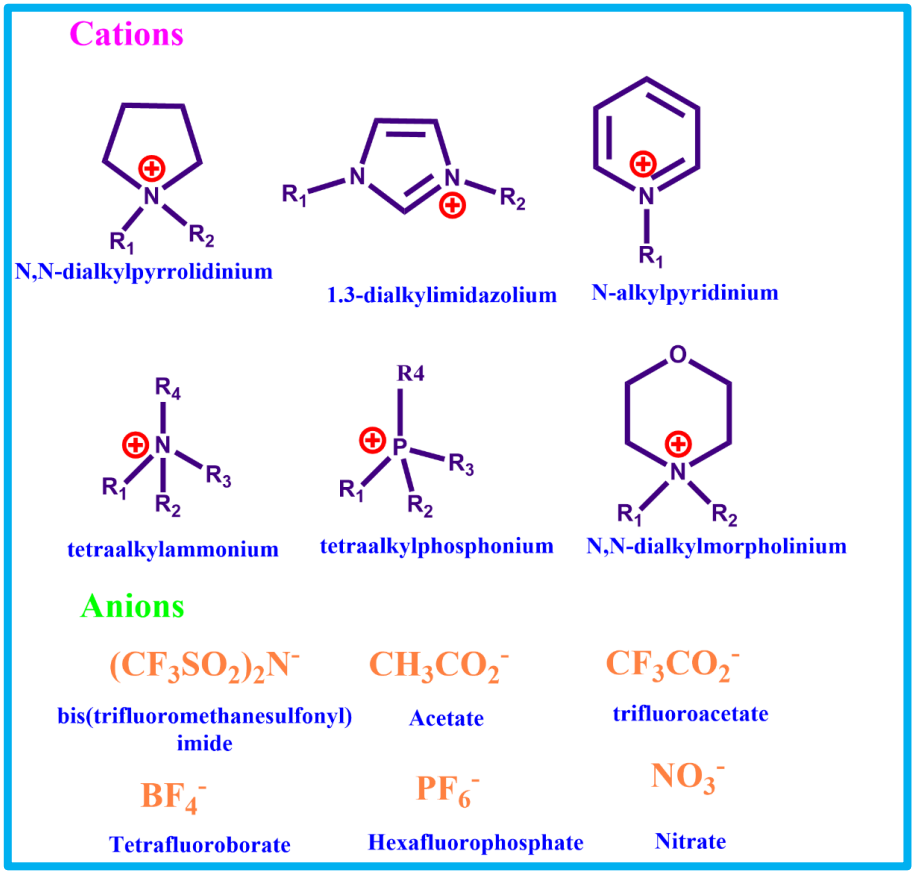

Scheme 1.1. Molecular structure of some common cation and anions that combine to form ILs. Here R represents the alkyl group with predominantly halide anions.

These ILs exhibit various interesting properties like high viscosity, low melting points, and high conductivity. However, some drawbacks were associated with these ILs, including production costs and a high affinity for binding with metal ions, which in turn could give rise to potential toxic effects. At the turn of the 21st century witnessed a surge of interest in

ionic liquids, with a growing understanding of their potential to revolutionize various industries. Their low volatility, thermal stability, and tuneable properties attracted attention across fields such as chemistry, materials science, and engineering.[8-9, 31] They found roles in green chemistry practices, serving as eco-friendly alternatives to traditional solvents that are often harmful to the environment. Furthermore, the concept of ionic liquids as "green solvents" extended their potential in sustainable technologies. Researchers also explored their applications in energy storage, electrochemistry, and even pharmaceutical formulations. Furthermore, the ability to tailor the properties of ILs by selecting specific combinations of cations and anions paved the way for the concept of "designer solvents."[8, 32-33] This concept allowed researchers to fine-tune the behaviour of ILs to suit specific tasks, from catalysis to separation processes and beyond. In more recent times, economically viable task-specific ILs are being devised for applications in energy materials.[5, 34-35]Beyond material applications, ILs based on amino acids were tailored for the utilization of ILs in pharmaceutics.[19, 31] Additionally, other categories of ILs, like geminal dicationic ILs (DILs), were formulated with anticipated applications in the realm of batteries and related technologies.[36-37] In this way, this designer material is consistently contributing to cleaner processes, energy efficiency, and ground-breaking innovations in shaping the future of various industries. As scientists keep learning about the hidden properties and possibilities of these substances, the story of ionic liquids will stay ever-evolving and influential. This journey will keep making big contributions to science and society.

1.2. General characteristics and properties of ionic liquids and applications

As mentioned earlier, ILs possess a range of distinctive characteristics and properties that set them apart from traditional solvents and materials. However, what makes ILs more fascinating is that the selection of both cations and anions substantially shapes the overall behaviour and traits of ionic liquids.[38-39] This ion-specific tunability opens up a wide range of

possibilities for designing ILs with desired properties for specific applications. Following are some ways in which the properties of an IL can be tuned by varying the constituent ions for specific applications.

1.2.1. **Melting point (m.p).** This property is indeed significant, as it determines the temperature range at which an ionic liquid remain in a liquid state. It can influence the applicability of an IL in various processes. The structure and chemical composition of ILs are closely tied to their melting points.[40] Cations with low symmetry, well-distributed charges, and weak intermolecular forces tend to decrease the melting point of ILs. The reduction in cation symmetry, for instance, has a significant impact on lowering the melting point. For example, the 1-butyl-3-methylimidazolium cation, which has only one methyl substituent and lower symmetry, has a lower melting point compared to the 1-butylpyridinium cation with higher symmetry. Likewise, when ammonium, pyrrolidinium, and phosphonium cations have symmetrical substituents, the resulting ILs tend to be in a solid state. Conversely, when asymmetric radicals are introduced as substituents, the melting point of these ILs is observed to be below room temperature. The choice of anion also affects the melting point of an ionic liquid. Larger anions tend to result in ILs with lower melting points. Conversely, anions that can form hydrogen bonds within the lattice structure of the ILs can lead to higher melting points. Understanding the relationship between the chemical structure of cations and anions and their impact on the melting point of ILs is crucial for designing and selecting ionic liquids with specific properties for various applications.

1.2.2. **Glass-transition temperature (T_g).** While most of the ILs are known for their low melting points and typically exist as liquids at or near room temperature, there are exceptions, and some ILs can exhibit a glassy or solid state under certain conditions,

particularly at very low temperatures or in specific environments.[36, 41] Indeed, in the context of ionic liquids (ILs), the glass transition temperature (T_g) can provide valuable insights into the cohesive energy within the salt and the interactions between the constituent ions. By altering the chemical structure of the cations and anions in an IL, it is indeed possible to influence its cohesive energy. For example, selecting cations and anions with weaker interactions or introducing steric hindrance that reduces ion-ion interactions can lower the cohesive energy of the IL. As a result, this can lead to a lower T_g, making the IL more fluid-like at lower temperatures

1.2.3. **Thermal stability and phase-behaviour.** ILs are known for their high thermal stability, which is one of their key advantages in various applications. Thermal stability refers to the ability of a substance to withstand high temperatures without undergoing significant decomposition or chemical reactions. It is important to note that the thermal stability of an IL can vary depending on its specific composition.[36, 40]For example, ILs that incorporate cations such as pyrrolidinium and imidazolium are generally known for their excellent thermal stability, whereas ILs based on pyridinium and ammonium cations tend to exhibit comparatively lower thermal stability. However, the thermal decomposition temperature of ILs is found to be mainly dependent on the nature of anions instead of the nature of the cation. Commonly, thermal stability of ILs containing same cation decreases with increase in the hydrophilicity of the anion. The thermal decomposition temperature of ILs generally vary from 100^0-400^0C.[36] ILs made up of a bis(trifluoromethane sulfonamide) anion (TFSI) and alkyl-ammonium cations or the imidazolium or pyrrolidinium cation and a variety of heterocyclic cations are known as the most stable ILs with decomposition temperatures above 200^0C. Interestingly, some ILs

can also shows various phase transitions before undergoing decomposition. These phase transitions are often associated with changes in the physical state of ILs and can include solid-solid transitions, solid-liquid transitions, or liquid-liquid transitions. While, some ILs undergo phase transitions within the solid state, leading to the formation of different crystalline structures or polymorphs, some exhibit a plastic-crystalline phase, which is an intermediate state between a crystalline solid and a disordered liquid. The thermal stability of an IL is a critical factor in determining its suitability for heat transfer applications. Selecting an IL with the appropriate thermal stability ensures safe and efficient heat transfer processes, helping to avoid equipment damage and maintain system integrity at high temperatures.

1.2.4. **Density (ρ).** The density of ILs is a crucial parameter as it plays a significant role in determining their flow behaviour and heat transfer characteristics. In general, the density (ρ) of ionic liquid is higher than water. Normally, the density of IL is found to be in the range of 1.04 to 1.50.[40] Exceptionally, phosphonium-based ILs are found to be less dense than water. The magnitude of density of an ionic liquid depends on the structure of constituent ions. The size of the cation influences the density in the way that a larger cation gives rise to the low density of IL. For instance, ILs with pyrrolidinium, pyridinium, and imidazolium cations are usually denser than that of ILs that contain phosphonium cations. Furthermore, the density of IL decreases as the length and number of the alkyl substituent attached to the cationic moiety increases. In some cases, the functional group attached to the cation also becomes the determinant of the density of ILs. Likewise, the density of ILs is also significantly influenced by the nature of the anions. For example, comparing the ILs with the common cation ([C_4mim]), the densities of the ILs follow the anion

order: [NTf_2] > [PF_6] > [TFO][C_1SO_4] > [$C(CN)_3$]. Density can affect mass transport properties, such as diffusion coefficients and solubility, which are important in applications like extraction and separations.[40] Matching the the density of IL to specific solutes or target molecules can optimize these processes.

1.2.5. **Viscosity.** Determining the viscosity of ILs is a critical aspect of their application because this property has direct implications for various important factors. Specifically, viscosity affects the energy expended in pumping fluids, the pressure drops in pipelines, and the rate of convective heat transfer.[40] In most cases, the viscosity of an IL is primarily influenced by two key factors: the length of the cationic chain and the size of the IL molecules. Smaller and symmetric cations with lower molecular weights tend to result in lower viscosities. Additionally, cations with higher molecular weights but shorter alkyl substituents also exhibit lower viscosities. For instance, pyrrolidinium-based ILs are more viscous than the imidazolium-based ILs.[36] Moreover, an increase in the chain length of the cation in an IL is associated with an increase in viscosity. This effect is attributed to strong van der Waals interactions between the longer alkyl chains, which result in greater resistance to flow. Longer chains lead to more extensive molecular interactions, contributing to higher viscosity. [42]The ability of the anion in an IL to participate in hydrogen bonding interactions can significantly impact its viscosity.[40] ILs with anions capable of forming hydrogen bonds tend to have higher viscosities. Hydrogen bonding interactions between the anion and surrounding ions contribute to the overall molecular cohesion and viscosity of the IL. Furthermore, ILs containing anions like PF_6^- and BF_4^- are found to be more viscous compared to those with Tf_2N^- anions.[40] This viscosity difference is attributed to electronic effects arising from the presence of fluoride atoms in these anions and the dispersion

of negative charge on the sulfoxide groups of Tf_2N^-anions. Moreover, temperature has a significant impact on the viscosity of ILs. Higher temperatures promote increased molecular mobility within the IL. As a result, the molecules in the IL have greater freedom to move, which eventually reduces their ability to aggregate. This enhanced ion mobility leads to a decrease in shear thinning and, consequently, a reduction in viscosity. The viscosity of ILs is often compared to that of conventional oils, but it can exhibit significant variation with changes in temperature. Even a relatively small temperature increase, such as 5 Kelvin (k), can result in a substantial decrease in viscosity, potentially up to 20%. The viscosity behaviour of ionic liquids (ILs) is often described using the Vogel-Tammann-Fulcher (VTF) equation[43], as presented in equation (1.1)

$$\ln(\eta) = \ln(\eta_0) + \frac{DT_C}{T-T_C} \quad (1.1)$$

In the eq. (1.1), η_0 represents viscosity at infinite temperature, D denotes the fragility parameter and T_C is the viscosity diverging temperature.

1.2.6. **Conductivity (σ)**. Ionic liquids exhibit reasonably good ionic conductivities, typically in the order of ~10 mS/cm, which is relatively higher as compared to many organic solvents. However, their high viscosity can limit their conductivity, especially at room temperature.[44] Furthermore, the conductivity of an electrolytic solution depends on both the mobility and the number of charge carriers within ILs. Some ILs contain larger ions, which can lead to reduced ion mobility. The size of ions affects how easily they can move through the medium.[42, 45] Consequently, the conductivity of ILs with relatively longer alkyl chains is low.[46] Similarly, the ionic conductivity of ILs increases with a less symmetrical cation structure and smaller molecular weight.[47] The tendency of ions to aggregate or form clusters within the

IL can also limit ion mobility as aggregated ions have limited freedom to move independently, decreasing overall conductivity.

1.2.7. **Electrochemical potential window**. Electrochemical potential is indeed a critical parameter in battery and electrochemical applications.[40] The electrochemical potential window, often referred to as the electrochemical stability window, represents the range of voltage within which an electrolyte or medium can be used without significant background current or undesirable chemical reactions. ILs are known for their exceptional electrochemical stability, making them valuable in various electrochemical applications. ILs typically exhibit a large electrochemical window, typically in the range of 4.5 to 5 volts.[40] The ability of ILs to maintain their integrity and conductivity over such a wide electrochemical potential window makes them attractive candidates for use in advanced energy storage devices, such as high-voltage batteries and supercapacitors, as well as in various electrochemical processes where stability at extreme potentials is essential.

1.2.8. **Other properties**. Besides the above-mentioned properties, ILs exhibit several other physical properties that can vary depending on the specific cations and anions used in their composition. For example, the surface tension of ILs is generally influenced by their molecular structure.[48-49] An increase in packing efficiency, often associated with smaller and more symmetric ions, can lead to a decrease in surface tension. Conversely, if ILs possess strong ionic or hydrogen bonding interactions, this can result in an increase in surface tension. Likewise, the refractive index is another interesting property of ILs that can provide insights into their polarity.[48] ILs are generally considered moderately polar media, similar to acetonitrile. However, the refractive index can be affected by factors such as the alkyl chain length of the cationic component.[49-50] Longer alkyl chains tend to decrease the refractive index,

while the addition of functional groups like hydroxyl groups can increase it. The solubility of an IL is an important parameter that determines the suitability of an IL to be used as a solvent for a given reaction. The solubility of an IL is primarily determined by the nature of its anionic species. ILs containing anions like PF_6^- and NTf_2^- are typically hydrophobic, meaning they are not easily soluble in water. In contrast, ILs with anions such as BF_4^- or halides (e.g., Cl^-) tend to be hydrophilic, exhibiting an affinity for water. Therefore, the hydrophobic or hydrophilic nature of the IL can have significant implications for its compatibility with other substances and its suitability for various applications.[51]

1.3. Microscopic structural organization in ILs and relevant properties

Microstructural and dynamical heterogeneities represent distinctive characteristics that can contribute to the unique properties exhibited by ILs.[24-25] Initially, within the IL community, these liquids were perceived to fit within the conventional model of molecular liquids, being coherent, irregular, and essentially homogeneous systems. Bulk ILs were commonly regarded as similar to high-temperature molten salts, such as NaCl, or highly concentrated salt solutions. However, more recently, it has been determined that ILs present diverse ordering structures compared to conventional molecular liquids. These distinctive mesoscopic organizations include hydrogen bonding networks, combinations of polar and apolar components with amphiphilic characteristics, and morphologies resembling micelles within the IL matrix. ILs exhibit structural heterogeneities at multiple length scales. The segregated structure observed in ILs emerges from a delicate balance of various inter and intramolecular forces that are operational between constituent ions. These molecular interactions span a spectrum from weak, isotropic, and nonspecific forces (e.g. solvophobic, van der Waals (vdW), dispersion forces, etc.) to strong (Coulombic), anisotropic, and specific forces (e.g., charge, dipole, and multiple interactions as well as

hydrogen bonding (HB) interactions, etc.).[52] These subtle interactions make significant entropic contributions, providing additional stabilization and leading to ionic cluster formation. This process sets the stage for the development of intricate, higher-order, self-assembled liquid structures within ionic liquids, both in bulk liquids and within confined environments.[24] Moreover, not all but a vast number of ILs can be categorized as having polar and apolar components and, therefore, can be regarded as nano-segregated fluids with polar (apolar) networks permeated by apolar (polar) domains. For example, Alkylammonium nitrate-based ILs are the most studied ILs since they are the first ILs ever synthesized in the laboratory. However, the crystal structure of methylammonium nitrate determined through DFT calculations by Bodo et al. shows that there is no nanoscale apolar segregation in methyl-ammonium nitrate (MAN) as methyl groups are too small.[53] However, Atkin and War and Umebayashi et al. independently investigated microstructures of ethyl ammonium nitrate (EAN) using complementary wide-angle X-ray scattering (WAXS) and small-angle neutron scattering (SANS) techniques, respectively.[7] Both studies indicated that nanoscale heterogeneity exists in EAN with polar and apolar domains throughout the bulk liquid matrix, suggesting a disordered, locally smectic, or discontinuous liquid structure. The hydrophobic interactions among alkyl units are essentially responsible for the formation of micro-heterogeneous structures. In addition, both electrostatic and HB interactions between amine and [NO_3] groups play a significant role in stabilizing microstructures in the EAN matrix. So, the above discussion shows that lengthening of the alkyl chains attached to cations leads to a more pronounced segregated liquid structure.[54] ILs composed of imidazolium cations paired with varied spherical anions (F^-, Cl^-, Br^-, BF_4^-, and PF_6^-) also present a similar picture of heterogeneous microstructures in IL matrixes but with a few differences.[55] Besides variation in the length of the alkyl chain, varying symmetry of cation, functionalization of cationic head and alkyl chain, and

the nature of anions have also resulted in different microscopic features and hence show different thermophysical properties.[47] For example, both pyrrolidinium and imidazolium cations are quaternary ammonium salts of symmetry. But, while the imidazolium cation is planar and aromatic, pyrrolidinium is non-planar. Due to this, pyrrolidinium-based ILs produce more viscous ionic liquid than imidazolium-cation-based ILs.[56-58] Also, the low-frequency Kerr spectra indicated lesser microheterogeneity in pyrrolidinium-based IL than in imidazolium-based ILs.[59] These are attributed to the distinct activation of translational and vibrational motions of different ion species at low-frequency regions. Mutating a methylene (methyl) group in imidazolium cation with specific atoms, like hydrogen, oxygen, fluorine, silicon, selenium, and even phenyl group, leads to a distinct structural arrangement in the heterogeneous IL matrices.[60-62] For instance, the silicon-substituted imidazolium cations have advantages in some applications in comparison with carbon-based imidazolium cations, and thus, they are frequently used as solvent electrolytes and gas absorbents. Both electronic and size effects make intermolecular correlations in [SiMIM] ILs weaker than in [C_nMIM] ILs, leading to a low viscosity of [SiMIM]-[NTF_2]. OHD-OKE spectroscopy revealed a generic correlation of low intermolecular vibrational frequencies for [SiMIM][NTF_2] with its decreased liquid viscosity, which is distinct from that of [C_nMIM][NTF_2] ILs.[24] Similarly, functionalizing imidazolium cations with aromatic moieties (benzyl groups) leads to significant and systematic changes in the thermophysical properties of ILs.[63] They have increased glass transition and melting temperatures arising from additional π–π interactions. Functionalization of alkyl chains of an imidazolium-based IL using ether and hydroxyl groups disturbs a delicate balance of Coulombic, HB, and dispersion interactions, contributing to enhanced intermolecular interactions between constituent ions.[64] Finally, regarding the impact of anions, they may result in different physical states in ILs. While NTf_2-based ILs generally form RTILs, halide anions mostly

give rise to ILs in the solid state. This is attributed to the differences in HB interactions of anions, which are reflected in macroscopic physicochemical properties, like melting points, glass transition temperatures, ion conductivities, and liquid viscosities of alkylammonium ILs.[8, 48, 65] From all the above discussion, it is clear that microstructural heterogeneity and the macroscopic behavior of ILs are intricately related. Due to the possibility of countless combinations of cation−anion moieties, a thorough understanding of their hierarchical structures and dynamics is highly significant for rational selection and design of ILs with desired properties and thereafter maximizing their functionalities in applications including catalysis, gas capture and separation, energy storage and harvesting, and lubrication. Many state-of-the-art experimental techniques such as spectroscopy (2D IR,[66] dielectric relaxation,[67] FT-IR,[68] NMR,[69-70] OHD-OKE,[71] ultrafast 2D-IR[72], SFG vibrational spectroscopy,[73-74] neutron diffraction,[54, 75] XPS[76] and theoretical studies[77-78] based on computer simulations have been employed to gain insights into the microstructures and dynamics of ILs. The current thesis work employs steady-state and time-resolved fluorescence spectroscopy techniques to understand the structural organization in ILs by investigating several photophysical processes in ILs.

1.4. Various photophysical processes used to understand the nano-structural organization in ILs

The preceding discussions make it evident that a comprehensive understanding of the intermolecular interactions, structure, and dynamics of this emerging class of material is imperative for their effective applications across diverse fields. This understanding not only offers valuable insights into the fundamental mechanisms governing the behaviour of ILs but also contributes to the strategic design of ILs with desired properties. A plethora of studies utilizing sophisticated experimental and computational techniques have been undertaken to thoroughly examine the interactions, structure, and dynamics of these

solvents. However, investigation of the microstructural organization and dynamics of these systems—especially through phoyoyhysical studies, employing meticulously chosen fluorescent probe molecules dissolved in these media represents an interesting area of investigation. [79-81]This is because the exceptional sensitivity, high selectivity, and simplicity of the fluorescence spectroscopic method have elevated its value significantly when compared with other available analytical techniques. This section illustrates a variety of photophysical phenomena and processes that are frequently employed to understand the structural organization and solute dynamics in ILs, with a special emphasis on those directly relevant to the present thesis.

1.4.1. **Excitation wavelength-dependent emission study.** Understanding and applying Kasha's rule is fundamental in the field of fluorescence spectroscopy. This rule provides a reliable framework for identifying the specific electronically excited state responsible for fluorescence emission.[82-83]This is crucial for gaining insights into the electronic structure and dynamics of molecules during fluorescence processes. Kasha's rule ensures that the emission spectrum of a fluorescent molecule is consistent, regardless of the excitation wavelength. That means the fluorescence of a molecule arises from the lowest vibrational energy level of the lowest electronically excited state with identical spin multiplicity, irrespective of the wavelength at which the molecule is excited. However, under specific conditions, it has been observed that the emission spectra of certain fluorophores monitored in a confined media get shifted towards a longer wavelength with an increase in the excitation wavelength. Interestingly, this phenomenon is found to be more noticeable when the sample undergoes excitation at the longer-wavelength, red end of the absorption spectrum.[83-84] For this reason, it is commonly referred to as the "red edge excitation shift (REES)" or the red edge effect (REE). REEs are typically observed in viscous solvents or glass-forming liquids like RTILs, especially at relatively low temperatures. In viscous

media like RTILs, where solvation of a solute fluorophore occurs more slowly compared to common solvents such as water, ethanol, and DMSO, fluorescence may also originate from various unrelaxed states of the solvent molecules surrounding the fluorophore.[85] Particularly, for example when the fluorescence lifetime (τ_f) of the fluorophore is considerably shorter than the average solvation time (τ_{solv}) in a given solvent, the fluorophores can exist in a condition where they are not completely equilibrated with the solvent environment. In such a situation, the local environments surrounding the fluorophores undergo distinct changes. Therefore, excitation at the red edge of the absorption band selectively triggers fluorophores with lower transition energy. As the relaxation of the solvent is slower than the fluorescence lifetime, the arrangement of solvent molecules remains almost unchanged throughout the excited state lifetime, resulting in a red-shifted emission. So, two conditions can give rise to excitation wavelength-dependent emission behaviour. Firstly, the ground state must exhibit a variety of energetically distinct species, contributing to the inhomogeneous broadening of the absorption band, and secondly, the rates of relaxation of the excited state of these distinct species must be slower than their respective fluorescence lifetimes. In the context of ILs, the REE was first revealed by Samanta and coworkers, and they have attributed its occurrence to the spatial heterogeneity within ILs.[85] Subsequently, Margulis and his group, using molecular dynamics (MD) simulations, have demonstrated that the source of REES can be related to the intrinsic dynamic heterogeneity of the medium.[86] They proposed that the medium heterogeneity in the ground state, which enables the photo-selection of the fluorophore, exists in ordinary fluid media as well. Nevertheless, the dependence on excitation wavelength becomes evident primarily in ILs due to the slow solvation rate and less effective energy transfer among distinct energetically excited species within the ILs. However, the dependence on excitation wavelength becomes apparent primarily in ILs

because of the slower solvation rate and less efficient energy transfer among various energetically excited species within the ILs. Although this method doesn't provide an exact prediction of the length scale of heterogeneity within the ILs, it serves as a valuable qualitative method for evaluating the micro-heterogeneous behaviour in ILs. Sarkar and colleagues have applied the same method for qualitatively determining the heterogeneity present in some specific IL medium.[87] In a separate work, Mandal and coworkers also, by employing this technique, have provided an idea about the size of the nano aggregates that persist in ILs.[88] The pictorial representation of this phenomenon is presented below (Scheme 1.2).

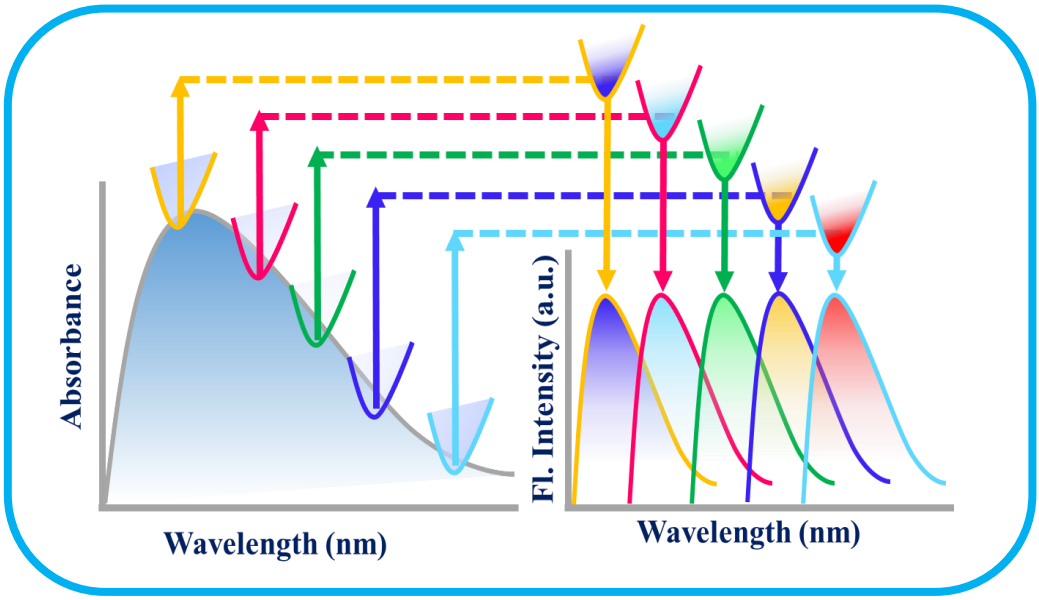

Scheme 1.2. Pictorial Representation of Red-Edge-Excitation Phenomena

1.4.2. Rotational dynamics. Investigation of the rotational dynamics of fluorescent probes within a given medium is of great significance across biochemistry, biophysics, and materials science. This approach is pivotal in studying intermolecular and intramolecular interactions and gaining insights into the properties of complex fluids. The commonly utilized fluorescence anisotropy technique proves particularly effective for examining the rotational dynamics of molecules in solution.[89-92] The anisotropy

process can be studied using either a combination or individual application of both steady-state and time-resolved fluorescence anisotropy techniques. However, when it comes to investigating complex micro-heterogeneous systems like ILs, time-resolved techniques can be more effective than steady-state measurements. This is attributed to their ability to reveal dynamic insights into molecular behaviour and interactions within the system. In contrast, steady-state measurements solely provide information about the equilibrium state of the system and lack the capability to capture transient behaviour, which is important for a comprehensive understanding of the dynamic properties of the systems. Time-resolved fluorescence anisotropy (TRFA) is a technique that involves measuring the decay of fluorescence anisotropy over time. The principle that forms the base of time-resolved fluorescence anisotropy is the selective excitation of fluorophores through photo-selection. According to this principle, when linearly polarized light is used to excite fluorophores, only those fluorophores whose absorption transition moments are aligned with the electric field vector of the incident light get preferentially excited. As a consequence of this selective excitation, an anisotropic orientation of fluorophores takes place in the excited state. However, such polarization is temporary and changes over time as a result of the rotational diffusion of fluorophores, which changes the orientation dipole of the fluorophore. This change in the orientation of the dipole moment vectors leads to a time-dependent evolution in the degree of anisotropy of the emitted fluorescence. A schematic diagram of illustrating the complete phenomena have been provided in scheme 1.3.

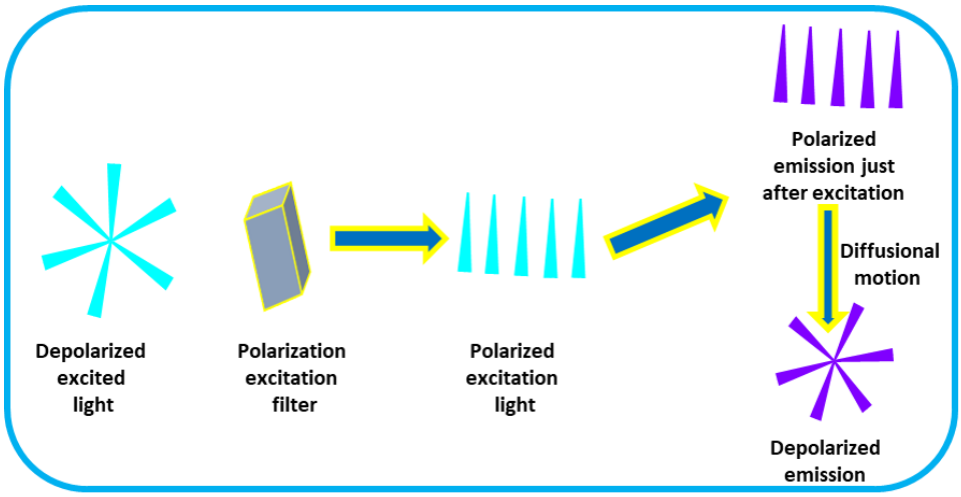

Scheme 1.3. Polarised Excitation light is depolarised due to the diffusional motion of the excited fluorophores.

Therefore, by measuring the decay of fluorescence anisotropy over time, one can gain information about the rotational dynamics of fluorophores in a given medium. Scheme 1.4 represents a typical anisotropy decay plot of a probe perylene in an IL medium.

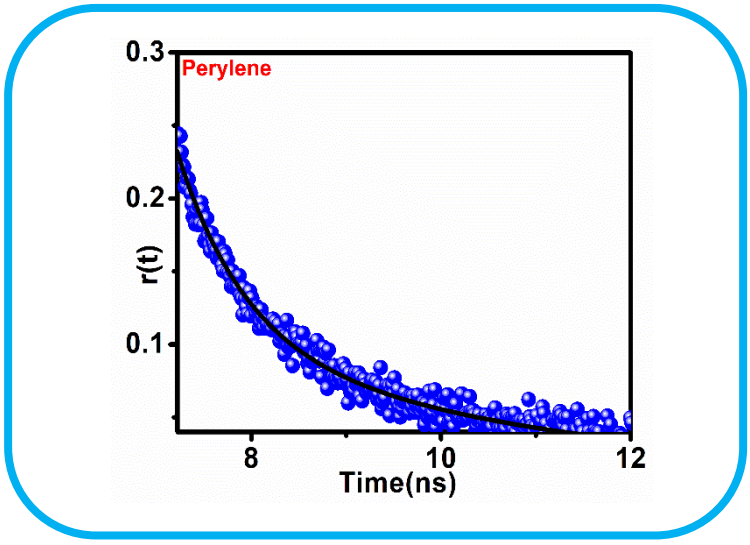

Scheme 1.4. Anisotropy decay of perylene in an imidazolium-based IL measured at room temperature

The anisotropy decay curve provides information about the rotational correlation time of the molecules. The rate at which the anisotropy decreases is related to the speed of the

rotational diffusion. This information can also be used to gather information about the size, and shape of the rotating species as well as factors like viscosity, temperature of the medium and interactions (electrostatic, hydrophobic or hydrogen-bonding) with surrounding solvent molecules.

After getting the anisotropy decay curve by means of TRFA techniques, the collected data can be analysed by means of different hydrodynamic model.[93-94] This theoretical approach provides a means to extract dynamic characteristics of both the solute and solvent media, offering valuable insights into their rotational behaviours and interactions within the system. One such commonly used model is the Stokes-Einstein-Debye (SED) hydrodynamic theory.[91, 93] According to the theoretical framework of SED theory, the solvent is considered as structureless continuous media where the rotational relaxation/reorientation/diffusion time for a solute of medium size is solely associated with to the bulk viscosity (η) of the medium through the equation provided below:

$$\tau_r = \frac{\eta V f C}{K_B T} \tag{1.2}$$

In the equation presented above, k_B represents the Boltzmann constant, T denotes the absolute temperature, V stands for the molecular volume of the solute molecule, calculated based on van der Waals radii, and the parameter f accounts for the shape factor of the solute molecule. The shape factor (f) plays a crucial role in addressing any departure of a solute molecule from a spherical shape. An f value of one indicates that the solute is perfectly spherical, whereas a higher f value is associated with an asymmetrical ellipsoid. Moreover, the SED models operate with two extreme boundary conditions (C): stick (C=1) and slip (0<C<1) limits. The value of C typically signifies the extent of solute-solvent coupling for a given solute and solvent. In cases where solute molecules exceed the size of solvent molecules, C is equal to one, signifying a stick boundary condition. Conversely, if the solute molecule is smaller or similar in size to the

solvent molecule, the value of C lies below one, signifying a slip boundary condition. The SED theory considers that solute molecules adhere to either symmetric or asymmetric ellipsoidal shapes. The limitation of SED theory is that it assumes that the hydrodynamic volume of a solute remains unaffected by the solvent continuum, but this assumption holds true only when the solute significantly surpasses the size of the solvent. In instances where the SED theory fails, quasi-hydrodynamic theories come into play, taking into account the sizes of both solvent and solute molecules. Two such theories are the Gierer-Wirtz (GW) and Dote-Kivelson-Schwartz (DKS), which elucidate the rotational behaviour of solute molecules, considering the dependence on solvent size.[94-95]According to the GW theory, the solvent molecules are present as concentric shells of spherical particles enveloping the spherical solute molecules.[93] The determination of the boundary parameter (CGW) in the GW theory relies on the use of angular viscosity. This value decreases with an increase in the number of concentric shells surrounding the solute molecule. In contrast, the DKS theory takes into account the available space between the solute and solvent molecules, along with their respective sizes.[94] According to this theory, when comparing the size of the solute molecule relative to the available space in the solvent, a weak connection between the solute and solvent emerges. Under such circumstances, the solute encounters reduced friction, resulting in an accelerated rotation within the solvent environment.

Looking forward to the investigations carried out by various groups on the rotational dynamics of a suitable solute in RTILs through TRFA measurements, Fayer and colleagues have explored the rotational dynamics of both polar and non-polar probes in imidazolium-based ILs.[93] Similarly, Dutt and his group have conducted extensive investigations into the rotational dynamics of various probes across a range of ILs.[89-91]Sarkar and co-workers have delved into the rotational dynamics of various solutes in

both mono-cationic and di-cationic ILs.[87, 96] Sarkar and coworkers have also examined the rotational motion of both charged and neutral solute molecules to probe the structure of both cationic and anionic IL-based micelle.[97] Across these studies, a consistent finding is that solute rotation is influenced not only by the viscosity of the medium but also by specific interactions between the solute and the solvent. Particularly, hydrogen bonding interactions play a significant role in affecting the rotational motion of solutes in ILs. Additionally, as ILs consist of ions, the electrostatic interactions between charged solutes and the ionic components of ILs can further impact the rotational behaviour of charged solute molecules. From the above discussions, it is apparent that monitoring the rotational dynamics of suitably chosen probe molecules by means of TRFA techniques is quite informative about the structural organization in microscopic scales and behaviors of this complex micro heterogeneous system like RTILs. Keeping this fact in mind, the current thesis work extensively incorporates rotational dynamics studies to understand the structural organization within ILs in a comprehensive manner.

1.4.3. Solvation dynamics. Understanding solvation dynamics is crucial in fields like chemistry and biochemistry because the interactions between solute and solvent molecules play a significant role in various chemical and biochemical processes. The study of solvation dynamics provides insights into how solvents reorganize and respond to changes in the environment around solute molecules over time, which can have implications for reaction mechanisms, molecular stability, and other related phenomena.[98] Various sophisticated methodologies, such as time-dependent fluorescence stokes shift measurement (TDFSS), FTIR/2DIR spectroscopy, dielectric relaxation measurements, optical Kerr effect (OKE) spectroscopy, molecular dynamics simulations, ab initio calculations, transient absorption spectroscopy have been employed to scrutinize and comprehend the intricate dynamics of in various solvent

systems.[99-102] Among the array of techniques, time-dependent fluorescence stokes shift measurement stands out as a pivotal and extensively employed method for monitoring the solvation dynamics of RTILs.[103-105] A visual representation of the solvation process is provided in scheme 1.5. In essence, TDFSS involves the application of a short laser pulse to excite the probe solute electronically. This excitation induces a change in the charge distribution of the solute without altering its molecular geometry. In the immediate aftermath of excitation, the solvent molecules undergo slow rearrangement among themselves around the solute in order to stabilize the modified charge distribution. The temporal evolution of this stabilization process, resulting from solvent reorganization, manifests as a red shift in the emission spectra. By quantifying the shift in the emission maxima over time, researchers can effectively monitor the intricate dynamics of solvent relaxation. In essence, TDFSS provides a dynamic and detailed insight into how the solvent environment adapts to and stabilizes the altered electronic state of the solute following laser excitation. This detailed understanding contributes significantly to the broader exploration of solvation phenomena in RTILs.

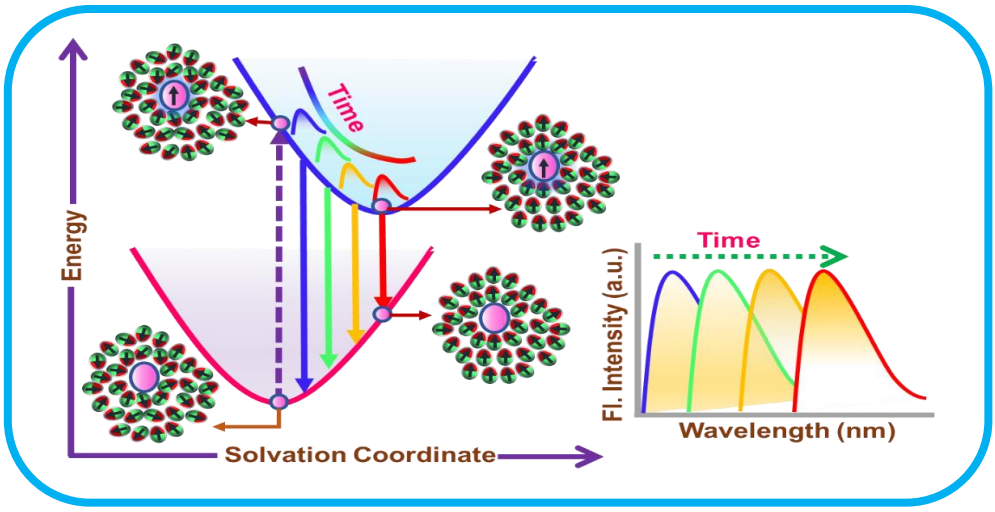

Scheme 1.5. Pictorial representation of the process of dynamics of solvation through time-dependent dynamic Stokes shift measurements.

Solvation dynamics in common dipolar solvents, such as water, have been studied extensively since the 1980s, offering a comprehensive understanding of temporal aspects. With the rise of ILs and their diverse applications, researchers turned their attention to unravelling solvation dynamics in such complex media. Karmakar and Samanta pioneered the examination of solvation dynamics in imidazolium-based ILs using TDDSS measurement. Subsequent contributions from groups led by Maroncelli, Castner, Bhattacharyya, Biswas, and others, through both experimental and theoretical approaches, have shed light on solvation dynamics in RTILs.[103, 106-111] Collectively, these studies reveal that solvation in RTILs occurs across multiple time scales and the slowest component corresponds to the bulk viscosity of the medium. In the same thread, Kobarak and Znamenskiy have suggested that collective cation-anion motion is responsible for the fast component.[112] Biswas and coworkers, Shim et.al, have also observed the ultrafast solvation response of ILs.[86, 113] So, this study has demonstrated that the multiple solvation component for a given probe molecule in ILs is due to the complex micro-heterogeneous structure of this medium.

1.4.4. Fluorescence correlation spectroscopy (FCS) studies. Fluorescence correlation spectroscopy is indeed a powerful technique because it can provide information about individual molecules rather than an ensemble average. Therefore, it becomes important in the context of investigating heterogeneity and dynamic behaviour of a system that may not be detected in the bulk measurements. Additionally, FCS can be utilized to study a range of molecular processes, including molecular diffusion, binding/unbinding events, and conformational changes.[114-116] Therefore, it is a widely used tool in fields such as cell biology, biochemistry, and pharmacology to investigate molecular interactions in live cells and complex environments.[117] This spectroscopic technique is based on measuring the fluctuations in the intensity of fluorescence emitted by the

fluorophores within a tiny volume (confocal volume) over time. These fluctuations are indicative of dynamic processes occurring in the sample. This fluctuation measured at two different times describes the correlation between fluorescence intensities at different points in time and gives rise to an autocorrelation function. The shape and decay time of the autocorrelation function provide information about the diffusion properties and interactions of the fluorescent molecules.[118] Therefore, investigating the rotational diffusion time of organic fluorophores within IL, for instance, if the fluorophores exhibit different diffusion behaviours in distinct areas of the ILs, it could indicate the existence of discrete structural domains within the ILs. Werner et al. were pioneers in examining the diffusion characteristics of rhodamine 6G and Atto 532 within imidazolium-based RTILs.[119] Subsequently, Bhattacharyya and collaborators delved into the study of the diffusion of two fluorescent probes, rhodamine 6G and pyrene, within three distinct RTILs featuring different anions. In that study, they observed more than one diffusion coefficient for a particular probe within a given IL. This explicitly suggests that the IL media are not homogeneous like common organic solvents or water; rather, they exhibit micro-heterogeneous domains of polar and non-polar character within them.[120] Moreover, Guo et al. and Patra et al. carried out separate investigations into the diffusion of specific fluorophores in pyrrolidinium and imidazolium-based ILs using FCS.[121-122] Their analyses of FCS data unveiled a bimodal diffusion pattern for the fluorophores in RTILs. This observation suggests the presence of two distinct diffusion rates for the fluorophores, indicating the presence of those fluorophores in a heterogeneous medium. An especially noteworthy discovery in the application of FCS to RTILs was made by Kim and his research team.[123] Expanding the work performed by Samanta and coworkers, who observed characteristic visible fluorescence in imidazolium-based ILs and ascribed it to the presence of aggregated

structures, Kim and colleagues have substantiated this assertion through the utilization of FCS techniques. In summary, all these findings underscore the relevance of the FCS techniques. Keeping all these facts in mind, this thesis also employs FCS techniques for understanding the structural organization and related solute dynamics in ILs

1.5. Motivation and objective of the thesis.

The focus of the research in the field of ILs is shifting beyond the mere measurement of physical properties and identification of trends related to specific structural features. Instead, scientists are now equally dedicated to exploring the nano-structural organization and associated complex behaviour of ILs. This represents a more comprehensive and detailed approach of studying these intriguing substances. This in-depth exploration is crucial for understanding how these molecular landscapes influence IL properties, particularly when fine-tuning ILs for specific applications. Despite these substantial advancements, there are particular challenges that persistently hinder the achievement of a thorough understanding and implication of this IL system. These challenges, in turn, impede the optimal utilization of these systems in their intended field. Some of the key issues that served as the motivation to carry out this thesis work are outlined below.

1. While mono-cationic ionic liquids (MILs) are being studied extensively, dicationic ionic liquids (DILs) have not been explored to their maximum potential. In this context, it is noteworthy that DILs are a subgroup of this broad category of ILs that contains two charge canters. Among them, one consisting of two cationic heads separated by an alkyl linker chain is the well-studied class of DILs.[36] Although their intriguing macroscopic characteristics, such as high viscosity, low vapour pressure, and exceptional thermal stability, have driven their widespread use in numerous scientific disciplines, the kinship between their microscopic structure and macroscopic physical attribute is not properly understood. Therefore,

exploring the DILs on a microscopic scale, i.e., their structural organization and their dynamic aspects can offer an opportunity to expand the understanding of ILs and discover novel applications for these compounds. Furthermore, we would also like to note here that the majority of studies on the above aspects have been carried out by taking imidazolium-based DILs. However, other groups of DILs, like pyrrolidinium-based DIL and morpholinium-based DILs, have not been explored yet. So, understanding the structural organization and microscopic properties of different cation-head-based DIL can help us realize the full potential of certain DIL systems for specific applications. Taking this fact in mind, the current thesis tries to investigate the difference in the behaviour of imidazolium and pyrrolidinium-based DIL. The focal point of this investigation lies in elucidating how the structural difference between imidazolium and pyrrolidinium cation i.e. planar and non-planar characteristics associated with each of them, is manifested in their overall structural arrangements and dynamic behaviour.

2. Owing to the superior physicochemical properties of DIL, they are being used across many fields, such as lubricants, high-temperature battery applications, etc.[124] However, the exploration of the implications originating from their microscopic structural attribute, i.e., how they behave in the presence of some of the critical analytes such as Lithium salt, molecular solvents like Ethylene glycol, and biological molecules like DNA, still presents an unexplored frontier.

   For example, due to the presence of polar and non-polar domain in the IL medium, they are being used to solubilize complex molecules like cellulose.[125-126] However, high viscosity of IL sometimes hinders their ability to properly interact with solute molecules. In solution to this issue, some cosolvent like methanol, acetonitrile and even water can be added in a trace amount to reduce the viscosity of the medium.[127-

[128] However, this addition of co-solvent may also affect the domain structure within the ILs, again hampering the solubility of the complex molecules. Therefore, it is also impetrative to understand the microscopic behaviour of ILs in the presence of molecular solvent. To understand this aspect, the current thesis also tries to investigate the structural organisation and diffusion dynamics of an imidazolium-based DIL and a MIL in the presence of an organic solvent, ethylene glycol. Similarly, owing to their wide thermal and electrochemical windows, low vapour pressure, low flammability, and high ionic conductivity ILs have gained substantial attraction as the substitution of volatile organic solvents in the pursuit of developing advanced electrochemical energy storage devices. These attributes have positioned ILs as promising candidates for designing safe and leakage-free electrolytes. This fact can also be visualized from scheme 1.6. In this context, the conventional approach of electrolytic selection often prioritizes to examine the bulk properties of ILs such as low viscosity, high electrochemical, and thermal stability although an optimal balance of these properties within a single IL system is a complex task. However, as IL represents a heterogeneous medium the simplistic reliance on only these macroscopic characteristics for selection of suitable electrolyte, might overlook its potential advantages from other critical aspects of ILs. For example, while ILs having longer alkyl chain often represents high viscous medium, at the same time they can exhibit more free-space within their molecular arrangement.[129-130] This intricate molecular arrangement at the microscopic level can enhance the conductivity of the medium. So, overlooking the potential of a highly viscous IL system may lead to loss of the benefits arising from this intricate microscopic feature. Overall, it can be said that, along with macroscopic properties, evaluating microscopic perspective of an IL system is essential for getting

optimized electrochemical performance. Furthermore, addition of salt, generally alkali metal salts have been shown to improve the electrolytic performance of an IL system. While this addition may help to achieve the desired conductivity, they also modify the inter-constituent interactions in the system and thus influence the microscopic structure and dynamics in ILs. In this regard, the robustness of the molecular arrangement within IL may be a demand to withstand the influences of such additives. Therefore, to understand the above aspects, an in-depth exploration of microscopic properties is indispensable for unlocking the full potential of ILs in enhancing the efficiency, speed, and overall performance of energy storage systems, such as batteries and other electrochemical devices. Keeping above issues in mind, the present thesis has made an attempt to investigate the microscopic structural organisation and lithium salt diffusion dynamics in some highly viscous pyrrolidinium-based ILs. The said chapter mainly focuses on understanding how differently a pyrrolidinium-based MIL and DIL consisting of similar alkyl chain behave in the presence of Lithium-salt.

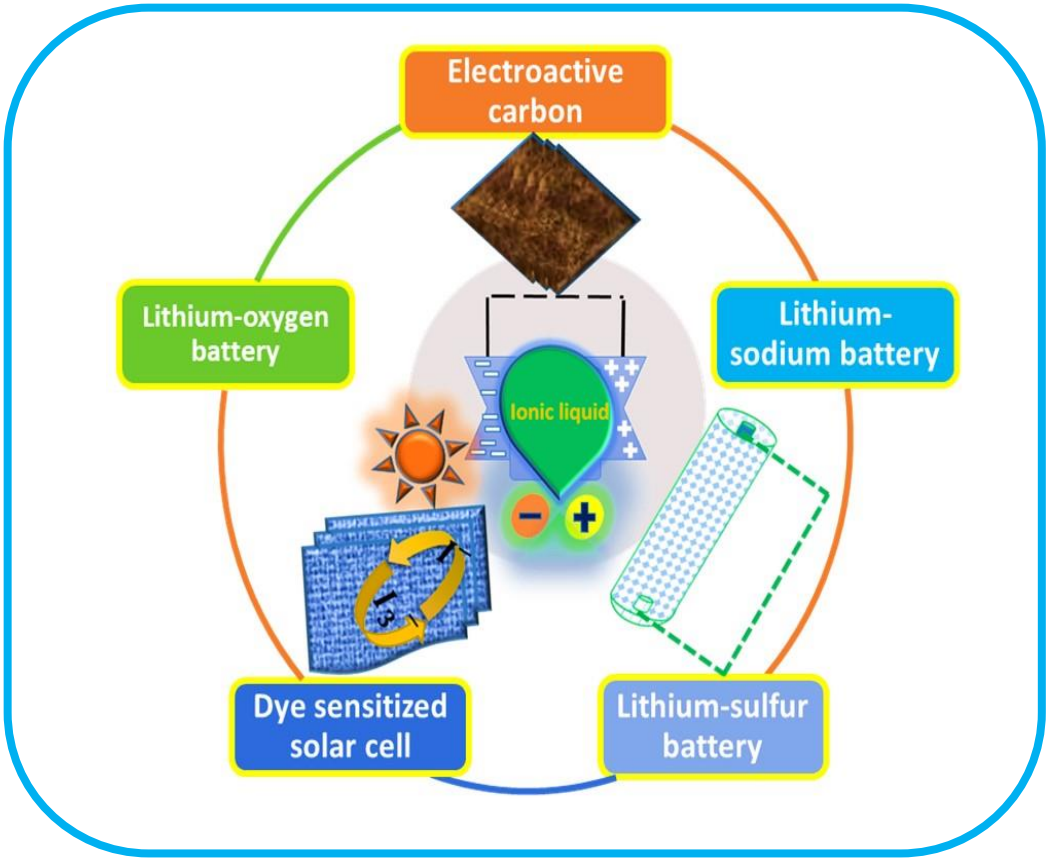

Scheme 1.6. This scheme represents the implication of ILs in various electrochemical applications.

3. In a similar manner ILs have profound implications in various biological applications as presented in scheme 1.7.[19] However, to fully leverage the potential of ILs in biological contexts, a thorough understanding of their microscopic structural feature in presence of target biomolecule is also essential. For example, the mode and the extent of interaction such as electrostatic, hydrophobic and Vander wall interaction of ILs with a biomolecule is a critical factor which may be influenced by their microscopic structure.[131] Keeping this fact in mind, the current thesis tries to examine the implications of the microscopic features of some pyrrolidinium-based MIL and DIL in governing the structure and stability of ct-DNA in aqueous solution of these ILs.

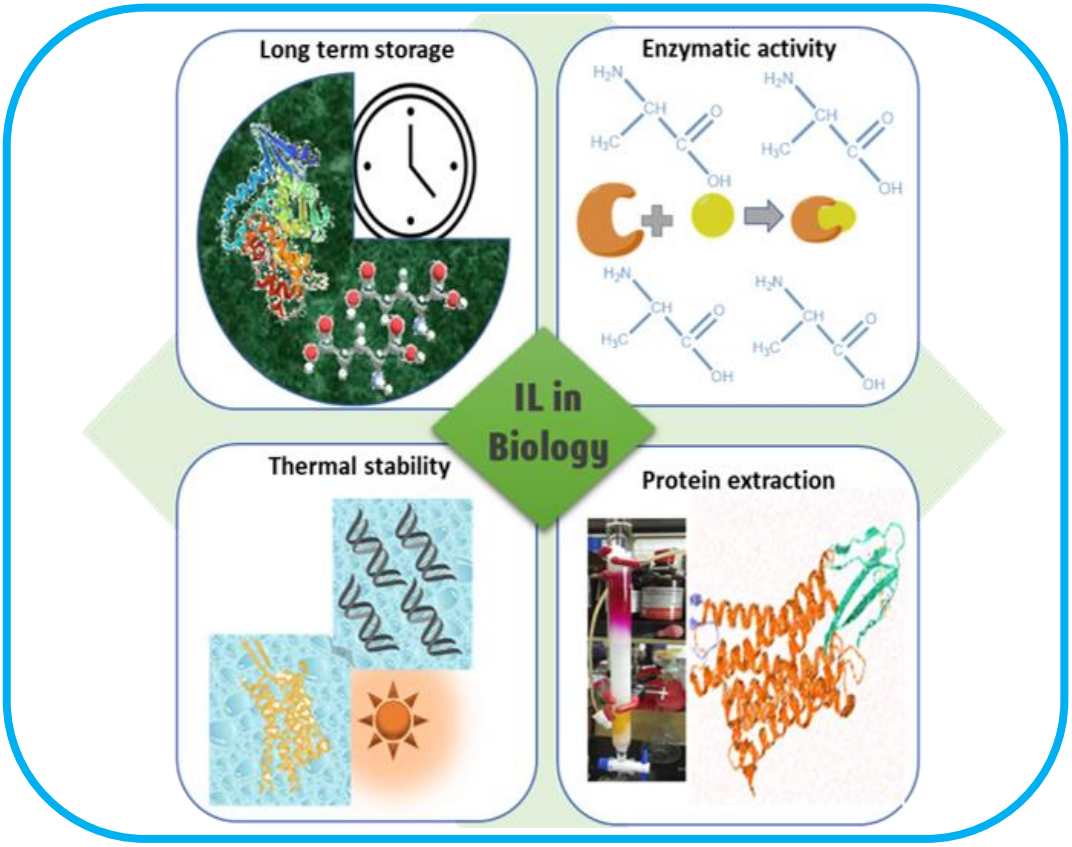

Scheme 1.7. This scheme represents the implication of ILs in various biological applications.

4. While RTILs are being explored, ILs that crystalize at room temperature have not been explored properly. These ILs are often termed as organic ionic crystals (OICs).[132-133] Similar to traditional ionic compounds, OICs consist of positively charged cations and negatively charged anions. However, OICs are composed of bulky organic cations and anions that form a stable crystal lattice at room temperature. OICs generally exhibit good thermal stability due to their crystalline structure. This stability is essential for applications in high-temperature environments, such as in solid-state battery and dye-sensitized solar cell. More over OICs are also devoid of leakage problem with RTIL-based electrolyte. Similar to ILs, OICs can also be tailored to attain specific properties, rendering them highly versatile for a multitude of electrochemical applications. While numerous studies focusing on the structure-properties relationship of OICs have cantered on

monocation-based OICs, there exists a notable gap in the investigation of their dicationic counterparts. Understanding the structure-properties dynamics of dication-based OICs is crucial for a comprehensive comprehension of their electrochemical behavior and potential applications. Therefore, the current thesis also tries to understand the structure and properties of some pyrroldinium-based geminal OICs and evaluating the suitability of these OICs as an electrolyte composite in all-solid-state dye-sensitized solar cells.

Keeping above issues in mind, the current thesis has been designed into the following chapters.

1.6. Organisation of the thesis.

The present thesis has been divided into six chapters. Chapter 1 provides a broad introduction to ILs from a historical perspective to the discovery and development of ILs. Subsequently, a brief discussion on the structure, physicochemical properties, and applications of various classes of ILs has been provided. Moreover, this chapter also provides a thorough discussion of the nano-structural organization of ILs and the intricate solvent dynamics by highlighting some recent literature reports. Moreover, photophysical processes such as excitation wavelength-dependent emission behaviour and rotational relaxation dynamics of some suitable solutes in ILs and translational diffusion dynamics of ILs, etc., which are often used to demonstrate the existence of nano-structural organization in ILs have also been described in detail.

In Chapter 2, fundamental principles of various experimental techniques which are employed for various measurements both at single molecular and ensemble-average levels in the current thesis work. Different spectroscopic techniques, such as absorption spectroscopy, steady-state and time-resolved fluorescence emission spectroscopy, and more specifically, the fundamental working principle of time-correlated single photon counting (TCSPC) and fluorescence

correlation spectroscopic (FC) technique, have been discussed in detail. Additionally, measurements of the self-diffusion coefficient through pulsed-field-gradient NMR (PFG-NMR) techniques have also been provided. Apart from this, various methodologies that are commonly used to obtain the fluorescence decay parameters, rotational relaxation parameters, and their analysis by employing hydrodynamic and quasi-hydrodynamic theories have been described.

Chapter 3 aims to understand the difference in the behaviour of imidazolium and pyrrolidinium-based dicationic ionic liquids (DILs) in terms of intermolecular interactions, microscopic structure, and dynamics by employing TRFA and NMR spectroscopic techniques. For this study two DILs, one imidazolium-based and another pyrrolidinium-based have been taken. To draw a comparison between MILs and DILs, MILs consisting of alkyl chain, close to the length of the alkyl spacer chain in DILs as well as consisting of alkyl chain, close to the half of the length of the alkyl spacer of DILs have been investigated in this study.

In Chapter 4a, the behaviour of imidazolium-based DILs in the presence of a molecular solvent, ethylene glycol (EG), is studied by employing TRFA and NMR spectroscopic techniques. To understand the structural organization and intermolecular interaction that prevails in the DIL+EG mixture in a better manner, a MIL consisting of a similar alkyl chain has also been employed. This study has provided an idea about the unique structural feature and response of DIL over a structurally similar MIL as a solvent system.

In Chapter 4b, the behaviour of a pyrrolidinium-based DIL in the presence lithium salt ($LiNTf_2$) has been studied by employing TRFA, FCS and NMR spectroscopic techniques as well as MD simulation studies. To better understand the structural organization and intermolecular interaction that prevails in Li^+ ion and DIL mixture, an MIL consisting of a similar alkyl chain has also been employed. The result of this study has shown that pyrrolidinium-based DIL, due

to its different structural organisation than MIL, can be used as an effective electrolytic media for lithium-ion conduction in energy-related applications.

In chapter 5a, the potential of a pyrrolidinium-based DIL in stabilizing ct-DNA has been investigated by following DNA-DIL interaction. Additionally, in order to understand the fundamental aspects of DNA-DIL interaction in a comprehensive manner, studies are also done by employing structurally similar MILs. The investigations have been carried out both at ensemble-average and single molecular levels by using various spectroscopic techniques. The molecular docking study has also been performed to throw more light into our experimental observations. This study has demonstrated that DILs can effectively be used as a better storage media for ct-DNA as compared to MILs. Investigations have also shown that the extra electrostatic interaction between the cationic head group of DIL as well as the structural feature of DIL, are primarily responsible for providing better stabilization to ct-DNA and thereby retaining its native structure in an aqueous medium.

Chapter 5b, tries to investigate and understand the structure and stability of ct-DNA in a series of imidazolium-based ILs comprising different anions spanning the Hofmeister series. The binding characteristics and thermodynamics of IL-DNA interaction have been investigated using various spectroscopic techniques such as UV-Vis absorption spectroscopy, steady-state, and time-resolved fluorescence spectroscopy. Furthermore, the conformational stability of ct-DNA is evaluated using circular dichroism (CD) spectroscopy. MD simulation study has also been employed to shed more light on the experimental observations. Quite interestingly, the findings of this study have underscored the significance of consideration of both the cation and anion of ILs in understanding the overall DNA-IL interaction event.

Chapter 6 investigates the structural features, thermal properties, and phase behaviours of a series of pyrrolidinium-based OICs. Additionally, their suitability as an efficient electrolyte composite (OIC: I2: TBAI) for all-solid-state dye-sensitized solar cells (DSSC) has been

assessed by employing various electro-analytical techniques. The finding of this study has demonstrated that the length of the alkyl bridge chain plays a significant role in determining the structural organization, morphology, and, eventually, the ionic conductivity of OICs.

REFERENCES

1. Wilkes, J. S., A Short History of Ionic Liquids—from Molten Salts to Neoteric Solvents. *Green Chemistry* **2002**, *4*, 73-80.
2. Seddon, K. R.; Stark, A.; Torres, M.-J., Influence of Chloride, Water, and Organic Solvents on the Physical Properties of Ionic Liquids. *Pure and applied chemistry* **2000**, *72*, 2275-2287.
3. Wasserscheid, P.; Welton, T., *Ionic Liquids in Synthesis*; Wiley Online Library, 2008; Vol. 1.
4. Wasserscheid, P.; Keim, W., Ionic Liquids—New "Solutions" for Transition Metal Catalysis. *Angewandte Chemie International Edition* **2000**, *39*, 3772-3789.
5. Visser, A. E.; Swatloski, R. P.; Reichert, W. M.; Mayton, R.; Sheff, S.; Wierzbicki, A.; Davis, J. J. H.; Rogers, R. D., Task-Specific Ionic Liquids for the Extraction of Metal Ions from Aqueous Solutions. *Chemical Communications* **2001**, 135-136.
6. Xue, H.; Verma, R.; Jean'ne, M. S., Review of Ionic Liquids with Fluorine-Containing Anions. *Journal of Fluorine Chemistry* **2006**, *127*, 159-176.
7. Umebayashi, Y.; Chung, W.-L.; Mitsugi, T.; Fukuda, S.; Takeuchi, M.; Fujii, K.; Takamuku, T.; Kanzaki, R.; Ishiguro, S.-i., Liquid Structure and the Ion-Ion Interactions of Ethylammonium Nitrate Ionic Liquid Studied by Large Angle X-Ray Scattering and Molecular Dynamics Simulations. *Journal of Computer Chemistry, Japan* **2008**, *7*, 125-134.
8. Tokuda, H.; Ishii, K.; Susan, M. A. B. H.; Tsuzuki, S.; Hayamizu, K.; Watanabe, M., Physicochemical Properties and Structures of Room-Temperature Ionic Liquids. 3. Variation of Cationic Structures. *The Journal of Physical Chemistry B* **2006**, *110*, 2833-2839.
9. Marsh, K. N.; Deev, A.; Wu, A. C. T.; Tran, E.; Klamt, A., Room Temperature Ionic Liquids as Replacements for Conventional Solvents – a Review. *Korean Journal of Chemical Engineering* **2002**, *19*, 357-362.
10. Pandey, S., Analytical Applications of Room-Temperature Ionic Liquids: A Review of Recent Efforts. *Analytica chimica acta* **2006**, *556*, 38-45.
11. Farzam, S.; Feyzi, F., Experimental Investigation and Thermodynamic Modeling of Equilibrium Extraction of Gold (III) from Hydrochloric Acid in 1-Butyl-3-Methylimidazolium Hexafluorophosphate. *Fluid Phase Equilibria* **2021**, *527*, 112839.
12. Damas, G. B.; Dias, A. B. A.; Costa, L. T., A Quantum Chemistry Study for Ionic Liquids Applied to Gas Capture and Separation. *The Journal of Physical Chemistry B* **2014**, *118*, 9046-9064.
13. Bara, J. E.; Camper, D. E.; Gin, D. L.; Noble, R. D., Room-Temperature Ionic Liquids and Composite Materials: Platform Technologies for CO_2 Capture. *Accounts of Chemical Research* **2010**, *43*, 152-159.
14. Zhang, X.; Zhang, X.; Dong, H.; Zhao, Z.; Zhang, S.; Huang, Y., Carbon Capture with Ionic Liquids: Overview and Progress. *Energy & Environmental Science* **2012**, *5*, 6668-6681.
15. Zheng, J.; Gu, M.; Chen, H.; Meduri, P.; Engelhard, M. H.; Zhang, J.-G.; Liu, J.; Xiao, J., Ionic Liquid-Enhanced Solid State Electrolyte Interface (SEI) for Lithium–Sulfur Batteries. *Journal of Materials Chemistry A* **2013**, *1*, 8464-8470.

16. Ma, F.; Zhang, Z.; Yan, W.; Ma, X.; Sun, D.; Jin, Y.; Chen, X.; He, K., Solid Polymer Electrolyte Based on Polymerized Ionic Liquid for High Performance All-Solid-State Lithium-Ion Batteries. *ACS Sustainable Chemistry & Engineering* **2019**, *7*, 4675-4683.
17. Wang, A.; Liu, X.; Wang, S.; Chen, J.; Xu, H.; Xing, Q.; Zhang, L., Polymeric Ionic Liquid Enhanced All-Solid-State Electrolyte Membrane for High-Performance Lithium-Ion Batteries. *Electrochimica Acta* **2018**, *276*, 184-193.
18. Zhuang, W.; Hachem, K.; Bokov, D.; Javed Ansari, M.; Taghvaie Nakhjiri, A., Ionic Liquids in Pharmaceutical Industry: A Systematic Review on Applications and Future Perspectives. *Journal of Molecular Liquids* **2022**, *349*, 118145.
19. Egorova, K. S.; Gordeev, E. G.; Ananikov, V. P., Biological Activity of Ionic Liquids and Their Application in Pharmaceutics and Medicine. *Chemical Reviews* **2017**, *117*, 7132-7189.
20. Shukla, S. K.; Mikkola, J.-P., Use of Ionic Liquids in Protein and DNA Chemistry. *Frontiers in Chemistry* **2020**, *8*.
21. Atkin, R.; Warr, G. G., The Smallest Amphiphiles: Nanostructure in Protic Room-Temperature Ionic Liquids with Short Alkyl Groups. *Journal of Physical Chemistry B* **2008**, *112*, 4164-4166.
22. Hayes, R.; Imberti, S.; Warr, G. G.; Atkin, R., Effect of Cation Alkyl Chain Length and Anion Type on Protic Ionic Liquid Nanostructure. *The Journal of Physical Chemistry C* **2014**, *118*, 13998-14008.
23. Greaves, T. L.; Kennedy, D. F.; Kirby, N.; Drummond, C. J., Nanostructure Changes in Protic Ionic Liquids (Pils) through Adding Solutes and Mixing Pils. *Physical Chemistry Chemical Physics* **2011**, *13*, 13501-13509.
24. Wang, Y.-L.; Li, B.; Sarman, S.; Mocci, F.; Lu, Z.-Y.; Yuan, J.; Laaksonen, A.; Fayer, M. D., Microstructural and Dynamical Heterogeneities in Ionic Liquids. *Chemical reviews* **2020**, *120*, 5798-5877.
25. Silva, W.; Zanatta, M.; Ferreira, A. S.; Corvo, M. C.; Cabrita, E. J., Revisiting Ionic Liquid Structure-Property Relationship: A Critical Analysis. *International Journal of Molecular Sciences* **2020**, *21*, 7745.
26. Trohalaki, S.; Pachter, R.; Drake, G. W.; Hawkins, T., Quantitative Structure−Property Relationships for Melting Points and Densities of Ionic Liquids. *Energy & Fuels* **2005**, *19*, 279-284.
27. Walden, P., Molecular Weights and Electrical Conductivity of Several Fused Salts. *Bull. Acad. Imper. Sci. (St. Petersburg)* **1914**, *1800*.
28. Hurley, F. H.; Wier, T. P., Electrodeposition of Metals from Fused Quaternary Ammonium Salts. *Journal of The Electrochemical Society* **1951**, *98*, 203.
29. Wilkes, J. S.; Zaworotko, M. J., Air and Water Stable 1-Ethyl-3-Methylimidazolium Based Ionic Liquids. *Journal of the Chemical Society, Chemical Communications* **1992**, 965-967.
30. J. Golding, J.; R. MacFarlane, D.; Spiccia, L.; J. Golding, J.; Forsyth, M.; W. Skelton, B.; H. White, A., Weak Intermolecular Interactions in Sulfonamide Salts: Structure of 1-Ethyl-2-Methyl-3-Benzyl Imidazolium Bis[(Trifluoromethyl)Sulfonyl]Amide. *Chemical Communications* **1998**, 1593-1594.
31. Vekariya, R. L., A Review of Ionic Liquids: Applications Towards Catalytic Organic Transformations. *Journal of Molecular Liquids* **2017**, *227*, 44-60.
32. Baker, G. A.; Baker, S. N.; Pandey, S.; Bright, F. V., An Analytical View of Ionic Liquids. *Analyst* **2005**, *130*, 800-808.
33. Newington, I.; Perez-Arlandis, J. M.; Welton, T., Ionic Liquids as Designer Solvents for Nucleophilic Aromatic Substitutions. *Organic Letters* **2007**, *9*, 5247-5250.

34. Wu, C.; De Visscher, A.; Gates, I. D., Comparison of Electronic and Physicochemical Properties between Imidazolium-Based and Pyridinium-Based Ionic Liquids. *The Journal of Physical Chemistry B* **2018**, *122*, 6771-6780.
35. Tang, S.; Baker, G. A.; Zhao, H., Ether- and Alcohol-Functionalized Task-Specific Ionic Liquids: Attractive Properties and Applications. *Chemical Society Reviews* **2012**, *41*, 4030-4066.
36. Anderson, J. L.; Ding, R.; Ellern, A.; Armstrong, D. W., Structure and Properties of High Stability Geminal Dicationic Ionic Liquids. *Journal of the American Chemical Society* **2005**, *127*, 593-604.
37. Fang, D.; Yang, J.; Jiao, C., Dicationic Ionic Liquids as Environmentally Benign Catalysts for Biodiesel Synthesis. *ACS Catalysis* **2011**, *1*, 42-47.
38. Ueno, K.; Tokuda, H.; Watanabe, M., Ionicity in Ionic Liquids: Correlation with Ionic Structure and Physicochemical Properties. *Physical Chemistry Chemical Physics* **2010**, *12*, 1649-1658.
39. Tokuda, H.; Tsuzuki, S.; Susan, M. A. B. H.; Hayamizu, K.; Watanabe, M., How Ionic Are Room-Temperature Ionic Liquids? An Indicator of the Physicochemical Properties. *The Journal of Physical Chemistry B* **2006**, *110*, 19593-19600.
40. Fabre, E.; Murshed, S. M. S., A Review of the Thermophysical Properties and Potential of Ionic Liquids for Thermal Applications. *Journal of Materials Chemistry A* **2021**, *9*, 15861-15879.
41. Bocharova, V., et al., Influence of Chain Rigidity and Dielectric Constant on the Glass Transition Temperature in Polymerized Ionic Liquids. *The Journal of Physical Chemistry B* **2017**, *121*, 11511-11519.
42. Ghandi, K., A Review of Ionic Liquids, Their Limits and Applications. *Green and Sustainable Chemistry* **2014**, *04,*10.
43. Okoturo, O. O.; VanderNoot, T. J., Temperature Dependence of Viscosity for Room Temperature Ionic Liquids. *Journal of Electroanalytical Chemistry* **2004**, *568*, 167-181.
44. Zhu, A.; Wang, J.; Han, L.; Fan, M., Measurements and Correlation of Viscosities and Conductivities for the Mixtures of Imidazolium Ionic Liquids with Molecular Solutes. *Chemical Engineering Journal* **2009**, *147*, 27-35.
45. Boruń, A., Conductance and Ionic Association of Selected Imidazolium Ionic Liquids in Various Solvents: A Review. *Journal of Molecular Liquids* **2019**, *276*, 214-224.
46. Litaiem, Y.; Dhahbi, M., Measurements and Correlations of Viscosity, Conductivity and Density of an Hydrophobic Ionic Liquid (Aliquat 336) Mixtures with a Non-Associated Dipolar Aprotic Solvent (DMC). *Journal of Molecular Liquids* **2012**, *169*, 54-62.
47. Zheng, W.; Mohammed, A.; Hines, L. G., Jr.; Xiao, D.; Martinez, O. J.; Bartsch, R. A.; Simon, S. L.; Russina, O.; Triolo, A.; Quitevis, E. L., Effect of Cation Symmetry on the Morphology and Physicochemical Properties of Imidazolium Ionic Liquids. *The Journal of Physical Chemistry B* **2011**, *115*, 6572-6584.
48. Hasse, B.; Lehmann, J.; Assenbaum, D.; Wasserscheid, P.; Leipertz, A.; Fröba, A. P., Viscosity, Interfacial Tension, Density, and Refractive Index of Ionic Liquids [Emim][$MeSO_3$], [Emim][MeOHPO2], [Emim][$OCSO_4$], and [BBim][NTf_2] in Dependence on Temperature at Atmospheric Pressure. *Journal of Chemical & Engineering Data* **2009**, *54*, 2576-2583.
49. Fröba, A. P.; Kremer, H.; Leipertz, A., Density, Refractive Index, Interfacial Tension, and Viscosity of Ionic Liquids [Emim][$EtSO_4$], [Emim][NTf_2], [Emim][$N(CN)_2$], and [OMA][NTf2] in Dependence on Temperature at Atmospheric Pressure. *The Journal of Physical Chemistry B* **2008**, *112*, 12420-12430.
50. Liu, W.; Zhao, T.; Zhang, Y.; Wang, H.; Yu, M., The Physical Properties of Aqueous Solutions of the Ionic Liquid [Bmim][BF_4]. *Journal of Solution Chemistry* **2006**, *35*, 1337-1346.

51. Spange, S.; Lungwitz, R.; Schade, A., Correlation of Molecular Structure and Polarity of Ionic Liquids. *Journal of Molecular Liquids* **2014**, *192*, 137-143.
52. Hayes, R.; Warr, G. G.; Atkin, R., Structure and Nanostructure in Ionic Liquids. *Chemical Reviews* **2015**, *115*, 6357-6426.
53. Bodo, E.; Postorino, P.; Mangialardo, S.; Piacente, G.; Ramondo, F.; Bosi, F.; Ballirano, P.; Caminiti, R., Structure of the Molten Salt Methyl Ammonium Nitrate Explored by Experiments and Theory. *The Journal of Physical Chemistry B* **2011**, *115*, 13149-13161.
54. Atkin, R.; Warr, G. G., The Smallest Amphiphiles: Nanostructure in Protic Room-Temperature Ionic Liquids with Short Alkyl Groups. *The Journal of Physical Chemistry B* **2008**, *112*, 4164-4166.
55. Urahata, S. M.; Ribeiro, M. C. C., Unraveling Dynamical Heterogeneity in the Ionic Liquid 1-Butyl-3-Methylimidazolium Chloride. *The Journal of Physical Chemistry Letters* **2010**, *1*, 1738-1742.
56. Ogbodo, R., et al., Structural Origins of Viscosity in Imidazolium and Pyrrolidinium Ionic Liquids Coupled with the Ntf2– Anion. *The Journal of Physical Chemistry B* **2023**, *127*, 6342-6353.
57. MacFarlane, D. R.; Forsyth, S. A.; Golding, J.; Deacon, G. B., Ionic Liquids Based on Imidazolium, Ammonium and Pyrrolidinium Salts of the Dicyanamide Anion. *Green Chemistry* **2002**, *4*, 444-448.
58. Men, S.; Lovelock, K. R. J.; Licence, P., X-Ray Photoelectron Spectroscopy of Pyrrolidinium-Based Ionic Liquids: Cation–Anion Interactions and a Comparison to Imidazolium-Based Analogues. *Physical Chemistry Chemical Physics* **2011**, *13*, 15244-15255.
59. Kakinuma, S.; Shirota, H., Femtosecond Raman-Induced Kerr Effect Study of Temperature-Dependent Intermolecular Dynamics in Molten Bis(Trifluoromethylsulfonyl)Amide Salts: Effects of Cation Species. *The Journal of Physical Chemistry B* **2018**, *122*, 6033-6047.
60. Xue, L.; Tamas, G.; Matthews, R. P.; Stone, A. J.; Hunt, P. A.; Quitevis, E. L.; Lynden-Bell, R. M., An Ohd-Rikes and Simulation Study Comparing a Benzylmethylimidazolium Ionic Liquid with an Equimolar Mixture of Dimethylimidazolium and Benzene. *Physical Chemistry Chemical Physics* **2015**, *17*, 9973-9983.
61. Shirota, H.; Matsuzaki, H.; Ramati, S.; Wishart, J. F., Effects of Aromaticity in Cations and Their Functional Groups on the Low-Frequency Spectra and Physical Properties of Ionic Liquids. *The Journal of Physical Chemistry B* **2015**, *119*, 9173-9187.
62. Yamada, S. A.; Bailey, H. E.; Tamimi, A.; Li, C.; Fayer, M. D., Dynamics in a Room-Temperature Ionic Liquid from the Cation Perspective: 2d Ir Vibrational Echo Spectroscopy. *Journal of the American Chemical Society* **2017**, *139*, 2408-2420.
63. Serra, P. B. P.; Ribeiro, F. M. S.; Rocha, M. A. A.; Fulem, M.; Růžička, K.; Santos, L. M. N. B. F., Phase Behavior and Heat Capacities of the 1-Benzyl-3-Methylimidazolium Ionic Liquids. *The Journal of Chemical Thermodynamics* **2016**, *100*, 124-130.
64. Fakhraee, M.; Zandkarimi, B.; Salari, H.; Gholami, M. R., Hydroxyl-Functionalized 1-(2-Hydroxyethyl)-3-Methyl Imidazolium Ionic Liquids: Thermodynamic and Structural Properties Using Molecular Dynamics Simulations and Ab Initio Calculations. *The Journal of Physical Chemistry B* **2014**, *118*, 14410-14428.
65. Fakhraee, M.; Gholami, M. R., Effect of Anion and Alkyl Side Chain on Structural and Dynamic Features of Ester Functionalized Ionic Liquids: Confirming Nanoscale Organization. *The Journal of Physical Chemistry B* **2016**, *120*, 11539-11555.
66. Bailey, H. E.; Wang, Y.-L.; Fayer, M. D., Impact of Hydrogen Bonding on the Dynamics and Structure of Protic Ionic Liquid/Water Binary Mixtures. *The Journal of Physical Chemistry B* **2017**, *121*, 8564-8576.

67. Gannon, T. J.; Law, G.; Watson, P. R.; Carmichael, A. J.; Seddon, K. R., First Observation of Molecular Composition and Orientation at the Surface of a Room-Temperature Ionic Liquid. *Langmuir* **1999**, *15*, 8429-8434.
68. Knorr, A.; Fumino, K.; Bonsa, A.-M.; Ludwig, R., Spectroscopic Evidence of 'Jumping and Pecking' of Cholinium and H-Bond Enhanced Cation–Cation Interaction in Ionic Liquids. *Physical Chemistry Chemical Physics* **2015**, *17*, 30978-30982.
69. Mbondo Tsamba, B. E.; Sarraute, S.; Traïkia, M.; Husson, P., Transport Properties and Ionic Association in Pure Imidazolium-Based Ionic Liquids as a Function of Temperature. *Journal of Chemical & Engineering Data* **2014**, *59*, 1747-1754.
70. Borodin, O.; Gorecki, W.; Smith, G. D.; Armand, M., Molecular Dynamics Simulation and Pulsed-Field Gradient Nmr Studies of Bis(Fluorosulfonyl)Imide (FSI) and Bis[(Trifluoromethyl)Sulfonyl]Imide (TFSI)-Based Ionic Liquids. *The Journal of Physical Chemistry B* **2010**, *114*, 6786-6798.
71. Shin, J. Y.; Yamada, S. A.; Fayer, M. D., Influence of Water on Carbon Dioxide and Room Temperature Ionic Liquid Dynamics: Supported Ionic Liquid Membrane Vs the Bulk Liquid. *The Journal of Physical Chemistry B* **2018**, *122*, 2389-2395.
72. Yan, C.; Thomaz, J. E.; Wang, Y.-L.; Nishida, J.; Yuan, R.; Breen, J. P.; Fayer, M. D., Ultrafast to Ultraslow Dynamics of a Langmuir Monolayer at the Air/Water Interface Observed with Reflection Enhanced 2d Ir Spectroscopy. *Journal of the American Chemical Society* **2017**, *139*, 16518-16527.
73. Santos, C. S.; Baldelli, S., Alkyl Chain Interaction at the Surface of Room Temperature Ionic Liquids: Systematic Variation of Alkyl Chain Length (R = C1−C4, C8) in Both Cation and Anion of [Rmim][R−OSO_3] by Sum Frequency Generation and Surface Tension. *The Journal of Physical Chemistry B* **2009**, *113*, 923-933.
74. Baldelli, S., Interfacial Structure of Room-Temperature Ionic Liquids at the Solid–Liquid Interface as Probed by Sum Frequency Generation Spectroscopy. *The Journal of Physical Chemistry Letters* **2013**, *4*, 244-252.
75. Humphreys, E. K.; Allan, P. K.; Welbourn, R. J. L.; Youngs, T. G. A.; Soper, A. K.; Grey, C. P.; Clarke, S. M., A Neutron Diffraction Study of the Electrochemical Double Layer Capacitor Electrolyte Tetrapropylammonium Bromide in Acetonitrile. *The Journal of Physical Chemistry B* **2015**, *119*, 15320-15333.
76. Olschewski, M.; Gustus, R.; Höfft, O.; Lahiri, A.; Endres, F., Monochromatic X-Ray Photoelectron Spectroscopy Study of Three Different Ionic Liquids in Interaction with Lithium-Decorated Copper Surfaces. *The Journal of Physical Chemistry C* **2017**, *121*, 2675-2682.
77. Dias, N.; Shimizu, K.; Morgado, P.; Filipe, E. J. M.; Canongia Lopes, J. N.; Vaca Chávez, F., Charge Templates in Aromatic Plus Ionic Liquid Systems Revisited: Nmr Experiments and Molecular Dynamics Simulations. *The Journal of Physical Chemistry B* **2014**, *118*, 5772-5780.
78. Voss, J. M.; Marsh, B. M.; Zhou, J.; Garand, E., Interaction between Ionic Liquid Cation and Water: Infrared Predissociation Study of $[Bmim]^+ \cdot (H_2O)_n$ Clusters. *Physical Chemistry Chemical Physics* **2016**, *18*, 18905-18913.
79. Subba, N.; Sahu, P.; Das, N.; Sen, P., Rational Design, Preparation and Characterization of a Ternary Non-Ionic Room-Temperature Deep Eutectic Solvent Derived from Urea, Acetamide, and Sorbitol. *Journal of Chemical Sciences* **2021**, *133*, 25.
80. Hossain, S. S.; Samanta, A., Solute Rotation and Translation Dynamics in an Ionic Deep Eutectic Solvent Based on Choline Chloride. *The Journal of Physical Chemistry B* **2017**, *121*, 10556-10565.
81. Kaur, S.; Gupta, A.; Kashyap, H. K., Nanoscale Spatial Heterogeneity in Deep Eutectic Solvents. *The Journal of Physical Chemistry B* **2016**, *120*, 6712-6720.

82. Valeur, B.; Weber, G., Anisotropic Rotations in 1-Naphthylamine. Existence of a Red-Edge Transition Moment Normal to the Ring Plane. *Chemical Physics Letters* **1977**, *45*, 140-144.
83. Weber, G.; Shinitzky, M., Failure of Energy Transfer between Identical Aromatic Molecules on Excitation at the Long Wave Edge of the Absorption Spectrum. *Proceedings of the National Academy of Sciences* **1970**, *65*, 823-830.
84. Mandal, P. K.; Paul, A.; Samanta, A., Excitation Wavelength Dependent Fluorescence Behavior of the Room Temperature Ionic Liquids and Dissolved Dipolar Solutes. *Journal of Photochemistry and Photobiology A: Chemistry* **2006**, *182*, 113-120.
85. Mandal, P. K.; Sarkar, M.; Samanta, A., Excitation-Wavelength-Dependent Fluorescence Behavior of Some Dipolar Molecules in Room-Temperature Ionic Liquids. *The Journal of Physical Chemistry A* **2004**, *108*, 9048-9053.
86. Hu, Z.; Margulis, C. J., Heterogeneity in a Room-Temperature Ionic Liquid: Persistent Local Environments and the Red-Edge Effect. *Proceedings of the National Academy of Sciences* **2006**, *103*, 831-836.
87. Majhi, D.; Seth, S.; Sarkar, M., Differences in the Behavior of Dicationic and Monocationic Ionic Liquids as Revealed by Time Resolved-Fluorescence, Nmr and Fluorescence Correlation Spectroscopy. *Physical Chemistry Chemical Physics* **2018**, *20*, 7844-7856.
88. Mandal, P. K.; Sarkar, M.; Samanta, A., Excitation-Wavelength-Dependent Fluorescence Behavior of Some Dipolar Molecules in Room-Temperature Ionic Liquids. *Journal of Physical Chemistry A* **2004**, *108*, 9048-9053.
89. Dutt, G. B., Influence of Specific Interactions on the Rotational Dynamics of Charged and Neutral Solutes in Ionic Liquids Containing Tris(Pentafluoroethyl)Trifluorophosphate (Fap) Anion. *The Journal of Physical Chemistry B* **2010**, *114*, 8971-8977.
90. Gangamallaiah, V.; Dutt, G. B., Rotational Diffusion of Nonpolar and Ionic Solutes in 1-Alkyl-3-Methylimidazolium Bis(Trifluoromethylsulfonyl)Imides: Is Solute Rotation Always Influenced by the Length of the Alkyl Chain on the Imidazolium Cation? *The Journal of Physical Chemistry B* **2012**, *116*, 12819-12825.
91. Karve, L.; Dutt, G. B., Rotational Diffusion of Neutral and Charged Solutes in Ionic Liquids: Is Solute Reorientation Influenced by the Nature of the Cation? *The Journal of Physical Chemistry B* **2011**, *115*, 725-729.
92. Horng, M. L.; Gardecki, J. A.; Maroncelli, M., Rotational Dynamics of Coumarin 153: Time-Dependent Friction, Dielectric Friction, and Other Nonhydrodynamic Effects. *The Journal of Physical Chemistry A* **1997**, *101*, 1030-1047.
93. Fruchey, K.; Fayer, M. D., Dynamics in Organic Ionic Liquids in Distinct Regions Using Charged and Uncharged Orientational Relaxation Probes. *The Journal of Physical Chemistry B* **2010**, *114*, 2840-2845.
94. Gierer, A.; Wirtz, K., Molekulare Theorie Der Mikroreibung. *Zeitschrift für Naturforschung A* **1953**, *8*, 532-538.
95. Dote, J. L.; Kivelson, D.; Schwartz, R. N., A Molecular Quasi-Hydrodynamic Free-Space Model for Molecular Rotational Relaxation in Liquids. *The Journal of Physical Chemistry* **1981**, *85*, 2169-2180.
96. Sahu, P. K.; Das, S. K.; Sarkar, M., Toward Understanding Solute–Solvent Interaction in Room-Temperature Mono- and Dicationic Ionic Liquids: A Combined Fluorescence Spectroscopy and Mass Spectrometry Analysis. *The Journal of Physical Chemistry B* **2014**, *118*, 1907-1915.
97. Kundu, N.; Roy, A.; Dutta, R.; Sarkar, N., Translational and Rotational Diffusion of Two Differently Charged Solutes in Ethylammonium Nitrate–Methanol Mixture: Does the

Nanostructure of the Amphiphiles Influence the Motion of the Solute? *The Journal of Physical Chemistry B* **2016**, *120*, 5481-5490.
98. Bagchi, B.; Jana, B., Solvation Dynamics in Dipolar Liquids. *Chemical Society Reviews* **2010**, *39*, 1936-1954.
99. Jin, H.; Baker, G. A.; Arzhantsev, S.; Dong, J.; Maroncelli, M., Solvation and Rotational Dynamics of Coumarin 153 in Ionic Liquids: Comparisons to Conventional Solvents. *The Journal of Physical Chemistry B* **2007**, *111*, 7291-7302.
100. Jimenez, R.; Fleming, G. R.; Kumar, P. V.; Maroncelli, M., Femtosecond Solvation Dynamics of Water. *Nature* **1994**, *369*, 471-473.
101. Chowdhury, P. K.; Halder, M.; Sanders, L.; Calhoun, T.; Anderson, J. L.; Armstrong, D. W.; Song, X.; Petrich, J. W., Dynamic Solvation in Room-Temperature Ionic Liquids. *The Journal of Physical Chemistry B* **2004**, *108*, 10245-10255.
102. Arzhantsev, S.; Jin, H.; Baker, G. A.; Maroncelli, M., Measurements of the Complete Solvation Response in Ionic Liquids. *The Journal of Physical Chemistry B* **2007**, *111*, 4978-4989.
103. Ito, N.; Arzhantsev, S.; Heitz, M.; Maroncelli, M., Solvation Dynamics and Rotation of Coumarin 153 in Alkylphosphonium Ionic Liquids. *The Journal of Physical Chemistry B* **2004**, *108*, 5771-5777.
104. Ito, N.; Arzhantsev, S.; Maroncelli, M., The Probe Dependence of Solvation Dynamics and Rotation in the Ionic Liquid 1-Butyl-3-Methyl-Imidazolium Hexafluorophosphate. *Chemical Physics Letters* **2004**, *396*, 83-91.
105. Karmakar, R.; Samanta, A., Solvation Dynamics of Coumarin-153 in a Room-Temperature Ionic Liquid. *The Journal of Physical Chemistry A* **2002**, *106*, 4447-4452.
106. Karmakar, R.; Samanta, A., Dynamics of Solvation of the Fluorescent State of Some Electron Donor−Acceptor Molecules in Room Temperature Ionic Liquids, [Bmim][(CF_3SO_2)2N] and [Emim][(CF_3SO_2)2N]. *The Journal of Physical Chemistry A* **2003**, *107*, 7340-7346.
107. Kashyap, H. K.; Biswas, R., Dipolar Solvation Dynamics in Room Temperature Ionic Liquids: An Effective Medium Calculation Using Dielectric Relaxation Data. *The Journal of Physical Chemistry B* **2008**, *112*, 12431-12438.
108. Seth, D.; Sarkar, S.; Sarkar, N., Solvent and Rotational Relaxation of Coumarin 153 in a Protic Ionic Liquid Dimethylethanolammonium Formate. *The Journal of Physical Chemistry B* **2008**, *112*, 2629-2636.
109. Zhang, X.-X.; Liang, M.; Ernsting, N. P.; Maroncelli, M., Conductivity and Solvation Dynamics in Ionic Liquids. *The Journal of Physical Chemistry Letters* **2013**, *4*, 1205-1210.
110. Bhattacharyya, K., Nature of Biological Water: A Femtosecond Study. *Chemical Communications* **2008**, 2848-2857.
111. Castner, E. W., Jr.; Wishart, J. F.; Shirota, H., Intermolecular Dynamics, Interactions, and Solvation in Ionic Liquids. *Accounts of Chemical Research* **2007**, *40*, 1217-1227.
112. Kobrak, M. N.; Znamenskiy, V., Solvation Dynamics of Room-Temperature Ionic Liquids: Evidence for Collective Solvent Motion on Sub-Picosecond Timescales. *Chemical Physics Letters* **2004**, *395*, 127-132.
113. Kashyap, H. K.; Biswas, R., Solvation Dynamics of Dipolar Probes in Dipolar Room Temperature Ionic Liquids: Separation of Ion−Dipole and Dipole−Dipole Interaction Contributions. *The Journal of Physical Chemistry B* **2010**, *114*, 254-268.
114. Ghosh, S.; Chattoraj, S.; Chowdhury, R.; Bhattacharyya, K., Structure and Dynamics of Lysozyme in Dmso–Water Binary Mixture: Fluorescence Correlation Spectroscopy. *RSC Advances* **2014**, *4*, 14378-14384.
115. Sen Mojumdar, S.; Chowdhury, R.; Chattoraj, S.; Bhattacharyya, K., Role of Ionic Liquid on the Conformational Dynamics in the Native, Molten Globule, and Unfolded States

of Cytochrome C: A Fluorescence Correlation Spectroscopy Study. *The Journal of Physical Chemistry B* **2012**, *116*, 12189-12198.
116. Mendivelso-Pérez, D. L.; Farooq, M. Q.; Santra, K.; Anderson, J. L.; Petrich, J. W.; Smith, E. A., Diffusional Dynamics of Tetraalkylphosphonium Ionic Liquid Films Measured by Fluorescence Correlation Spectroscopy. *The Journal of Physical Chemistry B* **2019**, *123*, 4943-4949.
117. Kim, S. A.; Heinze, K. G.; Schwille, P., Fluorescence Correlation Spectroscopy in Living Cells. *Nature Methods* **2007**, *4*, 963-973.
118. Yu, L.; Lei, Y.; Ma, Y.; Liu, M.; Zheng, J.; Dan, D.; Gao, P., A Comprehensive Review of Fluorescence Correlation Spectroscopy. *Frontiers in Physics* **2021**, *9*.
119. Werner, J. H.; Baker, S. N.; Baker, G. A., Fluorescence Correlation Spectroscopic Studies of Diffusion within the Ionic Liquid 1-Butyl-3-Methylimidazolium Hexafluorophosphate. *Analyst* **2003**, *128*, 786-789.
120. Sasmal, D. K.; Mandal, A. K.; Mondal, T.; Bhattacharyya, K., Diffusion of Organic Dyes in Ionic Liquid and Giant Micron Sized Ionic Liquid Mixed Micelle: Fluorescence Correlation Spectroscopy. *The Journal of Physical Chemistry B* **2011**, *115*, 7781-7787.
121. Guo, J.; Baker, G. A.; Hillesheim, P. C.; Dai, S.; Shaw, R. W.; Mahurin, S. M., Fluorescence Correlation Spectroscopy Evidence for Structural Heterogeneity in Ionic Liquids. *Physical Chemistry Chemical Physics* **2011**, *13*, 12395-12398.
122. Patra, S.; Samanta, A., Microheterogeneity of Some Imidazolium Ionic Liquids as Revealed by Fluorescence Correlation Spectroscopy and Lifetime Studies. *The Journal of Physical Chemistry B* **2012**, *116*, 12275-12283.
123. Cha, S.; Shim, T.; Ouchi, Y.; Kim, D., Characteristics of Visible Fluorescence from Ionic Liquids. *The Journal of Physical Chemistry B* **2013**, *117*, 10818-10825.
124. Watanabe, M.; Thomas, M. L.; Zhang, S.; Ueno, K.; Yasuda, T.; Dokko, K., Application of Ionic Liquids to Energy Storage and Conversion Materials and Devices. *Chemical Reviews* **2017**, *117*, 7190-7239.
125. Swatloski, R. P.; Spear, S. K.; Holbrey, J. D.; Rogers, R. D., Dissolution of Cellose with Ionic Liquids. *Journal of the American Chemical Society* **2002**, *124*, 4974-4975.
126. Zhu, S.; Wu, Y.; Chen, Q.; Yu, Z.; Wang, C.; Jin, S.; Ding, Y.; Wu, G., Dissolution of Cellulose with Ionic Liquids and Its Application: A Mini-Review. *Green Chemistry* **2006**, *8*, 325-327.
127. Chaban, V. V.; Prezhdo, O. V., Ionic and Molecular Liquids: Working Together for Robust Engineering. *The Journal of Physical Chemistry Letters* **2013**, *4*, 1423-1431.
128. Verma, C.; Mishra, A.; Chauhan, S.; Verma, P.; Srivastava, V.; Quraishi, M. A.; Ebenso, E. E., Dissolution of Cellulose in Ionic Liquids and Their Mixed Cosolvents: A Review. *Sustainable Chemistry and Pharmacy* **2019**, *13*, 100162.
129. Tiago, G. A. O.; Matias, I. A. S.; Ribeiro, A. P. C.; Martins, L. M. D. R. S., Application of Ionic Liquids in Electrochemistry—Recent Advances. *Molecules* **2020**, *25*, 5812.
130. Beichel, W.; Yu, Y.; Dlubek, G.; Krause-Rehberg, R.; Pionteck, J.; Pfefferkorn, D.; Bulut, S.; Bejan, D.; Friedrich, C.; Krossing, I., Free Volume in Ionic Liquids: A Connection of Experimentally Accessible Observables from Pals and Pvt Experiments with the Molecular Structure from Xrd Data. *Physical Chemistry Chemical Physics* **2013**, *15*, 8821-8830.
131. Benedetto, A.; Ballone, P., Room Temperature Ionic Liquids Meet Biomolecules: A Microscopic View of Structure and Dynamics. *ACS Sustainable Chemistry & Engineering* **2016**, *4*, 392-412.
132. He, T.; Wang, Y. F.; Zeng, J. H., Stable, High-Efficiency Pyrrolidinium-Based Electrolyte for Solid-State Dye-Sensitized Solar Cells. *ACS Applied Materials & Interfaces* **2015**, *7*, 21381-21390.

133. Vekariya, R. L.; Dhar, A.; Kumar, N. S.; Roy, S., Efficient Solid-State Dye-Sensitized Solar Cell Based on Tricationic Ionic Crystal Pyridinuim-Imidazolium Electrolytes. *Organic Electronics* **2018**, *56*, 260-267.

Chapter 2

Materials, Experimental and Methods

CHAPTER 2

Abstract

This chapter provides an overview of the general synthetic protocol of ionic liquids, various experimental techniques, theoretical perspectives, and an array of methodologies that have been vigorously employed to build up the current thesis. This chapter also delivers knowledge on the source of various chemicals used and methods followed for sample preparation for spectroscopic and microscopic investigations throughout the thesis work. The operational principles of various spectrophotometers such as fluorimeter, time-correlated single photon counting (TCSPC) setup, and time-resolved confocal fluorescence microscope (FCS) setup have been elaborated. In addition to this, this chapter also introduces different theories, such as hydrodynamic theory, quasi-hydrodynamic theories, etc., that have been adopted for subsequent data analysis. The standard error limits associated with different experimental measurements, including their calculation and incorporation methods, have been included towards the end of this chapter.

CHAPTER 2

2.1. Materials

The majority of the mono-cationic ILs used in the current thesis work were purchased from Sigma Aldrich, TCI chemicals, and Io-Li-Tech (Germany), depending on availability. These ILs include;

- 1-Butyl-3-methylimidazoliumbis(trifluoromethanesulfonyl)imide
- 1-Methyl-3-octylimidazoliumbis(trifluoromethanesulfonylimide)
- 1-Butyl-1-methylpyrrolidiniumbis (trifluoromethane sulfonyl imide)
- 1-Methyl-1-octylpyrrolidiniumbis(trifuoromethanesulfonyl)imide
- 1-Ethyl-3-methylimidazoilum bromide
- 1-Ethyl-3-methylimidazolium chloride
- 1-Ethyl-3-methylimidazolium terafluoroborate
- 1-Ethyl-3-methylimidazolium acetate
- 1-Ethyl-3-methylimidazolium hydrogensulfate
- 1-Ethyl-3-methylimidazolium nitrate

The ILs purchased are of the highest purity grade and were used without further purification. More importantly, the ILs were stored carefully in the vacuum desiccators to avoid any moisture absorption. However, some MILs namely 1-Butyl-1-methylpyrrolidinium bromide, 1-Methyl-1-octylpyrrolidiniumbromide and the DILs, 1,9-bis-(1-methylpyrrolidinium-1-yl) nonanebis(trifluoromethanesulfonyl)imide, 1,9-bis-(3-methylimidazolium-1-yl) nonane bis (trifluoromethanesulfonyl)imide, 1,9-bis-(1-methylpyrrolidinium-1-yl) nonane bromide, 1,8-bis-(1-methylpyrrolidinium-1-yl)octane bromide, 1,6-bis-(1-methylpyrrolidinium-1-yl)hexane bromide and 1,3-bis-(1-methylpyrrolidinium-1-yl)propane bromide were synthesized by simply following the reported synthetic protocols available in literatures.[1-5] For the synthesis of the aforementioned ILs, the reagents 1-Methylimidazole, 1-methyl pyrrolidine, 1-Bromobutane, 1-Bromooctane, 1,3-Dibromopropane, 1,6-Dibromohexane, 1,8-

Dibromooctane, 1,9-Dibromononane and Lithium bis(trifluoromethanesulfonyl)imide were obtained from TCI chemicals. The solvents Acetonitrile, Diethyl ether, Methanol, Ethyl acetate, and activated charcoal were purchased from SpectroChem. The solvents were distilled prior to their use in the synthesis using the standard distillation method. The deuterated solvents Chloroform-D ($CDCl_3$) and Dimethylsulfoxide-D_6 (DMSO-d6) for the characterization of synthesized ILs were purchased from Sigma Aldrich. All the synthesized ILs were subjected to vacuum drying prior to the characterization and spectroscopic studies. The *ct*-DNA employed in the biological study and tris-HCl buffer with a pH of 7.2 was obtained from Sigma Aldrich. Moreover, Ethylene Glycol, iodine, and Tetrabutylammonium iodide were also purchased from Sigma-Aldrich.

2.2. Synthesis procedure of ILs

2.2.1. 1-Butyl-1-methylpyrrolidinium bromide/ [C_4(MPyrr)Br] and 1-Methyl-1-octylpyrrolidinium bromide/[C_8(MPyrr)Br]

1-Methylpyrrolidine and the respective Bromoalkene solution were taken in a 1:1.2 molar ratio in acetonitrile. The mixture solution was transferred to a two-necked round bottom flask and stirred at 85^0C under reflux conditions in the nitrogen atmosphere. After 72 hours of continuous reflux, the resultant solvent from the reaction mixtures was evaporated and washed several times with diethyl ether to get the respective bromide salts. The obtained bromide salts were then recrystallized from methanol to get the pure white bromide salts. The bromide salts are dried under a vacuum for 24 hours before the characterization.[5]

2.2.2. 1, 9-bis-(1-methylpyrrolidinium-1-yl) nonanebis(trifluoromethanesulfonyl)imide/ [C_9(Mpyrr)$_2$][NTf_2]$_2$

1,9-Dibromononane and 1-Methylpyrrolidine were mixed in a 1:2.2 molar ratio and gradually added to a two-necked round bottom flask containing acetonitrile. Then, the flask containing

the reactant mixtures was left to reflux under a nitrogen atmosphere at 85^0C for 72 hours to get the bromide precursor. The residual solvents were decanted and evaporated using a rotary evaporator. The bromide salt was repeatedly washed with diethyl ether and ethyl acetate, and after evaporating the residual solvent, it was subjected to vacuum drying for 24 hours. Thereafter, the bromide salt was dissolved in water. The aqueous solution of Lithium bis(trifluoromethane sulfonyl)imide was gradually added to the bromide salt solution in water for the metathesis of bromide ion by $[NTf_2]$ ion. It should be noted here that the molar ratio of bromide salt to Lithium salt is maintained at 1:2.2. The mixture solution was stirred at room temperature for one day. An organic layer containing $[C_9(Mpyrr)_2][NTf_2]_2$ appeared. The resultant IL from aqueous solution was then extracted with ethyl acetate and condensed to get the desired DIL. The DIL was then post-treated with activated charcoal in acetonitrile for decolorization, and the subsequent evaporation yields the final product. The final product is dried under vacuum for 24 hours and stored in the desiccators.[1]

2.2.3. 1,9-bis-(3-methylimidazolium-1-yl) nonanebis(trifluoromethane sulfonyl)imide/ $[C_9(Mim)_2][NTf_2]_2$ and 1,8-bis-(3-methylimidazolium-1-yl) octane bis(trifluoromethane sulfonyl)imide/$[C_8(Mim)_2][NTf_2]_2$

For the synthesis of these two imidazolium-based DIL, the respective dibromoalkane and 1-Methylimidazole were mixed in a 1:2.2 molar ratio, and the mixture was gradually added to an appropriate amount of acetonitrile solution present in a two-necked round bottom flask. The reaction mixture in the flask was equipped with a reflux condenser and allowed to reflux with continuous stirring in a nitrogen atmosphere at 85^0C for 3 days to get the respective bromide precursor. The solvent layer was then removed by using a rotary evaporator, and bromide salt was washed repeatedly with diethyl ether and ethyl acetate to get the final bromide precursors. The bromide salts were kept under high vacuum for proper drying and then used for a metathesis reaction. For the metathesis reaction, an aqueous solution of the bromide salt and

Lithium bis(trifluoromethanesulfonyl)imide salt were mixed in a 1:2.2 molar ratio and stirred at room temperature for 24 hours. The resultant DILs were extracted with ethyl-acetate and condensed to get the desired ILs. The DILs were then treated with activated charcoal in acetonitrile solution to get the pure ILs. After that, the residual solvent was pumped out under a high vacuum, and the ILs were stored in the desiccator.[2]

2.2.4. 1,3-bis-(1-methylpyrrolidinium-1-yl) propane bromide/[$C_3(MPyrr)_2Br_2$] 1,6-bis-1-methylpyrrolidinium-1-yl) hexane bromide/[$C_6(MPyrr)_2Br_2$] 1,8-bis-(1-ethylpyrrolidinium-1-yl) octane bromide/[$C_8(MPyrr)_2Br_2$], 1,9-bis-(1-methylpyrrolidinium-1-yl) nonane bromide//[$C_9(MPyrr)_2Br_2$]

For the synthesis of these pyrrolidinium-based DILs (organic ionic crystals), briefly, 11 mL (0.09 mol) of 1-Methylpyrrolidine and 0.01mol of respective dibromo-alkane were added into 100 mL of acetonitrile. The resulting solution was stirred in a two-necked round bottom flask equipped with a reflux condenser at 90^0C for 8 hours under a constant nitrogen atmosphere. The resulting mixture was filtered to obtain the white precipitant. The crude product was washed successively with diethyl ether and ethyl acetate. The bromide salts are recrystallized from methanol. The pure products were obtained after vacuum drying at 40^0C for 24 hours.[1]

2.3. Sample Preparation for all spectroscopic measurements

For the steady-state and time-resolved fluorescence measurements, ILs were taken in a micro-cuvette made up of quartz with 1cm path length. The amount of fluorescence probe dissolved in the ILs was adjusted by measuring the optical density of the probe. The optical density of the probe solute was maintained at approximately 0.5 in each case to ensure an accurate result and minimize potential interference. Thorough precautions were taken during the sample preparation process to prevent moisture adsorption within the samples. For this purpose, the cuvettes were tightly sealed using a combination of parafilm and a rubber septum. The

deuterated solvents are taken in a small, thin capillary tube for NMR diffusion experiments. The height of the deuterated solvent in the capillary is maintained the same as the height of the IL in the NMR tube. For the biological study (Chapter 5a and Chapter 5b), all the IL and probe solutions were prepared in the tris-HCl buffer of pH 7.2 and stored in a refrigerator. The *ct*-DNA solutions were also prepared in tris-HCl buffer, and the optical density ratio at 260nm to 280nm was always verified to be less than 1.8.[6] For scanning electron microscopic analysis, the samples were prepared by drop casting the methanol to form a uniform layer of salt solution of OICs on a silicon wafer. The OIC-based electrolytes were prepared by mixing and grinding the ionic OIC, I^- source (TBAI), and iodine (I_2) in a molar ratio of 0.1:0.1:0.02.[7]

2.4. Instrumentation

2.4.1. Instruments used for characterization of ILs

The NMR spectra of synthesized ILs were recorded with a Bruker Avance 400 MHz NMR spectrometer. A Cone and Plate Viscometer (Brookfield LVDV-III Ultra) was utilized to measure the viscosity of the IL samples. Additionally, a Julabo water circulator bath was connected to the viscometer for temperature-dependent viscosity measurements. The X-ray source used was graphite-monochromatized high-intensity Mo Kα radiation with a wavelength (λ) of 0.71073 Å. These measurements were performed at room temperature. Powder X-ray diffraction data were collected on a Bruker D8 Advance X-ray powder diffractometer with Mo Kα radiation (λ =0.71073) as the X-ray source. The surface morphology of the samples was examined using a scanning electron microscope (FESEM, Merlin Compact with a GEMINI-I electron column, manufactured by Zeiss Pvt. Ltd., Germany). Thermal properties of the crystals were determined using a Mettler Toledo differential scanning calorimeter (DSC) at a scanning rate of 10°C/minute over the temperature range of 25°c to 250°c under an argon (Ar) atmosphere. Thermogravimetric analyses (TGA) were also carried out using a Discovery TGA instrument from TA Instruments-Waters Lab under a flow of nitrogen (N_2) gas at a ramp rate

of 10°C/minute. The ionic conductivity of the as-prepared ionic crystal electrolytes was ascertained through electrochemical impedance measurements (EIS), while Linear Sweep Voltammetry (LSV) measurements were conducted using a Swagelok cell comprising Teflon tubing and two conductive stainless-steel electrodes (each with a 1cm² surface area). These assessments were carried out using a computer-controlled Biologic Electrochemical workstation (SP-200) at room temperature, covering frequencies ranging from 1 MHz to 1 Hz. The samples had a thickness of 1 mm and a cross-sectional area of approximately 64 mm².

2.4.2. Instrumental techniques for steady-state absorption and fluorescence measurement

2.4.2.1. Steady-state absorption measurement

UV-Visible absorption spectroscopy is an effective tool for characterizing different types of chromophore systems and their immediate surroundings. Additionally, the absorption spectrum of a chromophore substance is influenced by several factors such as polarizability, solvent polarity, and hydrogen bonding interactions within the ground state. In this context, UV-visible absorption spectroscopy allows researchers to study the changes in absorbance at specific wavelengths, which can reveal details about the structure, electronic configuration, and local environment of the chromophore. This technique is beneficial for understanding the interactions and influences of the micro-environment on the electronic properties of the chromophore. This is achieved by observing the wavelength at which various absorption bands appear, along with their molar extinction coefficients. In the current thesis work, the UV-visible spectroscopy analysis was conducted using a Cary 100 Bio UV-Vis spectrophotometer. This spectrophotometer utilizes a deuterium lamp (D_2O lamp) for generating light in the UV range and a xenon lamp for producing light in the visible range. The UV-visible absorption spectroscopy is based on Lambert Beer's law.[8-9] This law describes the relationship between the concentration of a solute in a solution and the absorbance of light by that solution. This law

is crucial for quantifying the concentration of a substance in a solution based on its absorbance measurements. Mathematically, the Beer-Lambert law is expressed as

$$A_\lambda = log\left(\frac{I_o}{I}\right) = \epsilon_\lambda Cl \quad \textbf{(eq.2.1)}$$

where A_λ is the absorbance of the solution. It is a dimensionless value

I_o = Incident light intensity

I = Transmitted light intensity

C=is the concentration of the solute in the solution, typically measured in mol/L or m(molality)

l = path length of the light through the solution, typically measured in centimetres.

The Beer-Lambert law holds under certain assumptions, such as the absence of significant scattering of light and the solute not interacting with itself or other solutes in a nonlinear manner. This law provides most accurate results at relatively low concentrations, as higher concentrations can lead to deviations due to interactions between solute particles. The law is widely used in chemistry, biochemistry, and other fields to quantify the concentration of a solute in a solution using absorbance measurements, and it forms the basis of many quantitative analytical techniques.

2.4.2.2. Steady-state fluorescence measurement

Fluorescence spectroscopy is an extremely sensitive optical method generally employed to investigate a wide range of photophysical and photochemical processes occurring in the excited state of a fluorophore molecule. A slight alternation in the energetic properties or interactions among fluorophore molecules in their excited state as well as a change in the surrounding environment, can lead to alterations in the intensity, shape, and peak emission wavelength of the resulting emission spectra.[8-11] Therefore, by monitoring the fluorescence emission spectra of fluorophores in the presence of an analyte of interest, a deeper understanding of the microenvironment surrounding the emitting species can be achieved.

In this context, the current thesis work employs an Agilent Technologies (G9800A) Cary Eclipse fluorescence spectrophotometer for the steady-state fluorescence measurements of the sample. This instrument consists of a xenon lamp as the light source. Furthermore, for acquiring fluorescence spectra in a variable temperature range, the Edinburgh spectrofluorometer FS5 was also employed. A North West temperature controller (TC125) was employed to uphold a consistent temperature through the circulation of water through the cell holder.

2.4.3. Time-resolved fluorescence measurement

Time-resolved fluorescence measurements offer significant insights into the kinetics and dynamics of diverse photochemical and photophysical processes in the excited state. This technique involves the use of ultra-short pulsed light to excite fluorescent molecules, leading to an initial population of molecules in the excited state. Subsequently, the population of molecules in the excited state diminishes over time through both radiative and non-radiative pathways with a decay rate ($k_r + k_{nr}$), as described by the following relationship.[10, 12]

$$-\frac{dn(t)}{dt} = (k_r + k_{nr})n(t) \quad \textbf{(eq. 2.2)}$$

Where $n(t)$ represents the count of excited molecules at a specific time (t) after the excitation of the fluorophore molecule using the short-pulsed light. The parameters (k_r) and (k_{nr}) signify the radiative and non-radiative rate constants, respectively. Since emission is regarded as a random phenomenon, the probability of emission from excited fluorophores remains almost equal over a given time span. The decay of the excited state population follows an exponential pattern, as articulated in equation (2.3) below:

$$n(t) = n_o \exp\left(-\frac{t}{\tau}\right) \quad \textbf{(eq.2.3)}$$

In equation (2.3), it is evident that the fluorescence intensity correlates directly with the count of excited molecules within the solution. Consequently, equation (2.3) can be reformulated in terms of the time-dependent intensity *I(t),* and the resulting equation (2.4) is presented as follows:

$$I(t) = I_o \exp\left(-\frac{t}{\tau_f}\right) \quad \textbf{(eq.2.4)}$$

Where (I_o) represents the intensity at the initial time (time zero), and τ_f Signifies the fluorescence lifetime of the fluorophore. The fluorescence lifetime τ_f is interrelated with the radiative and non-radiative decay rate constants, as indicated by the following equation (2.5):

$$\tau_f = \frac{1}{k_r + k_{nr}} \quad \textbf{(eq. 2.5)}$$

The fluorescence lifetime of an excited fluorophore is determined using the time-correlated single photon counting (TCSPC) technique.[8, 10] It is important to note here that different molecules spend varying amounts of time in the excited state. Consequently, certain fluorophores may emit photons over a longer duration while others might undergo rapid emission. As a result, the time distribution of these emitted photons becomes evident as the measured fluorescence decay of the investigated sample. The fluorescence lifetime, determined through the TCSPC setup, signifies a statistical average of how long fluorophores tend to linger in their excited states. In this context, to carry out the time-resolved fluorescence measurement for this thesis work, the Edinburgh Life Spec II TCSPC, and OB920 setups instrument was employed. This device operates on the principles of TCSPC and includes crucial components that contribute to its functionality. Although TCSPC is a sophisticated tool for determining the excited lifetimes of fluorophores, it possesses a relatively wide resolution window of about 80 picoseconds. This limitation prevents it from capturing any ultrafast components that might be present in a fluorophore's behaviour. Therefore, fluorescence up-conversion spectroscopic (FLUPS) techniques are also certainly employed in some cases to capture ultrafast lifetime components with a sub-picosecond time resolution of approximately 300 femtoseconds. The basic operational procedure and the key elements relevant to the TCSPC and FLUPS setup are outlined below.

2.4.3.1. Basic principle of TCSPC techniques

The fundamental principle underlying TCSPC involves detecting a single photon when a fluorophore is subjected to pulsed excitation. In this technique, the time interval between the excitation pulse and the first detected photon is typically measured. The variations in fluorescence intensity that takes place over time when a specific fluorophore is excited correspond to the probability distribution of molecules existing in excited states, which can be observed through the device. As TCSPC relies on statistical methods, a high repetition rate for the excitation source is crucial to efficiently detect a significant number of photons within a short time period, ensuring accurate statistical data. This data is stored in the form of a histogram, essentially presenting the fluorescence decay profile of the fluorophore.[8] Conceptually, TCSPC functions similarly to a stopwatch, with the START pulse originating from either a photon emitted by the excitation source ("forward mode") or from the sample's emission ("reverse mode"). [12-13] Scheme 2.1 provides a diagrammatic representation of the TCSPC setup operating in the reverse mode.[10]

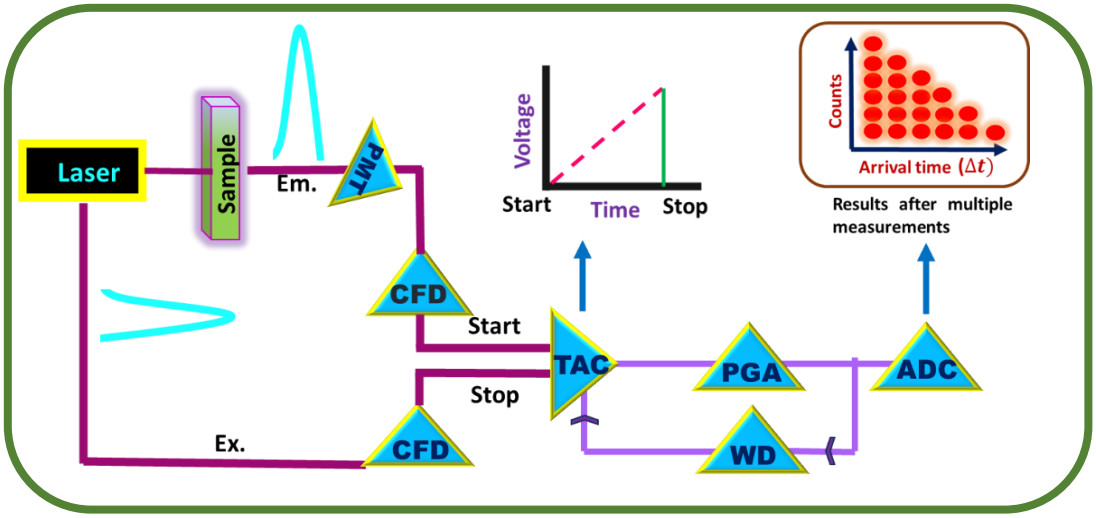

Scheme 2.1. A schematic diagram for the working principle of TCSPC setup

As illustrated in Scheme 2.1, in the initial step, the excitation pulse from diode LASER splits into two parts. While one part gets used in exciting the sample, the other part moves towards the electronic components. The optical signal produced by the emitted photon travels through

a Photomultiplier tube (PMT) and generates an electrical signal there, representing the START pulse. This START pulse then navigates through the Constant Fraction Discriminator (CFD), which precisely determines the arrival time of the pulse. Subsequently, this signal enters the time to amplitude converter (TAC) via the START input, creating a linearly increasing voltage ramp over time. Meanwhile, the second channel, consisting of excited photons, passes through an adjustable delay line and the CFD before reaching the TAC unit. These signals function as STOP pulses and serve as the STOP input for the same TAC unit. The TAC unit halts the voltage ramp upon detecting the initial STOP pulse. As a result, the TAC unit holds a voltage proportionate to the time interval (Δt) between the emission (start) and excitation (stop) pulses. The TAC output pulse signals are then directed to an Analog-to-Digital Converter (ADC) through a Pulsed Gain Amplifier (PGA). The ADC produces a numerical value, which is proportional to the height of the TAC output pulse signal, and this data is ultimately stored in a multichannel analyser (MCA). The above-mentioned cyclic process is repeated multiple times, producing histograms of counts in the MCA channels. Primarily, this TCSPC operational method is referred to as "reverse mode" functioning, and it is commonly employed in modern TCSPC measurements due to the high repetition rates of contemporary pulsed-light sources. The rapid succession of start signals necessitates the resetting and zeroing of the TAC before each start pulse. This precaution prevents the TAC from remaining in reset mode continuously and losing information. Importantly, the TCSPC conditions are adjusted to ensure that less than one photon is detected per hundred laser photons used for excitation. Thus, emission pulses trigger the voltage ramp initiation in the TAC, while subsequent laser pulses are utilized to halt the TAC. In the context of this thesis work, fluorescence decay data is collected using the Life Spec II and OB920 TCSPC spectrofluorometers. Analysis software (F980) provided by Edinburgh Instruments is utilized to fit experimental decay curves and extract fluorescence

lifetimes from the samples. Detailed procedures regarding the determination of average fluorescence lifetime from the decay profiles are also described towards the end of this chapter.

2.4.3.2. Basic principle of FLUPS techniques

Fluorescence Up-Conversion stands out as a highly used ultrafast spectroscopic technique that enables measurements of ultrafast dynamics or initial dynamics of any fluorophore with a time-resolution resolution range of 300 fs to 2 ns. The name itself conveys that this technique relies on the generation of a sum frequency signal referred to as an up-converted signal. This up- converted signal is formed by the combination of the emitted fluorescence and gate pulses. The pump-probe method forms the basis of this up-conversion process.[10, 14-17] In this method, a sample isexcited by an ultrafast laser pulse known as the pump pulse, and subsequently, the fluorescence decay is obtained by uniting the fluorescence from the sample and another additional laser pulse known as the probe pulse. A delay line causes the laser pulse to be time-delayed in relation to the fluorescence of the sample, and then both pulses are focused simultaneously on a nonlinear optical crystal (in our example, a BBO) to generate the unconverted UV signal. A delay line introduces a time lag to the laser pulse in relation to the sample's fluorescence, after which both pulses are concurrently directed onto a nonlinear optical crystal (such as a BBO in our scenario) to produce the unconverted UV signal. An overview of the steps and components involved in the process is outlined below.

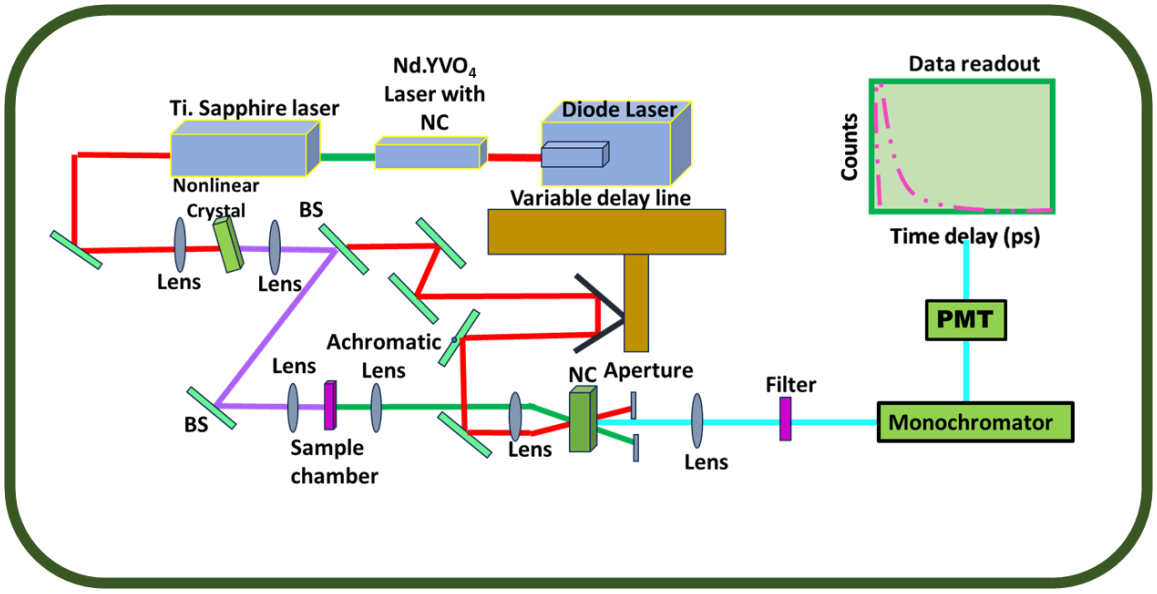

Scheme 2.2. A schematic representation of the up-conversion setup

The primary laser pulse (ω_p) is directed onto a nonlinear optical crystal (e.g., β-barium borate or BBO). This crystal generates a second harmonic beam ($2\omega p$) with the same repetition rate as the fundamental pulse. The combined output light passes through a dichroic mirror (BS1) that separates the fundamental beam (gate/probe pulse) and the second harmonic beam (excitation/pump pulse). The gate beam is transmitted through BS1, while the excitation pulse is reflected. The excitation pulse passes through a polarizer and is then focused onto the sample, inducing fluorescence. The fluorescence emitted by the sample is collected for further analysis. The collected fluorescence signal is filtered to allow only the fluorescence signal (ω_f) to pass through. The filtered fluorescence signal (ω_f) and the gate beam (ω_p) pass through a sum frequency generation (SFG) crystal (e.g., BBO) with precise alignment. The two signals interact, generating an up-converted signal with a frequency equal to the sum of the fluorescence and gate pulse frequencies ($\omega_{up} = \omega_f + \omega_p$). The up-converted signal is directed through an iris to block the fluorescence and gate beams. The up-converted signal is then sent through a monochromator to isolate specific wavelengths before being detected by a photomultiplier tube (PMT). The temporal and spatial alignment of the fluorescence and gate pulses is critical for efficient up-conversion. By varying the delay time for the gate pulse and

monitoring the intensity of the up-converted signal, the fluorescence decay profile can be deduced. To prevent photo-degradation, the sample is often contained in a rotating cell with a specific path length. The present thesis work employs FluoMax from IB Photonics Ltd. For excitation of the samples, a Ti-sapphire laser(Mai Tai HP, Spectra Physics, 80 MHz, center wavelength 800nm, 3W @800nm) with an adjustable range from 690 nm to 1040 nm to record the up-converted signal.

2.4.4. Single-Molecular Fluorescence Measurements

2.4.4.1. Time-resolved confocal fluorescence-microscopy

Optical microscopes play a vital role in magnifying small objects for observation.[18] However, visualization of clear images of micro-objects relies on the overall resolution of the microscope. The resolution of a microscope depends on several factors, such as the excitation wavelength and the numerical aperture of the objective lens. Modifying these aspects can effectively fine-tune the resolution of the microscop**e.** Confocal fluorescence microscopy (CFM) is a specialized and convenient technique that offers enhanced temporal resolution, potentially reaching down to the nanosecond range. CFM operates by incorporating multiple pinholes into the detection pathway.[18-20] These pinholes permit only focused light to pass through, facilitating measurements within a specific, confined region known as the confocal volume. This approach significantly improves image quality and minimizes background noise. The following scheme (scheme 2.3) shows the schematic diagram of a time-resolved confocal fluorescence microscop.

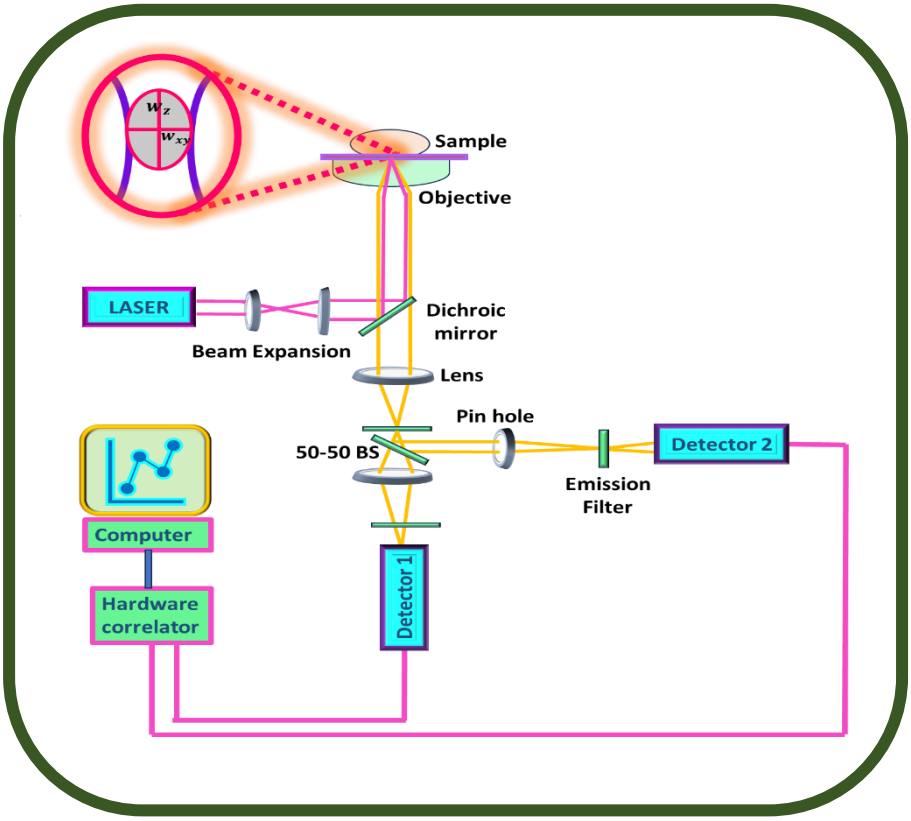

Scheme 2.3. Time-resolved confocal fluorescence microscope setup.

In this thesis work, all measurements at a single molecular level were conducted utilizing the PicoQuant MicroTime 200. A variety of pulsed picosecond diode lasers with distinct wavelengths (403 nm, 444 nm, 483 nm, and 519 nm) were employed alongside a continuum laser featuring an excitation wavelength spectrum ranging from 360 nm to 720 nm for excitation of the sample. To channel the laser output effectively, a polarization-maintaining single-mode optical fibre was employed. This optical path directed the laser light through a dichroic mirror, facilitating its subsequent entry into an inverted microscope of the Olympus IX71 model. A water immersion objective of high numerical aperture (UPlansApo NA 1.2, 60X) was strategically chosen to optimize imaging quality. A sample holder is utilized to place the sample on a coverslip effectively. Precise positioning of the sample is achieved either through manual adjustments using micro-meter screws or, alternatively, via an automated process utilizing a software-controlled piezo-scanner. This setup ensures accurate and

repeatable scanning along both the XY plane and the Z-position. The focus position on the sample surface was closely monitored using a charged-coupled device (CCD) detector. Furthermore, the emitted fluorescence from the sample was efficiently collected, subsequently passing through another dichroic mirror. The collected fluorescence was then filtered using a long-pass filter. The emitted fluorescence signal is then focused through a pinhole, measuring 50 μm in diameter. This strategic step serves to eliminate any extraneous signals arising from out-of-focus regions. Subsequently, the focused fluorescence signal is directed towards single-photon avalanche photodiodes (SPADs), a specialized type of photodetector capable of detecting individual photons. The acquired data is subjected to thorough analysis with the help of the SymPhoTime software-controlled PicoHarp 300 TCSPC (Time-Correlated Single Photon Counting) module. This analysis is conducted in a time-tagged time-resolved (TTTR) mode, which provides valuable insights into the temporal characteristics of the fluorescence signals.

2.4.4.2. Fluorescence Correlation Spectroscopy (FCS)

Fluorescence Correlation Spectroscopy (FCS) serves as a non-invasive method based on the analysis of fluctuations in fluorescence intensity with time within a very tiny volume measuring approximately 1fl (femtolitre). This technique yields insights into the dynamic processes underlying these fluctuations. In a solution sample, FCS operates by allowing fluorophores to move freely within the confines of a confocal volume, generating fluctuations in the signal. These fluctuations arise from various factors, including diffusion-related events.[15, 21] To attain distinct and well-defined fluctuations, it is essential to limit the number of participating molecular species. This is generally achieved by working with low concentrations, often in the nanomolar range. This choice is based on the fact that highly concentrated samples would exhibit relatively constant average signals over the duration of the measurement. Consequently, employing diluted solutions enhances the technique's sensitivity to single molecules, a

sensitivity contingent on the size of the observation volume. The acquired signals are subsequently subjected to correlation analysis, which involves analysing how the signals relate to one another over time. The experimental setup for FCS closely resembles the configuration depicted in Scheme 2.3. For the purpose of improving the Signal-to-Noise Ratio (SNR) and attaining enhanced temporal resolution, signals are commonly cross-correlated. In essence, FCS is a powerful tool for studying dynamic processes on the molecular scale, capitalizing on the inherent fluctuation-based behaviour of fluorescent species within confined volumes.

2.5. Methods

2.5.1. Analysis of the fluorescence decay curve

2.5.1.1. Lifetime analysis from the fluorescence decay curve

The magnitude of fluorescence lifetime is determined through the analysis of decay curves by using the re-convolution least squares method.[12, 15, 22-23] This is because, in the TCSPC measurement techniques, the determination of true intensity decay can be challenging. This is due to the fact that the fluorescence decay curve obtained from time-resolved measurements is a combination or convolution of both the laser pulse and the actual fluorescence emitted by the sample. This convolution arises because the estimated fluorescence decay time for any fluorophore tends to be longer than the pulse-width of the excitation source. In this scenario, several factors may contribute to the fluctuation of the experimental data. These include the response time of the photomultiplier tube (PMT), the finite decay time of the source pulse, and the effects of other related electronic components. Consequently, the instrument response function (IRF) is influenced not only by the decay time of the laser pulse but also by the response time of the detector and the associated electronic systems. Therefore, for the accurate determination of the true fluorescence lifetime of a sample, separation of the influence of the IRF from the measured fluorescence decay curve is essential. This separation is achieved

through a process known as deconvolution. Deconvolution aims to reverse the convolution process and isolate the genuine fluorescence decay signal from the combined effect of the laser pulse and instrumental response. Therefore, the iterative reconvolution least squares method was employed for the analysis of fluorescence decay profiles. Mathematically, this method can be described as the expression given below.

$$I_m(t) = \int_0^t I_R\,(t - t')R(t')dt' \qquad \textbf{(eq. 2.6)}$$

Here in the above relation $I_m(t)$ represents the fluorescence intensity at a given time t, $I_R(t\text{-}t')$ denotes the response function of the experimental system under consideration, and the intensity of the pulse (excitation) at time t' has been written as $R(t')$. The IRF was calculated using a ludox solution, and the iterative reconvolution approach was employed to develop a deconvolution algorithm.

The fitting fluorescence decay curves with an assumed functional form involves utilizing a nonlinear least squares (NLLS) data processing technique. This method is chosen to extract accurate information from the measured data. The least squares approach is effective when certain conditions are met, including having a sufficient number of independent data points, Gaussian-distributed uncertainties in the experimental data, and the absence of systematic errors. In this fitting method, both the intensity decay function $I_m(t)$ and the response function $R(t')$ are obtained experimentally from the TCSPC setup. The analysis begins by assuming a specific decay function $G(t)$ which is characteristic of the sample being studied. The aim is to deconvolute this assumed function with the observed response function $R(t')$ using equation 2.6. This deconvolution generates a calculated curve $Y(t)$. Subsequently, the calculated curve $Y(t)$ is compared with the experimentally observed decay curve $I_m(t)$. This comparison allows for an assessment of how well the assumed function $G(t)$ fits the actual data. To achieve a good fit between $Y(t)$ and, $I_m(t)$, the variables within the function $G(t)$ are adjusted iteratively. This iterative adjustment process aims to find the best combination of parameters

that minimize the discrepancy between the calculated and observed decay curves. The function $G(t)$ is commonly assumed to be a sum of some exponentials, as provided in equation 2.7.[24-25] This choice of functional form is based on the common behaviour exhibited by many fluorescent decay processes.

$$G(t) = \sum_i B_i \, exp\left(\frac{-t}{\tau_i}\right) \quad \textbf{(eq.2.7)}$$

Here B_i denotes the pre-exponential factor for the ith component and τ_i is the lifetime of the corresponding to the ith component. The average lifetime (< **τ** >) of the fluorophore is estimated using equation 2.8,

$$< \tau > = \sum i \; bi \; \tau i \quad \textbf{(eq.2.8)}$$

In the above expression b_i represent the normalized amplitude weighted components and τ_i denotes lifetime component corresponding to b_i.

2.5.1.2. Reduced chi-square (χ^2) values

To assess the quality of a fit between a model and experimental data, reduced χ^2 values are also evaluated by following the relation given below.

$$\chi^2 = \frac{\sum_i W_i\{Y_i - I_i\}^2}{n-p} \quad \textbf{(eq.2.9)}$$

In this equation:

- Y_i corresponds to the count in the ith channel of the calculated curve,
- I_i represents the count in the ith channel of the curve obtained through experimental measurement,
- W_i (with $W_i = I / I_i$) signifies the weighting factor applied to the counts in the ith channel,
- n signifies the number of channels used for analyzing the decay, and

- p stands for the degrees of freedom in the decay function considered for the analysis, which equates to the number of variables present in the function $G(t)$.

The χ^2 value, when close to unity, indicates a good fit between the model and the data. Typically, a range of χ^2 values from 1.0 to 1.2 is considered indicative of a well-fitted model for the data points.

2.5.1.3. Distribution of weighted residuals

Differences between the fitted decay function and the measured decay function are represented using weighted residuals. These residuals play a significant role in evaluating the quality of an analysis of Time-Correlated Single Photon Counting (TCSPC) data sets. The calculation of weighted residuals is based on the following equation (2.10).

$$r_i = \sqrt{W_i}(Y_i - I_i) \quad \textbf{(eq.2.10)}$$

An adequate fit is indicated by the occurrence of a random distribution of weighted residuals around the zero line across the entire range of data. In the current study, the F980 software, developed by Edinburgh Instruments, was employed for two primary purposes:

- **Deconvolution of the Instrument Response Function (IRF):** The software was utilized to carry out the deconvolution process, which separates the influence of the IRF from the measured fluorescence decay curves. This procedure is crucial for obtaining accurate fluorescence lifetime information.

- **Fitting Decay Curves:** The software was also employed to fit each decay curve to an appropriate mathematical function. This fitting process involves adjusting the parameters of the chosen mathematical function to achieve the best match between the calculated and experimental decay curves.

2.5.2. Analysis of the time-resolved fluorescence anisotropy data

Time-resolved fluorescence anisotropy is a technique used to investigate the rotational dynamics and molecular motion of fluorescent molecules in a sample. Anisotropy refers to the directional dependence of a physical property. In the context of fluorescence, anisotropy measures the polarization of emitted light relative to the polarization of the excitation light.[15] Scheme 2.4 represents a schematic diagram of the alignment of the polarizer in the TCSPC setup during the anisotropy measurement and scheme 2.5 represents the step-by-step process generally involved in the fluorescence anisotropy measurement.

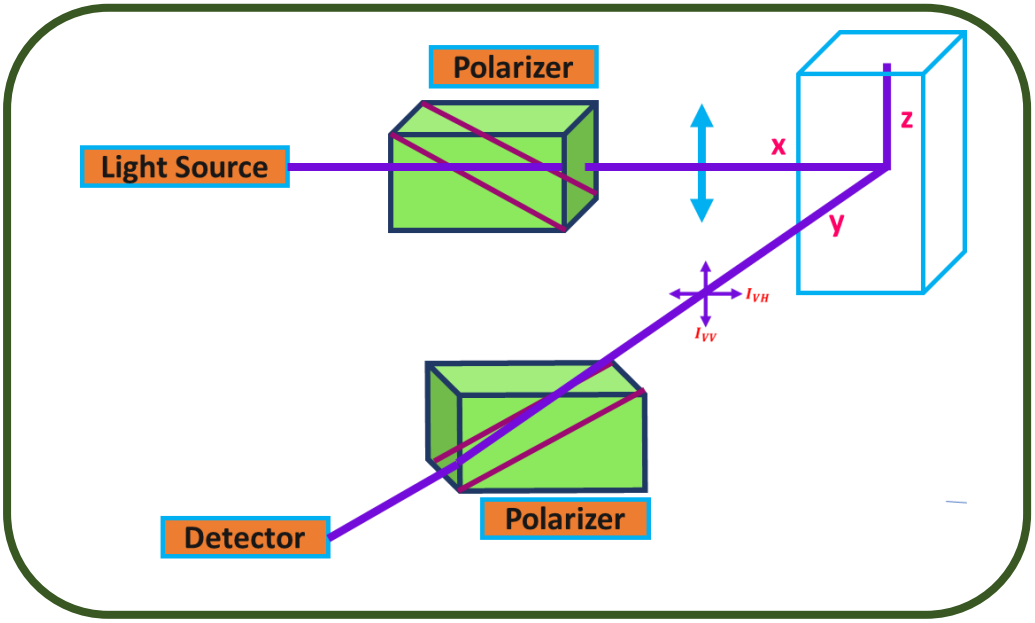

Scheme 2.4. A schematic view of fluorescence anisotropy measurements

The alignment of the emission polarization is determined by the electric vector of the excitation pulse. The terms I_{VV} and I_{VH} refer to the intensity of parallel polarization and perpendicularly polarized emission, respectively. In this context, it is worth mentioning that during parallel polarization, the excitation and emission polarizer are both placed vertically and for perpendicular polarization, the excitation and emission polarizer are placed vertically and horizontally, respectively. The concept of an ideal anisotropy *r(t)* is described through the following equation (2.11):

$$r(t) = \frac{I_{VV}(t) - GI_{VH}(t)}{I_{VV}(t) + 2GI_{VH}(t)} \quad \textbf{(eq.2.11)}$$

The fluorescence anisotropy is a dimensionless quantity. This is due to the fact that this quantity is obtained by normalizing the difference between parallel and perpendicular emission by the total emission intensity. The anisotropy of a given sample does not depend on the concentration of fluorophore as well as the total emission intensity.

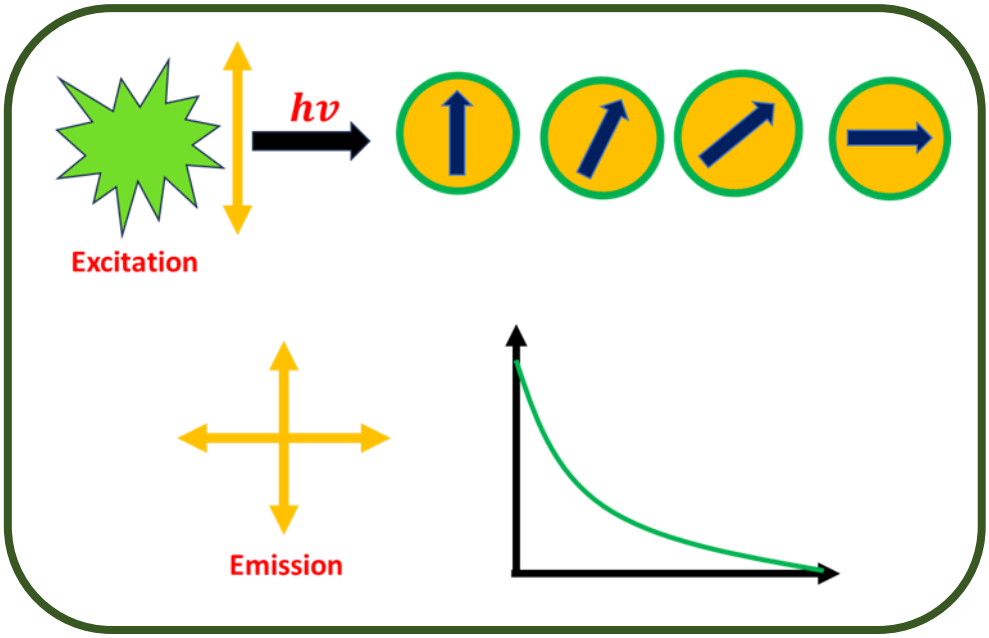

Scheme 2.5. A pictorial view of process involved in fluorescence anisotropy measurements

In TCSPC instruments, the accuracy of anisotropy measurements can be influenced by the sensitivity of the experimental setup and electronics, including components like monochromators. To eliminate these potential effects, it is important to introduce a correction factor denoted as G when estimating the anisotropy, $r(t)$. This correction factor compensates for variations in sensitivity across different orientations of polarizer. The correction factor G represents the relative sensitivity of the detection system to different polarizations. It indicates how the detection system responds to parallel (I_{HH}) and perpendicular (I_{HV}) orientation of polarizations of emitted light. The calculation of G is defined by equation (2.12), which is provided below[15].

$$G = \frac{I_{HH}}{I_{HV}} \quad \textbf{(eq.2.12)}$$

In the above equation, I_{HH} represents the intensity of emission detected when both the excitation and emission polarizers are in a horizontal position, while I_{HV} represents the intensity detected when the excitation polarizer is horizontal, and the emission polarizer is vertical.

The current thesis work employs the Edinburgh Life Spec II TCSPC setup for the measurement of time-resolved fluorescence anisotropy. To perform these measurements fluorescence intensities were collected with different polarization orientations, namely parallel (∥) and perpendicular (⊥), alternately. This process was repeated until a substantial peak difference between the parallel (∥) and perpendicular (⊥) decay curves reached approximately 5000 (at t = 0). The same procedure was applied to calculate the G-factor. However, for G-factor determination, the exciting laser beam was polarized horizontally. This process involved running five cycles of repetitions. To control the temperature during the temperature-dependent measurements, a Quantum instrument was used in conjunction with a North West TC 125 temperature controller. This setup maintains the cell temperature by circulating water through the cell holder. To derive information about the rotational relaxation time, the anisotropy data underwent fitting. The fitting process was carried out using the equation (2.13), which likely represents a mathematical expression used to model the relationship between time-resolved fluorescence anisotropy and other relevant parameters.

$$r(t) = r_0 e^{\langle -(t/\tau_r) \rangle} \quad \textbf{(eq.2.13)}$$

Here in the above equation, r_0 is referred as the initial anisotropy and τ_r denotes the reorientation time or rotational relaxation time. It can be noted here that the r_0 values can vary from 0.20 to 0.40 for a single-photon excitation. The data obtained from the time-resolved

anisotropy measurements were subsequently analyzed by using several hydrodynamic and quasi-hydrodynamic theories.[26-29]

2.5.2.1. Stoke Einstein Debye (SED) hydrodynamic theory

The SED theory posits that the rotational motion of a solute molecule in a solvent is influenced by the viscosity (η) of the fluid at a given temperature (T). The time it takes for the solute molecule to reorient itself is denoted as τ_r. This theory is an integrated approach of the Stokes-Einstein equation, Debye theory, and hydrodynamics to describe the behaviour of solute molecules in a fluid medium. The size and shape of the solute molecule are important factors in governing its rotation in the solvent. These properties are incorporated into the SED theory using the van der Waals volume (V) and the shape factor (f) to account for the non-spherical nature of the solute. In this model, the solute molecules are treated as symmetric or asymmetric ellipsoids, which allows for the consideration of their non-spherical shape in the model.[26] Moreover, the interaction between the solute and the solvent, if any (such as electrostatic or H-bonding, or hydrophobic), is a significant factor affecting the rotational diffusion of the solute molecule. A coupling parameter denoted as C is incorporated to account for this interaction. The axial ratio of the solute molecule and two limiting cases, stick and slip hydrodynamic boundary conditions, are considered to determine the value of C. The parameter C can take values between 0 (slip) and 1 (stick), with values close to 1 indicating strong coupling between the solute and solvent and values closer to 0 indicating weaker coupling.[30-34]

- **Stick Boundary Condition:** Assumes complete alignment between the motion of the solute and the solvent in the vicinity. This condition is favourable for larger solute molecules compared to the surrounding fluid molecules.

- **Slip Boundary Condition:** Assumes that the solvent does not move along with the rotating solute. This condition is applicable when the solute size is smaller or comparable to the fluid molecules.

Taking all the above factors in consideration, the SED equation has been described as follows.

$$\tau_r = \frac{\eta V f C}{kT} \qquad \textbf{(eq.2.14)}$$

The above equation involves the Boltzmann constant (k). The combination of V (van der Waals volume), f (shape factor), and C (boundary condition parameter) is termed the hydrodynamic volume (V_h), which represents the effective volume experienced by the solute within the solvent. The limitation of SED theory is that, in the SED framework, the determination of boundary parameters, the size of the solute molecule is only taken into consideration.[26, 34-36] However, The SED theory proves reasonably effective in explaining the rotational diffusion of solute molecules of medium size across various solvent types. In the context of the present study, the SED theory was applied to systems involving the solutes perylene, sodium 8-methoxypyrene-1,3,6-sulfonate (MPTS), Rhodamine 110 (R110), and 9-phenylantharcene (9-PA). The van der Waals volumes for these solutes were obtained through Edward's increment method. Relevant parameters such as solute dimensions, van der Waals volumes, shape factors, and boundary condition parameters (C_{slip}) values for perylene and MPTS are computed and provided in Table 2.1.[37-38]

Table 2.1. Van der Waals volumes (V), shape factors (f) and boundary condition parameters (C_{slip}) for the probe molecules used.

Probe	*V/ Å^3*	*f*	*C_{slip}*
Perylene	225	1.76	0.085
9-PA	236	1.73	0.12
MPTS	343	1.33	0.11
R110	275	2.02	0.15

2.5.2.2. Quasi-hydrodynamic theories

As described in the preceding section, the SED theory operates under the assumption that the hydrodynamic volume of the solute remains unaffected by the properties of the surrounding solvent continuum. However, this assumption remains valid primarily in cases where the solute's size greatly surpasses that of the solvent. The applicability of the SED theory becomes limited when attempting to analyse the hydrodynamic behaviour in cases where the solute size is not considerably larger than that of the solvent. In such scenarios, alternative theories like "quasi-hydrodynamic theories" have been developed, which take into account both the sizes of the solvent and solute molecules. Here in the present thesis work, such incidences have been explained by employing Dote-Kivelson-Schwartz (DKS) theories.[28, 39] DKS theory introduces an additional aspect by considering the available space between the solute and solvent molecules, in addition to their respective sizes. According to the DKS theory, when comparing the solute's size to the available space within the solvent, a condition arises where a relatively weak connection between the solute and solvent is evident. In this context, the solute encounters reduced friction, resulting in an accelerated rotational movement of the solute within the solvent medium. The aspects of DKS theory are described by the following equation (2.15)

$$C_{DKS} = (1 + \gamma/\phi)^{-1} \quad \textbf{(eq.2.15)}$$

Here, C_{DKS} is the boundary condition predicted by the DKS theory.

γ/ϕ gives the ratio of the available free volume of the solvent to the size of the solute molecule of interest. γ is determined by following equations (2.16)

$$\gamma = \frac{\Delta V}{V_p}\left(4\left(\frac{V_p}{V_s}\right)^{2/3} + 1\right) \quad \textbf{(eq.2.16)}$$

Where, ΔV is given by the relation given below

$$\Delta V = V_m - V_s \quad \textbf{(eq.2.17)}$$

$V_s =$ Volume of the solvent

$V_m =$ Molar volume of the solvent divided by Avogadro's number

$V_p =$ Volume of the solute

And$\phi = f C_{slip}$ **(eq.2.18)**

V_m is the solvent molar volume divided by the Avogadro number.

2.5.4. Pulse-field-gradient NMR measurements.

The pulse field gradient (PFG) NMR technique has been employed to compute the self-diffusion coefficient of IL samples.[39-44] To achieve this, a stimulated echo bipolar pulse-gradient pulse (stebpgp) sequence was employed, with a maximum gradient pulse strength of 50 G/cm. The variation in gradient pulse strength from 2% to 95%, at 16 equally spaced intervals, resulted in different echo heights. Then, the echo heights are fitted to the Stejskal-Tanner equation, which is given by equation (2.19)[45-47]

$$S(g) = S(0) \exp\left[-D\gamma^2\delta^2 g^2 \left(\Delta^{-\delta/3}\right)\right] \quad \textbf{(eq.2.19)}$$

In this equation, (g) represents the echo height at the gradient strength g, while S (0) is the echo height at 0 gradient strength. The symbols γ and δ correspond to the gyromagnetic ratio of the proton and the length of the gradient pulse, respectively. Additionally, Δ and D refer to the time between the two gradient pulses and the diffusion coefficient, respectively. This analytical approach allows us to extract the self-diffusion coefficients from the echo heights measured across different gradient strengths.

2.5.5. FCS data analysis

Fluorescence Correlation Spectroscopy (FCS) techniques represent a highly sensitive and reliable approach for determining the translational diffusion coefficient (D_t) of a probe molecule within a specific solvent system. In this procedure, a diluted sample (10-20 nM) is positioned on a coverslip, which is then positioned above the water-immersion objective. The excitation laser light passes through this setup. The intensity fluctuations of the samples are

monitored within an extremely minute observation volume (approximately 1 femtoliter) using a pinhole. The fluctuating fluorescence signals are simultaneously captured by two Single-Photon Avalanche Diode (SPAD) detectors. Subsequently, these signals are cross-correlated, resulting in the generation of correlation curves denoted as $G(\tau)$. By analysing the decay of these correlation functions with respect to time, valuable insights into the probe molecule's translational diffusion dynamics can be extracted. This method enables the determination of diffusion coefficients by exploiting the fine details of the fluorescence intensity fluctuations within the sample.[15, 19]

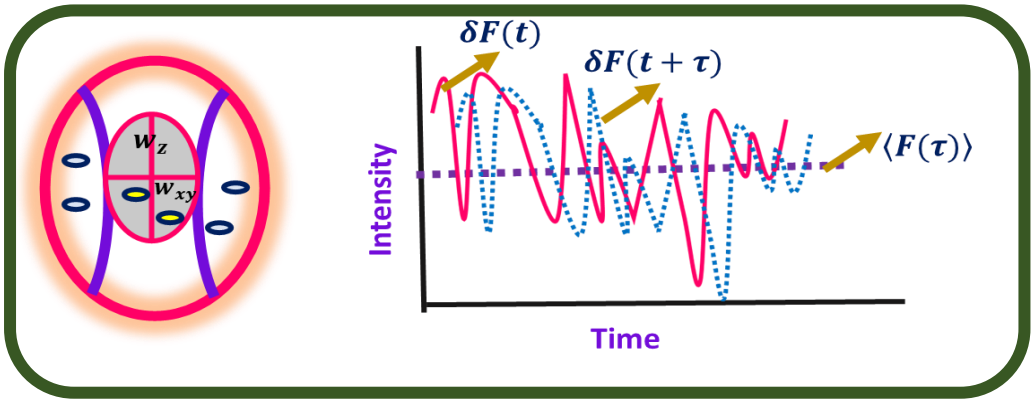

Scheme 2.6. Diffusion of fluorophores through the confocal volume and fluctuations in the relative intensities

Scheme 2.6 represents the diffusion of the particle within the illuminated volume of observation. The autocorrelation function is designated as the average product of the fluctuation of fluorescence intensities at time *t*, $\delta F(t)$, and $t + \tau$, $\delta F(t + \tau)$ obtained through a number of measurements. The autocorrelation function, $G(\tau)$ after normalization with the square of average fluorescence intensity (<*F(t)*>) is represented by the following equation (2.20);

$$G(\tau) = \frac{\langle \delta F(t) \delta F(t+\tau) \rangle}{\langle F(t) \rangle^2} \qquad \textbf{(eq.2.20)}$$

Here, $\delta F(t)$ and $\delta F(t + \tau)$ are given by the relation (2.21):

$$\delta F(t) = F(t) - \langle F(t) \rangle \; and \; \delta F(t + \tau) = F(t + \tau) - \langle F(t) \rangle \qquad \textbf{(eq.2.21)}$$

For simple diffusion of a molecule in three dimensions, the autocorrelation function can be fitted to the equation (2.22) provided below:

$$G(\tau) = \frac{1}{N}\left(1+\frac{\tau}{\tau_D}\right)^{-1}\left(1+\frac{\tau}{\kappa^2\tau_D}\right)^{-\frac{1}{2}} \quad \textbf{(eq.2.22)}$$

In equation 2.22, <*N*> represents the average number of fluorescent molecules found within the observation volume. The variable τ represents the lag time or delay, and (r_D) denotes the translational diffusion time constant. This constant corresponds to the duration it takes for a fluorophore molecule to diffuse through the observation volume. Additionally, *k* stands for the aspect ratio of the observation volume, calculated as $k = z/(w_{xy})$ where z and (w_{xy}) represent the longitudinal and combined transverse radii of the observation volume, respectively. The calibration of the FCS setup excitation volume was conducted using a diluted solution of Rhodamine 6G (R6G) in water, with a known translational diffusion coefficient (D_t) of 426 μm²/s. The calculated excitation volumes were approximately 0.45 femtoliters for the 405 nm laser source and around 0.80 femtoliters for the 483 nm laser source. From equation 2.22, the value of τ_D and using equation 2.23, the diffusion coefficient of the molecule can be calculated.

$$D_t = \frac{\omega_{xy}^2}{4\tau_D} \quad \textbf{(eq.2.23)}$$

In the current thesis work, the autocorrelation function obtained from the FCS measurement could be fitted successfully to the function provided below (equation 2.24).[48-50] This function takes into consideration the additional process such as triplet-state formation, photo-isomerization or protonation.

$$(\tau) = \frac{1-A+Aexp\left(\frac{\tau}{\tau_r}\right)^{\beta}}{N(1-A)}\left(1+\left(\frac{\tau}{\tau_D}\right)\right)^{-1}\left(1+\frac{\tau}{K^2\tau_D}\right)^{-1/2} \quad \textbf{(eq.2.24)}$$

In the equation provided above, A symbolizes the amplitude of τ_r, representing the proportion of non-fluorescent molecules in a separate state, while β is a stretching component ($0 < \beta < 1$)

that signifies a rate distribution. For a well-fitting autocorrelation function to equation 2.24, a β value of 0.44 was used (Chapter 5a). The fitting process yields (τ_D), which is then employed to compute the hydrodynamic radius (r_H) using equation 2.25. This equation proves particularly useful in compensating for alterations in diffusion time (τ_D) due to variations in the viscosity of the medium. Because Rh6G maintains its structural rigidity, its hydrodynamic radius (r_H) remains unchanged even when the viscosity of the surrounding medium changes. This unique property of Rh6G makes it ideal to be used as a standard. For this calculation, the (r_H) of Rh6G was determined with the aid of the Stokes-Einstein equation (2.26) from the known value of D_t in bulk water, and the diffusion time of free R6G in different solutions (IL solution of different viscosity) were calculated using equation 2.25.

$$\frac{{r_H}^{DNA}}{{r_H}^{Rh6G}} = \frac{{\tau_D}^{DNA}}{{\tau_D}^{Rh6G}} \quad \textbf{(eq.2.25)}$$

$$D_t = \frac{k_B T}{6\eta\pi r_H} \quad \textbf{(eq.2.26)}$$

Where η denotes the viscosity of the surrounding medium, k_B stands for the Boltzmann constant, and T represents the absolute temperature.

2.6. Standard error limit

The limit of error is a measure of the uncertainty or variability associated with the sample data

Table 2.2. Standard error limit of some experimental parameters

Parameters	Experimental Errors
λmax (abs./flu.)	±1-2 nm
Viscosity	±2
τ_f (> 1ns)	±5%
Rotational Relaxation time	±5%
Diffusion coefficient (through NMR)	3±%

Thermodynamics parameters $\Delta G, \Delta H$ & ΔS	3±%

REFERNCES

1. Anderson, J. L.; Ding, R.; Ellern, A.; Armstrong, D. W., Structure and Properties of High Stability Geminal Dicationic Ionic Liquids. *Journal of the American Chemical Society* **2005**, *127*, 593-604.
2. Ishida, T.; Shirota, H., Dicationic Versus Monocationic Ionic Liquids: Distinctive Ionic Dynamics and Dynamical Heterogeneity. *The Journal of Physical Chemistry B* **2013**, *117*, 1136-1150.
3. Shirota, H.; Mandai, T.; Fukazawa, H.; Kato, T., Comparison between Dicationic and Monocationic Ionic Liquids: Liquid Density, Thermal Properties, Surface Tension, and Shear Viscosity. *Journal of Chemical & Engineering Data* **2011**, *56*, 2453-2459.
4. Masri, A. N.; Mi, A. M.; Leveque, J.-M., A Review on Dicationic Ionic Liquids: Classification and Application. *Ind. Eng. Manag* **2016**, *5*, 197-204.
5. Montalbán, M.; Víllora, G.; Licence, P., Synthesis and Characterization Data of Monocationic and Dicationic Ionic Liquids or Molten Salts. *Data in brief* **2018**, *19*, 769-788.
6. Chandra, D., Effect of Ionic Liquids on DNA-Ligands Interaction: Studied by Fluorescence. *Asian J. Sci. Technol* **2015**, *6*, 2100-2103.
7. He, T.; Wang, Y. F.; Zeng, J. H., Stable, High-Efficiency Pyrrolidinium-Based Electrolyte for Solid-State Dye-Sensitized Solar Cells. *ACS Applied Materials & Interfaces* **2015**, *7*, 21381-21390.
8. Rohatgi-Mukherjee, K., Fundamentals of Photochemistry; New Age International, 1978.
9. Valeur, B.; Berberan-Santos, M. N., *Molecular Fluorescence: Principles and Applications*; John Wiley & Sons, 2012.
10. Lakowicz, J. R., Principles of Fluorescence Spectroscopy; Springer, 2006.
11. Lakowicz, J. R.; Lakowicz, J. R., Protein Fluorescence. Principles of fluorescence spectroscopy **1999**, 445-486.
12. Farr, E. P.; Quintana, J. C.; Reynoso, V.; Ruberry, J. D.; Shin, W. R.; Swartz, K. R., Introduction to Time-Resolved Spectroscopy: Nanosecond Transient Absorption and Time-Resolved Fluorescence of Eosin B. *Journal of Chemical Education* **2018**, *95*, 864-871.
13. Becker, W., Advanced Time-Correlated Single Photon Counting Techniques; Springer Science & Business Media, 2005; Vol. 81.
14. Becker, W.; Bergmann, A.; Kacprzak, M.; Liebert, A. In *Advanced Time-Correlated Single Photon Counting Technique for Spectroscopy and Imaging of Biological Systems*, Fourth International Conference on Photonics and Imaging in Biology and Medicine, SPIE: 2006; pp 261-265.
15. Lakowicz, J., In Principles of Fluorescence Spectroscopy. Springer, US: Boston, MA: 2006.
16. Xu, J.; Knutson, J. R., Chapter 8 Ultrafast Fluorescence Spectroscopy Via Upconversion: Applications to Biophysics. In *Methods in Enzymology*, Academic Press: 2008; Vol. 450, pp 159-183.
17. Zhao, L.; Luis Pérez Lustres, J.; Farztdinov, V.; Ernsting, N. P., Femtosecond Fluorescence Spectroscopy by Upconversion with Tilted Gate Pulses. *Physical Chemistry Chemical Physics* **2005**, *7*, 1716-1725.

18. Magde, D.; Elson, E.; Webb, W. W., Thermodynamic Fluctuations in a Reacting System—Measurement by Fluorescence Correlation Spectroscopy. *Physical review letters* **1972**, *29*, 705.
19. Elson, E. L., Fluorescence Correlation Spectroscopy: Past, Present, Future. *Biophysical journal* **2011**, *101*, 2855-2870.
20. Rigler, R.; Elson, E. S., Fluorescence Correlation Spectroscopy*: Theory and Applications*; Springer Science & Business Media, 2012; Vol. 65.
21. Kral, T.; Langner, M.; Beneš, M.; Baczyńska, D.; Ugorski, M.; Hof, M., The Application of Fluorescence Correlation Spectroscopy in Detecting DNA Condensation. *Biophysical chemistry* **2002**, *95*, 135-144.
22. O'Connor, D., *Time-Correlated Single Photon Counting*; Academic press, 2012.
23. Akhtar, M. B., Fluorescence Lifetime Measurement Using Time Correlated Single Photon Counting. **2010**.
24. McKinnon, A.; Szabo, A.; Miller, D., The Deconvolution of Photoluminescence Data. *The Journal of Physical Chemistry* **1977**, *81*, 1564-1570.
25. O' Connor, D.; Ware, W.; Andre, J., Deconvolution of Fluorescence Decay Curves. A Critical Comparison of Techniques. *Journal of Physical Chemistry* **1979**, *83*, 1333-1343.
26. Hu, C. M.; Zwanzig, R., Rotational Friction Coefficients for Spheroids with the Slipping Boundary Condition. *The Journal of Chemical Physics* **1974**, *60*, 4354-4357.
27. Gierer, A.; Wirtz, K., Molekulare Theorie Der Mikroreibung. *Zeitschrift für Naturforschung A* **1953**, *8*, 532-538.
28. Dote, J. L.; Kivelson, D.; Schwartz, R. N., A Molecular Quasi-Hydrodynamic Free-Space Model for Molecular Rotational Relaxation in Liquids. *The Journal of Physical Chemistry* **1981**, *85*, 2169-2180.
29. Mali, K.; Dutt, G.; Mukherjee, T., Do Organic Solutes Experience Specific Interactions with Ionic Liquids? *The Journal of chemical physics* **2005**, *123*.
30. Dutt, G., Molecular Rotation as a Tool for Exploring Specific Solute–Solvent Interactions. *ChemPhysChem* **2005**, *6*, 413-418.
31. Dutt, G., Influence of Specific Interactions on the Rotational Dynamics of Charged and Neutral Solutes in Ionic Liquids Containing Tris (Pentafluoroethyl) Trifluorophosphate (FAP) Anion. *The Journal of Physical Chemistry B* **2010**, *114*, 8971-8977.
32. Dutt, G.; Raman, S., Rotational Dynamics of Coumarins: An Experimental Test of Dielectric Friction Theories. *The Journal of Chemical Physics* **2001**, *114*, 6702-6713.
33. Karve, L.; Dutt, G., Rotational Diffusion of Neutral and Charged Solutes in Ionic Liquids: Is Solute Reorientation Influenced by the Nature of the Cation? *The Journal of Physical Chemistry B* **2011**, *115*, 725-729.
34. Biswas, R.; Bagchi, B., Ionic Mobility in Alcohols: From Dielectric Friction to the Solvent–Berg Model. *The Journal of chemical physics* **1997**, *106*, 5587-5598.
35. Edward, J. T., Molecular Volumes and the Stokes-Einstein Equation. *Journal of chemical education* **1970**, *47*, 261.
36. Lawler, C.; Fayer, M. D., The Influence of Lithium Cations on Dynamics and Structure of Room Temperature Ionic Liquids. *The Journal of Physical Chemistry B* **2013**, *117*, 9768-9774.
37. Gangamallaiah, V.; Dutt, G., Rotational Diffusion of Nonpolar and Ionic Solutes in 1-Alkyl-3-Methylimidazolium Bis (Trifluoromethylsulfonyl) Imides: Is Solute Rotation Always Influenced by the Length of the Alkyl Chain on the Imidazolium Cation? *The Journal of Physical Chemistry B* **2012**, *116*, 12819-12825.
38. Fruchey, K.; Fayer, M., Dynamics in Organic Ionic Liquids in Distinct Regions Using Charged and Uncharged Orientational Relaxation Probes. *The Journal of Physical Chemistry B* **2010**, *114*, 2840-2845.

39. Majhi, D.; Seth, S.; Sarkar, M., Differences in the Behavior of Dicationic and Monocationic Ionic Liquids as Revealed by Time Resolved-Fluorescence, Nmr and Fluorescence Correlation Spectroscopy. *Physical Chemistry Chemical Physics* **2018**, *20*, 7844-7856.
40. Mahapatra, A.; Ghosh, J.; Barik, S.; Parida, S.; Sarkar, M., Understanding the Influence of Ethylene Glycol on the Microscopic Behavior of Imidazolium-Based Monocationic and Dicationic Ionic Liquid. *Chemical Physics Impact* **2023**, *7*, 100331.
41. Damodaran, K., Recent Advances in Nmr Spectroscopy of Ionic Liquids. *Progress in Nuclear Magnetic Resonance Spectroscopy* **2022**, *129*, 1-27.
42. Menjoge, A.; Dixon, J.; Brennecke, J. F.; Maginn, E. J.; Vasenkov, S., Influence of Water on Diffusion in Imidazolium-Based Ionic Liquids: A Pulsed Field Gradient Nmr Study. *The Journal of Physical Chemistry B* **2009**, *113*, 6353-6359.
43. Annat, G.; MacFarlane, D. R.; Forsyth, M., Transport Properties in Ionic Liquids and Ionic Liquid Mixtures: The Challenges of Nmr Pulsed Field Gradient Diffusion Measurements. *The Journal of Physical Chemistry B* **2007**, *111*, 9018-9024.
44. Cui, J.; Kobayashi, T.; Sacci, R. L.; Matsumoto, R. A.; Cummings, P. T.; Pruski, M., Diffusivity and Structure of Room Temperature Ionic Liquid in Various Organic Solvents. *The Journal of Physical Chemistry B* **2020**, *124*, 9931-9937.
45. Daniel, C. I.; Vaca Chávez, F.; Feio, G.; Portugal, C. A. M.; Crespo, J. G.; Sebastião, P. J., 1h Nmr Relaxometry, Viscometry, and Pfg Nmr Studies of Magnetic and Nonmagnetic Ionic Liquids. *The Journal of Physical Chemistry B* **2013**, *117*, 11877-11884.
46. Davidowski, S. K.; Thompson, F.; Huang, W.; Hasani, M.; Amin, S. A.; Angell, C. A.; Yarger, J. L., Nmr Characterization of Ionicity and Transport Properties for a Series of Diethylmethylamine Based Protic Ionic Liquids. *The Journal of Physical Chemistry B* **2016**, *120*, 4279-4285.
47. Nordness, O.; Brennecke, J. F., Ion Dissociation in Ionic Liquids and Ionic Liquid Solutions. *Chemical Reviews* **2020**, *120*, 12873-12902.
48. Wennmalm, S.; Edman, L.; Rigler, R., Conformational Fluctuations in Single DNA Molecules. *Proceedings of the National Academy of Sciences* **1997**, *94*, 10641-10646.
49. Zhang, X.; Poniewierski, A.; Sozański, K.; Zhou, Y.; Brzozowska-Elliott, A.; Holyst, R., Fluorescence Correlation Spectroscopy for Multiple-Site Equilibrium Binding: A Case of Doxorubicin–DNA Interaction. *Physical Chemistry Chemical Physics* **2019**, *21*, 1572-1577.
50. Wu, E. C.; Kim, H. J.; Peteanu, L. A., Spectroscopic and Md Study of Dynamic and Structural Heterogeneities in Ionic Liquids. *The Journal of Physical Chemistry B* **2017**, *121*, 1100-1107.

Chapter 3

Comparison between Pyrrolidinium-based and Imidazolium-based Dicationic Ionic Liquids: Intermolecular Interaction, Structural Organization and, Solute Dynamics

---

Amita Mahapatra, Manjari Chakraborty, Sahadev Barik and Dr. Moloy Sarkar. *Physical Chemistry Chemical Physics* **2021**, 23, 21029-21041.

CHAPTER 3

Abstract

This chapter demonstrates the difference in the behaviour of imidazolium and pyrrolidinium-based dicationic ionic liquids (DILs) in terms of the intermolecular interactions, microscopic-structure and dynamics. For this purpose, two DILs, based on imidazolium and pyrrolidinium cation are synthesized subsequently investigated by exploiting combined steady sate and time resolved fluorescence, Electron paramagnetic resonance (EPR) and Nuclear magnetic resonance (NMR) spectroscopic techniques. Data obtained for DILs have also been compared with their corresponding mono-cationic counterpart (MILs) to evaluate and understand the distinctive characteristics of the DILs in contrast with the corresponding MILs. Steady state emission and EPR data has revealed that pyrrolidinium-based DIL is slightly less polar than that of imidazolium-based DIL. Temperature-dependent fluorescence anisotropy decay of two probes, perylene and MPTS (8-Methoxypyrene-1,3,6-trisulfonate), have been measured in DILs as well as in MILs. Solute−solvent coupling constants obtained from the experimentally measured reorientation times with the aid of Stokes−Einstein−Debye hydrodynamic (SED) theory have indicated appreciable differences in the dynamics of both the solutes on going from MILs to DILs. More interestingly, the outcome of the NMR study has suggested that the alkyl spacer chain in the imidazolium-based DIL exists in the folded form, but pyrrolidinium-based DIL remains in straight chain conformation. Inherently, the outcomes of all of these studies have depicted that the microscopic structural organisation in imidazolium and pyrrolidinium-based DILs are different from each other as well as from their respective mono-cationic counterparts.

CHAPTER 3

3. 1. Introduction

In the recent past room temperature ionic liquids (RTILs) have occupied a special place in the field of modern chemistry owing their importance in chemical, material and biologicalsciences[1-5]. In this context, one of the main focus of the current day research is to design and develop ionic liquids based solvent systems having desired physiochemical properties.[6-8] For this purpose, several pathways have been adopted, such as mixing of ILs, solvent co-ordination or by incorporation of a functional group to the constituent ions or by chemical synthesis of a dication.[9-10] Among them, geminal dicationic ionic liquids which consists of two singly charged distal cationic head linked through a simple hydrocarbon linker chain (alkyl spacer) or functional carbon chain and paired with too singly charged anion are found to have particular importance.[11]This is because as compared to monocation-based IL systems physicochemical properties of germinal dication-based ILs are found to be superior in terms higher density, higher viscosity, higher melting point, higher surface tension as well as higher thermal and electrochemical stability.[12-14] Since DILs are also structurally very close to traditional MILs, DILs can also be used as a good model system to identify the hidden effects in the IL that come from multiple charge centres rather than their individual identities. Although DILs have been used extensively in many different areas of chemistry, studies on the microscopic structure and dynamics of this non-molecular liquids are still at the early stage, [15-19] and majority of these studies are carried out on imidazolium- based DIL systems.[20-23]

Studies which focus on the local structures and inert molecular interactions involving imidazolium-based DILs have been carried out by exploiting X-ray scattering,[24] molecular dynamics simulation[25] and advanced spectroscopic techniques.[26,27]These studies have suggested that DILs possess significantly different nano-structural organization from MILs. A unique assembly pattern for long linkage chains (folded chain models) in imidazolium-based DILs have reported by MD simulation by several workers and subsequent evidences have been observed

experimentally.[25,26] Interestingly, in all the above studies it has been emphasized that the planarity of the ring and acidity of C(2)-H of the imidazolium moiety have significant roles in governing the structural organisation and dynamics in imidazolium-based DILs. Therefore, studies on structural analysis of the non-aromatic cation based DILs such as pyrrolidinium-based ILs are expected to be interesting as they are non-planar and do not possess acidic C(2)-hydrogen. Moreover, pyrrolidinium-based ILs have been recognized as an interesting system owing to their higher thermal stability, wider electrochemical window as well as lower toxicity compared to the many of the imidazolium-based analgues.[28,29] We would like to note here that both imidazolium and pyrrolidinium cations are quaternary ammonium salt of low symmetry. However, imidazolium ring is planar and aromatic but pyrrolidinium ring is non-planar. Due to the difference in the structure of cationic head such as existence of charge delocalisation in imidazolium ring and steric crowding owing to the alkyl group in the pyrrolidinium ring, a small change in the cation-anion interaction and their influence on microstructure and dynamic properties, especially concerning molecular motions, solute diffusion in these media have been observed. Saito and co-workers[30] have reported the lower melting point and enthalpy of fusion of pyrrolidinium-based MIL than that of imidazolium-based MIL containing same alkyl (butyl) chain. Tsuzuki and co-workers[31] observed faster diffusion of ions in imidazolium-based MILs than that of pyrrolidinium-based MILs on account of planar nature of imidazolium cation. In addition to physio-chemical properties, both these types of ionic liquids also show differences in the intermolecular vibrational and conformational flexibility.[32,33] From these discussions one can readily understand that most of the studies have been performed by focussing on the imidazolium and pyrrolidinium-based MILs.

It is pertinent to mention in this context that although germinal pyrrolidinium ILs are not particularly well known, germinal pyrrolidinium salts are well known and particularly common in their use as templates for the synthesis of porous metal organic framework systems.

Studies have shown that owing to their unique structural features, these molecules can assemble into solution, and above critical aggregation concentration, give rise to 3-dimensional networked structure.[34] In this context, Li and co-workers[35] have demonstrated that geminin surfactants are particularly superior than their single head partner in terms of surface activity and lower critical micellar concentration. All the above discussions also highlight that although geminal pyrrolidinium salt in solution state has been studied, solvent free DILs (neat DILs) based on germinal-pyrrolidinium dication have not been studied well. It should also be noted here that neat pyrrolidinium- based DILs may exhibit different properties than they show in their solution state. Hence, it would be a worthwhile objective to study both imidazolium and pyrrolidinium - based DILs along with the structurally similar MILs so as to understand the kinship among intermolecular interaction, structure and dynamics for these systems. Moreover, this study is also expected to be helpful in unravelling the role of cationic head groups, if any, on the structural organisation of the said DILs.

Keeping all the above facts in mind, in the present investigation, the structure and dynamics accompanying DILs composed of pyrrolidinium and imidazolium dications as well as their respective mono-cationic counterparts have been analysed by combined steady-state and TRFS, EPR and NMR techniques. For this study the DILs $[C_9(Mpyrr)_2][NTf_2]_2$ and $[C_9(Mim)_2][NTf_2]_2$ have been synthesized and characterized. In this study, in all the concerned ionic liquids (ILs) anion has been fixed as $[NTf_2]^-$. Moreover, in both the DILs alkyl spacer alkyl chain is kept constant (9-membered alkyl group) so that the effect of cationic head group on the overall structural organisation of ILs are understood. The nonyl spacer chain has been chosen due to the fact that the pyrrolidinium- based DIL consisting of a nonyl linker chain is the only pyrrolidinium-based DILs which is liquid at room temperature.[11]To draw a comparison between MILs and DILs, MILs consisting of alkyl chain, close to the length of the alkyl spacer chain in DILs, such as $[C_8Mim][NTf_2]$ and $[C_8MPyrr][NTf_2]$ as well as consisting of alkyl chain, close

to the half of the length of the alkyl spacer of DILs, such as [C_4Mim][NTf_2] and [C_4MPyrr][NTf_2] have been chosen in the study. Outcome of the comparative studies on these MILs and DILs are expected to be helpful in understanding the role of additional headgroup on the structural organisation of the concerned DILs. Steady state emission and EPR data have given idea about the medium polarity. Rotational dynamic of a neutral probe (perylene) and a negatively charged probe (MPTS) in the above DILs as well as in corresponding MILs have been investigated through time-resolved fluorescence anisotropy studies to have an in-depth understanding of the solute–solvent, solvent–solvent interactions and structural organization of the media. Additionally, NMR studies have also been used in understanding the structural organisation of DILs. The outcome of the present study has provided interesting insights in terms of understanding the microscopic behaviour of DILs in general and of pyrrolidinium-based DILs in particular. Chemical structure of ILs and probe molecules have been provided in scheme 3.1.

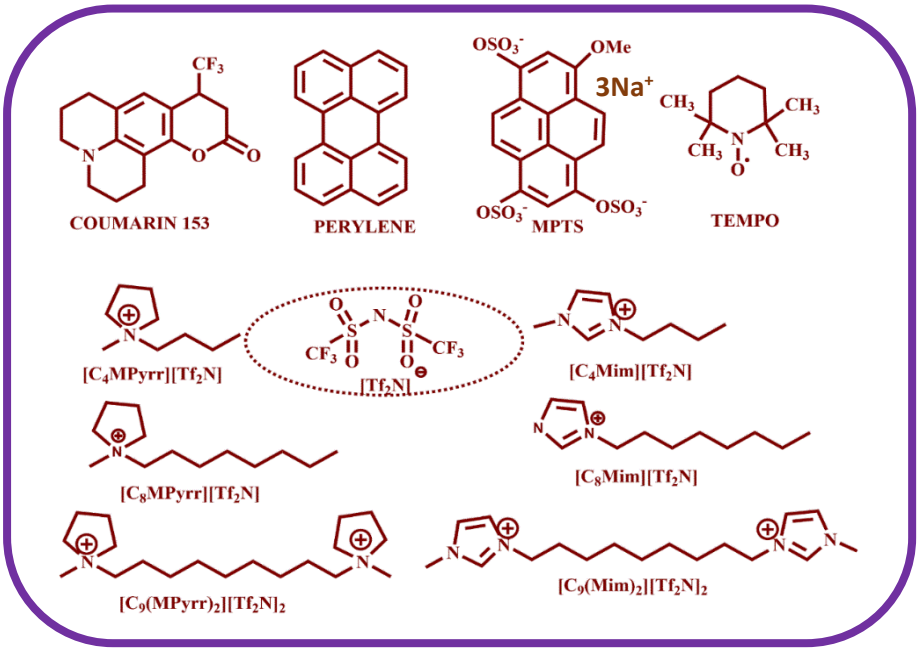

MPTS:8-methoxypyrene-1,3,6-trisulfonateTEMPO:2,2,6,6-tetramethylpiperidine-1-oxyl

[C_4MPyrr] [NTf_2]:1-butyl-1-methyl pyrrolidinium bis(trifluoromethanesulfonyl)imide.

[C_4Mim] [NTf_2]:1-butyl-3-methyl imidazolium bis(trifluoromethanesulfonyl)imide.

[C_8MPyrr] [NTf_2]:1-methyl-1-octyl pyrrolidinium bis(trifluoromethanesulfonyl)imide.

[C_8Mim] [NTf_2]:1-methyl-3-octyl imidazolium bis (trifluoromethanesulfonyl)imide.

$[C_9(Mpyrr)_2][NTf_2]_2$:1,9-bis-(1-methylpyrrolidinium-1-yl)nonanebis(trifluoromethylsulfonyl)amide.

$[C_9(Mim)_2][NTf_2]_2$:1,9-bis-(3-methylimidazolium-1-yl)nonanebis(trifluoromethylsulfonyl)amide.

Scheme 3.1. Structures and abbreviations of ionic liquids (ILs) and probe molecules used in the present study.

3. 2. Experimental techniques and methods

The MILs were purchased from TCI chemicals and IoLi-Tec. DILs have been prepared by following a standard procedure, as described in chapter 2. The NMR spectra of synthesized ILs can be found in Appendix 3 (Figures APX3.1, APX3.2 and APX3.3). The sample preparation methods, and the experimental framework for EPR, TRFS, and NMR studies are elaborated in Chapter 2.

3.3. Results and Discussion

3.3.1. Steady state emission and EPR data: Solute-solvent interaction, usually depends on various parameters like polarity, H-bond acidity and basicity, polarizability etc. A little variation in the structure of cation or anion can alter the solvent parameters of an IL, which in turn influences their solvation ability, diffusion as well as reaction rates.[36,37]It has been suggested in a recent paper that the cationic head of the ionic liquid is largely responsible for determining the polarity of an ionic liquid.[38]One of the methods often employed to estimate the polarity of solvents is based on the analysis of intramolecular charge-transfer (ICT) fluorescence band of C153 whose position is responsive to the polarity of the medium.[39]A shift in the emission maximum of C153 towards longer wavelength is observed with an increase in the polarity of the medium. The steady-state normalized emission spectra of C153 in both pyrrolidinium and imidazolium-based MILs and DILs are shown in Figure 3.1. No remarkable difference in the emission maxima of C153 in $[C_4MPyrr][NTf_2]$ (λ_{max}=519nm) and $[C_9(MPyrr)_2][NTf_2]_2$(λ_{max}=520nm) has been observed from Figure 3.1a. However, a red shift of about 5nm is observed in the emission maximum of C153 on going from $[C_4Mim][NTf_2]$ and $[C_9(Mim)_2][NTf_2]_2$ which consisted with earlier literature report.[26] Again, as compared to

the pyrrolidinium-based ILs the emission maxima in case of C153 has been observed to be at higher wavelength in imidazolium-based ILs (Figure 3.1b).This indicates that C153 experience slightly less polar enviroment in pyrrolidinium-based ILs in comparison toimidazolium-based ILs. This may be due to the non-planar nature of pyrrolidinium cation which is less polarizable than that of planar imidazolium cation.[33]

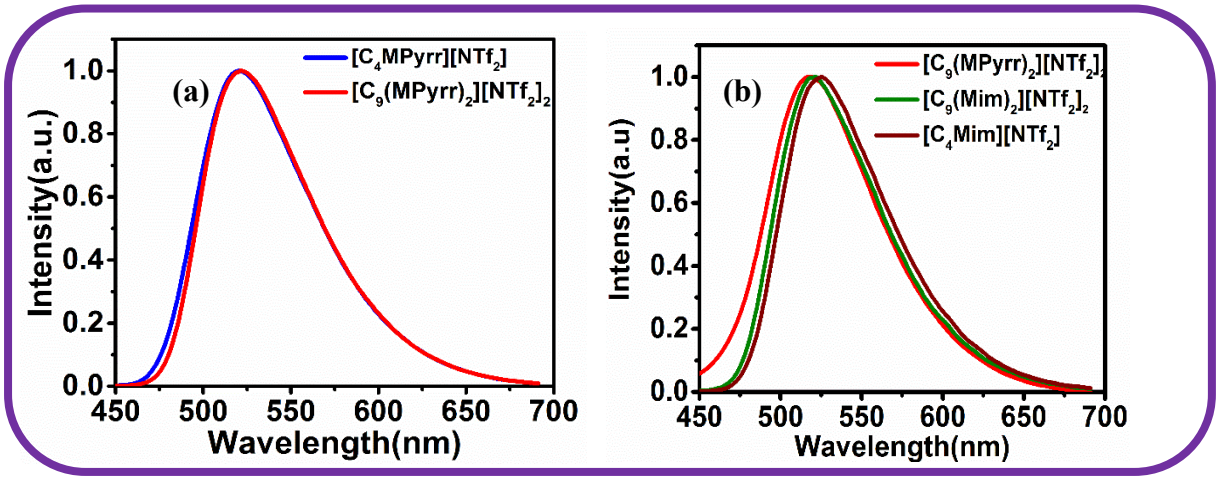

Figure 3.1. The normalized emission spectra ($\lambda_{exc.}$=375nm) of C153 in (a) $[C_4MPyrr][NTf_2]$ and $[C_9(MPyrr)_2][NTf_2]_2$ and (b) in$[C_4Mim][NTf_2]$, $[C_9(MPyrr)_2][NTf_2]_2$ and $[C_9(Mim)_2][NTf_2]_2$

However, the minute change in the micro-polarity of a given medium is not always predictable just by monitoring the steady-state fluorescence spectra of C153.[40]So, further attempt has been made to determine the micro-polarity of concerned ILs by exploiting EPR spectroscopy. We note here that^{14}N isotropic hyperfine splitting constant (a_N/G), in the EPR spectrum the charge transfer (CT) structure observed in N−O group determines the stability of the nitroxide free radicals like TEMPO. The polar solvent stabilises the ground-state CT structure of the N−O group and this increase in stabilisation is found to be proportional to the increased spin density around the nitrogen atom. Therefore, by estimating the value of a_N/G for TEMPO in the respective ILs the knowledge on the polarity of the corresponding medium can be obtained. Similar method has also been used previously by several workers to estimate the E_T(30) value

ILs.[41, 42]The EPR spectra of TEMPO has been represented in Figure 3.2 along with the corresponding simulated spectra in the concerned ILs. From Figure 3.2, an appreciable broadening of the line shape in EPR signals have been observed in DILs in comparison to MILs. The higher viscosity of DILs in comparison to MILs and the medium inhomogeneity is the key factor for the observed nature in the EPR signal.[26] Therefore, in the present scenario, the anisotropic nature of the EPR signal in both DILs compared to MILs indicates greater inhomogeneity in both DILs compared to MILs.

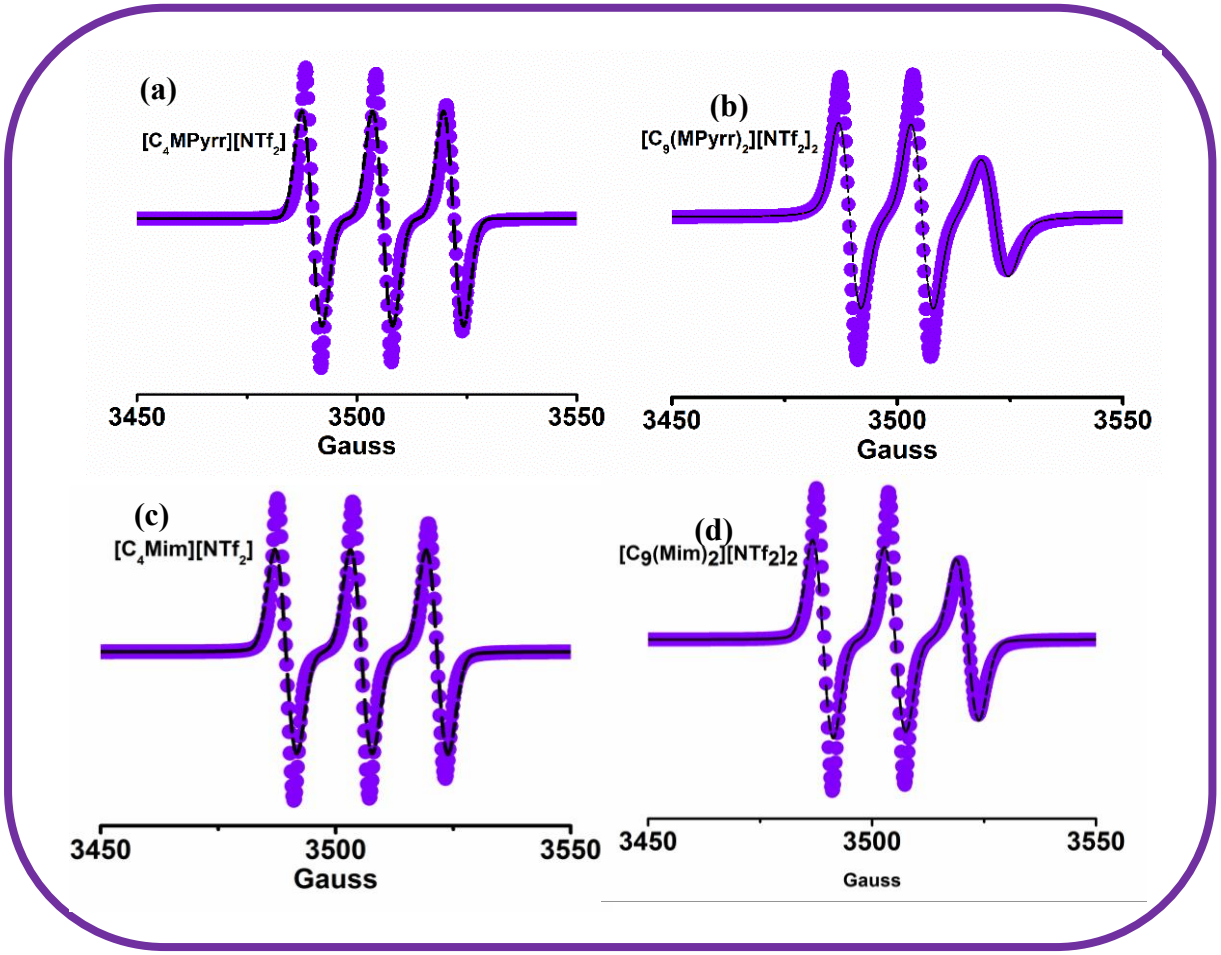

Figure 3.2. EPR spectra of TEMPO (a)[C_4MPyrr][NTf_2], (b)[C_9(MPyrr)$_2$][NTf_2]$_2$,(c) [C_4Mim][NTf_2] and (d)[C_9(Mim)$_2$][NTf_2]$_2$.The black lines indicate the simulated spectra.

To estimate the micro-polarity of the ILs quantitatively, E_T(30), the a_N/G value of each ILs are determined from their corresponding EPR spectra. The distance between the maxima of two consecutive hyperfine line usually represents the hyperfine coupling , a_N/G. But in the case of

DILs as spectral broadening has occurred, a_N/G values are calculated by taking the distance between the centres of the relevant adjacent hyperfine lines. After that, a plot of the hyperfine splitting parameters (a_N/G) of TEMPO in a few known organic solvents against the solvent polarity parameter E_T (30) for those solvents has been created.

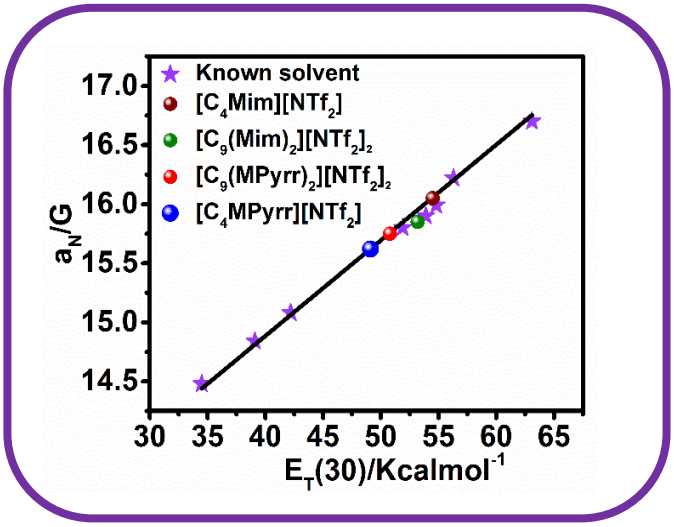

Figure 3.3. Plot of a_N/G Vs. E_T (30) values for TEMPO in MILs and DILs.

Table 3.1 enlists the E_T (30) values of the selected solvents. The plot of a_N/G versus E_T (30) for those solvent systems has been illustrated in Figure 3.3. From this graph the E_T (30) values of the unknown solvent system are calibrated. Several workers have compared the polarity of ionic liquids with conventional organic solvents such as alcohol, acetonitrile.[26,41]From E_T (30) values in the Table 3.1, it can be inferred that polarities of the imidazolium-based ILs are close to those of short chain alcohol and some poly hydroxyl alcohol, whereas polarities of pyrrolidinium-based ILs are close to long-chain mono-hydroxyl alcohols and benzyl alcohol.[43] This, further indicates that polarities of pyrrolidinium-based ILs are less compared to imidazolium-based ILs. These data also point out that along with the length of the apolar alkyl chain, [44] the charge distribution and symmetry of cationic head in has a vital role in determining their micro-polarity of the concerned medium.

Table 3.1 The a_N/G value of TEMPO in ILs and molecular solvents along with E_T (30) value

Systems	a_N/G	E_T (30) kcal/mol
Water	16.90	63.1[a]
Ethylene Glycol	16.22	56.3[a]
Benzene	14.48	34.5[a]
Chloroform	14.84	39.1[a]
Acetone	15.08	42.2[a]
Benzyl Alcohol	15.78	50.8[a]
$[C_4Mim]$ $[BF_4]$	15.99	54.8[a]
$[C_4Mim]$ $[PF_6]$	15.90	53.9[a]
$[C_4Mim]$ $[NTf_2]$	16.05	54.5[b]
$[C_4MPyrr][NTf_2]$	15.62	49.12[b]
$[C_9(MPyrr)_2][NTf_2]_2$	15.75	50.82[b]
$[C_9(Mim)_2]_2[NTF_2]_2$	15.85	53.21[b]

[a] Taken from reference,[26,41b]Estimated from calibration curve.

3.3.2. Time resolved fluorescence anisotropy studies: To further obtain insights into the microscopic environment of the pyrrolidinium and imidazolium-based DILs the rotational diffusion dynamic of two fluorescent probes, namely perylene (neutral) and MPTS (negatively charged) in these DILs and in the corresponding MILs are carried out by means of time resolved fluorescence anisotropy technique at various temperatures. As the rotational dynamics of a solute in a given solvent is a measure of the friction experienced by it in that medium, it can serve as a tool to probe the microenvironment in the vicinity solute. The two probes addressed here, depending on their different chemical characteristics (neutral or charged) posit themselves in the distinct micro- regions (polar and nonpolar) of the concerned ILs.[45,46]So, such studies may provide a clearer picture of any difference or similarity of microstructures in the imidazolium and pyrrolidinium-based DILs. Prior to the above studies the viscosities of the ILs are measured in the temperature range 293-313k.The viscosity at a particular temperature for pyrrolidinium-based ILs are found to be slightly higher than that of imidazolium-based ILs which is consistent with the earlier literature report.[11]The measured viscosities have also been

verified with the reported value in the literature.[11, 47]The temperature dependence of the viscosities of all the ILs fits well to the well-established Vogel−Fulcher Tammann (VFT) equation (equation 3.1).[48,49]

$$\eta = \eta_0 \, exp\left[\frac{B}{(T-T_0)}\right] \qquad (3.1)$$

Where η_0(cP), B (k), and T_0(k) are fitting parameters.

The VFT plots can be found in Figure APX3.3. The rotational correlation time (τ_r) of perylene and MPTS in the ILs at different temperature along with viscosities at corresponding temperature are enlisted in Table 3.2 and the detailed about the consequences are discussed below.

3.3.2.1.MPTS. MPTS being a negatively charged species, prefer to locate itself in the polar region in the ILs. Along with columbic interaction it can also interact with the solvent molecules through the formation of hydrogen bond using its SO_3^- moiety.[45]In the present case, MPTS has been chosen as the probe in time resolved fluorescence anisotropy study so that we can monitor the difference, if any, in the nature of polar domain formed by imidazolium and pyrrolidinium cationic head of the respective ILs effectively.

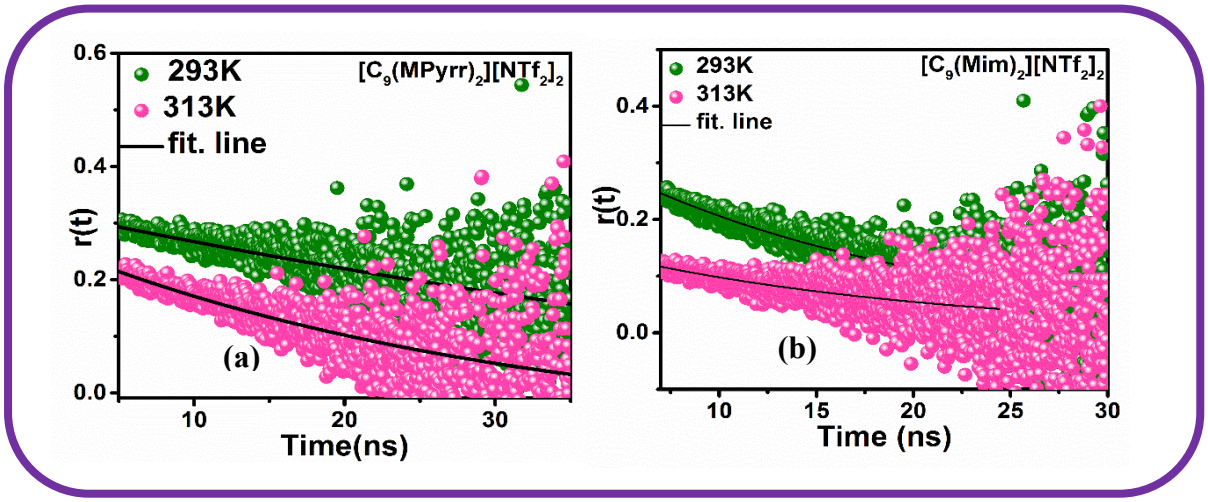

Figure 3.4. Decay plots for MPTS in(a) $[C_9(MPyrr)_2][NTf_2]_2$ and (b) $[C_9(Mim)_2][NTf_2]_2$

Table 3. 2. Rotational Relaxation Parameter of Perylene and MPTS in MILs and DILs.

Systems	T(k)	Viscositiy (cP)	Perylene		MPTS	
			τ_r(ns)	C_{rot}	τ_r(ns)	C_{rot}
[C_4Mim][NTf_2]	293	63.6	1.57	0.25	10.30	1.43
	298	49.6	1.34	0.28	7.98	1.45
	303	40.4	1.15	0.30	6.90	1.56
	308	33.4	0.97	0.31	5.89	1.64
	313	27.5	0.83	0.33	4.84	1.67
[C_4MPyrr][NTf_2]	293	90.3	1.61	0.18	12.90	1.26
	298	73.2	1.43	0.20	10.50	1.28
	303	58.9	1.23	0.22	9.08	1.41
	308	45.2	1.04	0.24	7.45	1.53
	313	39.2	0.87	0.25	6.50	1.57
[C_8Mim][NTf_2]	293	115.0	1.72	0.15	16.90	1.30
	298	90.3	1.45	0.17	13.50	1.34
	303	72.1	1.24	0.18	10.90	1.38
	308	57.0	1.10	0.20	9.20	1.51
	313	45.2	0.95	0.23	7.90	1.66
[C_8MPyrr][NTf_2]	293	128.2	1.80	0.14	18.30	1.26
	298	99.4	1.56	0.16	14.30	1.30
	303	81.1	1.35	0.17	12.10	1.36
	308	62.8	1.15	0.19	9.55	1.41
	313	51.0	0.99	0.21	8.50	1.57
[C_9($Mim)_2$][NTf_2]$_2$	293	960.1	5.05	0.05	47.04	0.43
	298	655.9	4.30	0.07	37.11	0.51
	303	486.6	3.76	0.08	30.06	0.57
	308	361.5	3.36	0.10	24.30	0.62
	313	272.8	3.14	0.12	19.00	0.66
[C_9($MPyrr)_2$][NTf_2]$_2$	293	1024	6.45	0.06	44.60	0.37
	298	710.2	5.13	0.07	40.95	0.51
	303	535.2	4.36	0.08	35.11	0.60
	308	404.6	3.81	0.11	32.86	0.76
	313	312.5	3.3	0.115	28.59	0.87
Experimental error = ±5%						

The decay plot of MPTS at two different temperature in two DILs [C_9($MPyrr)_2$][NTf_2]$_2$ and [C_9($Mim)_2$][NTf_2]$_2$ are shown in Figure 3.4. The rotational correlation time (τ_r) of MPTS at corresponding temperatures are obtained by fitting the curve with single-exponential function[45] and collected in Table 3.2. From the Figure 3.4 and Table 3.2 it has been observed that the

rotational correlation time (τ_r) of MPTS has been decreased with increase in temperature which are consistent with the lowering of the bulk viscosity of the medium at higher temperature. Moreover, to get an idea about nature of interaction in imidazolium and pyrrolidinium-based ILs, the analysis of rotational diffusion data of MPTS have been done by using the Stokes-Einstein−Debye (SED) hydrodynamic theory.[50]The details regarding SED theory and analysis has been described in Chapter 2 (eq.2.14). The log (τ_r) vs. log (η/T) plots of MPTS along with the boundary conditions for the MILs and DILs have been illustrated in Figure 3.5. From Figure 3.5a, it can be seen that the experimentally determined rotational correlation time (τ_r) of MPTS fall above the stick boundary condition in both the imidazolium and pyrrolidinium-based MILs. As per hydrodynamic terminology this behaviour of MPTS in MILs is called super-stick behaviour. This super-stick behaviour shows that rotation of MPTS in MILs has been hindered due to strong solute-solvent interaction.[45]This can also be confirmed when the data were analysed by estimating the solute-solvent coupling constant (C_{rot}) value, which usually indicate the degree of solute–solvent coupling.

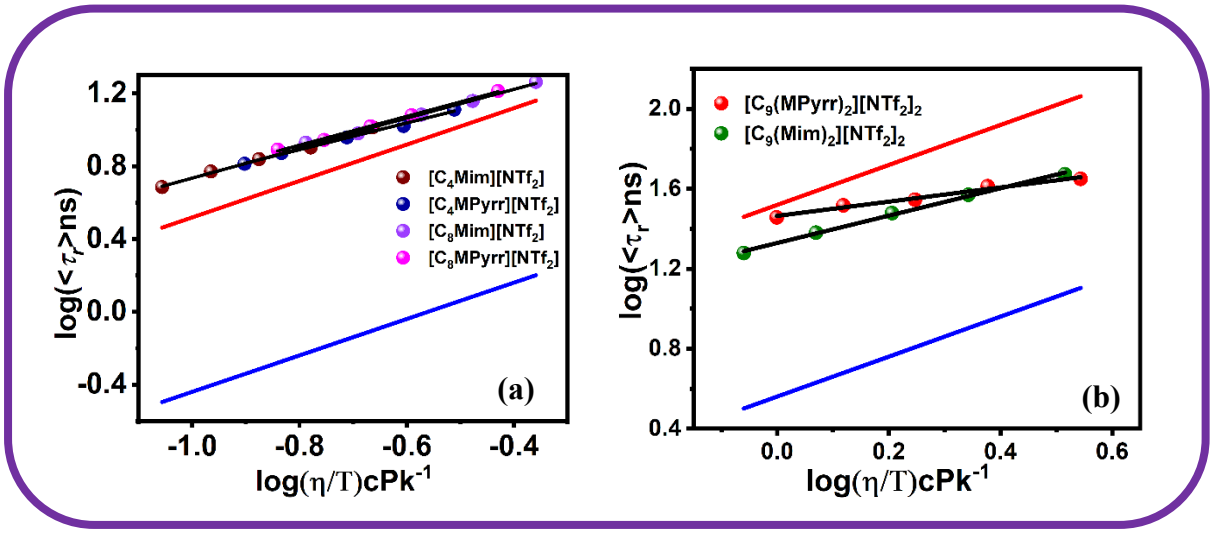

Figure 3.5 SED plot for MPTS in (a) MILs and (b) DILs. The blue, red and black line indicates slip, stick and fit. Line respectively.

The C_{rot} value is determined by $C_{rot} = \tau_r^{exp} / \tau_r^{stk}$, where, τ_r^{exp} and τ_r^{stk} are the experimental and theoretically calculated rotational correlation times, respectively. The average C_{rot} values of MPTS observed in MILs $[C_4MPyrr][NTf_2]$ and $[C_4Mim][NTf_2]$ were found to be 1.41 and 1.55 respectively, whereas the corresponding value in $[C_8MPyrr][NTf_2]$ and $[C_8Mim][NTf_2]$ are found to be 0.17 and 0.19 respectively(The average C_{rot} values have been obtained by averaging this parameter at five different temperature). This higher C_{rot} value (C_{rot}>1) indicates significantly hindered rotation of MPTS in MILs. Previous studies suggest super stick behaviour of MPTS in imidazolium-based MILs are due to the specific hydrogen bond formation between the C(2)-H of imidazole moiety (pK_a = 23.8) and SO_3^- moiety of MPTS.[45]However, in case of pyrrolidinium-based MIL the electrostatic interaction between the pyrrolidinium cation[52]and negatively charged MPTS may have caused the hindered rotation of MPTS . Moreover, the comparable average C_{rot} value indicates that MPTS perhaps present in a similar micro-environment in both the MILs. Again, the experimental rotational correlation time (τ_r) of MPTS has been observed to lie just below the stick boundary in the DILs (Figure 3.5b). Interestingly, relatively less hindered rotation of MPTS have been found in DILs as compared to that in MILs despite of the presence of two cationic heads in the former. The average C_{rot} value for DILs $[C_9(MPyrr)_2][NTf_2]_2$ and $[C_9(Mim)_2][NTf_2]_2$ is estimated to be 0.62 and 0.55 respectively which are lower than that of average C_{rot} value of corresponding MILs. Interestingly, from the comparison of average C_{rot} values of MPTS for butyl, octyl chain containing MILs and DILs one can realize that the behaviour of DILs is neither like butyl chain containing MILs nor like octyl chain containing MILs whose alkyl chain length remains close to the alkyl spacer length of the DIL. Moreover, Figure 3.5a reveals that (τ_r) of MPTS in $[C_8MPyrr][NTf_2]$ and $[C_8Mim][NTf_2]$ still lies above the stick line despite the fact that the length of the alkyl chain in MIL is close to the length of the alkyl spacer in the DILs. The considerable difference in the rotational behaviour of the MPTS in DIL and in the MIL essentially indicates that structural organisation in MILs and

DILs are different and thus clearly establishes the role of the cationic head groups of the DILs for this behaviour. Again, the average rotational coupling constant of MPTS in both the DILs are also found to be nearly similar. But decrease of rotational correlation (τ_r) time with temperature is found not to be same in both the cases. For example, as can be noticed from Table 3.2, that for both the DILs, on-going from 293-313k the viscosity decreases by a factor of 9-fold, whereas the (τ_r) value of MPTS, although decreases by more than two fold in $[C_9(Mim)_2][NTf_2]_2$, it decreases only less than two fold in $[C_9(MPyrr)_2][NTf_2]_2$.This observation indicates that the interaction between MPTS and $[C_9(Mim)_2][NTf_2]_2$ is comparatively stronger than that with $[C_9(MPyrr)_2][NTf_2]$. This data also indicates that the structural organisation of pyrrolidinium and imidazolium-based DILs may be different. In this context we would like to mention that Majhi et.al have reported that the alkyl spacer chain in the imidazolium-based DIL get folded to maximize the cation-anion interaction.[26]Due to this geometry of cation the bulky MPTS couldn't make strong hydrogen bonding interaction with the C (2)-H of imidazolium ring hence inducing faster rotation of MPTS in imidazolium-based DIL. However, Armstrong and co-workers[11] have shown that in the presence of nonaromatic pyrrolidinium rings along with the spacer propyl chain exhibit an elongated molecular shape bearing two nitrogen atoms laying on the C-3 plane of $[C_3(MPyrr)_2]^{2+}$in contrary to that observed in dication of $[C_3(Mim)_2]^{2+}$ where the propyl chain becomes highly twisted. Cummings and co-workers have also suggested that the alkyl linker chain in the imidazolium- based DILs get folded as the flexibility of the chain increases with increase in the number of carbon atom.[25] So, to obtain more idea about the role of cationic head group of ILs on the structural organization of apolar domain formed by alkyl group (tail part), the rotational dynamics of a neutral probe, perylene, has been investigated in all these ILs.

3.3.2.2. Perylene. Perylene is a neutral probe and due to its apolar nature it generally locates itself in the apolar (alkyl) region of RTILs.[45]It is important to note here that the nature of the cationic heads in ILs has profound effect on the overall micro-heterogeneous nano-structure

of ILs, and in particular, on the formation apolar domain formed due to the segregation of alkyl chain [53-55] We have chosen a fixed alkyl chain length in case of DILs and MILs. So, the analysis of the rotational motion of perylene is expected to give idea about the nature of apolar domain in pyrrolidinium and imidazolium-based DILs as well as in the MILs. The decay plot of perylene at two different temperature in two DILs $[C_9(MPyrr)_2][NTf_2]_2$ and $[C_9(Mim)_2][NTf_2]_2$ are shown below in Figure 3.6. The rotational correlation time (τ_r) of perylene at all temperatures are obtained by fitting the curve with bi-exponential function[45] and collected in Table 3.2. From the Figure 3.6 and Table 3. 2 it is observed that the rotational correlation time (τ_r) of perylene has been decreased with increase in temperature which are consistent with the lowering of viscosity at higher temperature. For a given temperature, the rotational correlation time (τ_r) of $[C_9(MPyrr)_2][NTf_2]_2$ is found to be slightly higher than that of $[C_9(Mim)_2][NTf_2]_2$ due to the higher viscosity of the former than the later. A similar trend is also observed when we compare the corresponding MILs. But, interestingly, upon going from MILs to DILs, although there is around 15-fold increase in bulk viscosity, the (τ_r) value has been increased only by two-fold indicating a faster rotation of perylene in DILs than that of MILs.

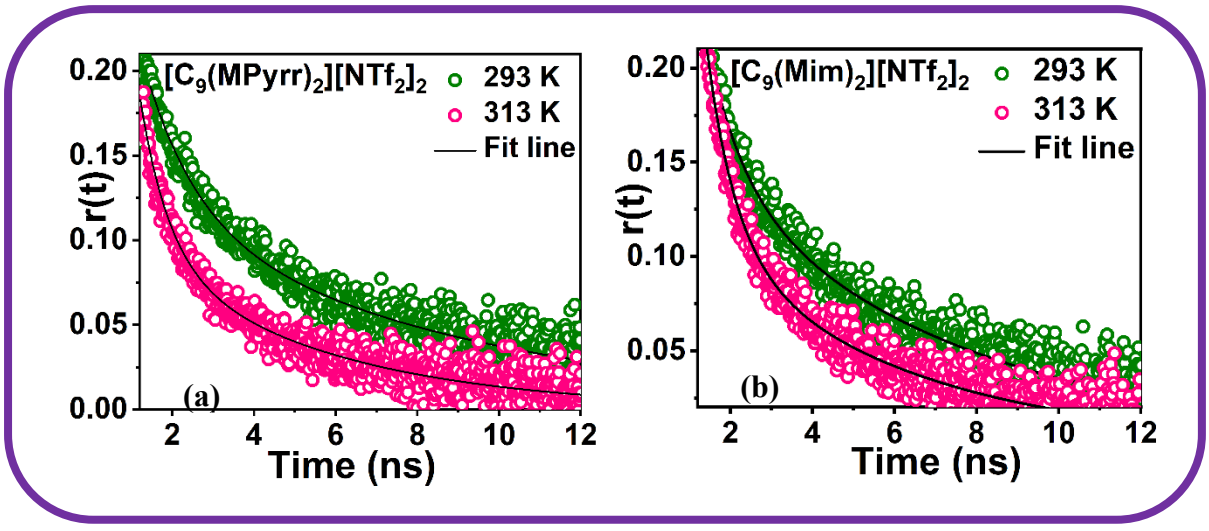

Figure 3.6. Decay plots of perylene (a) in $[C_9(MPyrr)_2][NTf_2]_2$ and (b) $[C_9(Mim)_2][NTf_2]_2$

To get more insight to the perylene and ILs interaction we have analysed the experimental results using SED theory. The log (τ_r) vs. log (η/T) of perylene in the MILs and the DILs are provided in Figure 3.7. From Figure 3.7a, it is clear that the rotational correlation time (τ_r)of perylene in both of the DILs $[C_9(MPyrr)_2][NTf_{2s}]_2$ and $[C_9(Mim)_2][NTf_2]_2$ lies close to slip line, even crosses the slip line while that of corresponding MILs lies in between theoretically predicted stick and 1slip line (Figure 3.7b). The average C_{rot} values of perylene in $[C_8MPyrr][NTf_2]$ and $[C_8Mim][NTf_2]$ are found to be 0.17 and 0.19 respectively whereas the corresponding values in MILs, $[C_4MPyrr][NTf_2]$ and $[C_4Mim][NTf_2]$,are found to be 0.21 and 0.26 respectively. The lower C_{rot} value in octyl chain containing MIL can be attributed to the larger size of the solvent molecule which induces lower friction to the rotating solute. The distinct feature of DILs can again be realized by looking at Figure 3.7b. As can be seen, the(τ_r)of perylene still lies in between stick and slip line in $[C_8MPyrr][NTf_2]$ and $[C_8Mim][NTf_2]$ even though the length of the alkyl chain for these MILs remains close to that present in DILs, $[C_9(MPyrr)_2][NTf_2]_2$ and $[C_9(Mim)_2][NTf_2]_2$. This dependence can be understood by considering the pertinent of the van der Waals interactions between the neutral perylene with the alkyl chain of the ILs.

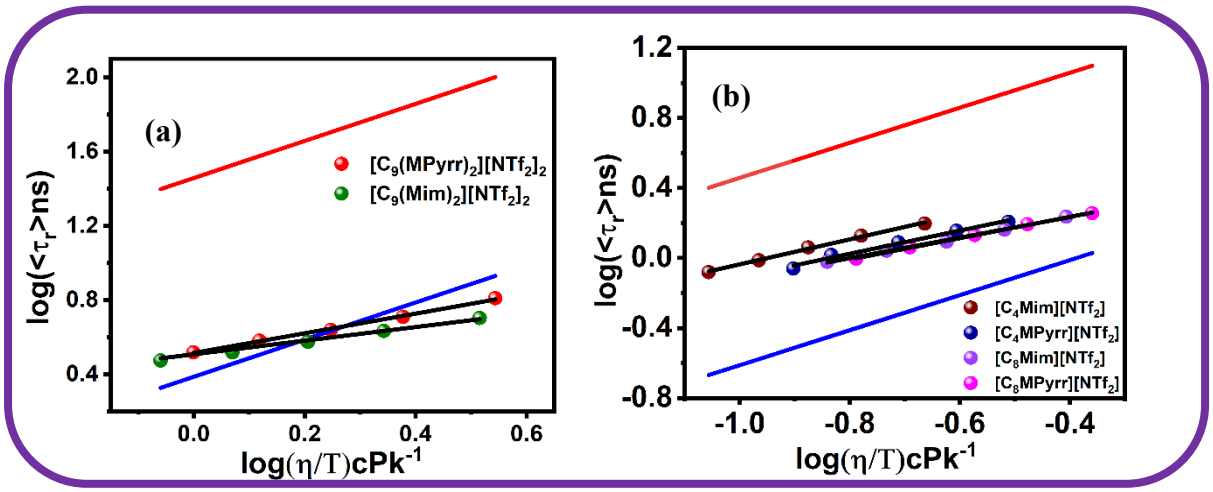

Figure 3.7. SED plot for perylene in (a) DILs and (b) MILs. The blue, red and black line indicates slip, stick and fit. line respectively.

There of course is a strong attractive interaction between perylene and MILs than that of DILs. It is evident from the Table 3.2 the average C_{rot} values of perylene with $[C_9(MPyrr)_2][NTf_2]_2$ and $[C_9(Mim)_2][NTf_2]_2$ are 0.088 and 0.084 respectively, which are close to theoretically predicted C_{slip} value (0.085) of perylene. But, according to SED theory the rotational dynamics of a solute follows slip hydrodynamic if the size (van der Waals volume) of the solute and solvent are similar.[56]But the van der Waals volume of $[C_9(MPyrr)_2][NTf_2]_2$ and $[C_9(Mim)_2][NTf_2]_2$ are found to be 387cm^3 and 366cm^3(calculated following literature method) respectively, which are quite bigger than the van der Waals volume of perylene ($V_m = 225cm^3$). Several workers have explained the faster rotation of non-polar solute in the vicinity of bigger sized solvent molecules with the help of Dote–Kivelson–Schwartz (DKS) theory.[57] The details regarding DKS theory have been provided in chapter 2. Figure 3.8 illustrates a plot of $\log(\tau_r)$ vs. $\log(\eta/T)$ for perylene with their modified boundary condition obtained from DKS theory. It can be observed from Figure 3.8 that the (τ_r) of perylene in DILs fall within the boundary predicted by DKS theory. The dotted green and yellow lines corresponds to the DKS line for $[C_9(MPyrr)_2][NTf_2]_2$ and $[C_9(Mim)_2][NTf_2]_2$ respectively. This observation illustrates that the free volume in DILs has significantly influenced the rotational behaviour of perylene due to the fact that free volume offers lower friction to the perylene and thereby induces its faster rotation. This behaviour of perylene in DILs in terms of hydrodynamic theory is termed as the sub-slip behaviour.[58,59]

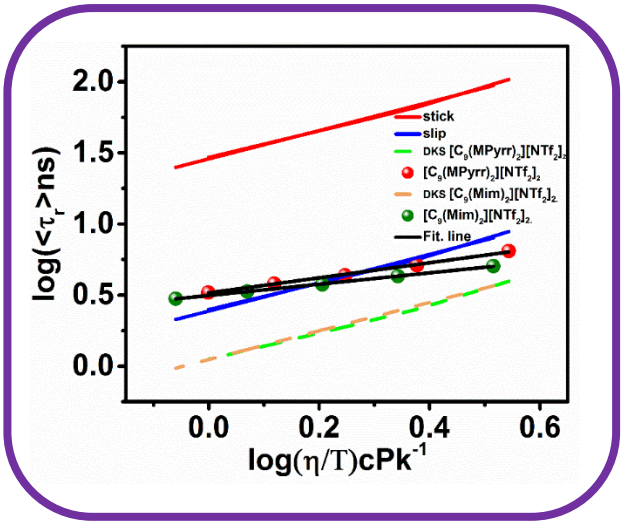

Figure 3.8 log (τ_r) vs. log (η/T) plot of Perylene with modified boundary condition C_{DKS}.

Further evidences are found when the data are analysed with the help of power law empiricalrelationship.[60] The power law equation,$\tau_r = A(\eta/T)^n$where A and n are constants and exponent n represents the extent of non-linearity. Table 3.3 represents the parameter obtained by fitting the (τ_r) value at different temperature and viscosity to the power law equation and the plots can be found in Figure APX.3.4. From Table 3.3 it is clear that the value of the n deviate from unity for all the ILs and such deviation has clearly informed the disassociation of rotational diffusion motion of the perylene in ILs from the bulk viscosity of the ILs. It has been previously shown by several workers that the decoupling of rotational diffusion of solute from bulk viscosity indicates inhomogeneity in IL media.[61,62] Further, from Table 3.3 we can see that the extent of deviation from unity is more in case of DILs than that of MILs, indicting more structural heterogeneity in DILs. Such deviation has been seen to be more as the alkyl chain length in MILs has been increased.

Table 3.3. Parameters A and n obtained from the fitting of the Power law equation $\tau_r = A(\eta/T)^n$

Systems	A	n
$[C_4Mim][NTf_2]$	4.73±0.01	0.71 ± 0.025
$[C_4MPyrr][NTf_2]$	3.57±0.02	0.67 ± 0.045
$[C_8Mim][NTf_2]$	2.88±0.01	0.58±0.021
$[C_8MPyrr][NTf_2]$	2.95±0.01	0.60±0.010
$[C_9(Mim)_2][NTf_2]_2$	3.22±0.01	0.31 ± 0.021
$[C_9(MPyrr)_2][NTf_2]_2$	3.27±0.03	0.52 ± 0.015

Again, comparing the n value of DILs deviation from linearity is found to be more in imidazolium-based DIL. This indicates that the inhomogeneity is more pronounced in imidazolium-based DIL than that of pyrrolidinium-based DIL. This may be the result of different structural organisation of alkyl chain in DILs, thereby the micro-viscosity felt by perylene in both the DILs are also different.

3.3.3. PFG-NMR Studies. We have further exploited PFG-NMR technique to monitor self-diffusion of cations in all the concerned ILs. The translational diffusion coefficient (D_T) depends on the nature size, shape as well as geometry of the diffusing species.[63]So, the estimation of self-diffusion coefficients of cationic moieties in all the ILs may give us idea about the nature of diffusing species. The diffusion coefficients of cations in both DILs and MILs obtained at variable temperature range of 293-313k and collected in Table 3.4.

Table 3.4. Estimated Translational Diffusion Coefficient of MILs and DILs at various temperature with slope value obtained by fitting to Stoke Einstein equation

system	Temp. (k)	Viscosity (cP)	Diffusion coefficient[a] (D_tx 10^{-11}) m^2/s	slope= $\frac{k}{6\pi R}$ ($Jk^{-1}m^{-1}$)
$[C_4Mim][NTf_2]$	298	49.6	2.65	0.39±0.02
	303	40.4	3.31	
	308	33.4	4.05	
	313	27.5	4.73	
$[C_4MPyrr][NTf_2]$	298	73.2	1.62	0.38±0.01
	303	58.9	2.04	
	308	45.2	2.55	
	313	39.2	3.11	
$[C_8Mim][NTf_2]$	298	90.3	1.15	0.29±0.05
	303	72.1	1.41	
	308	57.0	1.79	
	313	45.2	2.22	
$[C_8MPyrr][NTf_2]$	298	99.4	0.66	0.24±0.01
	303	81.1	0.89	
	308	62.8	1.14	
	313	51.0	1.44	
$[C_9(Mim)_2][NTf_2]_2$	298	655.9	0.12	0.35±0.00
	303	486.6	0.18	
	308	361.5	0.26	
	313	272.8	0.36	
$[C_9(MPyrr)_2][NTf_2]_2$	298	710.2	0.06	0.19±0.02
	303	535.2	0.08	
	308	404.6	0.12	
	313	312.5	0.17	

[a] Experimental error = ±5%

The effect of temperature and viscosity on the molecular diffusion is quite noticeable from the Figure 3.9 and Table 3.4. The diffusion coefficients of DILs are found to be less than that of corresponding MILs. The higher bulk viscosity of DILs than that of MILs have been assigned as the cause of such behaviour. Again, the diffusion coefficients of imidazolium-based ILs are found to be higher than that of pyrrolidinium-based ILs despite of their comparable viscosity and van der Waals volume. The planarity of aromatic imidazolium cations is responsible for such

enhanced diffusion rate in imidazolium based ILs in comparison to ILs containing bulky quaternary alkyl pyrrolidinium cations.[31]The current finding has asserted that, besides molecular size, the diffusion in said ILs have also been controlled by the structure and chemistry of cation.

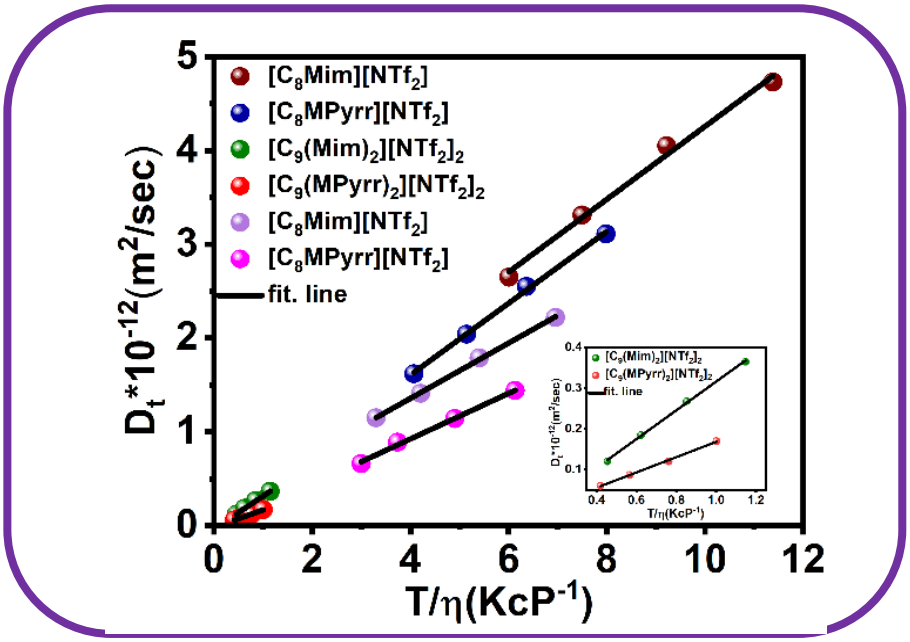

Figure 3.9 Plot of the diffusion coefficient (D_t) vs. (T/η) for MILs and DILs. (The inset represents enlarged view for DILs).

We further analysed our data using Stokes−Einstein (SE) relation as follows. As per SE theory, the slope of the plot D_t versus (T/η) given by$k/c\pi r_h$, where k is the Boltzmann constant and r_h = hydrodynamic radius, c is a constant whose value is equal to 4.66.[48, 65]The expression for slope indicates that, steeper the slope smaller would be the hydrodynamic radius of diffusing species.[66,67]From Table 3.4 we can see that the slope value ($0.35 Jk^{-1}m^{-1}$) obtained for imidazolium-based DIL is almost close to that obtained for cation in $[C_4Mim][NTf_2]$ ($0.39 Jk^{-1}m^{-1}$). Moreover, the slope for $[C_9(Mim)_2][NTf_2]_2$ is found to be relatively larger than that for $[C_8Mim][NTf_2]$. This observation indicates the smaller hydrodynamic radii for imidazolium-based DIL than that for corresponding imidazolium-based MILs However, in case of pyrrolidinium-based IL systems, the slope (Table 3.4) is found to be steepest for $[C_4MPyrr][NTf_2]$, when the same is compared for MILs $[C_8MPyrr][NTf_2]$ and

$[C_9(MPyrr)_2][NTf_2]_2$. This suggests larger hydrodynamic radii for $[C_9(MPyrr)_2][NTf_2]_2$ when compared with $[C_4MPyrr][NTf_2]$ and$[C_8MPyrr][NTf_2]$ independently. The data in Table 3.4 also suggests relatively larger hydrodynamic radii for pyrrolidinium-based IL than that for imidazolium-based DIL. The smaller hydrodynamic radii for imidazolium-based DIL than that for MIL can be rationalized by considering the folding of alkyl spacer chain.[25,26] In this context, the relatively larger hydrodynamic radii for pyrrolidinium dication than that for corresponding MILs is an interesting observation. The observation of relatively larger hydrodynamic radii for $[C_9(MPyrr)_2][NTf_2]_2$ than that for $[C_9(Mim)_2][NTf_2]_2$ clearly suggest that unlike in imidazolium-based DIL, pyrrolidinium-based DIL in the experimental condition remain in a straight chain conformation. We note here that when the size of the solvent molecule is relatively larger than the solute molecule SED relation can break down due to the creation of void space created by larger solvent molecules.[68,69] In view of this, the relatively faster rotation of the MPTS in pyrrolidinium-based DIL as compared to that in MIL can be attributed to the relatively longer alkyl spacer chain length in that DIL.[70]

3.3.4. To obtain further insight into the micro-heterogeneous behaviour of the imidazolium and pyrrolidinium-based ILs, the change of viscosity, rotational diffusion time of perylene and translational diffusion coefficient of cations in ILs with respect to temperature have been fitted to Arrhenius equation. The Arrhenius equation provides the value of activation energy for viscous flow, rotational and translational diffusion, which, in turn, can provide some structural information regarding the diffusive species.[71]

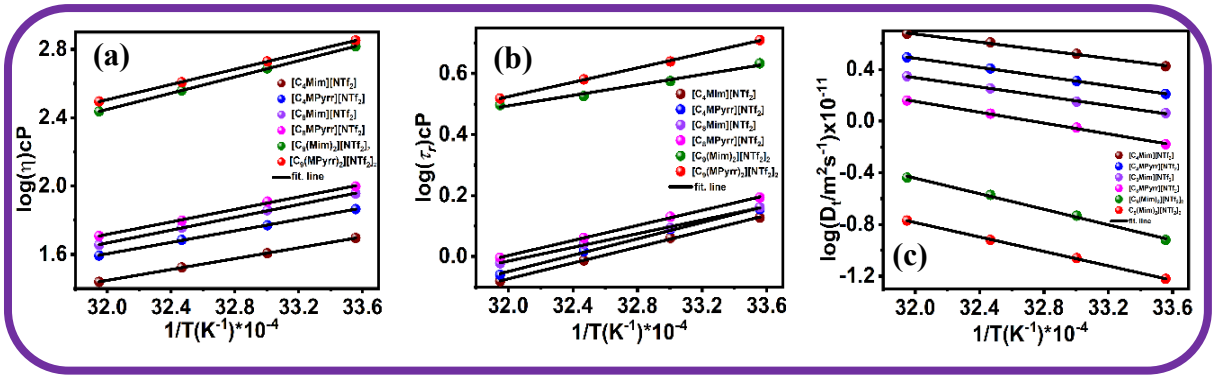

Figure 3.10. The variation of the (a) viscosity (b) rotational diffusion coefficient and (c) translational diffusion coefficient as a function of temperature.

The activation energies of the various flow, calculated from the slope of the Arrhenius equation are presented in Table 3.5. Figures 3.10a, b and c represent the Arrhenius behaviour in terms of viscosity (η), rotational diffusion of perylene (τ_r) diffusion coefficients (D_t) and respectively.

Table 3.5 Activation energy for viscous flow (E_η), rotational diffusive flow (E_R) and translational diffusive flow (E_T) of ILs, perylene in ILs and cation of ILs respectively

Systems	Viscousflow E_η/(kJ/mol)	Translational diffusive flow E_T/ (kJ/mol)	Rotational diffusive flow E_R /(kJ/mol)
$[C_4Mim][NTf_2]$	30.40±1.52	30.12±1.50	24.92±1.24
$[C_4MPyrr][NTf_2]$	32.10±1.60	33.12±1.69	25.71±1.28
$[C_8Mim][NTf_2]$	35.84±1.79	34.29±1.71	21.53±1.07
$[C_8MPyrr][NTf_2]$	35.01±1.75	40.17±2.00	23.64±1.18
$[C_9(Mim)_2][NTf_2]_2$	45.43±2.27	57.56±2.87	16.40±0.82
$[C_9(MPyrr)_2][NTf_2]_2$	42.54±2.12	53.45±2.67	22.62±1.13

From Table 3.5, it can be seen that, for all ILs, the activation energies for translational diffusive flow are similar to those for viscous flow. However, the activation energy for rotational diffusion of solute have not been found to vary reciprocally with viscosity. This evidence crucially suggests that while translational diffusion is more closely associated with the

viscosity of the medium but, there is relatively less association of rotational diffusion perylene with viscosity of ILs.

Here we would like to note that the diffusion motion of ions in ILs can originate from non-hydrodynamic "jump" like motion,[72] where the collective diffusion of cation and anion takes place. The activation energy accounts for the extent of inter and intra-molecular interaction, which play an important role in governing their diffusion. Table 3.5 shows that in case of MILs the activation energies related to viscous flow and diffusive flow have been increased with increase in the alkyl chain length on the cationic part, whereas activation energies for rotational diffusion of perylene has been found to decrease. Furthermore, going from MILs to DILs, the deviation of activation energy of rotational diffusion from the activation energy of bulk viscosity of the medium has also been found to increase. Again, the difference in the activation energy required for the viscous flow and rotational diffusive flow of peryleneis observed to be more in $[C_9(Mim)_2][NTf_2]_2$.This observation further indicates that the imidazolium-based DILs are more micro-heterogeneous in nature than the pyrrolidinium-based DIL. This analysis also reveals that the difference in the nature and symmetry of cationic head group of DIL has an important role in governing the overall structural organisation and micro-heterogeneous behaviour of DILs.

3.4. Conclusions

This study reports the differences in the microscopic behaviour of imidazolium and pyrrolidinium-based DILs in terms of structure, dynamic and intermolecular interaction. The behaviour of the concerned media has been investigated by exploiting combined steady state and time resolved fluorescence, EPR and NMR studies. Specially the investigation have been carried out by employing two DILs, namely $[C_9(MPyrr)_2][NTf_2]_2$ and $[C_9(Mim)_2][NTf_2]_2$. Additionally, mono-cationic counterparts (MILs) of the respective DILs have also been used

for the study so that proper comparison of the microscopic behaviour of DILs with that of MILs can be obtained. The steady state emission and EPR spectral data have revealed that the polarities of pyrrolidinium and imidazolium-based DILs reskemble to mono-hydroxyl and poly-hydroxyl alcohol respectively. The rotational correlation times (τ_r) corresponding to two chemically different probes perylene and MPTS at various temperatures in both MILs and DILs are found to be different. The analysis of the rotational motion of the solutes with the help of Stoke-Einstein-Debye (SED) theory has revealed that nature of solute solvent interactions in these media are different from each other. Additionally, differences in the dynamics of both the solutes in the DILs as compared to the MILs have also been emerged from the studies. Interestingly, it has been observed that the rotational diffusion of both charged and neutral solute have been found to be faster in DILs than that in MILs, despite of the fact that DILs are relatively bulkier than their MILs counterparts. The observation of relatively larger decoupling of rotational motion of solute from the medium viscosity for $[C_9(Mim)_2][NTf_2]_2$ than that of $[C_9(MPyrr)_2][NTf_2]_2$ further suggest that the former is dynamically more heterogeneous than the later. More interestingly, measurements and analysis of temperature dependent translational self-diffusion coefficient of cationic components of MILs and DILs through PFG-NMR technique suggested that the alkyl spacer chain in $[C_9(Mim)_2][NTf_2]_2$ exists in folded form but in $[C_9(MPyrr)_2][NTf_2]_2$ remains in straight chain conformation. The outcome of all these studies essentially indicates that the structural organisation of both DILs is different from each other as well as different from theirs mono-cationic counterparts and the local structure of ILs contribute significantly to the dynamics of the solute.

3.5. Appendix 3

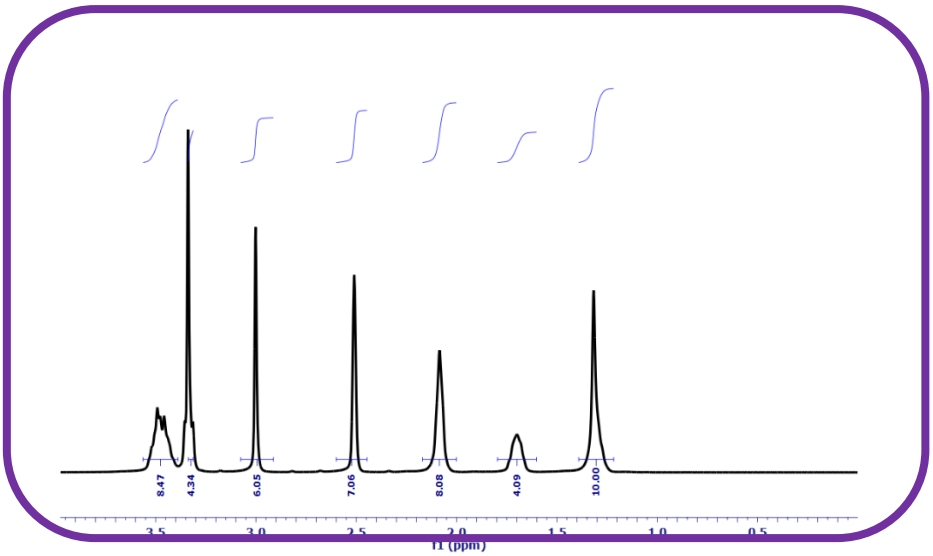

Figure APX 3.1. ^{1}H NMR spectra of (a) $[C_9(MPyrr)_2][NTf_2]_2$

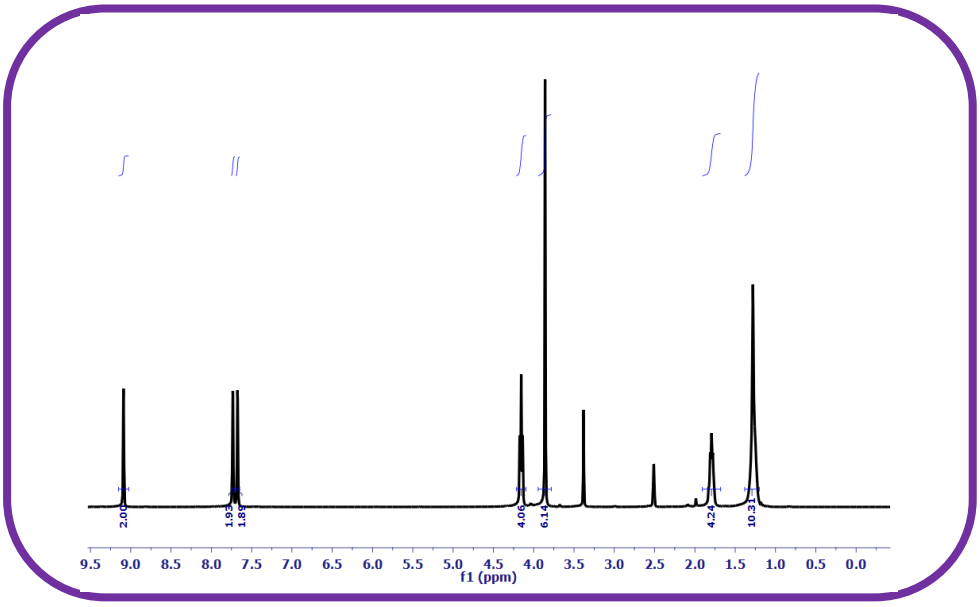

Figure APX 3.2. ^{1}H NMR spectra of (a) $[C_9(Mim)_2][NTf_2]_2$

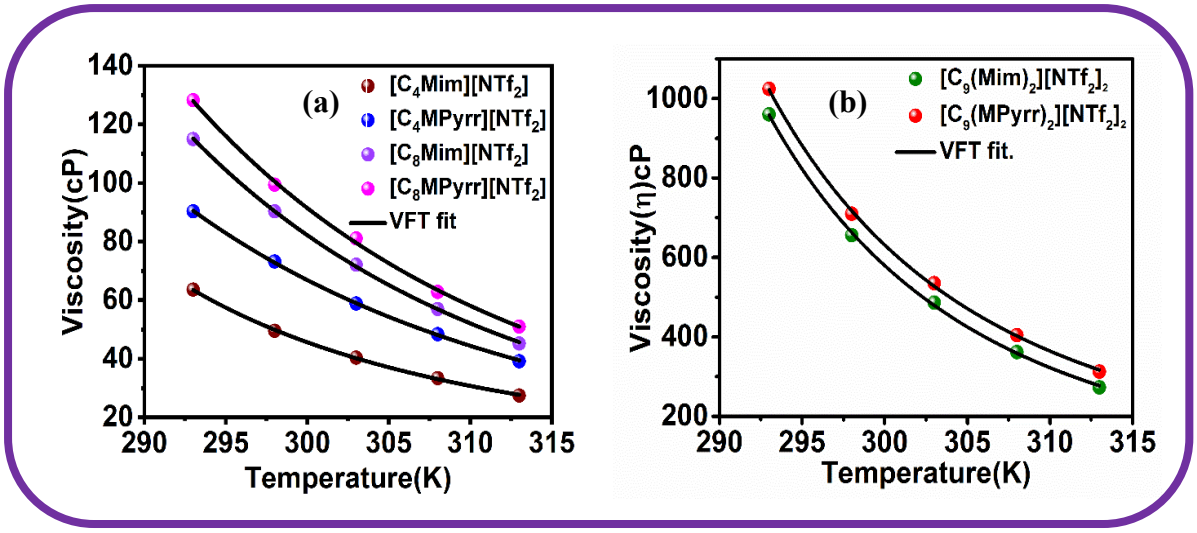

Figure APX 3.3. Vogel-Tamman-Fulcher (VTF) fitting of Viscosity (η/cP) of (a) MILs and (b) DILs with Temperature (k).

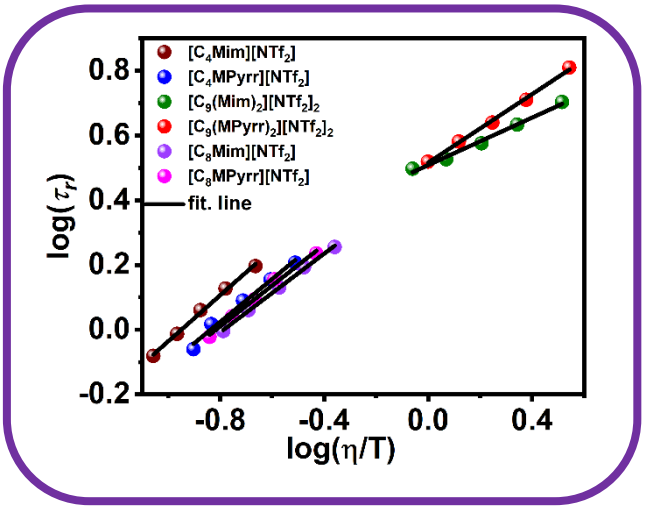

Figure APX 3.4. Power law plot

REFERENCES

1. Hallett, J. P.; Welton, T. Room-temperature ionic liquids: solvents for synthesis and catalysis. *Chemical Review* **2011**, *111*, 3508-3576.
2. Pârvulescu, V. I.; Hardacre, C. Catalysis in ionic liquids. *Chemical Review* **2007**, *107*, 2615–2665.
3. Wang, H.; Gurau, G.; Rogers, R. D. Ionic liquid processing of cellulose. *Chemical Society Reviews* **2012**, *41*, 1519–1537.
4. Brandt, A.; Gräsvik, J.; Hallet, J. P.; Welton, T. Deconstruction of lignocellulosic biomass with ionic liquids. *Green Chemistry* **2013**, *15*, 550-583.
5. Zhang, X.; Zhang, X.; Dong, H.; Zhao, Z.; Zhang, S.; Huang, Y. Carbon capture with ionic liquids: overview and progress. *Energy & Environmental Science* **2012**, *5*, 6668-6681.

6. Guo, J.; Han, K.S.; Mahurin, S. M.; Baker, G.A.; Hillesheim, P.C.; Dai, S.; Hagaman, E.W.; Shaw, R.W. Rotational and translational dynamics of rhodamine 6G in a pyrrolidinium ionic liquid: a combined time-resolved fluorescence anisotropy decay and NMR study. *The Journal of Physical Chemistry B* **2012**, *116*, 7883–7890.
7. Alam, T. M.; Dreyer, D. R.; Bielawski, C. W.; Ruoff, R. Combined measurement of translational and rotational diffusion in quaternary acyclic ammonium and cyclic pyrrolidinium ionic liquids. *The Journal of Physical Chemistry B* **2013**, *117*, 1967–1977.
8. Cabeza, O.; Rilo, E.; Segade, L.; Pe´rez, M.D.; Garabal, S. G.; Ausı´n, D.; ´pez-Lago, E.L.; Varela, L. M.; Vilas, M.; Verdıa, P.; Tojo. E. Imidazolium decyl sulfate: A very promising selfmade ionic hydrogel. *Material Chemistry Frontier* **2018**, *2*, 505-513.
9. Hojniak, S. D.; Khan, A. L.; Hollóczki, O.; Kirchner, B.; Vankelecom, I. F. J.; Dehaen, W.; Binnemans, K. Separation of carbon dioxide from nitrogen or methane by supported ionic liquid membranes (SILMs): Influence of the cation charge of the ionic liquid. *The Journal of Physical Chemistry B* **2013**, *117*, 15131-15140.
10. Zhang, X. X.; Breffke, J.; Ernstingb, N. P.; Maroncelli. M. Observations of probe dependence of the solvation dynamics in ionic liquids. *Physical Chemistry Chemical Physics* **2015**, *17*, 12949-12956.
11. Anderson, J. L.; Ding, R.; Ellern, A.; Armstrong, D. W. Structure and properties of high stability geminal dicationic ionic liquids. *Journal of American Chemical Society* **2005**, *127*, 593–604.
12. Montalbán, M. G.; Víllora , G.; Licence , P. Synthesis and characterization data of monocationic and dicationic ionic liquids or molten salts. *Data in Brief* **2018**, *19*, 769–788.
13. Shirota, H.; Mandai , T.; Fukazawa, H.; Kato, T. Comparison between dicationic and monocationic ionic liquids: liquid density, thermal properties, surface tension, and shear viscosity. *Journal of Chemical & Engineering Data* **2011**, *56*, 2453–2459.
14. Pitawala, J.; Matic, A.; Martinelli, A.; Jacobsson, P.; Koch, V.; Croce, F. Thermal properties and ionic conductivity of imidazolium bis(trifluoromethanesulfonyl)imide dicationic ionic liquids. *The Journal of Physical Chemistry B* **2009**, *113*, 10607–10610.
15. Bodo, E.; Chiricotto, M.; Caminiti, R. Structure of geminal Imidazolium bis(trifluoromethylsulfonyl)imide dicationic ionic liquids: a theoretical study of the liquid phase. *The Journal of Physical Chemistry B* **2011**, *115*, 14341–14347.
16. Yeganegi, Y.; Soltanabadi, A.; Farmanzadeh, D. Molecular dynamic simulation of dicationic ionic liquids: Effects of anions and alkyl chain length on liquid structure and diffusion *The Journal of Physical Chemistry B* **2012**, *116*, 11517–11526.
17. Sahu, P. K.; Das, S. K.; Sarkar, M. Toward understanding solute–solvent interaction in room-temperature mono- and dicationic ionic liquids: a combined fluorescence spectroscopy and mass spectrometry analysis. *The Journal of Physical Chemistry B* **2014**, *118*, 1907–1915.
18. Bui-Le, L.; Hallett, J.P.; Licence, P. Thermally-stable imidazolium dicationic ionic liquids with pyridine functional groups. *ACS Sustainable Chemistry and Engineering* **2020**, *8*, 8762–8772.
19. Paul, A.; Mandal, P. K.; Samanta. A. On the optical properties of the imidazolium ionic liquids. *The Journal of Physical Chemistry B* **2005**, *109*, 9148–9153.

20. Patra, S.; Samanta, A. Microheterogeneity of some imidazolium ionic liquids as revealed by fluorescence correlation spectroscopy and lifetime studies. *The Journal of Physical Chemistry B* **2012**, *116*, 12275−12283.
21. Cha, S.; Shim, T.; Ouchi, Y.; Kim, D. Characteristics of visible fluorescence from ionic liquids. *The Journal of Physical Chemistry B* **2013**, *117*, 10818−10825.
22. Ishida, T.; Shirota. H. Dicationic versus monocationic ionic liquids: Distinctive ionic dynamics and dynamical heterogeneity. *The Journal of Physical Chemistry B* **2013**, *117*, 1136–1150.
23. Wang, Y. L.; Li, B.; Sarman, S.; Mocci, F.; Lu, Z.Y.; Yuan, J.; Laaksonen, A.; Fayer, M.D. Microstructural and dynamical heterogeneities in ionic liquids. *Chemical Review*s **2020**, *120*, 5798−5877.
24. Zhang, H.; Li, M.; Yang, B. Design, synthesis, and analysis of thermophysical properties for imidazolium-based geminal dicationic ionic liquids. *The Journal of Physical Chemistry C* **2018**, *122*, 2467–2474.
25. Li, S.; Feng, G.; Bañuelos, J. L.; Rother, G.; Fulvio , P. F.; Dai, S.; Cummings, P. T. Distinctive nanoscale organization of dicationic versus monocationic ionic liquids. *The Journal of Physical Chemistry C* **2013**, *117*, 18251–18257.
26. Majhi, D.; Seth, S.; Sarkar, M. Differences in the behaviour of dicationic and monocationic ionic liquids as revealed by time resolved-fluorescence, NMR and fluorescence correlation spectroscopy. *Physical Chemistry Chemical Physics* **2018**, *20*, 7844-7856.
27. Shirota, H.; Ishida, T. Microscopic aspects in dicationic ionic liquids through the low-frequency spectra by femtosecond raman-induced kerr effect spectroscopy. *The Journal of Physical Chemistry B* **2011**, *115*, 10860–10870.
28. Ghatee, M. H.; Zare, M.; Zolghadr, A. R.; Moosavi, F. Temperature dependence of viscosity and relation with the surface tension of ionic liquids. *Fluid Phase Equilibria* **2010**, *291*, 188-194.
29. Salminen, J.; Papaiconomou, N.; Kumar, R. A.; Lee, J. M.; Kerr, J.; Newman, J.; Prausnitz, J. M. Physicochemical properties and toxicities of hydrophobic piperidinium and pyrrolidinium ionic liquids. *Fluid Phase Equilibria* **2007**, *261*, 421-426.
30. Shimizu, Y.; Ohte, Y.; Yamamura, Y.; Tsuzuki, S.; Saito, K. Comparative study of imidazolium- and pyrrolidinium-based ionic liquids: thermodynamic properties. *The Journal of Physical Chemistry B* **2012**, *116*, 5406–5413.
31. Tsuzuki, S.; Matsumoto, H.; Shinodaa, W.; Mikamia, M. Effects of conformational flexibility of alkyl chains of cations on diffusion of ions in ionic liquids. *Physical Chemistry Chemical Physics* **2011**, *13*, 5987–5993.
32. Koyama, Y.; Matsuishi, K.; Takekiyo, T.; Abe, H.; Yoshimura, Y. How does the flexibility of pyrrolidinium cations affect the phase behaviour of 1-alkyl- 1-methylpyrrolidinium bis (trifluoromethanesulfonyl) imide homologues under stressful conditions? *Physical Chemistry Chemical Physics* **2019***, 21,* 11290-11297.
33. Endo, T.; Hoshino, S.; Shimizu, Y.; Fujii, K.; Nishikawa, K. Comprehensive conformational and rotational analyses of the butyl group in cyclic cations: DFT calculations for imidazolium, pyridinium, pyrrolidinium, and piperidinium *The Journal of Physical Chemistry B* **2016**, *120*, 10336–10349.
34. Mandal, P. K.; Samanta, A. Fluorescence studies in a pyrrolidinium ionic liquid: polarity of the medium and solvation dynamics. *The Journal of Physical Chemistry B* **2005**, *109*, 15172–15177.
35. M. A. T.; Jr, E. S.; Andrea, L. D,; Purcell, S. M.; Costen, M. L.; Bruce, W. D.; Slattery, J. M.; Minton, T. K.; McKendrick, K. G . Hiding the headgroup?

Remarkable similarity in alkyl coverage of the surfaces of pyrrolidinium- and imidazolium-based ionic liquids. *The Journal of Physical Chemistry C* **2016**, *120*, 27369–27379.

36. Laszlo, J. A.; Compton, D. L. Comparison of peroxidase activities of hemin, cytochrome *c* and microperoxidase-11 in molecular solvents and imidazolium-based ionic liquids. *Jornal of Molecular Catalysis B: Enzym*atic **2002**, *18*, 109-120.
37. Gazitua, M.; Tapia, R.A.; Contreras, R.; Campodonico, P. R. Mechanistic pathways of aromatic nucleophilic substitution in conventional solvents and ionic liquids. *New Journal of Chemistry* **2014**, *38*, 2611-2618.
38. Muldoon, M. J.; Gordon, C. M.; Dunkin, I. R. Investigations of solvent–solute interactions in room temperature ionic liquids using solvatochromic dyes. *Journal of the Chemical Society, Perkin Transaction 2* **2001**, *2*, 433–435.
39. Samanta, A. Dynamic stokes shift and excitation wavelength dependent fluorescence of dipolar molecules in room temperature ionic liquids. *Journal of Physical Chemistry B* **2006**, *110*, 13704-13716.
40. Pandey, A.; Rai, R.; Pal, M.; Pandey, S. How polar are choline chloride-based deep eutectic solvents? *Physical Chemistry Chemical Physics* **2014**, *16*, 1559−1568.
41. Lee, J. M.; Ruckes, S.; Prausnitz, J. M. Solvent polarities and Kamlet-Taft parameters for ionic liquids containing a pyridinium cation. *Journal of Physical Chemistry B* **2008**, *112*, 1473–1476.
42. Guan, W.; Chang, N.; Yang, L.; Bu, X.; Wei, J.; Liu, O. Determination and prediction for the polarity of ionic liquids. *Journal of Chemical Engineering Data* **2017**, *62*, 2610−2616.
43. Carrascoa, J. P.C.; Jacquemina, D.; Laurencea, C.; Planchata, A.; Reichardt, C.; Sraïdid, K. Solvent polarity scales: determination of new E_T (30) values for 84 organic solvents. *Journal of Physical Organic Chemistry* **2014**, *27*, 512–518.
44. Ab Rani, M. A.; A. Brant, A.; Crowhurst, L.; A. Dolan, A.; Lui, M.; Hassan, N. H.; J. P. Hallett, J. P.; Hunt, P.A.; Niedermeyer, H.; Arlandis, J. M. P.; Schrems, M.; Welton, T.; Wilding, R. Understanding the polarity of ionic liquids. *Physical Chemistry Chemical Physics* **2011**, *13*, 16831–16840.
45. Fruchey, K.; Fayer, M. D. Dynamics in organic ionic liquids in distinct regions using charged and uncharged orientational relaxation probes. *The Journal of Physical Chemistry B* **2010**, *114*, 2840–2845**.**
46. Khara, D.C.; Samanta, A. Rotational dynamics of positively and negatively charged solutes in ionic liquid and viscous molecular solvent studied by time- resolved fluorescence anisotropy measurements**.** *Physical Chemistry Chemical Physics* **2010, *12*,** 7671-7677.
47. Vranes. M.; Dozic, S.; Djeric, V.; Gadzuric, S. Physicochemical characterization of 1-butyl-3-methylimidazolium and 1-butyl-1-methylpyrrolidinium bis(trifluoromethylsulfonyl)imide . *Journal of Chemical Engineering Data* **2012**, *57*, 1072–1077.
48. Moosavi, M.; Khashei, F.; Sharifi, A.; Mirzaei, M. Transport properties of short alkyl chain length dicationic ionic liquids: The effects of alkyl chain length and temperature. *Industrial & Engineering Chemistry Research* **2016**, *55*, 9087–9099.
49. Vila, J.; Ginés, P.; Pico, J. M.; Franjo, C.; Jiménez, E.; Varela, L. M.; Cabeza, O. Temperature dependence of the electrical conductivity in EMIM-based ionic liquids. *Fluid Phase Equilibria* **2006**, *242*, 141–146.
50. Edward, J. T. Molecular volumes and the Stokes-Einstein equation. *Journal of Chemical Education* **1970**, *47*, 261−270.

51. Fleming, G. R. *Chemical applications of ultrafast spectroscopy*; Oxford University Press: New York, **1986**, 989.
52. Men, S.; Lovelock, K. R. J.; Licence, P. X-ray photoelectron spectroscopy of pyrrolidinium-based ionic liquids: cation–anion interactions and a comparison to imidazolium-based analogues. *Physical Chemistry Chemical Physics* **2011**, ***13***, 15244-15255.
53. Tokuda, H.; Hayamizu, K.; Ishii, K.; Susan, Md. A. B. H.; Watanabe, M. Physicochemical properties and structures of room temperature ionic liquids. 1. Variation of Anionic Species. *The Journal of Physical Chemistry B* **2004**, *108*, 16593–16600.
54. Wang, H.; Wang, J.; Zhang, S.; Xuan, X. Structural effects of anions and cations on the aggregation behavior of ionic liquids in aqueous Solutions. *The Journal of Physical Chemistry B* **2008**, *112*, 16682–16689.
55. Men, S.; Jin, Y.; Licence, P. Probing the impact of the N3-substituted alkyl chain on the electronic environment of the cation and the anion for 1, 3-dialkylimidazolium ionic liquids. *Physical Chemistry Chemical Physics* **2020**, *22*, 17394—17400.
56. Gangamallaiah, V.; Dutt, G. B. Rotational diffusion of nonpolar and ionic solutes in 1-Alkyl-3-Methylimidazolium bis(trifluoromethylsulfonyl)imides: is solute rotation always influenced by the length of the alkyl chain on the imidazolium cation? *The Journal of Physical Chemistry B* **2012**, *116*, 12819-12825.
57. Amotz, D. B.; Drake, J. M. The solute size effect in rotational diffusion experiments: A test of microscopic friction theories. *The Journal of Chemical Physics* **1988**, *89*, 1019-1029.
58. Dutt, G. B.; Sachdeva, A. Temperature-dependent rotational relaxation in a viscous alkane: interplay of shape factor and boundary condition on molecular rotation. *The Journal of Chemical Physics* **2003**, *118*, 8307-8314.
59. Dutt, G. B.; Raman, S. Rotational dynamics of coumarins: an experimental test of dielectric friction theories. *The Journal of Chemical Physics* **2001**, *114*, 6702-6712.
60. Xia, X.; Wolynes, P. G. Microscopic theory of heterogeneity and nonexponential relaxations in supercooled liquids. *Phys Rev Lett.* **2001**, *86*, 5526-5529.
61. Das, A.; Biswas, R.; Chakrabarti, J. Solute rotation in polar liquids: Microscopic basis for the Stokes-Einstein-Debye model. *The Journal of Chemical Physics* **2012,** *136*, 014505.
62. Chakraborty, M.; Ahmed, T.; Dhale, R.S.; Majhi, D.; Sarkar, M. Understanding the microscopic behavior of binary mixtures of ionic liquids through various spectroscopic techniques. *The Journal of Physical Chemistry B* **2018**, *122*, 12114-12130.
63. Tsuzuki, S. Factors controlling the diffusion of ions in ionic liquids. *Chem Phys Chem*. **2012**, *13*, 1664 – 1670.
64. Tsuzuki, S.; Matsumoto, H.; Shinoda, W.; Mikami, M. Physicochemical properties and structures of room-temperature ionic liquids. 3. Variation of cationic structures effects of conformational flexibility of alkyl chains of cations on diffusion of ions in ionic liquids. *Physical Chemistry Chemical Physics* **2011**, ***13***, 5987-5993.
65. Kowsari, M.; Alavi, S.; Ashrafizaadeh, M.; Najafi, B. Molecular dynamics simulation of imidazolium-based ionic liquids. I. dynamics and diffusion coefficient. *The Journal of Chemical Physics* **2008**, *129*, 224508.
66. Atkins, P. W.; Julio De, P. *Physical Chemistry*, 9th ed.; Oxford University Press: **2010**.
67. Sahu, P.K.; Ghosh, A.; Sarkar, M. Understanding structure–property correlation in monocationic and dicationic ionic liquids through combined fluorescence and

pulsed-Field gradient (PFG) and relaxation NMR experiments. *The Journal of Physical Chemistry B* **2015**, *119*, 14221–14235.
68. Guo, J.; Mahurin, S.M.; Baker, G. A.; Hillesheim, P.C.; Dai, S.; Shaw, R.W. Influence of solute charge and pyrrolidinium ionic liquid alkyl chain length on probe rotational reorientation dynamics. *The Journal of Physical Chemistry B* **2014**, *118*, 1088–1096.
69. Das, S. K.; and Sarkar. M. Rotational Dynamics of Coumarin-153 and 4-Aminophthalimide in 1-Ethyl-3-methylimidazolium alkyl sulfate ionic liquids: Effect of alkyl chain length on the rotational dynamics. *The Journal of Physical Chemistry B* **2012**, 116, 194–202.
70. Davila, M.J.; Aparicio, S.; Alcalde, R.; Garcı´a, B.; Leal, J.M. On the properties of 1-butyl-3-methylimidazolium octylsulfate ionic liquid. *Green Chemistry* **2007**, 9, 221–232.
71. Barik, S.; Chakraborty, M.; Sarkar, M. How does addition of lithium salt influence the structure and dynamics of choline chloride-based deep eutectic solvents? *The Journal of Physical Chemistry B* **2020**, *124*, 2864–2878.
72. Taylor, A. W.; Licence, P.; Abbott, A. P. Non-classical diffusion in ionic liquids. *Physical Chemistry Chemical Physics* **2011**, *13*, 10147–10154.

Chapter 4a

Understanding the Influence of Ethylene Glycol on the Microscopic Behavior of Imidazolium-based Monocationic and Dicationic Ionic Liquid

---

Amita Mahapatra, Joyoti Ghosh, Sahadev Barik, Subhakanta Parida, and Moloy Sarkar. *Chemical Physics Impact* **2023**,7, 100331.

Abstract

In this chapter, the influence of a molecular co-solvent, ethylene glycol (EG) on the microscopic behaviour of an imidazolium-based DIL is analyzed by employing TRFA) and NMR spectroscopic techniques. In order to have a clear understanding of the specific role of DIL, a MIL containing an alkyl side chain unit, same as the alkyl spacer chain length of DIL, have also been investigated. The rotational diffusion of two fluorescent probes 9-PA and R110 have been carried out in both neat MIL and DIL and their mixtures with various fraction of EG. The analysis of the results has demonstrated that, within the studied concentration range, the microstructure of MIL encompassing both polar and nonpolar domains gets disrupted as the mole fraction of EG increases. However, a similar investigation in DIL have revealed that the micro-structure of DIL gets affected slightly when the similar proportions of EG is added to DIL. This behaviour of DIL is attributed to the enhanced rigidity of the DIL structure due to its folded structural arrangements. Furthermore, NMR studies have provided additional insights into the interactions between the components of ILs and the added solvent. It has been observed that EG can form strong hydrogen-bonding interactions with the imidazolium-ring and alkyl chain protons of MIL. However, such interaction has not been observed in DIL. Moreover, the translational diffusion coefficient (D_t) value for the cationic moiety of both MIL and DIL, measured through NMR, have depicted that in presence of EG, the change in $D_t$value is much higher for MIL than that for DIL. Overall, the outcome of the combined fluorescence and NMR studies have pointed out that the behaviour of DIL and MIL in presence of a co-solvent is very different from one another and thus the individual mixture (IL+solvent) can be used for various targeted industrial applications.

4a.1. Introduction

In recent times, binary mixtures of ILs and a molecular solvent have emerged as suitable alternative to pure IL-based system in numerous analytical applications, such as separation, extraction, and synthesis [1-5]. The idea of combining ionic liquids with molecular solvent has led to the formation of new solvents systems with improved physicochemical properties [6-7]. Moreover, proper choice of co-solvents can allow one to effectively customize the physicochemical characteristics of a (IL+ co-solvent) mixture which can facilitate their use in diverse fields [8-10]. In addition to this, the most crucial characteristics that IL possess is the heterogeneous microstructure in them. Due to presence of polar and nonpolar domain in the fluid structure, they play significant role in the dissolution of complex molecules and ion-transport [11-13]The microscopic structural organization within ILs can be disturbed with the addition of molecular solvents. Therefore, it is beneficial in many ways to understand how added co-solvents affect the relevant microscopic properties in ILs as well. While most of the research work in this regard has been conducted by employing mono-cation based ILs, such studies on an alternative class of ILs, for example, DIL, are notably limited[14-18]. In fact, it has been demonstrated that the properties DILs are superior to the MILs in terms of the higher glass transition temperature, higher surface tension, and larger electrochemical window [19-22]. Therefore, it would be interesting to know the structural organization and various intermolecular interactions that prevail in DIL-molecular solvent mixtures. This can be achieved with proper understanding on the structure and dynamics of DILs in the absence and the presence of co-solvent. Additionally, understanding this aspect of mixture (IL+co-solvent) may also be helpful in developing suitable solvent system for targeted application.

An extensive amount of experimental and theoretical studies on RTILs have been carried out in order to investigate the behaviour of IL in its neat condition as well as in presence of water, alcohol, and other polar or nonpolar organic compounds [23-24]. Specifically, to understand the

behaviour and the heterogeneity of IL/ molecular liquid mixtures, nuclear magnetic resonance (NMR) and neutron/X-ray diffraction, IR, fluorescence-based techniques have been employed [11, 24-26]. These studies have shown that the presence of hydrogen bonding interaction between ILs and co-solvent molecules can decrease the electrostatic interaction between cation and anions in an IL and thereby reduce the total binding energy of ILs, which eventually decreases the viscosity of the given of ILs [27-29]. In this context, investigations carried out by Dutt and co-workers are note-worthy. They have observed significant change in the micro-viscosity of the mixture containing of imidazolium-based MIL $[C_8(Mim)][BF_4]$ and di-ethylene glycol (DEG) mixture than that have been observed for the individual neat solvent [30]. The new hydrogen bonding network formed by $[C_8(Mim)][BF_4]$ with EG is considered to be the main reason behind the enhancement of the microviscosity of the concerned medium. In a separate study, while examining the influence of an organic solvent, tetraethylene glycol dimethyl ether (TEGDME) on the structure and microscopic behaviour of an imidazolium-based MIL, 1-butyl-3-methylimidazolium hexafluorophosphate ($[C_4(Mim)][PF_6]$), Guo and co-workers, have observed the dissipation of the polar regions as well as the nonpolar regions of the $[C_4(Mim)][PF_6]$, with an increase in the mole fraction of TEGDME[10]. In an another work, Sarkar and co-workers have observed faster solvation and rotational diffusion time of coumarin 153 in $[C_4(Mim)][PF_6]$–water mixture as compared to neat $[C_4(Mim)][PF_6]$, due to the weakening of electrostatic interaction between ions of ILs as a result of the addition of water to neat ILs. It is evident from the above discussions, most of the studies on this aspect have been carried out by employing monocation-based ILs [15, 31-32]. However, there have been no reported studies that investigate how molecular solvents affect the microscopic characteristics and structural arrangement within the context of DIL. In this scenario, we would like to mention that DILs are structurally more micro-heterogeneous than MILs [33-34]. Due to the presence of an extra cationic head, the mode and extent of interaction with a particular

molecular solvent is expected to be different in DIL than that has been generally observed with a similar class of MILs [19-20]. Therefore, investigating the effect of molecular solvents on both microscopic and macroscopic behavior in DIL in terms of its structural organization, intermolecular interaction is expected to be interesting.

With the aforementioned issues in mind, the aim of this chapter is to understand the structural organization of some MIL and DIL and the intermolecular interaction that prevails in IL-solvent mixture in the presence of an organic solvent. For this purpose, a DIL, 1,8-bis(3-methylimidazolium-1-yl) octane bis(trifluoromethanesulfonyl)imide $[C_8(Mim)_2][NTf_2]_2$ and a MIL 1-methyl-3-octylimidazolium bis(trifluoromethanesulfonyl)imide $[C_8(Mim)][NTf_2]$ have been synthesized and are investigated. EG has been chosen as the molecular solvent in this study because it is extensively used in many industrial applications and is miscible with all ILs studied here at ambient conditions [14]. We would like to note here that, the MIL has been chosen in a way that the alkyl chain length of the MILs matches with the spacer chain length of the DIL. The choice of system is expected to provide a comparative view of the changes that may happen during IL-EG interaction events. To probe the structural organization in the apolar and polar domains of ILs in absence and presence of EG, the rotational diffusion of selected solutes are carried out using TRFA. For example, two probes, 9-Phenylanthracene (9-PA) and Rhodamine 110 (R110), are used for TRFA measurements. 9-PA, being apolar, help in probing solute-solvent interactions in the apolar domain, while R110, being polar, help in monitoring activities in the polar domain of the ILs [30]. Furthermore, NMR studies have also been carried out to shed more light on the intermolecular interaction at the molecular level. The outcomes of this study are expected to advance our knowledge in understanding the behaviour of both MIL and DIL in presence of organic solvent and the acquired knowledge may also be helpful to formulate new solvent mixtures for targeted application. Scheme 4a.1. represents the chemical structure of ILs and probe molecules used in this chapter.

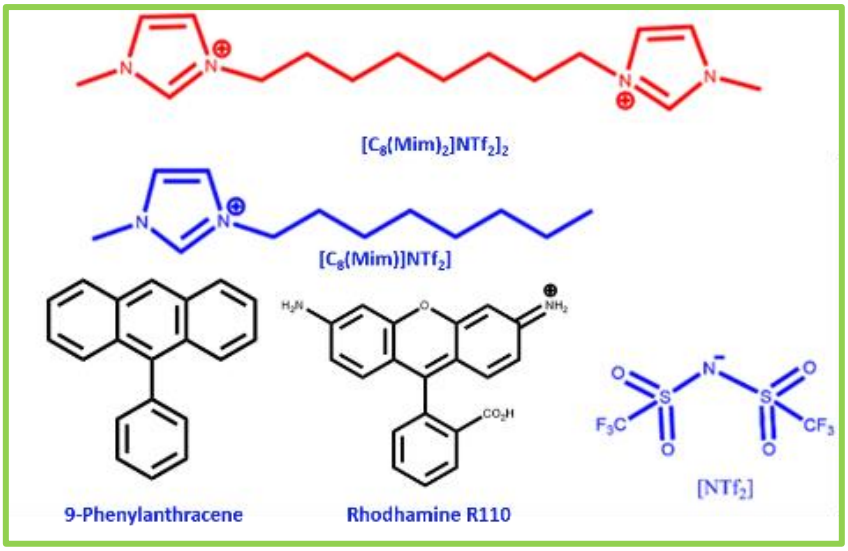

Scheme 4a.1. Chemical structure of the ionic liquid and molecular probe used in this study.

4a. 2. Materials, Instruments and Methods.

Rhodamine 110, 9-PA, Ethylene glycol (EG) was purchased from Sigma-Aldrich. Both the DILs, 1,8-bis(3-methylimidazolium-1-yl) octane bis(trifluoromethanesulfonyl)imide ($[C_8(Mim)_2][NTf_2]_2$) and MIL, 1-methyl-3-octyl imidazolium bis(trifluoromethylsulfonyl)imide ($[C_8(Mim)][NTf_2]$) were synthesized using standard protocols that were reported in the literatures and has been described in details in chapter 2 [19-20, 35]. The NMR spectra of the respective ILs are provided in Figure APX.4a.1 and Figure APX4a.2. The mixture of ILs with EG were prepared by simply mixing them with proper molar ratio. Specifically, three compositions with EG fraction 0.2, 0.4, 0.6 were prepared. We want to note here that the ILs and EG were easily miscible under atmospheric conditions by simply shaking the mixtures. The solution of fluorophore molecules, 9-PA and R110 of micro-molar concentration are carefully prepared for the TRFS studies. The sample solution was further evacuated with nitrogen gas and was then transferred into a micro-cuvette for the measurements. The methodology for TRFA and PFG-NMR measurement can be found in chapter 2.[35-38]

4a.3. Results and Discussion

4a.3.1. Time-resolved fluorescence anisotropy study. Rotational diffusion study is an important tool to extract several valuable information about the solute-solvent and solvent-solvent interactions[38,39]. Therefore, in order to understand the influence of increasing concentration of EG on the structural organization of both MIL and DIL, the rotational diffusion of two suitably chosen molecule 9-PA and R110 have been monitored in the neat ILs as well as in the IL+EG mixtures as a function of temperature. As the rotational diffusion time is directly related to the viscosity of the solvent, at the beginning of this study, viscosity of (EG+IL) mixtures are measured and collected in Table APX4a.1. The fluorescence anisotropy decays of 9-PA and R110 in both IL and (IL+EG) mixtures over the temperature range of 298−323k are measured and these decay plots at a particular temperature 298k for both MIL and DIL in the absence and presence of EG are illustrated in Figure 4a.1.

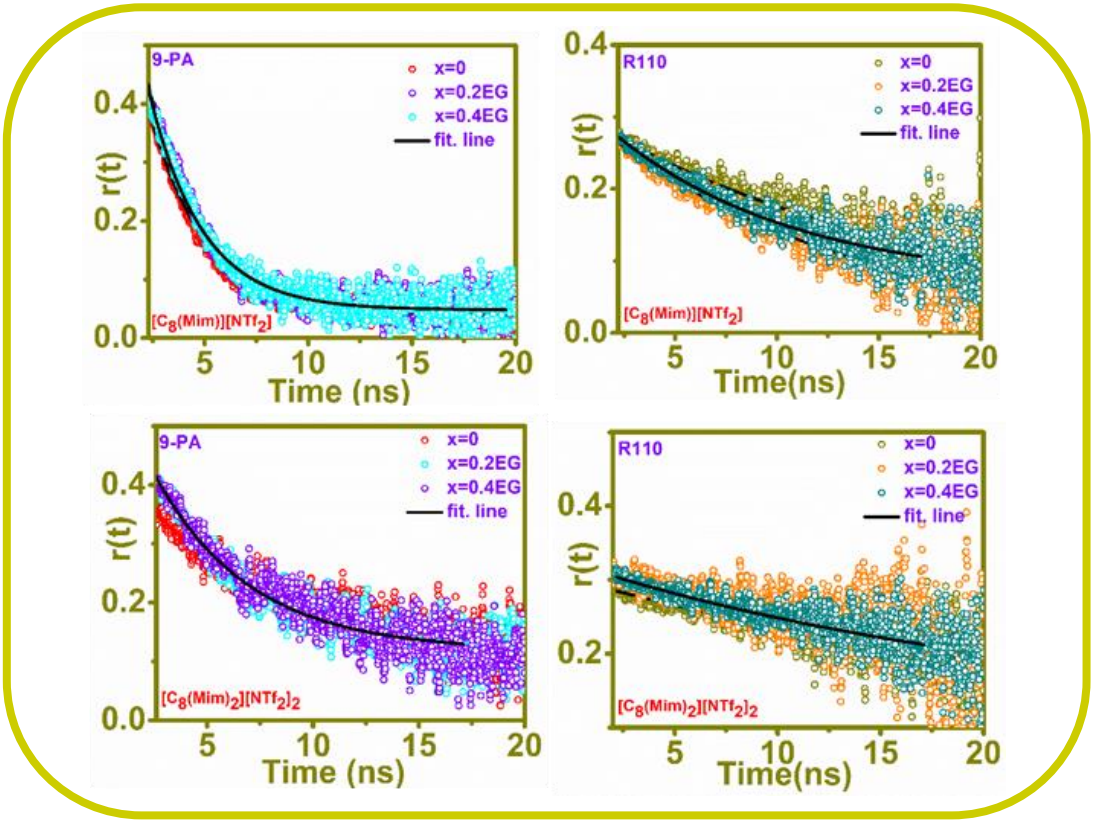

Figure 4a.1. Decay plots for 9-PA and R110 in MIL and DIL with increasing fraction (X) of EG at 298k.

The estimated reorientation times (τ_r) of the two solutes along with the viscosities of the solvent systems are provided in Table APX4a.1. From the table, it is clear that at a particular temperature the reorientation time (τ_r) of both 9-PA and R110 in MIL is relatively less as compared to those observed in the DIL. This is due to the higher viscosity of the DIL as compared to MIL. Interestingly, one can also find from Table APX4a.1 that with an increase in the mole fraction of EG, τ_r values of both the probes decreases in both MIL and DIL indicating the faster rotation of solutes with decrease in the viscosity of the medium. However, since it would be difficult to assess that this lower τ_r value of the probe in the concerned media is due to change in the bulk viscosity of the media or due to the change in micro-viscosity of the media in presence of EG, we estimated the reorientation time (τ_r) of probe molecules in pure ILs and their mixtures with EG under iso-viscous conditions. For this purpose, we have conducted additional measurements of the (τ_r) for both the probe molecules in pure ILs as well as their EG mixtures by carefully controlling the temperature so that the viscosity of the mixtures match with the viscosity of the pure ILs. This allowed us to eliminate the influence of viscosity and gain precise insight into the effect of EG on the rotation of solute molecules. The results of these measurements are summarised in Table 4a.1. We would like to note here that, the τ_r the MIL systems are measured at a viscosity 34cP and that of for DIL systems at 165cP.

Table 4a.1. The rotational relaxation time of different probes in both the MIL and DIL systems under iso-viscous conditions

X (EG)	τ_r/ns			
	$[C_8(Mim)][NTf_2]$		$[C_8(Mim)_2][NTf_2]_2$	
	9-PA	R110	9-PA	R110
0	1.5	9.9	3.3	18.0
0.2	1.7	8.6	3.0	15.7
0.4	1.9	7.1	2.8	13.3
0.6	2.3	5.9	2.5	13.0

Upon analysing the data presented in Table 4a.1, a distinct pattern can be observed regarding the impact of EG on the rotational behavior of the probe molecules in MIL and DIL. For example, while examining the rotational behavior of 9-PA, it is evident that the addition of EG gradually slows down its rotational diffusion in the MIL system. However, intriguingly, in case of DIL the rotational motion of 9-PA become faster when EG is added to it. Conversely, while probing the rotation of R110 we find that the rotation of R110 become faster with the introduction of EG to the MIL. Similarly, when EG is added into the DIL, the rotation of R110 is observed to be increased. The current findings suggest that EG exhibits very different effects on the behaviour of MIL and DIL systems. Specifically, these observations suggest that EG influences the micro-environment experienced by the probe molecules differently in MIL and DIL. This observation can be attributed to various factors such as molecular interactions, solvation effects, or structural changes induced by EG in the IL systems. In order to declutter these issues, we have analyzed the data using Stoke-Einstein-Debye (SED) hydrodynamic theory [30, 33, 40]. The details of SED theory have been described in chapter 2 and the SED equation has been given by eq. 2.14. To analyse the data, the probe parameters such as $V, f \ and \ C_{slip}$ are collected from available literature [30]. The log-log plots of reorientation time (τ_r) vs (η/T) for 9-PA in MILs and DIL in the absence and presence of EG are shown in Figure 4a.2. Figure 4a.2a clearly demonstrates that the rotational relaxation behaviour of 9-PA in neat MIL, $[C_8(Mim)][NTf_2]$ tends to remain within the boundary condition parameters predicted by SED theory. However, with the gradual addition of EG, the rotational diffusion of 9-PA become slower and eventually approaches the stick line. This observation is quite interesting in the sense that rotational motion of 9-PA slows down even when the bulk viscosity of the medium get reduced due to the addition of EG. This departure of the hydrodynamic behaviour of the probe solute reflects the important role of the micro-viscosity of the concerned media in driving the solute rotation.

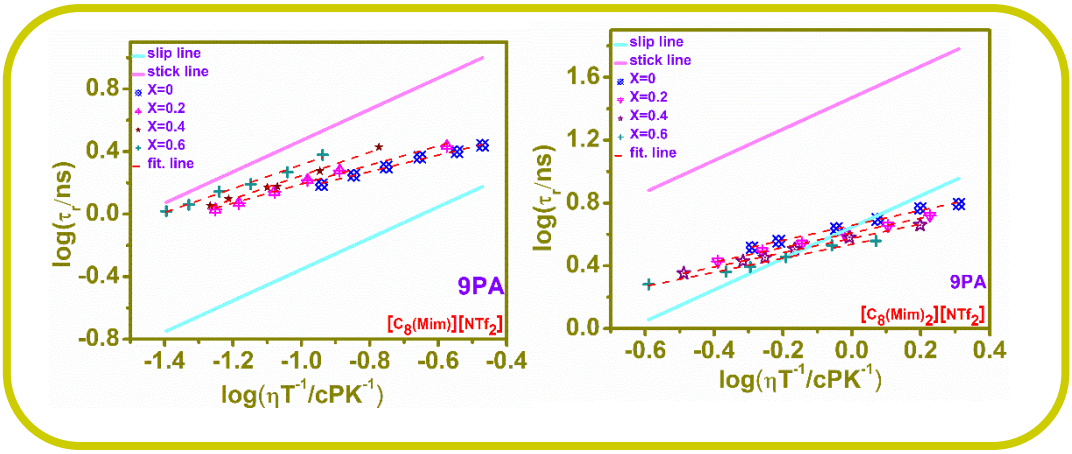

Figure 4a.2. Log–log plots of rotational reorientation time of 9-PA in (a) $[C_8(Mim)][NTf_2]$ (b) $[C_8(Mim)_2][NTf_2]_2$ in neat condition as well as with their mixture with EG of various composition as marked in the legend of the figures. Here, cyan and magenta lines indicate the slip and stick boundary conditions, respectively. The dashed red line indicates the fit to data points.

In this context, we would like to note that such viscosity-diffusion decoupling behaviour is suggestive of the change in the micro heterogeneous behaviour of the relevant media [20, 33, 41-42]. It has been well established in the literatures that the micro heterogeneous nature is intricately related to the change in the structural organization of the medium where the solute rotation occurs [21, 30]. Therefore, in the present case, the change in the rotational behaviour of 9-PA can be attributed to the alteration in the micro-heterogeneous behaviour and structural organization of the MIL caused by the introduction of EG to IL media. Quite interestingly, in case of neat DIL (Figure 4a.2b), one can see that the rotational relaxation behaviour of 9-PA falls close to slip boundary (faster rotation) condition at lower temperature and even cross the slip line at higher temperature. Based on the result stated above, the rotation of 9-PA in DIL is noticeably faster than that in MIL, and according to hydrodynamic terminology, this faster rotation of 9-PA in DIL is referred as sub-slip behaviour [33]. Previous literature reports also demonstrate the sub-slip behaviour of apolar molecules in DIL[42]. Please note that 9-PA being

apolar molecule locate itself in the apolar domain of both MIL and DIL. In this connection, we would also like to recall that the length of alkyl chain corresponding to the MIL and DIL investigated here are the same. Despite this, the faster rotation of 9-PA in DIL as compared to MIL clearly points out that the length of the alkyl chain (side chain in MIL and spacer chain in DIL) is not the only factor affecting the rotation of the solute in the given medium. Instead, it demonstrates that the nano-structural organization of MIL and DIL are very distinct; as a result, the rotating solute experiences substantially different degrees of micro-viscosity in these two media. Moreover, it has also been observed that with the addition of EG in the DIL medium, the rotational motion of 9-PA becomes slightly faster only at higher temperature. The results presented here clearly shows that relaxation behaviour of 9-PA in (MIL + EG) mixtures differs remarkably from that in (DIL + EG) mixtures. Moreover, the influence of EG on the relaxation properties of 9-PA is more pronounced in the presence of MIL compared to DIL.

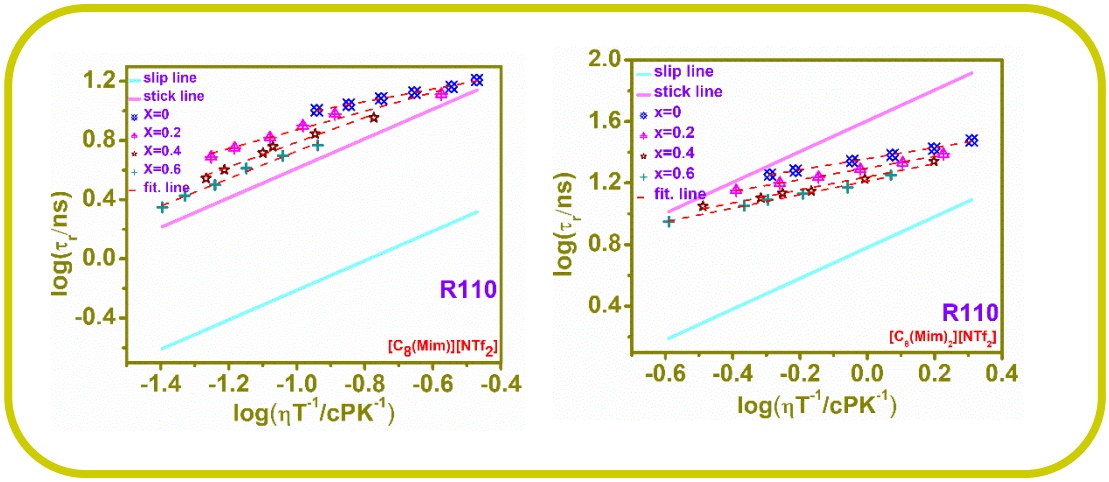

Figure 4a. 3. Log−log plots of rotational reorientation time of R110 in (a) $[C_8(Mim)][NTf_2]$, (b) $[C_8(Mim)_2][NTf_2]_2$ in neat condition as well as with their mixture with EG of various composition as marked in the legend of the figures. Here, cyan and magenta lines indicate the slip and stick boundary conditions, respectively. The dashed red line indicates the fit to data points.

Again, in order to probe how the nano-structural organization of the polar domains of ILs is influenced by the presence of EG, which is expected to make hydrogen bonding interaction

with the cation and anion of the given IL, a positively charged probe R110 has been used for the study. Please note that the R110 being polar probe help in monitoring the polar domains of the concerned ILs. Figure 4a.3 illustrates the log−log plots of average rotational relaxation time (τ_r) versus (η/T) for R110 in MIL (Figure 4a.3a) and DIL (Figure 4a.3b) in absence and presence of EG at various temperatures. As evident from Figure 4a.3a, in the case of MIL, the rotational relaxation behaviour of R110 is significantly hindered as compared to that has been observed in the case of 9-PA. As per hydrodynamic terminology, this particular rotational behavior of R110 can be termed as super-stick behavior (above stick boundary limit) [33]. The super-stick behavior of solute (R110) usually indicates a strong solute−solvent specific interaction[32]. In this context we would like to mention here that R110 is positively charged, and it is a hydrogrn bond donating solute.[30] Therefore, in neat MIL, the R110 experience a strong hydrogen bonding as well as electrostatic interaction with the NTf_2^- (anion) of ILs and hence experience hindered rotation. At the same time, EG can also form strong hydrogen bonding interactions with the imidazolium cation and NTf_2^- anion in IL. Therefore, upon introducing EG into the MIL, the competitive interaction of EG and R110 with the NTf_2^- reduces the extent of solute-solvent interaction, thereby facilitating the faster rotation of R110. On the contrary, the rotation of R110 is found to be appreciably faster in DIL than in MIL. The (τ_r) value of R110 in DIL fall just below the stick boundary condition (Figure 4a. 3b). The faster rotation of charged solute like MPTS in DIL as compared to that in MIL despite the fact that both containing the same alkyl chain has been reported in previous literature[43]. Quite interestingly, upon careful look at Figure 4a. 3b, one can also realize that even after the addition of EG, the rotational behavior of R110 remains almost unaltered; in fact, R110 continues to fall within the slip and stick boundary limit as predicted by the SED theory. This result suggests that the DIL-EG interaction is weaker than the MIL-EG interaction. It is essential to note here that a series of experimental and theoretical studies have provided compelling evidence regarding the

distinct nano-structural organization found in MILs and DILs, particularly those featuring longer alkyl chains [33-34, 43]. In MILs, the alkyl sidechain exhibits a relatively greater degree of freedom and flexibility. This inherent flexibility leads to a distinct behavior where the alkyl chains tend to aggregate due to hydrophobic interactions between them, and in such arrangements, the anion (here NTf_2^-) tends to be present near the head group (imidazolium) ensuring maximum cation-anion electrostatic interaction. Conversely, when considering DILs, the situation is remarkably different. In DILs, the alkyl chain is buried between the two head groups of the molecule. As the length of the alkyl chain in DILs increases (C>6), its flexibility also increases. This increased flexibility results in an arrangement where the alkyl chains tend to become folded, and simultaneously, head groups in DILs are compelled to come closer to each other and in such arrangement, two anions become available for each imidazolium cation. Keeping this in mind, we can conjecture that the folded structural configuration of DILs imposes a restriction for EG to strongly interact with the cation and anion in DIL, and perhaps due to this reason, upon addition of EG, the rotation of R110 remains least affected in DIL.

To have a better realization of this distinct behaviour of MIL and DIL in the presence of EG, the friction coefficient values($C_{rot} = {}^{\tau_r}/_{\tau_{exp}}$) of 9-PA and R110 estimated utilizing the data from Table APX4a.1 for both MILs and DIL are plotted individually against the mole fraction of EG added to the neat ILs (Figure 4a. 4). Friction coefficient is a measure of the extent of solute-solvent interaction. Figure 4a. 4a and Figure 4a. 4b have collectively shown that the change in the friction coefficient of 9-PA and R110 with the addition of EG is relatively higher in MIL than that have been observed for DIL. The outcome of the current analysis has conveyed that the presence of EG bring about significant perturbation in the structural organization in MIL. However, the structural organization of the DIL remains intact even after a similar proportion of EG is added to the DIL.

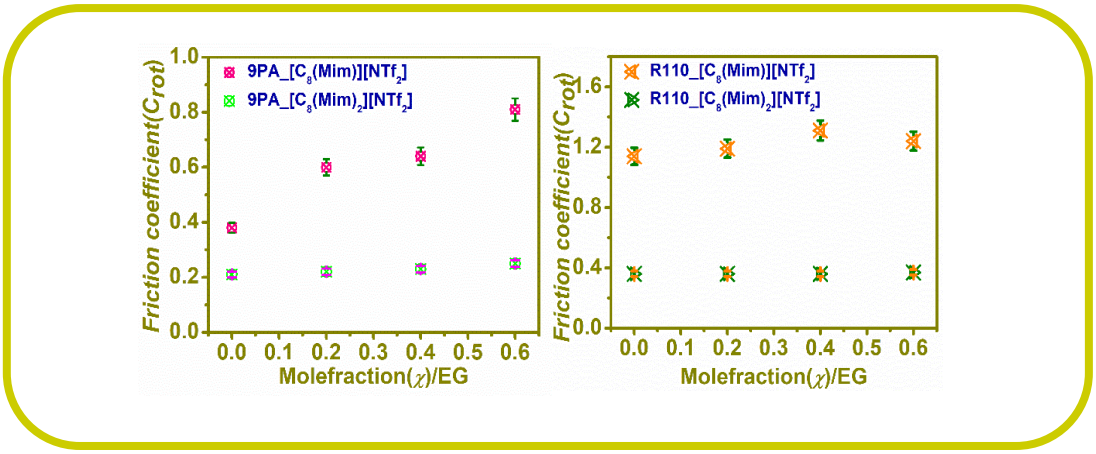

Figure 4a.4. Friction coefficient for 9-PA (a) and R110 (b) in MIL and DIL as a function of EG molefraction.

From SED analysis one can also realize that the rate of change in (τ_r) for both the solute with respect to the addition of EG to MIL and DIL is not in accordance with the decrease in bulk viscosity of the medium. This indicates that the rotational motion of the solute is decoupled with the medium viscosity, which is known as viscosity-diffusion decoupling behaviour. The literatures suggest that this η-(τ_r) decoupling happens due to the micro-heterogeneous behaviour of the concerned medium.[42-44] Since the introduction of EG into the ILs can influence the micro-heterogeneous behaviour of the ILs, understanding these aspects of ILs in the absence and presence of EG is essential. In order to understand how the presence of EG affects the micro-heterogeneous behaviour in MIL and DIL, the rotational anisotropy data are analyzed further by employing an empirical relationship, $\tau_r=A(\eta/T)^n$, where A is the constant and n is the exponent [30, 42, 44]. Previous literature studies have also depicted that by looking at the departure in 'n' value from unity one would be able to get an idea about the micro-heterogeneous behaviour of the medium. The values of n for 9-PA in MIL and DIL are estimated using the data presented in Table APX4a.1 and collected in Table 4a.2.

Table 4a. 2. The n value for 9-PA for in MIL and DIL and their respective mixture with EG

X(EG)	n/(9-PA)	
	$[C_8(Mim)][NTf_2]$	$[C_8(Mim)_2][NTf_2]_2$
0.0	0.527	0.476
0.2	0.609	0.466
0.4	0.747	0.455
0.6	0.763	0.446

It can be observed from Table 4a.2 that the value of n is 0.52 and 0.48 for 9-PA in neat MIL and DIL respectively, suggesting the microheterogeneous stucture of both the media. Interstingly, one can see from same table that upon gradual addition of EG, in case of MIL, the n value approachs to unity (n=0.76 at 0.6 molefraction of EG), indicating a partial loss in micro-hetergeneous structurein MIL. On the other hand, in the case of DIL, even in the presence of 0.6 mole fraction of EG, the estimated n value (0.44) remains much below unity indicating micro-heterogeneous structure in DIL does not change appericiably in the presence of EG. Therefore, we can say here that the micro-structure for DIL is more rigid as compared to that for MIL.

4a. 3.2. NMR Studies.

To ascertain how the electronic environment of different protons in both MILs and DILs changes in the presence of EG, a molecular level analysis has been carried out by employing ^{1}H NMR spectroscopy. In 1-alkyl-3-methylimidazolium-based ILs, it is commonly observed that the protons of the cationic head group participate in hydrogen bonding interactions even with weak hydrogen bond acceptor (HBA) anions, along with other type of interactions such as ionic and van der Waals interactions.[31] The addition of hydrogen bond donors (HBDs), such as EG, can induce significant changes in the strength of hydrogen bonding interactions between the constituents of ILs. This can occur through the formation of new hydrogen bonds or by

breaking/weakening the existing hydrogen bonds present in the pure ILs. Therefore, the interaction between the constituents of ILs and EG has been further investigated by measuring the chemical shift (δ) of various protons in the binary mixture of ILs with EG. Figure 4a.5a and a' show the chemical shift of different protons in pure ILs $[C_8(Mim)][NTf_2]$ and $[C_8(MIM)_2][NTf_2]_2$), while Figure 4a. 5b and b' represent the chemical shift of these protons in their corresponding binary mixtures with 0.6 mole fraction of EG. Upon analyzing Figure 4a.5b and b', it is evident that after the addition of EG to both ILs, an additional peak appeared in the range of ~ 3.5 ppm to 3.6 ppm, which is attributed to the resonance peaks originating from EG.[31] Again, a careful inspection of the stacked spectra (Figure 4a. 5c and c') revealed an up-field shift of the C (4,5)-proton (attached to the imidazolium ring proton) as well as C (6,7)-proton (alkyl chain proton, Scheme 4a. 2) after addition of EG to the MIL. However, no such shift has been observed in case of DIL $[C_8(Mim)_2][NTf_2]_2$. In this context, we would like to draw attention to the fact that previous literature has provided strong evidence for the significant impact of EG on both C (4,5) and C(2) proton of the imidazolium rings, as well as some protons of the alkyl chains.[14] This observed up field shift in the ring protons as well as alkyl chain protons of MIL indicates their strong interactions with ethylene glycol.[31] However, such interactions appear to be absent in the case of DILs, which essentially suggests that the imidazolium ring proton as well as alkyl chain proton in DIL, due to their folded structure, are less available for making interaction with ethylene glycol. This fact is further manifested by monitoring the translational diffusion of the ILs, specifically the cationic part of the ILs, in the absence and presence of EG utilizing PFG NMR technique.

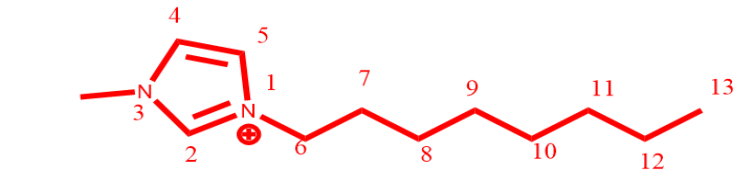

$[C_8(Mim)]$

*$[C_8(Mim)][NTf_2]$:^{1}H NMR ($CDCl_3$, 400 MHz)

δ 8.87 (s, 1H, N-C(2)H-N), 7.58 (d, 2H, N-C(4)H-C(5)H-N), 4.20 (t, 2H, N-C(6)H2-C(7)H_2, 3.92 (s, 3H, N-CH_3), 1.94-1.83 (m, 2H, N-CH2-CH2-C5H10-CH3), 1.37-1.28 (m, 10H, N-CH2-CH2-C5H10-CH3), 0.90 (t, 3H, N-CH2-CH2-C5H10-CH3)

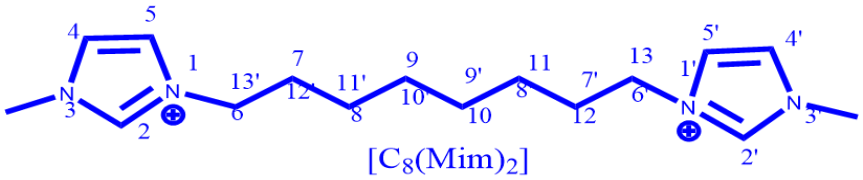

$[C_8(Mim)_2]$

* $[C_8(Mim)_2][NTf_2]_2$:1H NMR ($CDCl_3$, 400 MHz)

δ (ppm) = 9.02 (s, 2H, N-C(2)H-N), 7.69 (s, 2H, N-C(4)H-C(5)H-N), 7.64 (s, 2H, N-C(4)H-C(5)H-N), 4.08 (t,4H), 3.79 (s, 6H, N-CH_3), 1.71 (m, 4H), 1.21 (m, 8H).

Scheme 4a.2. The number assigned to the carbon atoms and the chemical shift of the protons attached to those carbon atoms.

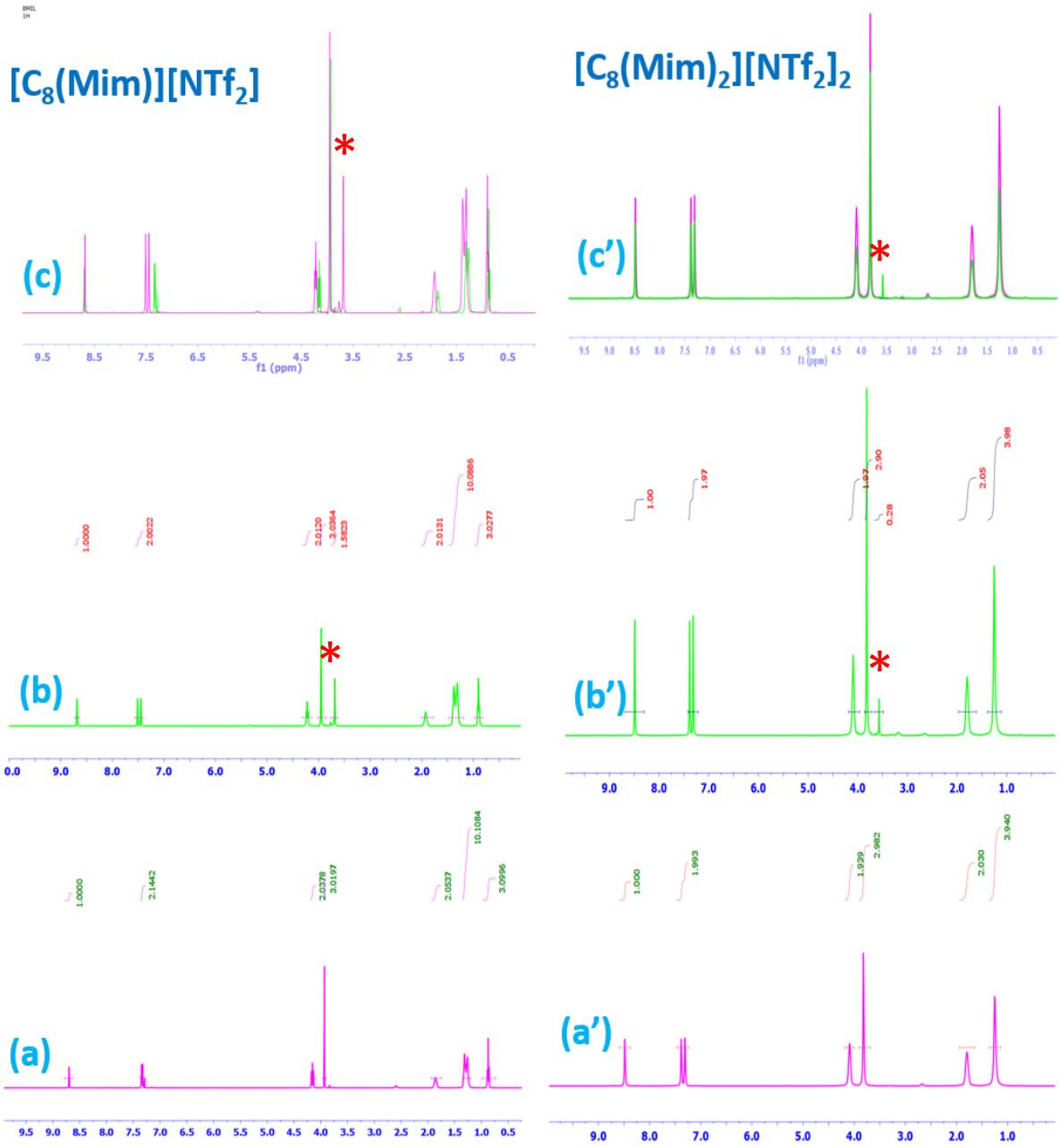

Figure 4a.5. Selected ^{1}H NMR spectra, i.e. those collected for pure (a) $[C_8(Mim)][NTf_2]$ and (a') $[C_8(MIM)_2][NTf_2]_2$ and the respective EG/IL mixture with X = 0.6 (b and b'). The carbon number and the chemical shifts referenced to tetramethylsilane (TMS) are assigned as per scheme 4a.2. The stars in the intermediate spectrum (i.e. that of the mixture of ILs with X = 0.6 EG) indicate resonance peaks arising from EG. Figure c and c' indicates the overlapped NMR spectra of MIL and DIL respectively in absence (Magenta line) and presence of Ethylene Glycol (green line).

Table 4a.3. Translational diffusion coefficients of cationic part of IL systems in absence and presence of ethylene glycol at 298k.

System	Diffusion Coefficient (D_t*$10^{-11}/m^2s^{-1}$)
[C_8(Mim)][NTf_2]	1.20
{EG (0.6)+ [C_8(MIM)][NTf_2]}	2.40
[C_8(MIM)$_2$][NTf_2]$_2$	0.30
{EG (0.6)+ [C_8(MIM)$_2$][NTf_2]$_2$}	0.40

Table 4a. 3 illustrates the estimated D_t values of the respective cations of both MIL and DIL in the absence and presence EG (X=0.6) at room temperature. Table 4a. 3 shows that in the absence of EG, the value of D_t for the DIL is substantially smaller than for the MIL, which is consistent with their respective masses and medium viscosities. However, with the addition of EG, the $D_t$value of both the ILs increases, which can be attributed to the decrease in the bulk viscosities of these media. Interestingly, upon a careful inspection of Table 4a.3 it can be seen that for the MIL, with addition of 0.6 M.F. of EG the decrease in viscosity is more than 3 times whereas the increase in the D_t value is almost 2 times. This observation essentially suggests a significant interaction between the constituents of MIL and EG, causing this disproportionate change in the D_t value of the MIL in the presence of EG. Conversely, in the case of the DIL, it is observed that the changes in viscosity and D_t value align more closely with each other when EG is added, indicating minimal interaction between EG and DIL. Overall, analysis of the NMR data shows that the influence of EG on the nano-structural organization of MILs and DILs differs significantly, with MIL being more affected upon addition EG. In contrast, the folded structure of DIL remains unchanged even at higher concentrations of EG. Essentially,

the outcomes of the NMR measurement highly corroborate the findings obtained from the rotational dynamic study.

4a.4. Conclusions

In summary, the influence of a molecular co-solvent, ethylene glycol (EG), on the structural organization of imidazolium-based MIL and DIL have been investigated. For this purpose the relevant DIL, $[C_8(Mim)_2][NTf_2]_2$ and a MIL $[C_8(Mim)][NTf_2]$, has been synthesized and their microscopic behaviour have been investigated using time-resolved fluorescence and NMR spectroscopic techniques both in absence and presence of EG. The rotational anisotropy of data two selected probes (9-PA and R110) has revealed contrasting behaviour in MIL and DIL in presence of EG. Specifically, in case of MIL, the rotational relaxation of 9-PA became progressively slower as the mole fraction of EG increases, suggesting the formation of a more compact structure in the apolar region (composed of the alkyl chain) in the presence of EG. Meanwhile, the faster rotation of R110 in MIL in presence of EG indicated the interaction of EG with the polar domain of the MIL. In contrast to this, the addition of EG to DIL induces marginal effect on the relaxation behaviour of 9-PA and R110. This observation suggests that the folded structural arrangement of DIL become an important factor in preventing the direct interaction between the imidazolium cation and EG. In a similar fashion the rotational motion of the solute is found to be more decoupled from the medium viscosity in case of (EG+MIL) mixture. However, the decoupling remained largely unchanged in case of (EG+DIL) mixture, indicating relatively stronger interaction of EG with MIL as compared to DIL. Interestingly, the shift in the NMR signals of some specific protons of MIL in presence of EG has indicated the H-bonding interaction of EG with MIL. However, no such shift was observed for equivalent protons in DIL when EG was present. More interestingly, the diffusion coefficient of the cation in MIL, which exhibited significant changes in the presence of EG, showed minimal changes in the case of DIL. Collectively, these results have led us to conclude that among ILs, having

the same alkyl chain, DIL retains its nano-structural organization to a greater extent in the presence of the co-solvent EG compared to MIL. The present study is expected to enrich our understanding of the underlying principles governing the interactions between ILs and molecular solvents, which in turn can be helpful in designing a suitable IL+cosolvent mixture suitable for a specific application.

4a.5.Appendix 4a

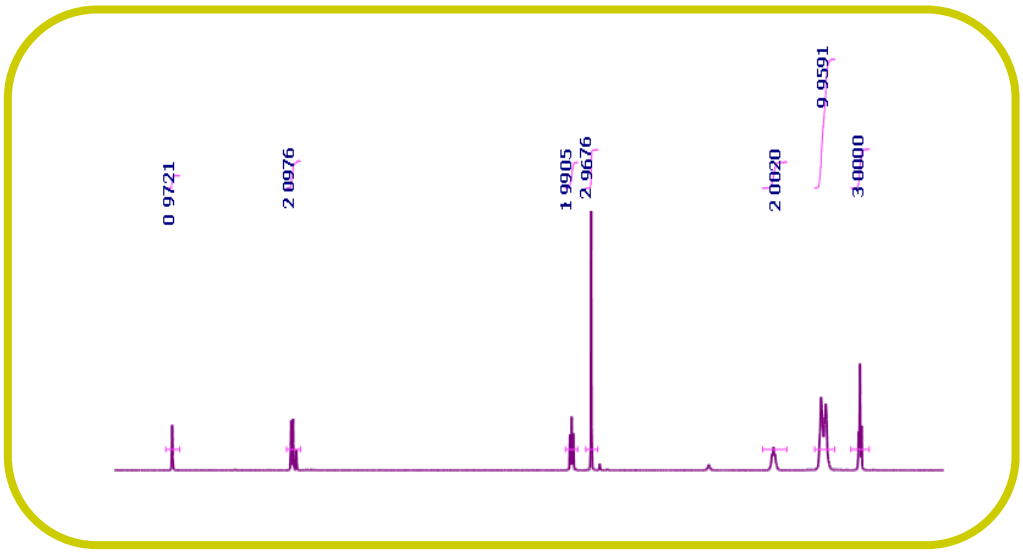

Figure APX4a.1. ^{1}H NMR spectra of MIL ([C$_8$(Mim)][NTf$_2$]) with reference to CDCl$_3$.

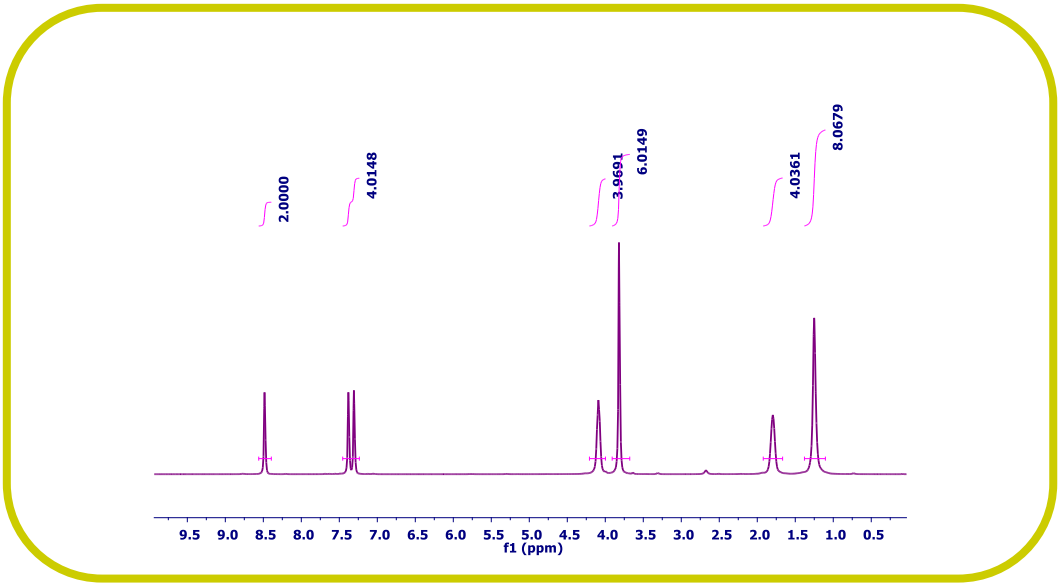

Figure APX4a.2. ^{1}H NMR spectra of MIL ([C$_8$(Mim)$_2$][NTf$_2$]$_2$) with reference to CDCl$_3$.

Table APX4a.1. The viscosity and rotational reorientation time of 9-PA and R110 in IL systems

Systems	T (k)	η(cP)	9PA		R110	
			τ_r (ns)	C_{rot}	τ_r (ns)	C_{rot}
$[C_8(Mim)][NTf_2]$	298	108.8	2.75	0.28	15.9	1.15
	303	86.30	2.50	0.30	14.7	1.26
(neat)	308	68.30	2.31	0.35	13.2	1.46
	313	55.40	2.00	0.38	12.1	1.67
	318	45.20	1.77	0.42	11.2	1.93
	323	37.00	1.54	0.46	10.1	2.16
	298	79.30	2.72	0.35	13.0	1.19
	303	39.20	1.90	0.50	9.70	1.83
(X=0.2EG)	308	32.10	1.65	0.54	8.00	1.88
	313	26.10	1.52	0.62	6.70	1.96
	318	20.90	1.23	0.63	5.75	2.14
	323	18.10	1.12	0.68	4.90	2.14
	298	50.20	2.55	0.51	9.05	1.31
	303	34.30	1.88	0.56	7.10	1.53
(X=0.4EG)	308	26.20	1.50	0.60	5.70	1.64
	313	24.90	1.44	0.63	5.20	1.60
	318	19.50	1.19	0.66	4.00	1.59
	323	17.50	1.08	0.68	3.50	1.58
	298	34.40	2.28	0.67	5.88	1.25
	303	27.60	1.85	0.69	5.10	1.37
(X=0.6EG)	308	21.90	1.45	0.69	4.10	1.41
	313	18.00	1.39	0.82	3.20	1.36
	318	14.91	1.15	0.83	2.64	1.38
	323	13.01	1.03	0.86	2.20	1.34
$[C_8(Mim)_2][NTf_2]_2$	298	609.20	6.20	0.10	30.00	0.37
	303	479.02	5.82	0.12	26.50	0.42
(neat)	308	366.07	4.95	0.14	24.10	0.52
	313	282.37	4.34	0.16	22.02	0.61
	318	195.00	3.60	0.20	19.10	0.77
	323	165.00	3.27	0.22	17.99	0.87
	298	501.47	5.15	0.10	24.50	0.36
	303	386.20	4.50	0.12	21.50	0.42
(X=0.2EG)	308	293.65	3.98	0.14	19.50	0.51
	313	224.32	3.47	0.16	17.30	0.60
	318	174.70	3.10	0.19	16.20	0.67
	323	131.77	2.65	0.22	14.20	0.86
	298	470.20	4.48	0.10	23.02	0.36

	303	298.00	3.80	0.13	16.85	0.43
(X=0.4EG)	308	210.00	3.20	0.16	14.05	0.51
	313	175.15	2.83	0.17	13.60	0.60
	318	153.52	2.68	0.19	13.00	0.67
	323	104.95	2.24	0.21	11.20	0.86
	298	350.15	3.62	0.10	17.85	0.38
	303	265.00	3.39	0.13	14.80	0.42
(X=0.6EG)	308	198.00	2.85	0.15	13.50	0.52
	313	158.60	2.47	0.17	12.30	0.60
	318	137.00	2.31	0.18	11.42	0.66
	323	82.97	1.93	0.20	8.90	0.86

REFERENCES

1. Fang, A.; Smolyanitsky, A., Large Variations in the Composition of Ionic Liquid–Solvent Mixtures in Nanoscale Confinement. *ACS applied materials & interfaces* **2019**, *11*, 27243-27250.
2. Pavlov, S.; Danilova, V.; Sivakov, V.; Kislenko, S., The Effect of a Mixture of an Ionic Liquid and Organic Solvent on Oxygen Reduction Reaction Kinetics. *Physical Chemistry Chemical Physics* **2022**, *24*, 16746-16754.
3. Ren, F.; Wang, J.; Yu, J.; Zhong, C.; Xie, F.; Wang, S., Dissolution of Cellulose in Ionic Liquid–Dmso Mixtures: Roles of Dmso/Il Ratio and the Cation Alkyl Chain Length. *ACS Omega* **2021**, *6*, 27225-27232.
4. Xia, J.; King, A. W.; Kilpeläinen, I.; Aseyev, V., Phase-Separation of Cellulose from Ionic Liquid Upon Cooling: Preparation of Microsized Particles. *Cellulose* **2021**, *28*, 10921-10938.
5. Yang, Q.; Xing, H.; Su, B.; Yu, K.; Bao, Z.; Yang, Y.; Ren, Q., Improved Separation Efficiency Using Ionic Liquid–Cosolvent Mixtures as the Extractant in Liquid–Liquid Extraction: A Multiple Adjustment and Synergistic Effect. *Chemical Engineering Journal* **2012**, *181*, 334-342.
6. Stoppa, A.; Hunger, J.; Buchner, R., Conductivities of Binary Mixtures of Ionic Liquids with Polar Solvents. *Journal of Chemical & Engineering Data* **2009**, *54*, 472-479.
7. Yang, F.; Feng, P., Thermophysical Properties of 1-Octyl-3-Methylimidazolium Acetate with Organic Solvents. *International Journal of Chemical Engineering* **2020**, *2020*, 1-12.
8. Ghazipour, H.; Gutiérrez, A.; Alavianmehr, M.; Hosseini, S.; Aparicio, S., Tuning the Properties of Ionic Liquids by Mixing with Organic Solvents: The Case of 1-Butyl-3-Methylimidazolium Glutamate with Alkanols. *Journal of Molecular Liquids* **2022**, *347*, 117953.
9. Meng, J.; Pan, Y.; Yang, F.; Wang, Y.; Zheng, Z.; Jiang, J., Thermal Stability and Decomposition Kinetics of 1-Alkyl-2, 3-Dimethylimidazolium Nitrate Ionic Liquids: Tga and Dft Study. *Materials* **2021**, *14*, 2560.
10. Guo, Q.; Liu, Q.; Zhao, Y., Insights into the Structure and Dynamics of Imidazolium Ionic Liquid and Tetraethylene Glycol Dimethyl Ether Cosolvent Mixtures: A Molecular Dynamics Approach. *Nanomaterials* **2021**, *11*, 2512.
11. Wang, Y.-L.; Li, B.; Sarman, S.; Mocci, F.; Lu, Z.-Y.; Yuan, J.; Laaksonen, A.; Fayer, M. D., Microstructural and Dynamical Heterogeneities in Ionic Liquids. *Chemical Reviews* **2020**, *120*, 5798-5877.

12. Kaintz, A.; Baker, G.; Benesi, A.; Maroncelli, M., Solute Diffusion in Ionic Liquids, Nmr Measurements and Comparisons to Conventional Solvents. *The Journal of Physical Chemistry B* **2013**, *117*, 11697-708.
13. Cha, S.; Shim, T.; Ouchi, Y.; Kim, D., Characteristics of Visible Fluorescence from Ionic Liquids. *The Journal of Physical Chemistry B* **2013**, *117*, 10818-10825.
14. Pal, A.; Kumar, B.; Kang, T. S., Effect of Structural Alteration of Ionic Liquid on Their Bulk and Molecular Level Interactions with Ethylene Glycol. *Fluid Phase Equilibria* **2013**, *358*, 241-249.
15. Mancini, P.; Fortunato, G.; Vottero, L., Molecular Solvent/Ionic Liquid Binary Mixtures: Designing Solvents Based on the Determination of Their Microscopic Properties. *Physics and Chemistry of Liquids* **2004**, *42*, 625-632.
16. Islam, M. R.; Warsi, F.; Khan, A. B.; Kausar, T.; Khan, I.; Ali, M., Solvatochromism of Binary Mixtures of 2, 2, 2-Trifluoroethanol+ Ionic Liquid [Bmim][NTf_2]: A Comparative Study with Molecular Solvents. *Journal of Chemical & Engineering Data* **2019**, *64*, 1140-1154.
17. Kodama, K.; Tsuda, R.; Niitsuma, K.; Tamura, T.; Ueki, T.; Kokubo, H.; Watanabe, M., Structural Effects of Polyethers and Ionic Liquids in Their Binary Mixtures on Lower Critical Solution Temperature Liquid-Liquid Phase Separation. *Polymer journal* **2011**, *43*, 242-248.
18. Ausín, D.; Parajó, J. J.; Trenzado, J. L.; Varela, L. M.; Cabeza, O.; Segade, L., Influence of Small Quantities of Water on the Physical Properties of Alkylammonium Nitrate Ionic Liquids. *International Journal of Molecular Sciences* **2021**, *22*, 7334.
19. Anderson, J. L.; Ding, R.; Ellern, A.; Armstrong, D. W., Structure and Properties of High Stability Geminal Dicationic Ionic Liquids. *Journal of the American Chemical Society* **2005**, *127*, 593-604.
20. Shirota, H.; Mandai, T.; Fukazawa, H.; Kato, T., Comparison between Dicationic and Monocationic Ionic Liquids: Liquid Density, Thermal Properties, Surface Tension, and Shear Viscosity. *Journal of Chemical & Engineering Data* **2011**, *56*, 2453-2459.
21. Chakraborty, M.; Barik, S.; Mahapatra, A.; Sarkar, M., Effect of Lithium-Ion on the Structural Organization of Monocationic and Dicationic Ionic Liquids. *The Journal of Physical Chemistry B* **2021**, *125*, 13015-13026.
22. Nirmale, T. C.; Khupse, N. D.; Kalubarme, R. S.; Kulkarni, M. V.; Varma, A. J.; Kale, B. B., Imidazolium-Based Dicationic Ionic Liquid Electrolyte: Strategy toward Safer Lithium-Ion Batteries. *ACS Sustainable Chemistry & Engineering* **2022**, *10*, 8297-8304.
23. Noack, K.; Leipertz, A.; Kiefer, J., Molecular Interactions and Macroscopic Effects in Binary Mixtures of an Imidazolium Ionic Liquid with Water, Methanol, and Ethanol. *Journal of Molecular Structure* **2012**, *1018*, 45-53.
24. Bandlamudi, S. R. P.; Benjamin, K. M., Thermodynamics of Ionic Liquid Cosolvent Mixtures Using Molecular Dynamics Simulation: 1-Ethyl-3-Methylimidazolium Acetate. *Journal of Chemical & Engineering Data* **2018**, *63*, 2567-2577.
25. Borodin, O.; Gorecki, W.; Smith, G. D.; Armand, M., Molecular Dynamics Simulation and Pulsed-Field Gradient Nmr Studies of Bis (Fluorosulfonyl) Imide (FSI) and Bis [(Trifluoromethyl) Sulfonyl] Imide (TFSI)-Based Ionic Liquids. *The journal of physical chemistry B* **2010**, *114*, 6786-6798.
26. Hardacre, C.; Holbrey, J. D.; Mullan, C. L.; Youngs, T. G.; Bowron, D. T., Small Angle Neutron Scattering from 1-Alkyl-3-Methylimidazolium Hexafluorophosphate Ionic Liquids ([CNMim][PF_6], N= 4, 6, and 8). *The Journal of chemical physics* **2010**, *133*, 074510.
27. Chakrabarty, D.; Seth, D.; Chakraborty, A.; Sarkar, N., Dynamics of Solvation and Rotational Relaxation of Coumarin 153 in Ionic Liquid Confined Nanometer-Sized Microemulsions. *The Journal of Physical Chemistry B* **2005**, *109*, 5753-5758.

28. Seth, D.; Chakraborty, A.; Setua, P.; Sarkar, N., Dynamics of Solvent and Rotational Relaxation of Coumarin-153 in Room-Temperature Ionic Liquid 1-Butyl-3-Methyl Imidazolium Tetrafluoroborate Confined in Poly(Oxyethylene Glycol) Ethers Containing Micelles. *The Journal of Physical Chemistry B* **2007**, *111*, 4781-4787.
29. Fumino, K.; Wulf, A.; Ludwig, R., Strong, Localized, and Directional Hydrogen Bonds Fluidize Ionic Liquids. *Angewandte Chemie International Edition* **2008**, *47*, 8731-8734.
30. Prabhu, S. R.; Dutt, G., Rotational Diffusion of Organic Solutes in 1-Methyl-3-Octylimidazolium Tetrafluoroborate–Diethylene Glycol Mixtures: Influence of Organic Solvent on the Organized Structure of the Ionic Liquid. *The Journal of Physical Chemistry B* **2014**, *118*, 5562-5569.
31. Yaghini, N.; Abdurrokhman, I.; Hasani, M.; Martinelli, A., Transport Properties and Intermolecular Interactions in Binary Mixtures Based on the Protic Ionic Liquid Ethylimidazolium Triflate and Ethylene Glycol. *Physical Chemistry Chemical Physics* **2018**, *20*, 22980-22986.
32. Khodadadi-Moghaddam, M.; Habibi-Yangjeh, A.; Gholami, M. R., Solvatochromic Parameters for Binary Mixtures of an Ionic Liquid with Various Protic Molecular Solvents. *Monatshefte für Chemie-Chemical Monthly* **2009**, *140*, 329-334.
33. Majhi, D.; Seth, S.; Sarkar, M., Differences in the Behavior of Dicationic and Monocationic Ionic Liquids as Revealed by Time Resolved-Fluorescence, Nmr and Fluorescence Correlation Spectroscopy. *Physical Chemistry Chemical Physics* **2018**, *20*, 7844-7856.
34. Li, S.; Feng, G.; Bañuelos, J. L.; Rother, G.; Fulvio, P. F.; Dai, S.; Cummings, P. T., Distinctive Nanoscale Organization of Dicationic Versus Monocationic Ionic Liquids. *The Journal of Physical Chemistry C* **2013**, *117*, 18251-18257.
35. Montalbán, M.; Víllora, G.; Licence, P., Synthesis and Characterization Data of Monocationic and Dicationic Ionic Liquids or Molten Salts. *Data in brief* **2018**, *19*, 769-788.
36. Barik, S.; Chakraborty, M.; Sarkar, M., How Does Addition of Lithium Salt Influence the Structure and Dynamics of Choline Chloride-Based Deep Eutectic Solvents? *The Journal of Physical Chemistry B* **2020**, *124*, 2864-2878.
37. Stejskal, E. O.; Tanner, J. E., Spin Diffusion Measurements: Spin Echoes in the Presence of a Time-Dependent Field Gradient. *The journal of chemical physics* **1965**, *42*, 288-292.
38. Sahu, P. K.; Das, S. K.; Sarkar, M., Toward Understanding Solute–Solvent Interaction in Room-Temperature Mono- and Dicationic Ionic Liquids: A Combined Fluorescence Spectroscopy and Mass Spectrometry Analysis. *The Journal of Physical Chemistry B* **2014**, *118*, 1907-1915.
39. Fruchey, K.; Fayer, M., Dynamics in Organic Ionic Liquids in Distinct Regions Using Charged and Uncharged Orientational Relaxation Probes. *The Journal of Physical Chemistry B* **2010**, *114*, 2840-2845.
40. Chakrabarty, D.; Chakraborty, A.; Seth, D.; Hazra, P.; Sarkar, N., Dynamics of Solvation and Rotational Relaxation of Coumarin 153 in 1-Butyl-3-Methylimidazolium Hexafluorophosphate [Bmim][PF_6]–Water Mixtures. *Chemical physics letters* **2004**, *397*, 469-474.
41. Das, S.; Biswas, R.; Mukherjee, B., Reorientational Jump Dynamics and Its Connections to Hydrogen Bond Relaxation in Molten Acetamide: An All-Atom Molecular Dynamics Simulation Study. *The Journal of Physical Chemistry B* **2015**, *119*, 274-283.
42. Pal, T.; Biswas, R., Heterogeneity and Viscosity Decoupling in (Acetamide+ Electrolyte) Molten Mixtures: A Model Simulation Study. *Chemical Physics Letters* **2011**, *517*, 180-185.

43. Mahapatra, A.; Chakraborty, M.; Barik, S.; Sarkar, M., Comparison between Pyrrolidinium-Based and Imidazolium-Based Dicationic Ionic Liquids: Intermolecular Interaction, Structural Organization, and Solute Dynamics. *Physical Chemistry Chemical Physics* **2021**, *23*, 21029-21041.
44. Dueby, S.; Dubey, V.; Daschakraborty, S., Decoupling of Translational Diffusion from the Viscosity of Supercooled Water: Role of Translational Jump Diffusion. *The Journal of Physical Chemistry B* **2019**, *123*, 7178-7189.

Chapter 4b

Probing Lithium-Ion Driven Micro-Environment Changes in Pyrrolidinium-Based Mono-cationic and Di-cationic Ionic Liquid

Abstract

In recent times, the mixture of lithium salt and ionic liquid (IL) has emerged as an alternative electrolyte for lithium-ion batteries demonstrating notable improved conductivity than pure IL-based electrolyte. However, this promising advancement is not without its complexities, as the introduction of lithium salt has been identified to influence the structural organization within ILs. In this chapter, the structural organisation and diffusion dynamics of a pyrrolidinium-based MIL and DIL containing same alkyl units have been studied in the absence and presence of lithium salt. The inherent findings of this study have revealed that the coordination of Li^+ ions with the anions of both MILs and DILs triggers a change in the structural arrangement of the nonpolar regions within these respective media. Quite interestingly, our results have also indicated that the introduction of Li^+ can ions induce a significantly more pronounced perturbation in the nano-structural organization of MILs as compared to its impact on DILs. Analysis of the data have suggested that the robust nano-structural organization in pyrrolidinium-based DIL remains only slightly affected by the influence of lithium salt. These findings contribute valuable insights into the intricate interplay between lithium salt, ILs, and the resulting electrochemical characteristics, offering a promising avenue for the continued development of high-performance lithium-ion batteries.

4b.1. Introduction

The continuous quest for safer, more efficient, and environmentally friendly energy-storage device have driven researchers to explore innovative formulations for lithium-ion batteries (LIBs).[1-3] Recently, a promising avenue has emerged with the utilization of mixtures comprising lithium salts and ILs as electrolytes, presenting an intriguing alternative to traditional organic solvent-based LIB electrolytes.[4-5] ILs being characterized by their low volatility and flammability has not only mitigated the safety risks but also has contributed to enhance the overall stability of the electrolyte system.[6-7] Moreover, addition of lithium salts has long been recognized for their ability to enhance ionic conductivity. [7]However, the synergy of lithium salt with ILs and the consequent impact on the microscopic structural organizations within ILs still represents a less explored frontier. In this context, recent studies have shed light on a noteworthy phenomenon i.e. the aggregation of IL anions in the presence of lithium (Li) ions.[8-13] Therefore, understanding how the introduction of lithium salts alters the intricate arrangement of ions and molecules within ILs is also crucial for optimization of an electrolyte. In this context we would like to note here that while most of the studies on the above-mentioned aspects have been carried out by employing MILs, investigations involving another category of ILs, specifically DILs, are notably scarce. [14-16]As DIL are advantageous as compared to MILs particularly in terms of high thermal stability and wider electrochemical potential window, detailed examination of their potential attributed to their microscopic feature is also crucial to fully realize the potential of a DIL-based electrolytic system for various-energy related applications.

Focusing on some recent studies carried on the coordination effect of Li ion with the ILs, Varela and co-workers through combined small angle X-ray scattering (SAXS) experiments and atomic simulations have shown that the structure of alkyl ammonium nitrate (EAN) IL remains almost intact upon addition of lithium nitrate ($LiNO_3$) salt.[17] The analysis of their data have

revealed that although coordination of Li^+ ion take place with the polar nano-domain within the IL formed by the anions in both monodentate and bidentate fashion, the inter-constituent interaction in ILs gets only slightly affected. In this context, we would like to mention here that solvated Li-ion can coordinate with the IL media in distinct ways. [18-19]This coordination mode can be intricately related to the idea of "structure-making" and "structure-breaking" where the solvated inorganic ions induce different local structure of water molecules in the first and even the second or third solvation shells to accommodate the dissolved species. [19-21] In this context, Atkin and co-workers have shown "structure-breaking" effect of $LiNO_3$ in EAN, where the incorporation of $LiNO_3$ into the polar domain of EAN, are shown to disrupt in the neat alignment of ethyl chains in the apolar domain.[21] Conversely, in the case ethanolammonium nitrate (EtAN) IL, "structure-making" effect of $LiNO_3$ have also been observed. This phenomenon has been attributed to the long-range rearrangement of EtAN in the presence of Li^+ ions. [21]Fayer and co-workers while investigating the effect of lithium bis(trifluoromethylsulfonyl)imide ([LiNTf2]) salt on imidazolium-based MIL through optically heterodyne-detected optical Kerr effect (OHD-OKE) spectroscopy have observed the influences of lithium salt addition on the ion mobility and rotational dynamics of ions in IL−Li solvent system attributed to increase in viscosity of the medium.[22] Furthermore, it has also been demonstrated by Sakai and colleague that the binding of lithium to the polymeric sites of the gel-based electrolyte helps in enhancing the diffusion of lithium-ion in the medium due to the segmental motion of the polymer chain.[23] Overall, all the above-mentioned studies that are carried out by employing MILs have demonstrated that the introduction of Li^+ ion can cause significant perturbation in the structural organization of the IL medium.

In addition to this, a recent investigation by Sarkar and coworkers on the same aspects by employing structurally similar MIL and DIL has revealed that structural organisation DIL remains less affected by introduction of Li salt as compared to MIL.[24] This study highlights the

robust structural integrity of the DIL. It is important to note here that the aforementioned work has been carried out by imidazolium-based DIL.[25] However, similar work by employing other cation-based DIL has not been carried out yet. Interestingly, pyrrolidinium-based DIL have been demonstrated to have superior physicochemical properties as well as different structural organisation than imidazolium-based DIL.[26-27] Therefore, it is imperative to understand the influence of lithium salt on the structural organisation in pyrrolidinium-based DIL. This investigation can help one in making proper choice in selecting of DIL-based electrolyte for targeted applications.

Keening above facts in mind, the present chapter aims to investigate the structural organization of a pyrrolidinium-based DIL and MIL in the absence and presence of lithium salt. For this purpose, a DIL, 1,9-bis(1-methylpyrrolidinium-1-yl) nonane bis(trifluoromethanesulfonyl)imide $[C_9(MPyrr)_2][NTf_2]_2$ and a MIL 1-methyl-1-octylpyrrolidinium bis(trifluoromethanesulfonyl)imide $[C_8(MPyrr)][NTf_2]$ have been synthesized and are investigated. Lithium bis(trifluoromethanesulfonyl) imide has been chosen as the salt in this study because it possesses anion NTf_2^- same as that of IL possess. Moreover, we would like to note here that, the MIL has been chosen in such a way that the alkyl chain length of the MILs matches with the spacer chain length of the DIL. The choice of system is expected to provide a comparative view of the changes that may happen during IL-Li^+ interaction events. To probe the structural organization in the apolar and polar domains of ILs in absence and presence of lithium ion, the rotational diffusion of selected solutes are carried out using TRFA. Two probes, 9-Phenylanthracene (9-PA) and Rhodamine 110 (R110), are also used here for TRFA measurements. 9-PA, being apolar, help in probing solute-solvent interactions in the apolar domain, while R110, being polar, help in monitoring activities in the polar domain of the ILs. Furthermore, NMR studies have also been carried out to shed more light on the intermolecular interaction at the molecular level. The results of this research are

anticipated to enhance our understanding of the behaviour exhibited by both MIL and DIL in the presence of lithium salt. The chemical structures of ILs used in this study has been provided in Scheme 4b.1.

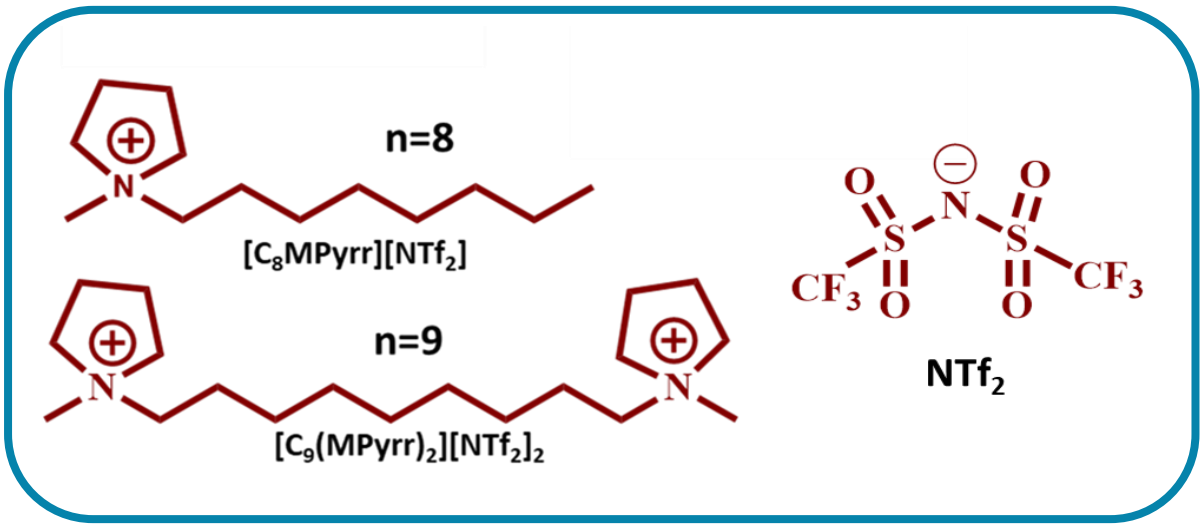

Scheme 4b.1. Chemical structure of the ILs used in this study

4b.2. Materials, Instruments and Methods.

The ionic liquid has been synthesized by following standard protocols as described in the chapter 1. The methods followed to carry out the experiments in this chapter is same as described in chapter 4a and chapter 2.

4b.3. Results and Discussion

4b.3.1. Time resolved fluorescence anisotropy studies. To declutter the impact of increasing concentration of Li^+ ions on the structural organization of both MIL and DIL, as we did in the chapter 4a, the rotational diffusion of two meticulously chosen probe molecules, 9-PA and R110, has been monitored in neat ILs as well as (IL+$LiNTf_2$) mixtures at various temperature ranging from 303k-353k. Fluorescence anisotropy decays of 9-PA and R110 were measured in both IL and (IL+$LiNTf_2$) mixtures at corresponding temperatures. A single exponential decay function satisfactorily fits the data.

Table 4b.1. The viscosity and rotational reorientation time of 9-PA and R110 in IL systems

Systems	T (k)	η(cP)	9PA		R110	
			τ_r (ns)	C_{rot}	τ_r (ns)	C_{rot}
$[C_8(MPyrr)][NTf_2]$	303	81.1	2.29	0.29	12.7	1.16
	313	51.0	1.55	0.32	7.80	1.17
(X=0)	323	43.0	1.30	0.33	6.60	1.21
	333	28.5	0.97	0.38	4.30	1.22
	343	21.7	0.82	0.44	3.30	1.27
	353	17.5	0.69	0.47	2.55	1.28
	303	129.5	2.82	0.22	15.5	0.89
	313	84.3	2.03	0.25	10.0	0.90
(X=0.05 Li^+)	323	57.0	1.41	0.27	7.10	0.98
	333	38.9	1.09	0.31	4.91	1.03
	343	28.1	0.88	0.36	3.55	1.05
	353	20.5	0.71	0.41	2.60	1.09
	303	153.1	3.01	0.20	16.6	0.80
	313	98.5	2.10	0.22	10.8	0.83
(X=0.1 Li^+)	323	66.1	1.44	0.23	7.30	0.87
	333	45.1	1.12	0.27	5.10	0.92
	343	32.7	0.90	0.31	3.64	0.93
	353	23.8	0.73	0.36	2.70	0.97
	303	269.1	3.90	0.15	20.2	0.56
	313	159.2	2.50	0.17	13.0	0.62
(X=0.2 Li^+)	323	92.2	1.60	0.19	8.05	0.69
	333	55.5	1.12	0.23	5.16	0.76
	343	37.2	1.00	0.31	3.75	0.84
	353	27.0	0.75	0.32	2.84	0.90
$[C_9(MPyrr)_2][NTf_2]_2$	303	815.0	9.00	0.11	27.0	0.25
	313	485.6	6.10	0.13	20.0	0.31
(X=0)	323	286.1	4.10	0.15	12.8	0.35
	333	180.7	2.80	0.17	7.93	0.36
	343	121.0	1.90	0.18	5.63	0.39
	353	82.6	1.50	0.21	4.00	0.41
	303	900.9	9.45	0.10	27.7	0.22
	313	526.5	6.45	0.13	20.5	0.29
(X=0.05Li^+)	323	310.6	4.27	0.15	13.0	0.33
	333	189.7	2.91	0.17	8.33	0.35
	343	126.0	1.96	0.18	5.75	0.38
	353	90.0	1.54	0.20	4.15	0.39
	303	1055.0	10.0	0.09	28.2	0.20
	313	581.2	7.00	0.12	20.6	0.27
(X=0.1 Li^+)	323	349.0	4.74	0.14	13.2	0.30
	333	215.0	3.05	0.16	8.72	0.33
	343	139.8	2.05	0.17	5.81	0.34
	353	96.5	1.60	0.20	4.28	0.38
	303	1211.0	10.5	0.08	28.9	0.17
	313	704.0	8.30	0.12	21.1	0.23
(X=0.2 Li^+)	323	406.0	5.38	0.14	13.5	0.26
	333	287.0	3.96	0.15	9.20	0.27
	343	162.0	2.30	0.16	5.89	0.30
	353	109.0	1.70	0.18	4.37	0.34

The decay plots at a specific temperature (323k) for both MIL and DIL in the absence and presence of $LiNTf_2$ are provided in the Appendix 4b (Figure APX.4b.1). The estimated reorientation times (τ_r) of the two solutes along with the viscosities of the solvent systems are provided in Table 4b.1. However, since it would be difficult to assess that this lower (τ_r) value of the probe in the concerned media is due to change in the bulk viscosity of the media or due to the change in micro-viscosity of the media in presence of $LiNTf_2$, we also estimated the reorientation time (τ_r) of probe molecules in pure ILs and their mixtures with $LiNTf_2$ under iso-viscous condition. For this purpose, we have conducted additional measurements of the (τ_r) for both the probe molecules in pure ILs as well as their $LiNTf_2$ mixtures by carefully controlling the temperature so that the viscosity of the mixtures match with the viscosity of the pure ILs. This allowed us to eliminate the influence of viscosity and gain precise insight into the effect of $LiNTf_2$ on the rotation of solute molecules. The results of these measurements are summarised in Table 4b.2. We would like to note here that, the τ_r the MIL systems are measured at a viscosity 55cP and that of for DIL systems at 185cP.

Table 4b.2. Rotational relaxation parameters of different probes in both the MIL and DIL systems under iso-viscous conditions.

X/ (Li^+)	τ_r (ns)			
	$[C_8(MPyrr)][NTf_2]$		$[C_9(MPyrr)_2][NTf_2]_2$	
	9-PA	R110	9-PA	R110
0.0	1.75	9.40	2.86	7.93
0.05	1.42	7.20	2.79	7.80
0.1	1.24	6.40	2.55	7.27
0.2	1.13	5.20	2.40	6.45

Upon careful inspection of the data presented in Table 4b.2, it can be revealed that the rotational diffusion time for both the probe 9-PA and R110 decreases upon the addition of $LiNTf_2$ salt even under iso-viscous conditions. This observation clearly implies that the presence of Li^+ ions induce structural perturbation in both MIL and DIL, leading to a change in the rotational

behaviour of the probe molecules in these media. Moreover, the extent of change of τ_r for both the probe is found to be different for MIL and DIL. For example, the τ_r of 9-PA, which has been decreased by 1.5-fold with addition of 0.2 M. F of $LiNTf_2$ in case of MIL, decreased only marginally in case of DIL. Similarly, while τ_r of R110 has been decreased almost by two-fold in case of MIL, decreased only marginally in case of DIL. Therefore, these observations partcularly suggest that the micro-environment experienced by the probe in presence of Li^+ ion is not unform in both MIL and DIL.

In order to address, how presence Li^+ ion influence the strctural organisations in MIL and DIL, we furthe analysed the data by means of Stoke-Einstein-Debye (SED) hydrodynamic theory (eq. 2.14.).[28] The SED plots for 9-PA and R110 in the presence of MIL and DIL and their imixture with various molefraction of $LiNTf_2$ have been been provided in Figure 4b.1 and Figure 4b.2 respectively.

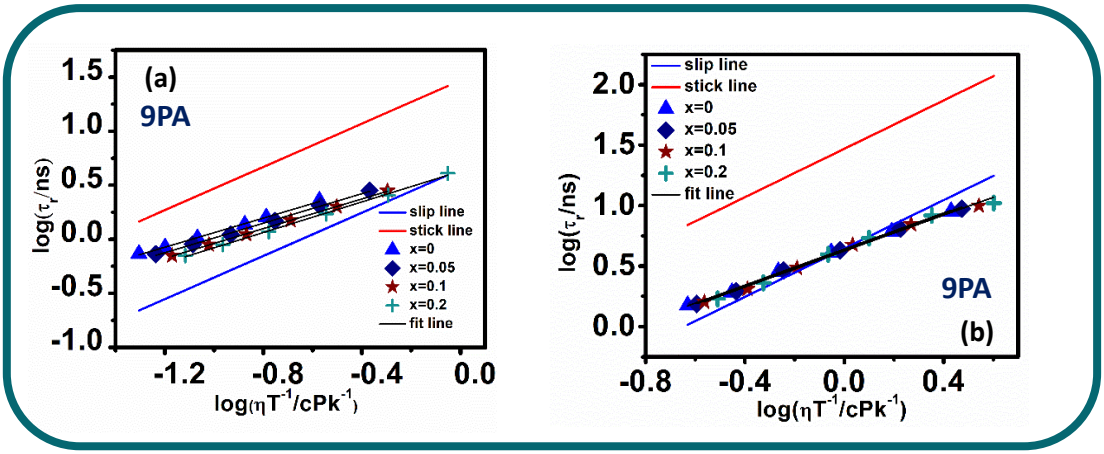

Figure 4b.1. Log–log plots of rotational reorientation time of 9-PA in (a) $[C_8(MPyrr)][NTf_2]$ (b) $[C_9(MPyrr)_2][NTf_2]_2$ in neat condition as well as with their mixture with $LiNTf_2$ of various composition as marked in the legend of the figures. Here, blue and red lines indicate the slip and stick boundary conditions, respectively. The solid black line indicates the fit to data points.

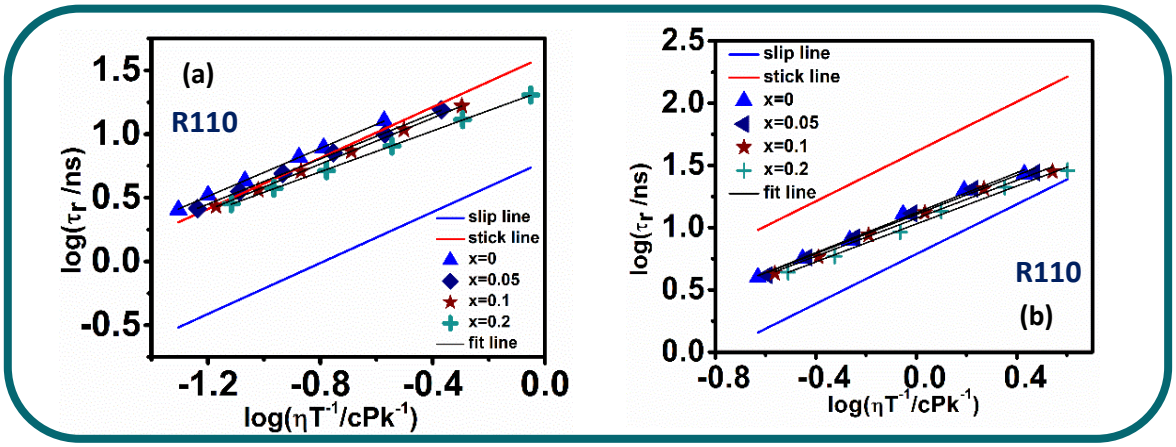

Figure 4b.2. Log−log plots of rotational reorientation time of R110 in (a) $[C_8(MPyrr)][NTf_2]$, (b) $[C_9(MPyrr)_2][NTf_2]_2$ in neat condition as well as with their mixture with LiNTf2 of various composition as marked in the legend of the figures.

Upon careful analysis of SED plots, we found that the presence of lithium salt is perhaps affecting the structural organisation in DIL to a greater extent. To have a better visualization of the difference in the behaviour of MIL and DIL in the presence of $LiNTf_2$, the average friction coefficient values($C_{rot} = {}^{\tau_r}/_{\tau_{exp}}$) of 9-PA and R110 are estimated utilizing the data from Table 4b.1 for both MILs and DIL and are plotted individually against the mole fraction of $LiNTf_2$ added to concerned neat ILs (Figure 4b.3). In this context we would like to note here that the friction coefficient is a measure of the extent of solute-solvent interaction. Figure 4b.3a and Figure 4b.3b have collectively shown that the change in the friction coefficient of 9-PA and R110 with the addition of $LiNTf_2$ is found to be relatively higher in MIL than that in DIL. The outcome of the current analysis has clearly pointed out that the presence of $LiNTf_2$ can cause significant perturbation in the structural organization of MIL, whereas the structural organization of the DIL remains almost intact even after a similar proportion of $LiNTf_2$ is added to the DIL.

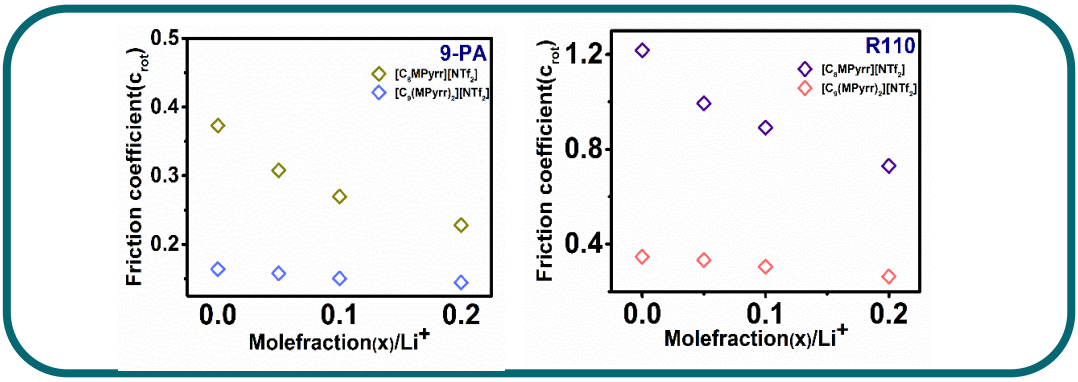

Figure 4b.3. Friction coefficient for 9-PA (a) and R110 (b) in MIL and DIL as a function of $LiNTf_2$ molefraction.

4b. 3. 2. PFG-NMR studies.

To verify these aspects further, we the temperature dependent self-diffusion coefficient (D_t) of the cationic parts of both MIL and DIL in the absence and presence of various mole fraction of $LiNTf_2$ has been determined by using PFG-NMR technique and are collected in Table 4b.3.

Table 4b. 3. Translational diffusion coefficients of cationic part of IL systems in absence and presence of ethylene glycol at 303-343k.

	Diffusion Coefficient (D_t*10^{-11}/m^2s^{-1})					
Systems	X($LiNTf_2$)	303k	313k	323k	333k	343k
[C_8(MPyrr)][NTf_2]	0	1.08	1.72	2.34	3.63	5.56
	0.05	0.76	1.26	1.90	2.92	4.90
	0.1	0.55	1.10	1.74	2.58	4.03
	0.2	0.27	0.48	0.81	1.55	2.50
[C_9(MPyrr)$_2$][NTf_2]$_2$	0	0.09	0.16	0.29	0.5	0.85
	0.05	0.08	0.16	0.29	0.49	0.83
	0.1	0.07	0.17	0.28	0.47	0.79
	0.2	0.06	0.14	0.26	0.39	0.71

From Table 4b.3. it can be seen that the diffusion coefficient of both MIL and DIL at a given temperature decreases with increasing amount of lithium salt. This happens due to the increase in viscosity of the medium upon addition of lithium salt (Table 4b.1). However, upon a more careful look, one can find that the rate of decrease of D_t value with the increase fraction of lithium salt is relatively larger in presence of MIL as compared that in DIL. This study also indicated that addition of same fraction of lithium salt to both MIL and DIL brings about more changes in the structural organisation of MIL than that of DIL. However, we note here that studies by employing molecular dynamic simulation is expected to throw more light on the reason behind the distinct influence of lithium ion on the nano-structural organisation in MIL and DIL in better manner.

4b.4. Conclusions

In this section, we have investigated the structural arrangement and diffusion dynamics of a pyrrolidinium-based MIL and DIL featuring identical alkyl units, both in the absence and presence of lithium salt by employing TRFA and NMR spectroscopy techniques. The results of our study reveal that the coordination of Li^+ ions with the anions in both MILs and DILs initiates a shift in the structural organization of the nonpolar regions within these media. Notably, our findings highlight that the introduction of Li^+ ions cause a more significant disruption in the nano-structural organization of MILs compared to its impact on DILs. Our data analysis suggests that the robust structural organization observed in pyrrolidinium-based DIL is only minimally affected by the influence of lithium salt. These insights provide valuable information on the complex interplay between lithium salt and ILs. This is expected to open up research opens up a promising avenue for advancing the development of high-performance lithium-ion batteries.

4b.5. Appendix 4b

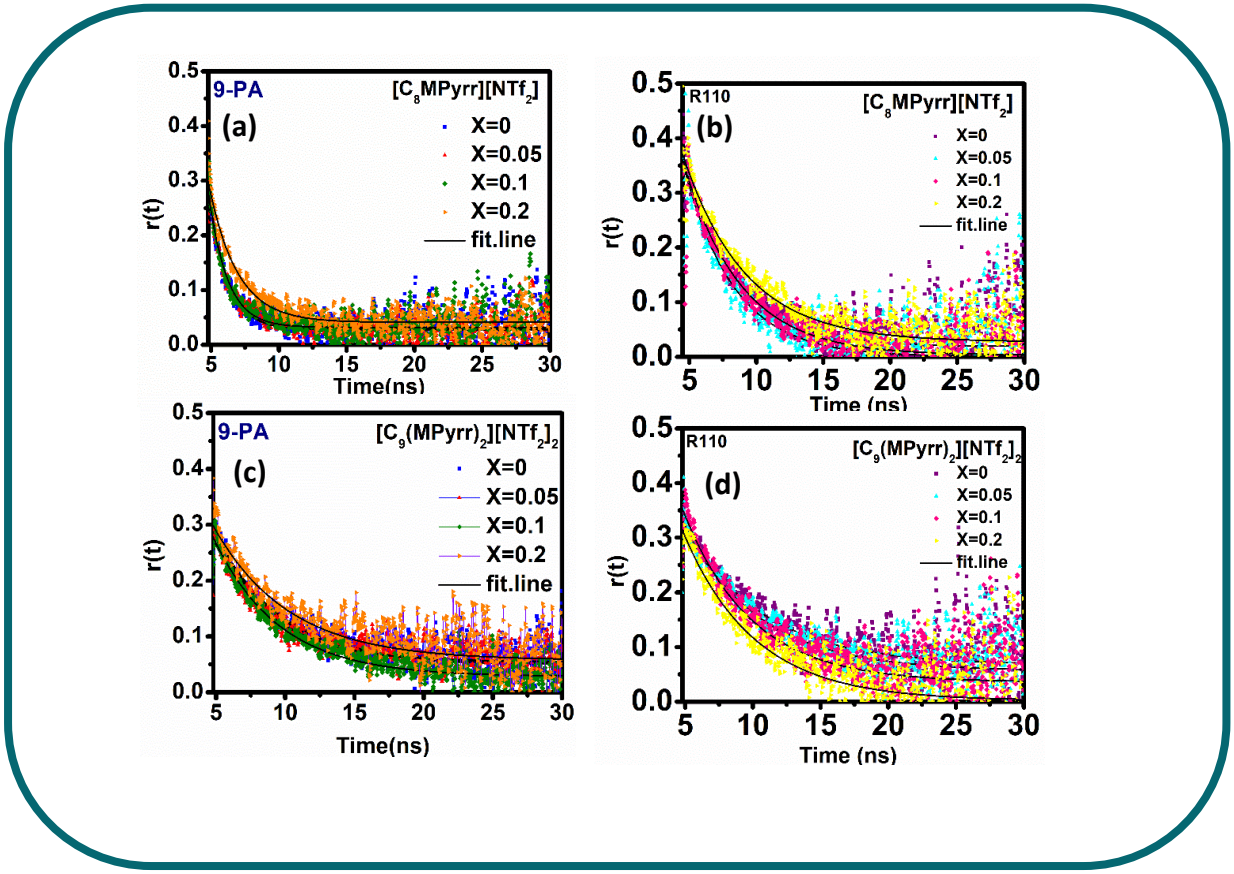

Figure APX.4b.1. Decay profiles of 9-PA and R110 in MIL and DIL at 323k in abascence and presence of lithium salt.

REFERNCES

1. Miyamoto, H.; Yokota, Y.; Imanishi, A.; Inagaki, K.; Morikawa, Y.; Fukui, K.-i., Potential Dependent Changes in the Structural and Dynamical Properties of 1-Butyl-3-Methylimidazolium Bis (Trifluoromethanesulfonyl) Imide on Graphite Electrodes Revealed by Molecular Dynamics Simulations. *Physical Chemistry Chemical Physics* **2018**, *20*, 19408-19415.

2. Zhu, H.; Wang, X.; Vijayaraghava, R.; Zhou, Y.; MacFarlane, D. R.; Forsyth, M., Structure and Ion Dynamics in Imidazolium-Based Protic Organic Ionic Plastic Crystals. *The journal of physical chemistry letters* **2018**, *9*, 3904-3909.

3. Wang, Y.-L.; Li, B.; Sarman, S.; Mocci, F.; Lu, Z.-Y.; Yuan, J.; Laaksonen, A.; Fayer, M. D., Microstructural and Dynamical Heterogeneities in Ionic Liquids. *Chemical reviews* **2020**, *120*, 5798-5877.

4. Liu, K.; Wang, Z.; Shi, L.; Jungsuttiwong, S.; Yuan, S., Ionic Liquids for High Performance Lithium Metal Batteries. *Journal of energy chemistry* **2021**, *59*, 320-333.

5. Zhou, G.; Sun, X.; Li, Q.-H.; Wang, X.; Zhang, J.-N.; Yang, W.; Yu, X.; Xiao, R.; Li, H., Mn Ion Dissolution Mechanism for Lithium-Ion Battery with Limn2o4 Cathode: In Situ Ultraviolet–Visible Spectroscopy and Ab Initio Molecular Dynamics Simulations. *The journal of physical chemistry letters* **2020**, *11*, 3051-3057.

6. Pigłowska, M.; Kurc, B.; Galiński, M.; Fuć, P.; Kamińska, M.; Szymlet, N.; Daszkiewicz, P., Challenges for Safe Electrolytes Applied in Lithium-Ion Cells—a Review. *Materials* **2021**, *14*, 6783.
7. Kim, H.-T.; Kang, J.; Mun, J.; Oh, S. M.; Yim, T.; Kim, Y. G., Pyrrolinium-Based Ionic Liquid as a Flame Retardant for Binary Electrolytes of Lithium Ion Batteries. *ACS Sustainable Chemistry & Engineering* **2016**, *4*, 497-505.
8. Ray, P.; Vogl, T.; Balducci, A.; Kirchner, B., Structural Investigations on Lithium-Doped Protic and Aprotic Ionic Liquids. *The Journal of Physical Chemistry B* **2017**, *121*, 5279-5292.
9. Lawler, C.; Fayer, M. D., The Influence of Lithium Cations on Dynamics and Structure of Room Temperature Ionic Liquids. *The Journal of Physical Chemistry B* **2013**, *117*, 9768-9774.
10. Dutt, G., How Does the Alkyl Chain Length of an Ionic Liquid Influence Solute Rotation in the Presence of an Electrolyte? **2016**.
11. Kadyan, A.; Pandey, S., Florescence Quenching within Lithium Salt-Added Ionic Liquid. *The Journal of Physical Chemistry B* **2018**, *122*, 5106-5113.
12. Duluard, S.; Grondin, J.; Bruneel, J. L.; Pianet, I.; Grélard, A.; Campet, G.; Delville, M. H.; Lassègues, J. C., Lithium Solvation and Diffusion in the 1-Butyl-3-Methylimidazolium Bis (Trifluoromethanesulfonyl) Imide Ionic Liquid. *Journal of Raman Spectroscopy: An International Journal for Original Work in all Aspects of Raman Spectroscopy, Including Higher Order Processes, and also Brillouin and Rayleigh Scattering* **2008**, *39*, 627-632.
13. Aguilera, L.; Völkner, J.; Labrador, A.; Matic, A., The Effect of Lithium Salt Doping on the Nanostructure of Ionic Liquids. *Physical Chemistry Chemical Physics* **2015**, *17*, 27082-27087.
14. Russina, O.; Caminiti, R.; Méndez-Morales, T.; Carrete, J.; Cabeza, O.; Gallego, L. J.; Varela, L. M.; Triolo, A., How Does Lithium Nitrate Dissolve in a Protic Ionic Liquid? *Journal of Molecular Liquids* **2015**, *205*, 16-21.
15. Nicotera, I.; Oliviero, C.; Henderson, W. A.; Appetecchi, G. B.; Passerini, S., Nmr Investigation of Ionic Liquid−Lix Mixtures: Pyrrolidinium Cations and Tfsi- Anions. *The Journal of Physical Chemistry B* **2005**, *109*, 22814-22819.
16. Oh, S.; Keating, M. J.; Biddinger, E. J., Physical and Electrochemical Properties of Ionic-Liquid- and Ester-Based Cosolvent Mixtures with Lithium Salts. *Industrial & Engineering Chemistry Research* **2022**, *61*, 12118-12131.
17. Mendez-Morales, T.; Carrete, J.; Cabeza, O.; Russina, O.; Triolo, A.; Gallego, L. J.; Varela, L. M., Solvation of Lithium Salts in Protic Ionic Liquids: A Molecular Dynamics Study. *The Journal of Physical Chemistry B* **2014**, *118*, 761-770.
18. Méndez-Morales, T.; Carrete, J.; Rodriguez, J. R.; Cabeza, O.; Gallego, L. J.; Russina, O.; Varela, L. M., Nanostructure of Mixtures of Protic Ionic Liquids and Lithium Salts: Effect of Alkyl Chain Length. *Physical Chemistry Chemical Physics* **2015**, *17*, 5298-5307.
19. Hjalmarsson, N.; Atkin, R.; Rutland, M. W., Effect of Lithium Ions on Rheology and Interfacial Forces in Ethylammonium Nitrate and Ethanolammonium Nitrate. *The Journal of Physical Chemistry C* **2016**, *120*, 26960-26967.
20. Mahapatra, A.; Chowdhury, U. D.; Barik, S.; Parida, S.; Bhargava, B. L.; Sarkar, M., Deciphering the Role of Anions of Ionic Liquids in Modulating the Structure and Stability of Ct-DNA in Aqueous Solutions. *Langmuir* **2023**, *39*, 17318-17332.
21. Hayes, R.; Bernard, S. A.; Imberti, S.; Warr, G. G.; Atkin, R., Solvation of Inorganic Nitrate Salts in Protic Ionic Liquids. *The Journal of Physical Chemistry C* **2014**, *118*, 21215-21225.

22. Nicolau, B. G.; Sturlaugson, A.; Fruchey, K.; Ribeiro, M. C.; Fayer, M. D., Room Temperature Ionic Liquid− Lithium Salt Mixtures: Optical Kerr Effect Dynamical Measurements. *The Journal of Physical Chemistry B* **2010**, *114*, 8350-8356.
23. Umecky, T.; Saito, Y.; Okumura, Y.; Maeda, S.; Sakai, T., Ionization Condition of Lithium Ionic Liquid Electrolytes under the Solvation Effect of Liquid and Solid Solvents. *The Journal of Physical Chemistry B* **2008**, *112*, 3357-3364.
24. Chakraborty, M.; Barik, S.; Mahapatra, A.; Sarkar, M., Effect of Lithium-Ion on the Structural Organization of Monocationic and Dicationic Ionic Liquids. *The Journal of Physical Chemistry B* **2021**, *125*, 13015-13026.
25. Nirmale, T. C.; Khupse, N. D.; Kalubarme, R. S.; Kulkarni, M. V.; Varma, A. J.; Kale, B. B., Imidazolium-Based Dicationic Ionic Liquid Electrolyte: Strategy toward Safer Lithium-Ion Batteries. *ACS Sustainable Chemistry & Engineering* **2022**, *10*, 8297-8304.
26. Mahapatra, A.; Chakraborty, M.; Barik, S.; Sarkar, M., Comparison between Pyrrolidinium-Based and Imidazolium-Based Dicationic Ionic Liquids: Intermolecular Interaction, Structural Organization, and Solute Dynamics. *Physical Chemistry Chemical Physics* **2021**, *23*, 21029-21041.
27. Patil, R. A.; Talebi, M.; Xu, C.; Bhawal, S. S.; Armstrong, D. W., Synthesis of Thermally Stable Geminal Dicationic Ionic Liquids and Related Ionic Compounds: An Examination of Physicochemical Properties by Structural Modification. *Chemistry of Materials* **2016**, *28*, 4315-4323.

Chapter 5a

Assessing the Suitability of a Dicationic Ionic Liquid as a Stabilising Material for Storage of DNA in Aqueous Medium

---

Amita Mahapatra, Sahadev Barik, Lakkoji Satish, Manjari Chakraborty and Moloy Sarkar. *Langmuir* **2022**, 38, 48, 14857–14868.

Abstract

In this chapter, the potential of a pyrrolidinium based DIL in stabilizing *ct*-DNA in aqueous solution has been investigated by following DNA-DIL interaction. Additionally, in order to understand the fundamental aspects regarding DNA-DIL interaction in a comprehensive manner, studies are also done by employing structurally similar MILs. The investigations have been carried out both at ensemble-average and single molecular level by using various spectroscopic techniques. The molecular docking study has also been performed to throw more light into our experimental observations. The combined steady-state and time-resolved fluorescence, FCS and circular dichroism (CD) measurements have demonstrated that DILs can effectively be used as a better storage media for *ct*-DNA as compared to MILs. Investigations have also shown that the extra electrostatic interaction between cationic head group of DIL and the phosphate backbone of DNA is primarily responsible for providing better stabilisation to *ct*-DNA retaining its native structure in aqueous medium.

5a.1. Introduction

DNA is a special class of bio-macromolecule, which stores genetic information in living cell. This special molecule is gaining considerable importance owing to their suitability in several applications ranging from biosensors, bio-catalysis, nano-medicines to programmable drug delivery devices.[1-3] However, the long-term storage of this material possesses a great challenge, as they get denatured by means of slow hydrolytic reaction when stored in aqueous medium.[4] Therefore, the quest for a suitable alternative storage media which can ensure long term preservation of DNA in its native form has remained a worth-while objective to the scientific community to pursue. The traditional strategy of using organic solvents systems such as ethylene glycol, DMSO for storing DNA are not effective as these solvents are toxic that leads to denaturation or biotransformation of DNA.[5] Moreover, it has been observed that several surfactants and multivalent ions like polyamines which are also used to compact and store DNA in aqueous medium induce structural changes in DNA due to strong electrostatic interaction.[6-8] Recently, several researchers have acknowledged the use of ILs and more specifically MILs in DNA technology.[9-10] The adjustable hydrophilic and hydrophobic properties of MILs have provided a unique microenvironment for many nucleic acid-based application such extraction, solubilisation and stabilization of DNA in aqueous medium.[11-17] However, the perspective of DILs which are shown to be more versatile than MILs, towards nucleic-acid based applications have not been explored yet.[18-21] As DILs possess a different structural backbone from MILs; the presence of two cationic head groups is expected to induce extra stabilisation due to dication-DNA interaction. Therefore, understanding the fundamental aspects of interaction behaviour of DILs with DNA is quite essential to include such systems in nucleic-acid based research.

In recent past enormous studies have been carried out in order to unravel the mechanism of DNA-IL interactions in aqueous medium. In this context, Ding et al. using both analytical

techniques and molecular dynamic (MD) simulation study have demonstrated that the binding between a butyl imidazolium-based IL, [C_4Mim][Cl] and DNA involves both electrostatic and hydrophobic forces.[22] Later on, Cui and co-workers conducted study on same imidazolium-based ILs [C_nMIM][Cl], with variable alkyl chain (n = 4, 6, 8, 10, 12) have observed that the electrostatic interaction between DNA and imidazolium ion of the ILs is the dominant factor in the binding event.[23] In a similar way when the binding mechanism of choline-based ILs with DNA are investigated, the involvement of H- bonding between the hydroxyl group of choline cation and DNA have also been established in some literature report.[24-25] Moreover, along with structural factor, the geometry of IL cations also found to have a great role in the interaction behaviour of ILs with DNA.[26] In this context, Senapati and a co-worker have demonstrated relatively stronger binding affinity of planar imidazolium-based ILs over choline cation-based ILs at the minor grove of DNA.[27] Furthermore, the effect of length of the alkyl chain in the ILs during the interaction event with DNA has also been examined in several studies. The results of those studies have depicted an increased binding affinity of ILs with DNA in presence of relatively longer alkyl chain.[28] It is evidenced from the above discussion that the binding characteristics and of ILs with DNA depends upon the nature of constituent ions of the ILs. Apart from this, several reports are there which suggests the stability of DNA in presence of ILs are also dependent upon the nature of ILs. In this regard, Prasad and co-workers using choline-based bio-ionic liquids mentioned that significant hydrogen bonding and electrostatic interactions between DNA and ILs provides stability to DNA.[24] MacFarlane and co-workers studied the structural stability of DNA in presence of choline based ILs and showed that the native structure of *ct*-DNA has been remained unaltered at room temperature for a period of one year.[29] Choline based ILs has been reported to provide better thermal stability to *ct*-DNA than imidazolium based ILs.[30] Moreover, higher thermal stability of DNA in presence of longer alkyl chain containing ILs has also been demonstrated in a recent work.[28] The above studies

have provided a lot of valuable information in-terms of understanding the details of DNA-IL interaction event. Moreover, the above discussions have also conveyed that DNA-ILs interaction studies have been done exclusively by exploiting only MILs. However, similar studies by exploiting DILs are elusive. DILs can be a more worth material for storage of DNA as their physiochemical properties are more tailorable owing to greater variability in their structure.[31-33]Therefore, comparative studies of IL−DNA interaction by employing structurally similar class of MIL and DIL are expected to provide a significant step forward in our understanding of the mechanism of DNA−DIL interaction.

Keeping above facts in mind, in this chapter, the potential of a pyrrolidinium based DIL in maintaining structural integrity of *ct*-DNA in aqueous solution has been investigated. The pyrrolidinium-based DIL has been specifically chosen for study because, the pyrrolidinium cation which is devoid of any complex interaction mechanism like π- π interaction and H-bond, unlike imidazolium- based ILs, is expected to provide a simplified picture of the role of extra cation in DIL during their interaction with DNA.[34-35] To understand how DNA-DIL interactions are different from DNA-MIL interactions, two structurally similar MILs, MIL1 and MIL2 have also been employed in this study. It is to be noted here that the MIL1 contains an alkyl chain of length (four -CH_2 unit) which is exactly half of that the MIL2 and DIL have (eight-CH_2 unit) and all of them contain a fixed anion bromide anion (Br^-). The chemical structure of the ILs and the abbreviations used for these ILs are provided in Scheme 5a.1. The presence of similar alkyl chain in MIL2 and DIL is expected to help us to unravel the role of extra cation head in DIL in the interaction event with *ct*-DNA. The investigations have been carried out both at ensemble-averaged and single molecular level by employing various biophysical techniques such as UV-Visible, steady-state and time-resolved fluorescence spectroscopy, FCS, CD spectroscopy and UV-melting experiments. In addition to these, the molecular docking studies have also been performed to rationalise the acquired experimental data. The outcomes of these

studies have suggested that DIL can be used as a better alternative storage media for DNA as compared to MILs.

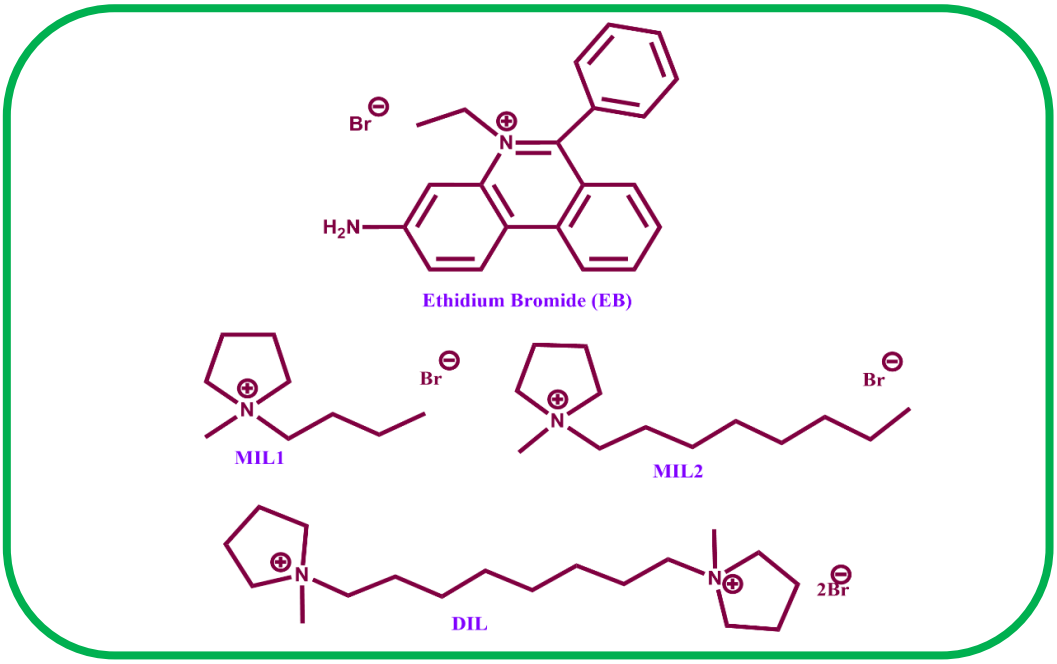

Scheme 5a.1. Schematic structure of ILs, probe molecules and the abbreviation used for the investigated ILs and the probe.

5a.2. Materials, Experimental techniques and methods[36-39]

1-Methylpyrrolidine, 1-Bromobutane, 1-Bromooctane, 1, 8-Dibromooctane, were purchased from TCI Chemicals India. Calf thymus DNA (*ct*-DNA) and Ethidium bromide (EB) [3, 8-diamino-5-ethyl-6-phenylphenanthridium bromide] and tris-HCl buffer (1M) of pH 7.4 were obtained from Sigma-Aldrich. The ionic liquids (ILs) used in this study i.e. MILs, 1-Butyl-1-Methylpyrrolidinum bromide (MIL1), 1-methyl-1-Octylpyrrolidinium bromide (MIL2) and a DIL 1,8-bis (1-methylpyrrolidinium-1-yl) octane bromide were synthesized following the method described in the chapter 2. The purity of the products was analysed using NMR spectroscopy. ^{1}H-NMR spectra of these ILs are provided in Appendix 5a. The sample preparation procedure and the experimental methods has been described in chapter 2.

5a.3. Results and Discussion

5a.3.1. Characteristics of binding of ILs with *ct*-DNA: UV-Vis. absorption measurements

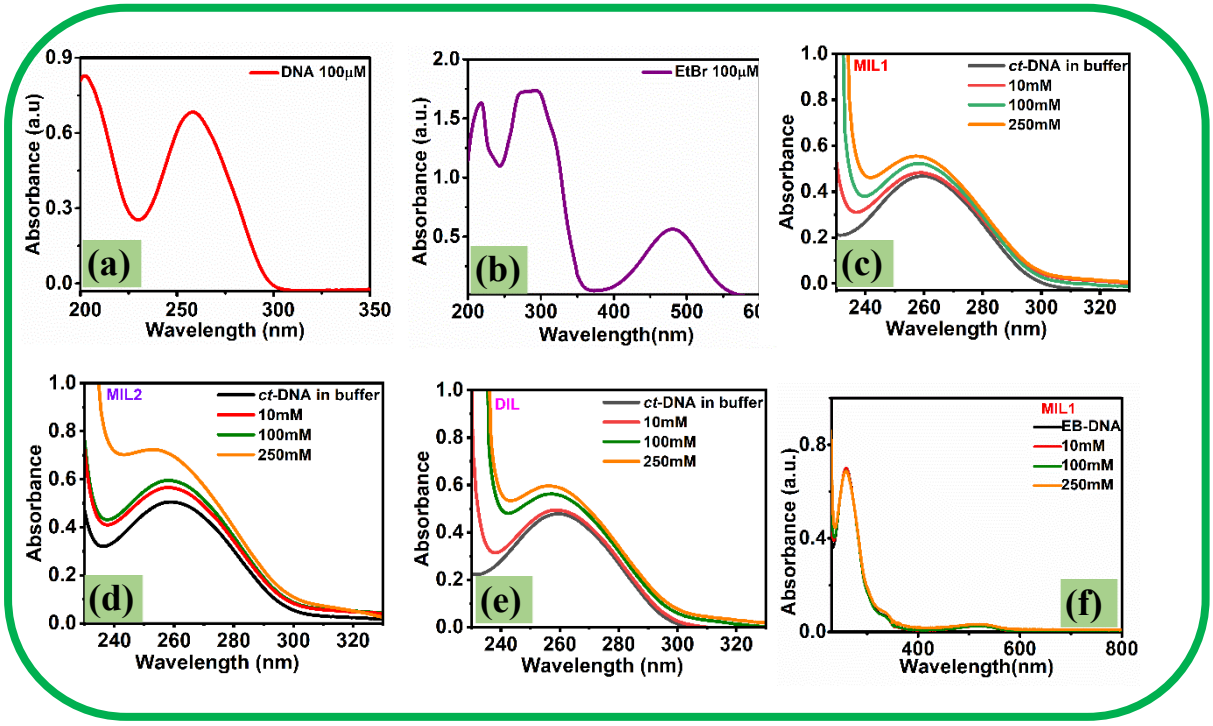

Figure 5a.1. Absorption spectra of (a) Free *ct*-DNA (100 μ*M*), (b) Free EB (100 μ*M*), Absorption spectra of *ct*-DNA (40 μ*M)* in presence of increasing concentration of (c) MIL1, (d) MIL2 and (e) and (f) DNA -EB (5 μ*M* EB and 40 μ*M* DNA) complex in absence and presence of varying concentration of MIL1.

UV–Visible absorption spectroscopy is one of the simplest and most effectual instrumental technique for studying both the stability and interaction of DNA with small ligand molecules. Both the binding potency and the mode of DNA-IL interactions can be perceived through Uv–Visible absorption spectroscopy by monitoring the changes in the absorption properties of the DNA in the presence of ILs.[40] Figure 5a.1a and Figure 5a.1b represents the absorption spectra of free *ct*-DNA and EB in buffer with absorption maxima (λ_{max}) at 260 *nm* and 480 *nm* respectively. As a preliminary investigation, the absorption of *ct*-DNA has been monitored in presence of all the chosen ILs and the results clearly showed a gradual increase in absorbance along with a moderate blue shift upon addition of ILs (Figures 5a.1c, 1d and 1e). These

observations suggest that there may exist more than one type of interaction between *ct*-DNA and chosen IL systems.[15, 25]Figure 5a.1f shows the absorption spectra of EB-DNA complex (5μM EtBr and 40 μM DNA) in absence and presence of three different concentrations of MIL1 as marked in the legend of the Figure 5a.1. Similar spectra for other two IL systems, MIL2 and DIL are provided in Figure APX5a.1 (Appendix 5a). No appreciable changes in the absorption of EB-DNA complex have been noticed in presence of these ILs. This observation clearly suggests the preferential interaction of ILs with *ct*-DNA.[25]In addition to this, the absorption spectra of ILs that are employed in this study are also recorded and have been provided in Appendix 5a (Figure APX5a.1). The negligible absorption of ILs further confirms that the absorption due to ILs do not interfere with the absorption of EB.

5a.3.2. Steady state and Time resolved Fluorescence measurements

Steady-state fluorescence measurements are routinely used to characterize the nature of interaction of DNA with small molecules.[41] In this experiment, EB has been used to probe the interactions between *ct*-DNA and ILs using the fluorescence quenching studies. It may be noted here that EB is an intercalating probe which shows enhanced fluorescence intensity when the planar ring of this molecule stacks inside the base pairs of *ct*-DNA protecting itself from potential quenchers like oxygen etc.[36] Any induced change in the structure of *ct*-DNA owing to its interaction with ILs will affect the microenvironment of the EB and hence can lead to a modulation in its fluorescence behaviour. In the present study for estimating the extent of interaction of different ILs with *ct*-DNA, EB exclusion method has been followed in presence of selected ILs by employing temperature dependent spectrofluorometric titration experiments. Figure 5a.2 shows fluorescence spectra of EB-DNA complex in absence and presence of increasing concentrations of different ILs (10mM to 250mM) at 293k and the equivalent spectra at other temperatures are presented in the Appendix 5a (Figures APX5a.2, APX5a.3 and APX5a.4).

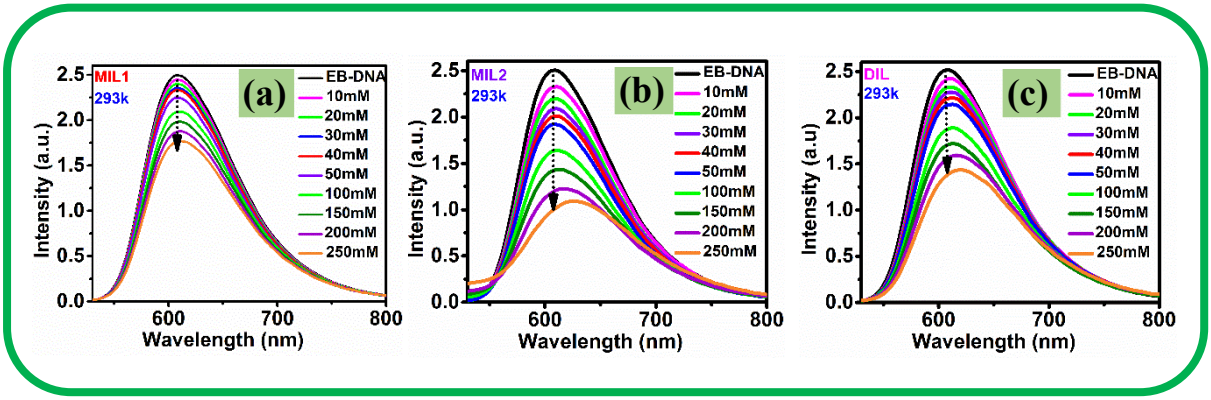

Figure 5a.2. The fluorescence emission spectra of EB-DNA complex in absence and presence of gradual addition of (a) MIL1 (b) MIL2 and (c) DIL at 293k.

As can be seen from above Figures, EB-DNA complex shows an emission maximum at 610 nm when excited at 480 nm. Moreover, from the Figure 5a.2 it is also evident that the fluorescence intensity of EB-DNA complex gradually decreases in the presence of all the three ILs and the emission maxima which remain unchanged at lower concentration, become gradually red-shifted at higher concentration of ILs. The fluorescence quenching of EB-DNA complex upon addition of ILs is expected to arise due to the exclusion of EB from the DNA base pair microenvironment toward the aqueous bulk. The red shift in the emission peak has further revealed dissociation of EB from the EB-DNA complex.[22] However, the extent of quenching is observed to be different in the presence of different ILs. It can be observed that EB-DNA complex shows around 30% reduction in fluorescence intensity in the presence of MIL1, whereas the same is estimated to be around 55% to 45% for MIL2 and DIL respectively. These observations indicate that more EB leaches out from EB-DNA complex in presence of MIL2 than in the presence of either MIL1 or DIL. According to the previous literature reports, the interaction of ILs with *ct*-DNA can take place by means of electrostatic as well as hydrophobic interactions. [22, 30]In the present case the continuous decrease in fluorescence intensity with a gradual red shift of the emission peak also signify that the fluorescence quenching process is driven by both electrostatic and hydrophobic interaction between *ct*-DNA and ILs. This

observation is also consistent with the result obtained from steady state absorption measurements. The relatively higher fluorescence quenching by MIL2 than that by MIL1 may have happened due to the presence of longer alkyl chain (eight -CH_2) in the former IL system. The longer alkyl chain containing IL system is expected to induce more hydrophobic interaction with DNA resulting more exclusion of EB out of the DNA microenvironment.[41]Interestingly, despite the fact that both DIL and MIL2 contain same alkyl chain, the lower fluorescence quenching in presence DIL than that in presence MIL2 in clearly indicates the role of extra pyrrolidinium ring head of the DIL in DNA-IL interaction event. These observations also indicate that the DIL has a different interaction pattern with DNA than that is usually observed for DNA-MIL interactions.

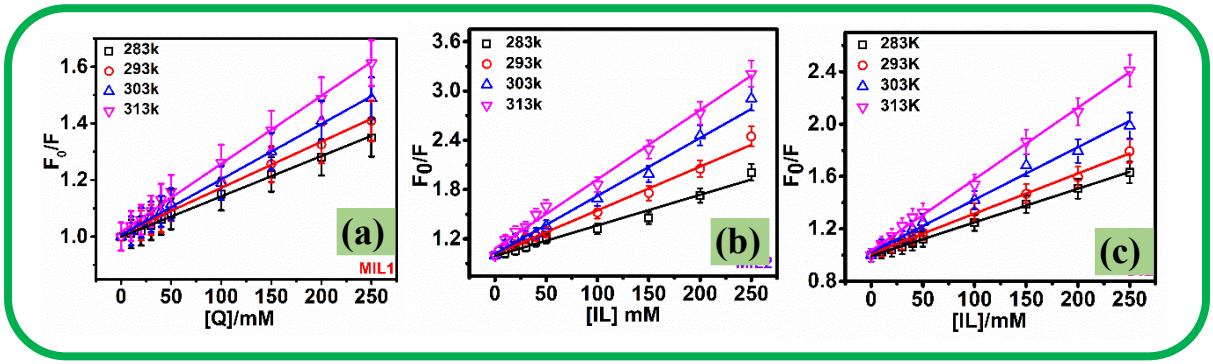

Figure 5a.3. The Stern-Volmer plot for quenching of fluorescence of EB-DNA complex by (a) MIL1 (b) MIL2 and (c) DIL at four different temperatures marked in the legend. (The solid lines are the fitted line)

Again, in order to ascertain the nature of the quenching process during interaction of ILs with DNA, the fluorescence quenching data at four different temperatures (283k, 293k, 303k and 310k) were analysed using the Stern-Volmer equation (eq.5a.1).[42]

$$\frac{F_0}{F} = 1 + K_{sv}\,[IL] \qquad \text{(eq.5a.1)}$$

Here, K_{sv} is Stern-Volmer quenching constant, F_0 and F are the fluorescence intensity of the EB-DNA complex in the absence and presence of quenchers (ILs). The Stern-Volmer plots for EB-DNA fluorescence intensity variation in presence of three ILs are shown in Figure 5a.3. The linearity of the plots for all the three IL systems at the experimental temperatures suggests that the quenching process is either pure static or pure dynamic. The K_{sv} value obtained from the slope of the plots at 293K are estimated to be 0.00163mM^{-1}, 0.00532mM^{-1} and 0.00257mM^{-1} for MIL1, MIL2 and DIL respectively. The K_{sv} value of the respective system at other three temperatures have been provided in the Appendix 5a (Table APX5a.1). The K_{sv} value for the current DNA-IL interaction runs paralleled with the values that have been reported in previous literatures. [25] Relatively higher K_{sv} value for MIL2 than that of DIL, further indicates a different interaction pattern of DIL with *ct*-DNA.

5a.3.2.1. Time resolved fluorescence measurement

Further, to confirm whether the quenching follows dynamic or static process we have carried out fluorescence lifetime measurements of EB-DNA complex with gradual addition of ILs. The measured fluorescence decay profiles of EB−DNA complex in presence of various ILs are shown in Figure APX5a.5 (Appendix 5a) and the calculated decay parameters obtained from exponential fitting according to eq.2.8 is listed in the Table 5a.1. The decay plots of EB-DNA complex (Figure APX5a.5) indicate that lifetime decreases in the presence of increasing concentration of ILs. We note here that the fluorescence decay of EB−DNA complex is found to be biexponential with lifetimes components of 1.63ns (τ_1) and 21.37ns (τ_2). These two lifetime values are typical of the two forms of EB in its free and DNA-bound state respectively. [43,44] From the Table 5a.1 it is evident that, with gradual addition of ILs the longer lifetime component corresponding to EB-DNA complex i.e. (τ_2) decreases along with increase in the contribution from the shorter component (τ_1), which corresponds to lifetime of free EB in

buffer. Again, the appearance of a short-lived third component (τ_3) at higher concentrations of ILs is consistent with the release of EB into the aqueous environment from DNA due to the interaction with ILs. [26] Further the decrease in the average lifetime (τ_{avg}) calculated using eq.2.8. with addition of ILs, demonstrates that the quenching processes by ILs are dynamic in nature.[42] In addition, the increase in K_{sv} values obtained from steady-state fluorescence measurements of a particular system with an increase in temperature further supports the dynamic nature of the fluorescence quenching processes.

Table 5a.1. Decay parameters of EB-DNA complex in the presence of different ILs.

EB-DNA- MIL1							
[IL]mM	τ_1(ns)	B_1	τ_2(ns)	B_2	τ_3(ns)	B_3	τ_{avg}(ns)
0	1.63	0.05	21.37	0.95			20.38
20	1.63	0.05	21.35	0.95			20.36
50	1.63	0.09	21.25	0.91			19.48
100	1.63	0.10	21.19	0.90			19.23
150	1.63	0.11	21.14	0.71	0.24	0.18	15.23
200	1.63	0.13	21.10	0.61	0.19	0.27	13.12
EB-DNA- MIL2							
[IL]mM	τ_1(ns)	B_1	τ_2(ns)	B_2	τ_3(ns)	B_3	τ_{avg}(ns)
20	1.63	0.08	21.32	0.91			19.53
50	1.63	0.12	21.06	0.67	0.19	0.21	14.34
100	1.63	0.13	20.97	0.45	0.09	0.42	9.69
200	1.63	0.25	18.27	0.25	0.15	0.50	5.05
EB-DNA- DIL							
[IL]mM	τ_1(ns)	B_1	τ_2(ns)	B_2	τ_3(ns)	B_3	τ_{avg}(ns)
20	1.63	0.07	21.34	0.93			19.96
50	1.63	0.24	21.08	0.76			16.41
100	1.63	0.25	21.04	0.65	0.50	0.10	14.13
200	1.63	0.26	21.00	0.49	0.52	0.25	10.84

5a.3.2.2. Thermodynamic parameters and nature of binding forces.

To get more insight into the thermodynamics of binding of ILs to *ct*-DNA the fluorescence intensity data has been further analysed by using double logarithmic regression curve of log $(F_0 - F)/F$ versus log [Q], which is obtained by using eq.5a.2. This equation can also be used for determination of the binding constant (K_B) and the number of binding sites. [45-48]

$$\log\frac{F_0-F}{F} = \log K_B + n\log[IL] \qquad \text{(eq. 5a.2)}$$

Here, in the above equation, K_B denotes the binding constant and n denotes the number of binding sites per ligand molecules. The double logarithmic curve for all the three systems at all experimental temperatures are shown in Figure 5a.4.

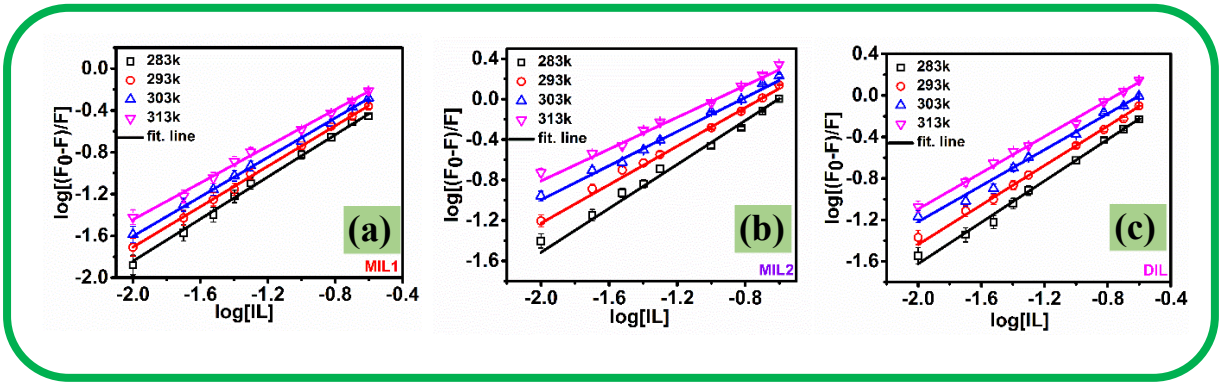

Figure 5a.4. Double logarithm plot for (a) MIL1 (b) MIL2 and (c) DIL at four different temperatures marked in the legend. The slope and intercept of this linear plot give the number of binding site (n) and the binding constant (K_B) according to eq.5a.2. The solid lines represent the fitted line to eq.5a.2.

The values of K_B and n estimated from the intercept and slope of the linear plots respectively are enlisted in Table 5a.2. As can be seen from Table 5a.2, the estimated K_B values for the IL-DNA binding interaction are found to be substantially lower than the K_B values obtained from the binding of DNA with several classical intercalator. Here, it is to be noted that K_B values for classical intercalator are in the order of 10^4 *to* 10^7. This clearly indicates that ILs that are employed in the current study do not intercalate in the DNA, rather they bind to the minor groove of DNA.[48] This is obvious as the pyrrolidinium moiety being non-planar it does not fit into the DNA base pairs in order to intercalate.[35] It is to be noted here that, to explain the lower K_B value similar arguments have also been provided by several researches. [30] Again, the number of binding sites for all the three ILs with *ct*-DNA are found to be nearly equal to 1.

This also indicates that although the strength of binding is different for DIL and MIL, they interact only through one class of binding site (minor groove) during the interaction *ct*-DNA. This unusual binding behaviour has led us to realize that microenvironment of DILs around DNA has been modified due to the presence of extra cationic head of the DIL.

The interaction of organic ligands at the minor groove of DNA usually involves several non-covalent forces such as hydrogen bonding, electrostatic and hydrophobic interaction.[23] Several researches have demonstrated that estimation of the value of thermodynamic parameters corresponding to the binding event can help to get an idea about the nature of forces that are operational during the interaction of ligands with *ct*-DNA.[23, 49-51]

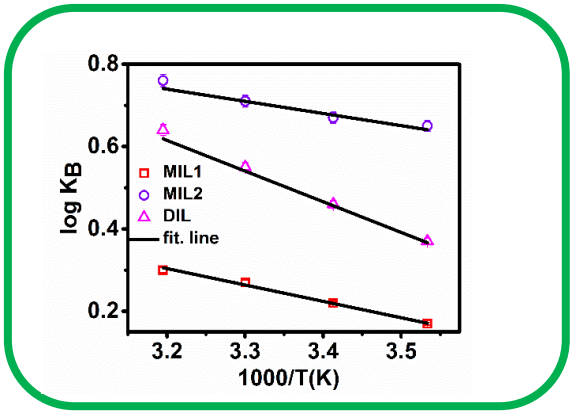

Figure 5a.5. Van't Hoff plot for the binding events of MIL1, MIL2 and DIL as marked in the legend. Solid lines represent the fitting to the data points.

Therefore, in order to estimate the relevant thermodynamic parameters such as enthalpy (ΔH), entropy (ΔS) and free energy (ΔG) of the interaction event of ILs and DNA, we have used the well-known Van' t Hoff equation (eq.5a.3), where R is the universal gas constant. [51]

$$\log K_B = \frac{-\Delta H}{2.303RT} + \frac{\Delta S}{2.303R} \qquad \text{(eq.5a.3)}$$

$$\Delta G = \Delta H - T\Delta S \qquad \text{(eq.5a.4)}$$

Figure 5a.5 shows the linear relationship between $\log K_B$ and $^1/_T$. ΔH and ΔS are obtained from the slope and intercept of the plots respectively and using these values in eq.5a.4, the free energies (ΔG) of the corresponding binding event have been calculated. The thermodynamic data thus obtained are collected in Table 5a.2.

Table 5a.2. Binding Constants (K_B), Number of Binding Sites (n), and Other Relative Thermodynamic Parameters for the Interaction of (a) MIL1 (b) MIL2 and (c) DIL.

EB-DNA-MIL1					
Temp/k	K_B/M^{-1}	ΔH/kJ mol^{-1}	ΔS/$Jk^{-1}mol^{-1}$	ΔG/kJ mol^{-1}	n
283	1.47±0.03	7.61±0.15	30.06±0.60	-0.89±0.01	1.00±0.02
293	1.65±0.03			-1.19±0.01	0.96±0.009
303	1.86±0.03			-1.49±0.01	0.94±0.009
313	1.99±0.03			-1.79±0.03	0.87±0.008
EB-DNA-MIL2					
Temp/K	K_B/M^{-1}	ΔH/kJ mol^{-1}	ΔS/$Jk^{-1}mol^{-1}$	ΔG/kJ mol^{-1}	n
283	4.43±0.08	5.65±0.11	32.16±0.64	-3.45±0.06	1.08±0.01
293	4.67±0.09			-3.77±0.07	0.95±0.009
303	4.89±0.09			-4.09±0.08	0.84±0.008
313	5.75±0.10			-4.41±0.08	0.78±0.007
EB-DNA-DIL					
Temp/K	K_B/M^{-1}	ΔH/kJ mol^{-1}	ΔS/$Jk^{-1}mol^{-1}$	ΔG/kJ mol^{-1}	n
283	2.34±0.05	14.26±0.28	57.24±1.14	-1.94±0.03	0.99±0.009
293	2.88±0.05			-2.51±0.05	0.95±0.009
303	3.54±0.06			-3.09±0.06	0.86±0.008
313	4.46±0.07			-3.36±0.07	0.87±0.008

The negative value of free energy for all the three system confesses the thermodynamic feasibility of the binding process of ILs with DNA.[23] Furthermore, the positive value of both ΔH and ΔS can be a symbol of participation the hydrophobic force during the interaction events.[49] However, it has also been reported by Subramanian and co-worker that the electrostatic interaction between biomolecules and ligand is accompanied by no or little change in enthalpy of either sign. As the ILs contain a pyrrolidinium cation, contribution from electrostatic interaction between ILs and DNA which is an anionic polyelectrolyte, to the

positive value of ΔH cannot be excluded.[52] So, from the above discussion it can be said that the interaction between ILs and DNA has been mediated by both the combination of electrostatic and hydrophobic interaction. But the large change in enthalpy and entropy with positive sign indicates that the hydrophobic interaction between base pair of *ct*-DNA and ILs has the major contribution than to the overall binding energy than the electrostatic interaction between cationic moiety of ILs and phosphate back bone of DNA.[52] We also note here that, the above results are consistent with the result obtained by Rahman and co-workers.[28] They have seen that although there exists significant electrostatic interaction between cationic head of ILs and phosphate group of *ct*-DNA, the hydrophobic interaction between alkyl chain and the bases of DNA becomes predominant one as the length of the alkyl chain increases. In this context, several researchers have also observed that the minor groove binding of ILs with DNA primarily takes place through hydrophobic interaction although the electrostatic interaction is essential one.[23, 28] With the above discussion it may be noted here that as the hydrophobic interaction is predominant, on-going from MIL2 to DIL the binding strength should not change much as both of them contain same hydrophobic (8-CH_2) unit. But in the present case K_B value for DIL is found to be even lower than MIL2. All these observations essentially indicates that the hydrophobic environment provided by DIL is quite different than that of MIL2. For an in-depth understanding of these observations, we here resorted to a more microscopic analysis by employing fluorescence correlation spectroscopy.

5a.3.3 Conformational stability of DNA in presence of ILs: FCS studies

FCS technique is a pivotal technique in molecular biology to understand the dynamics of biomolecules, molecular diffusion, bimolecular complexion, and binding affinity with single-molecular sensitivity.[42] In principle, single molecular measurements are more precise and informative since these allow probing individual molecules independently with their immediate microenvironment.[53] The primary tool that FCS measurements offer is the autocorrelation

function which can be greatly utilised to extract parameters such as diffusion time (τ_D), number of molecule (N) and diffusion coefficients etc. [42] In the current study we have made use of the autocorrelation function to investigate the effect of both MILs and DIL on the size and conformational dynamics of DNA that are intricately related to its interaction events with ILs. It has been shown that the size as well as conformational stability of *ct*-DNA can be effectively studied by means of FCS using dyes which are bound non-covalently with *ct*-DNA.[54] EB is an intercalating probe and it gets located inside the base pair of *ct*-DNA in the interior position through non-covalent interaction. Any changes in the *ct*-DNA structure due to interaction with the ILs will be reflected in the change in the diffusion properties of EB-DNA complex. For this purpose, we have monitored the fluorescence of EB−DNA complex, and the experiment is done by gradually adding different ILs to EB-DNA complex.

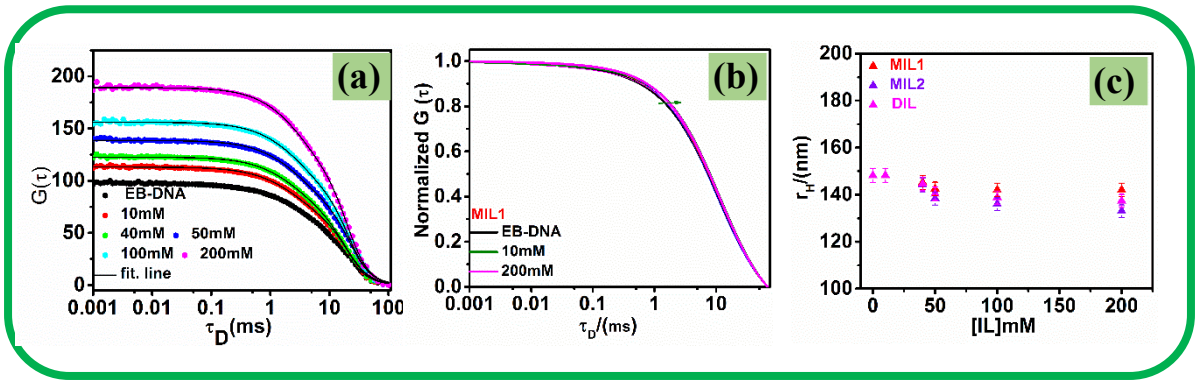

Figure 5a.6. (a) Variation of *G(0)* value in the presence of increasing concentration of MIL1, (b) Normalised autocorrelation curve corresponding to Figure 5a.6a, (c) The hydrodynamic radii of *ct*-DNA in absence and presence of ILs at different concentration ILs as shown in the X-axis in the plot.

Figure 5a.6a displays a series of FCS traces of the EtBr-DNA complex in the presence of increasing MIL1 concentration (as shown in the caption), and Figure 5a.6b presents its normalised fitted curve, which was generated by fitting the data to eq.2.24. The analogous traces for other two ILs are also provided in Appendix 5a (Figure APX5a.6 and Figure

APX5a.7). It can be clearly seen from Figure 5a.6a and Figure APX5a.6 that *G(0)* value increases with the addition of ILs. This suggests a decrease in the *N* value which indicates that EB exposed out to the aqueous environment from its DNA bound state in the presence of ILs.[26] Again, from the normalized fitted traces (Figure 5a.6b, Figure APX5a.7) of respective systems a minor increase in the diffusion time (τ_D) of EB-DNA complex has been noticed with addition of ILs. The slight increase in the τ_D value perhaps observed due to the increase in the viscosity of the medium with the addition of ILs. So, the hydrodynamic radius (r_H) of *ct*-DNA in absence and presence of concerned ILs have been determined by applying eq.2.25, which corrects the overestimated value of τ_D due to increased viscosity of the medium. The plots of variation of hydrodynamic radii (r_H) with concentration of three different IL systems have been provided in Figure 5a.6c. The hydrodynamic radius of *ct*-DNA is estimated to be 148 nm in absence of ILs, which is pretty close to the value that has been reported in literature. [26]Now, with addition of MIL1, the (r_H) value of *ct*-DNA is found to remain almost unchanged. However, a slight decrease in the r_H value of *ct*-DNA has been observed in the presence of MIL2 and DIL, particularly at higher concentration. For example, the r_H values of *ct*-DNA reduced to 130 nm and 137 nm with addition of 250 mM of MIL2 and DIL respectively. This observation suggests that the structure of *ct*-DNA is slightly compacted in the presence of the two above mentioned IL systems. In this context it is relevant to mention here that several researchers by means of DLS (Dynamic Light Scattering) as well as FCS measurements have also observed that the hydrodynamic radius of *ct*-DNA decreases upon addition of ILs.[55] It's also crucial to note that, depending on the concentration of ILs, the structure of ct-DNA may undergo compaction, changing from an extended coil state (r_H = 65 nm) to a compact globule state (r_H = 320 nm). [22,55] But in the present case minimal changes in the hydrodynamic radius also subsequently confirmed that conformational stability of *ct*-DNA does not change significantly in the presence of given ILs. However, relatively more decrease in hydrodynamic radii of *ct*-DNA

upon addition of MIL2 as compared to upon addition of MIL1, essentially suggests more the hydrophobicity of the alkyl chain more is the compactness in the DNA structure. The partial compaction of DNA structure due to the hydrophobic association with the alkyl chain of ILs has been reported earlier.[55] However, in our case the DIL which also contain same hydrophobic unit as that of MIL2, is found to be less efficient in bringing compaction in the *ct*-DNA. In this context the role of folded structure of DILs comes in to picture. We note here that the alkyl side chain attached to pyrrolidinium-cation is fully free in the case of MILs, whereas in DIL the eight-membered alkyl chain forms a bridge between two pyrrolidinium rings. Moreover, recently, it has been proven both by experimental and theoretical studies that relatively longer alkyl spacer chain containing DILs tend to exist in the folded form.[56,57] Perhaps due to this reason, the hydrophobic alkyl spacer in DIL gets less exposed to interact with *ct*-DNA which in turn bring less compaction in the *ct*-DNA structure. Keeping above discussion in mind, it can be said that structural organisation of ILs play a key role in controlling the DNA-IL interaction. Furthermore, it has been also commented in some literature that several multivalent cations such as polyamine can cause rapid *ct*-DNA compaction due to the strong electrostatic interaction which may eventually lead to change in *ct*-DNA micro-structure even when they are added at smaller concentration.[6,7] But such effects are perhaps less pronounced in the presence DIL due to the comparatively weaker electrostatic interactions between DNA and DILs. Thus, above results clearly suggests that possibly DILs can be considered as a preferred media over MILs as well as several multivalent cationic species in maintaining the structural integrity of *ct*-DNA. To verify the result obtained from FCS measurement we step forward for circular dichroism measurement.

5a.3.4. Circular dichroism studies. Circular dichroism (CD) spectroscopy has been admired as the most appropriate tool to have both structural and conformational information on *ct*-DNA.[14] The CD spectra (230-320 nm) of *ct*-DNA in buffer as well as in the presence of

concentration gradient of three IL systems ($25mM$ to $250mM$) are displayed in Figure 5a.7. As can be seen from Figure 5a.7, the CD spectra of native *ct*-DNA exhibits a positive maximum at 277 nm and a negative band at 241 nm corresponding to corresponding to $\pi - \pi$ base packing and helicity of the *ct*-DNA respectively.[14] It may be noted here that these band are the characteristics peaks for so call native B-form of *ct*-DNA.

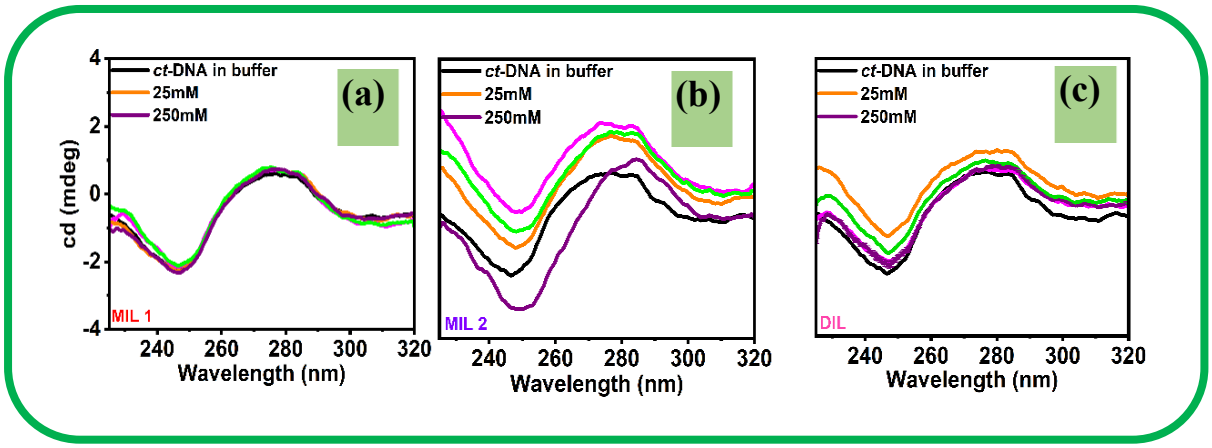

Figure 5a.7. Near UV-CD spectra of *ct*-DNA in the presence of varying concentration (a) MIL1, (b) MIL2 and (c) DIL.

Comparing the spectral signatures of *ct*-DNA in the presence of three IL systems (Figures 5a.7a, 7b and 7c), a slight alternation in the amplitude of both the positive and negative band of *ct*-DNA can be noticed in the presence of both MIL2 as well as DIL. These changes in the spectral shape with respect to that of native *ct*-DNA alone in buffer can be due to minor change in helicity as well as base stacking due to the interaction with these ILs.[61] Furthermore, a small shift along with a deep decrease in amplitude in the positive band of *ct*-DNA has been observed in the presence of only higher concentration ($250mM$) of MIL2 (Figure 5a.7b). This could be due to slight compaction of *ct*-DNA as a result of hydrophobic association of alkyl chain in MIL2 with *ct*-DNA.[27, 30] Interestingly, such shift has not been observed in the presence of DIL. This observation essentially suggests the comparatively stronger binding tendency MIL2 with DNA over DIL. We note here that, the observed spectral changes of *ct*-DNA in presence

of ILs are not significant and cannot be assigned as the conformational changes in *ct*-DNA. This suggests that native B-form of DNA remains more or less unaltered in the presence of all the three ILs employed in the study. Again, when the above results are also looked at in conjunction with the FCS data, the DIL is found out to be better in maintaining the native structure of DNA.

5a.3.5. UV melting study. Along with the conformational stability, the thermal stability of DNA is an important factor that determine the suitability of a given media for its storage. Therefore, UV melting experiments on *ct*-DNA have been performed in the presence of three IL systems and representative melting profiles are provided in the Appendix 5a (Figure APX5a.8). Plots of melting temperature (T_m) of *ct*-DNA as a function of concentration of different ILs are also provided in Figure 5a.8.

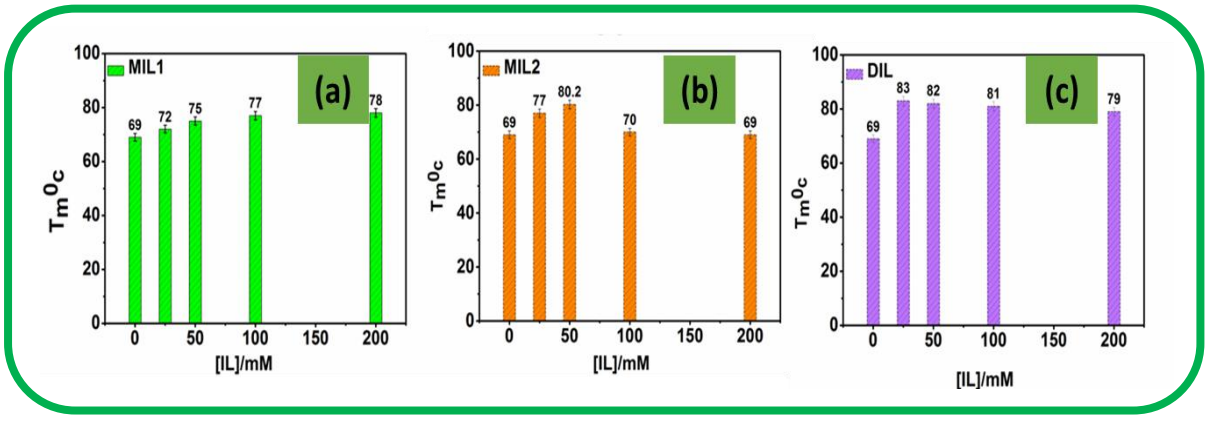

Figure 5a.8. UV melting temperature T_m of *ct* -DNA in the presence of (a) MIL1, (b) MIL2 and (c) DIL at different concentration of ILs marked in the X-axis of the plots. The label on the top of each column represents the melting temperature (T_m) of *ct*-DNA at respective ILs concentration.

From Figure 5a.8 it can be observed that native *ct*-DNA shows a thermal transition temperature (T_m) around 69^0C, which is increased subsequently in presence of all the chosen ILs. Moreover, upon comparing the (T_m) of *ct*-DNA in presence of the concerned ILs, the highest T_m value

(83^0c) of *ct*-DNA has been achieved in presence of DIL. In this context we would like to mention here that the stabilisation of double helical structure of *ct*-DNA in the presence of longer alkyl chain containing surfactants has been reported and well explained in several literatures.[58] In the present case also the (T_m) value for *ct*-DNA is found to be higher in presence of MIL2 which contain a longer alkyl chain than that of MIL1. In contrast to those results the current observation which shows higher thermal stabilisation of *ct*-DNA in presence of DIL over MIL2 despite they contain the similar hydrophobic unit is quite interesting. This perhaps has happened due to the presence of extra cationic head in DIL which facilitate comparatively stronger electrostatic interaction with the phosphate backbone of DNA.[30,59-61] Further a close inspection of Figures 5a.8b and 8c reveal that the stabilisation effect of MIL2 gets saturated quite early at relatively higher concentration of MIL2 and the melting temperature of *ct*-DNA decreases drastically. Before discussing the above result, it is to be remembered that the thermal stability of *ct*-DNA not only depends on the displacement of water from the spine of hydration, but also depends on the penetration ability of IL cations into the hydration layer. [27] The current observation shows that the intrusion of DIL into the hydration layer is perhaps less facile. This might have happened due to the bulkier folded form of DIL which find less exposure of its hydrophobic alkyl chain to interact with DNA. Moreover, due to this structural arrangement DIL also not fit into the hydration shell in the minor groove. However, MIL2 which contain a free alkyl chain may permeate easily into the hydration layer. Moreover, they may also get settled there due to the hydrophobic association of the alkyl chain of with sugar residues of the DNA after dislodging a large number of water molecules from DNA surface.[4, 27]consequently, further increase in concentration of MIL2 cause partial compaction in DNA and ultimately resulting decrease in melting T_m of DNA. All the above discussions indicates that among the ILs used, DIL can provide better thermal stability to DNA over MILs even at higher concentration.

5a.3.6. Molecular docking studies

In order to rationalize our experimental observations, the DNA binding site of IL cations are further analysed by employing molecular docking studies. The best docking pose with the lowest absolute value of energy that are selected for analysis are shown in Figure 5a.9. Moreover, the 2D molecular diagram presenting the participating nucleic acids and the type of interaction are also provided in Appendix 5a (Figure APX5a.9). The docking affinities of IL cations to DNA are found to be in order MIL 2 > DIL > MIL 1.

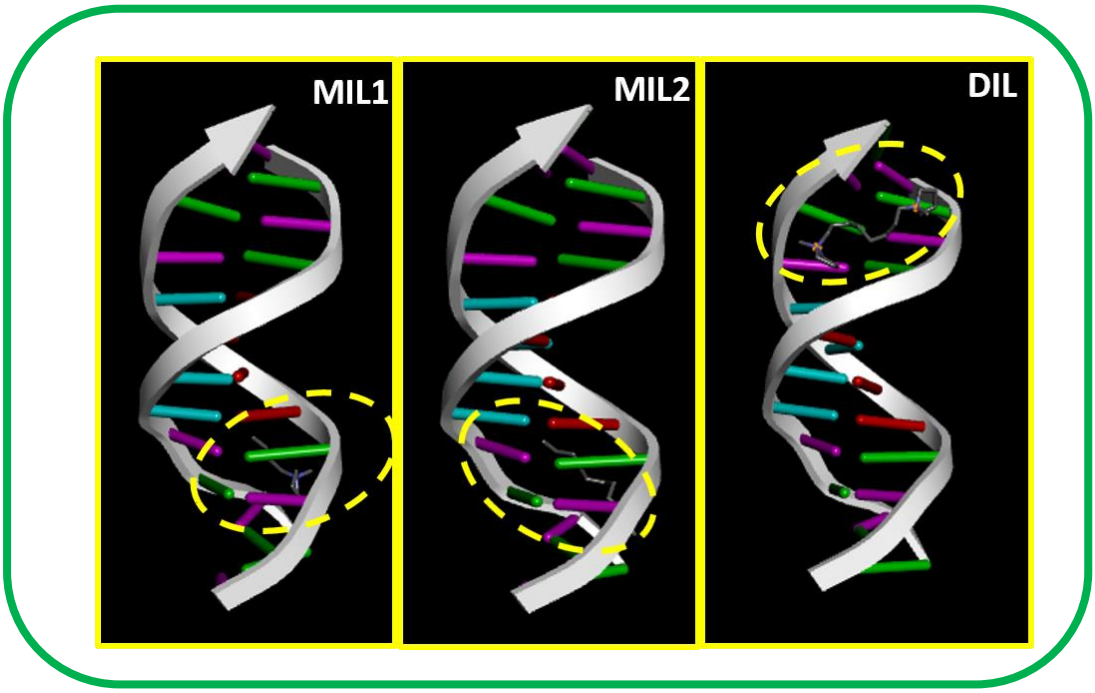

Figure 5a.9. View of the binding position of ILs with DNA. Picture shown here represents the lowest energy binding mode of ILs with DNA.

The binding energy *(ΔG_b)* values for the respective systems calculated to be -4.8 kcal, -4.6 kcal, -4.1 kcal which are somewhat lower than those are found previously for imidazolium and cholinium based ILs.[25-26] The weaker binding of chosen ILs is beneficial in terms of regeneration of DNA for its further utilization. Furthermore, the magnitude of ΔG_b also supported the preferential binding of pyrrolidinium cations to the minor groove of DNA. [26]

From the 2D molecular interaction diagram (Figure APX5a.9), it can be noticed that the interaction between all ILs and nucleic acid residues mostly involve hydrophobic interaction. All these findings nicely corroborate the results that are obtained through experimental studies.

5a.4. Conclusions

In the midst of several studies on both the fundamental and applied aspects of MILs in nucleic-acid based applications, the present report describes the suitability of a new class solvent system, DIL, towards structural integrity of *ct*-DNA. With an aim to achieve this goal, the binding affinity as well as stabilisation effects of a pyrrolidinium based DIL has been compared with two structurally similar MILs. These ILs are purposefully chosen so that the effect of both hydrophobicity and structural arrangements of the cationic moiety of ILs, if any, on the interaction event is understood. Investigations are done both at ensemble-average and single molecular level by using various spectroscopic techniques. Molecular docking studies have also been performed to throw more light into the present investigations. The fluorescence quenching studies of EB-DNA complex in the presence of concerned ILs, have depicted that the DNA-IL interaction is relatively less for DIL than that for MIL2. Analysis of thermodynamic parameters have suggested that the interactions between DNA and chosen ILs are thermodynamically feasible and mainly governed by hydrophobic forces. Similar results are also obtained from molecular docking studies. Moreover, FCS and CD measurements combinedly demonstrated that structure of *ct*-DNA remains less perturbed in presence of DIL than in presence of MIL2 despite of the fact that both of they contain similar hydrophobic unit. Furthermore, higher thermal stability of *ct*-DNA has also been observed in presence of DIL even at higher concentration. These unique response of DIL as compared to MILs have been explained by folded structural organisation of DILs. The outcomes of the present study may provide a fundamental understanding in designing various multi-cationic- based ILs, which can be used in various nucleic acid-based applications.

5a.5.Appendix 5a

^{1}H NMR Spectra of MIL1

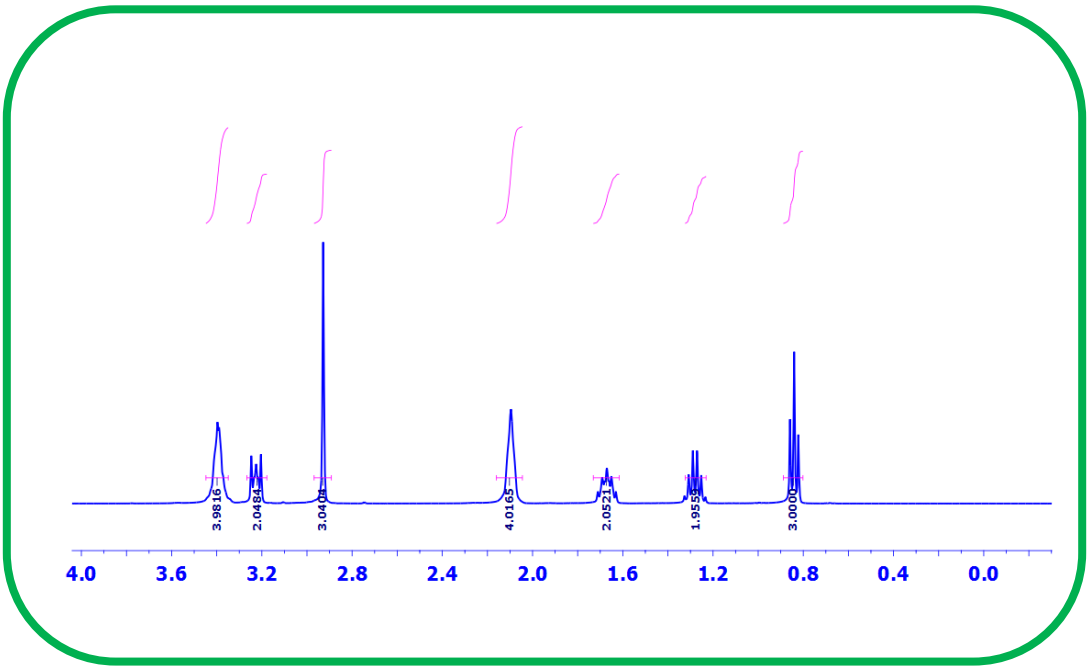

^{1}H NMR Spectra of MIL2

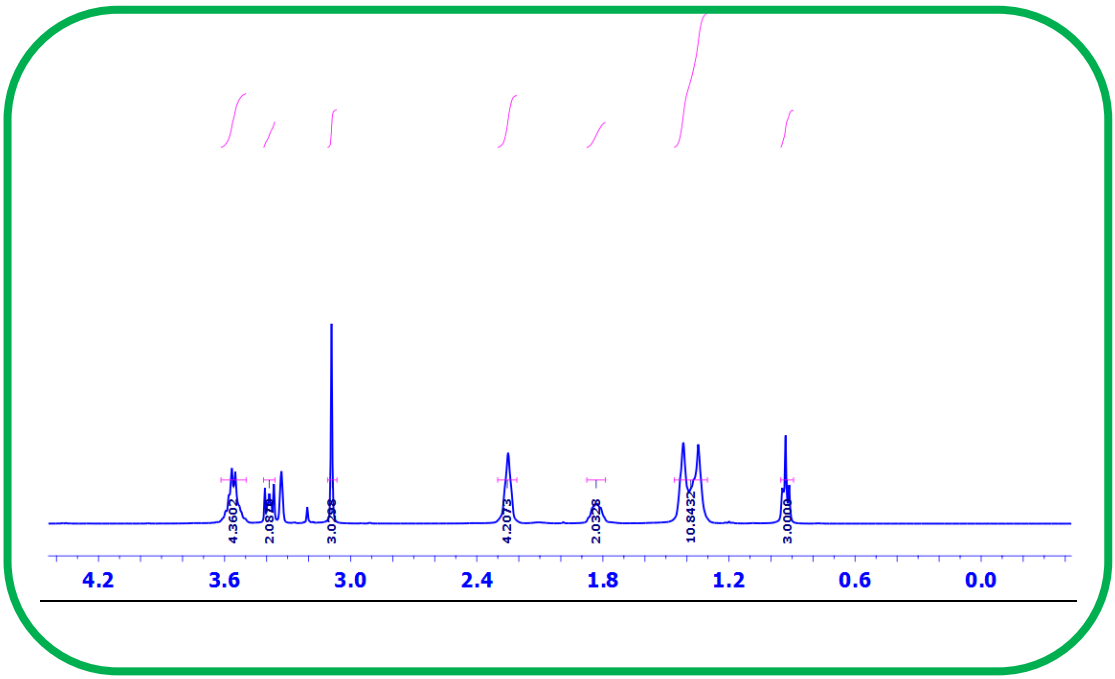

^{1}H NMR Spectra of DIL

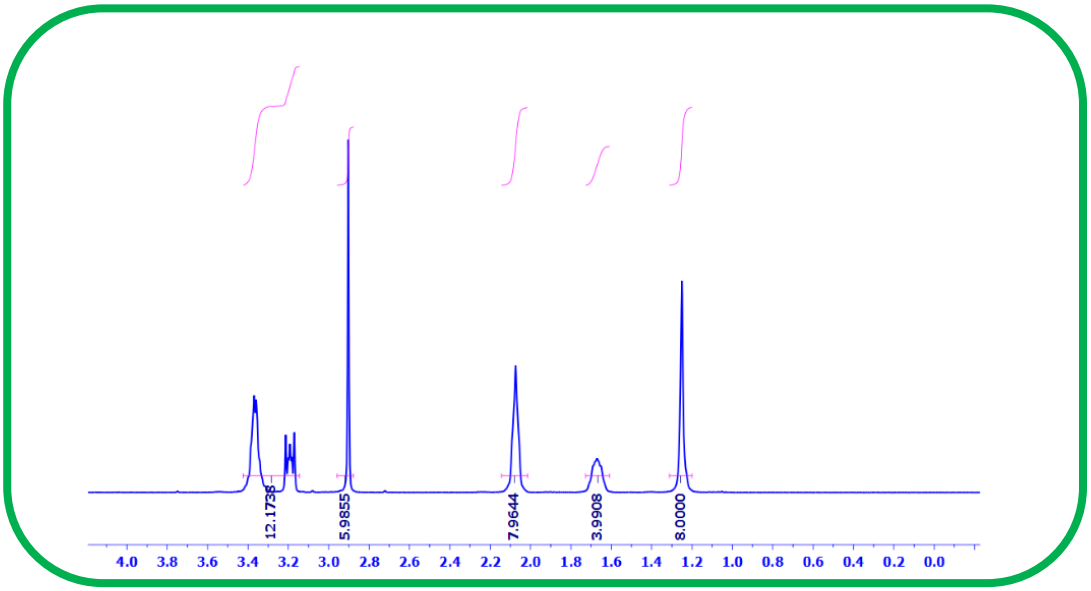

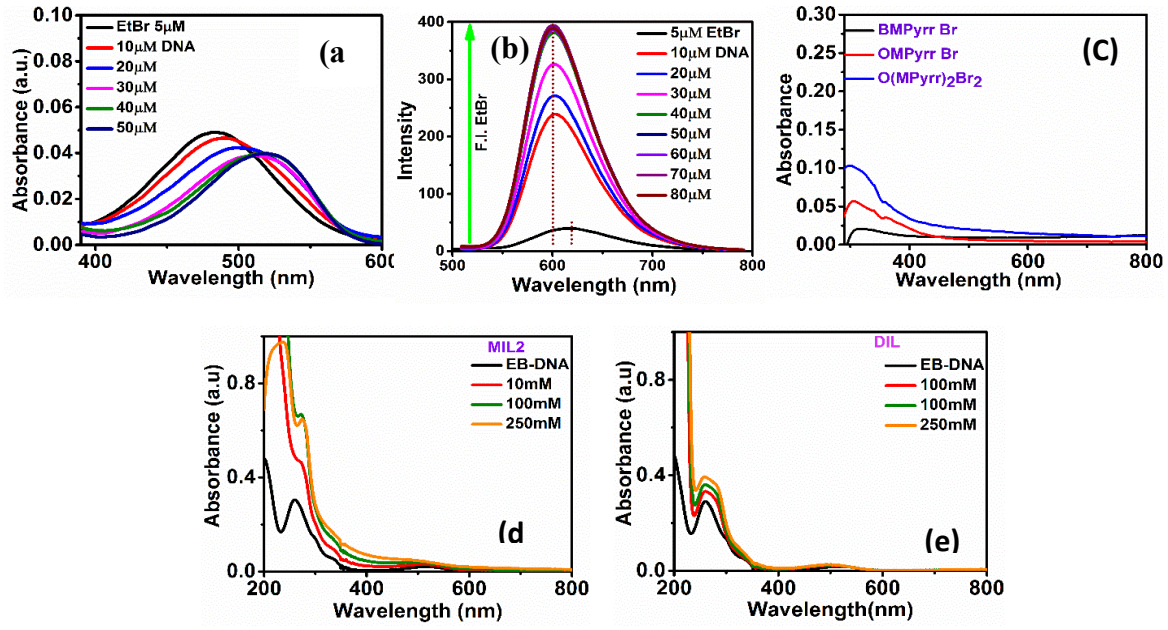

Figure APX.5a.1. (a) Represents the absorption spectra of $5uM$ EB ($\lambda_{max} = 480\ nm$) and it's complex with *ct*-DNA. The absorbance of EB gradually decreases with a redshift with the addition of *ct*-DNA as marked in the legend. An isosbestic point at around 510nm indicates the complexation of EB with *ct*-DNA. (b) Represents the fluorescence emission spectra of $5uM$ EB ($\lambda_{max} = 610\ nm$) when excited at $480nm$ and its' complexes with *c*t-DNA. The emission intensity of EB has been increased gradually with the subsequent addition of *ct*-DNA as marked in the legend. No more increase emission intensity has been observed when the concentration after the addition of $40uM$ *ct*-DNA. This indicates that at this concentration maximum EtBr is present in the bound form with *ct*-DNA. (c) Shows the absorption spectra of ILs employed in the study. No, significant absorption after $400\ nm$ have been found. This indicates the absorption of ILs will not interfere with the absorption of EB (EB). (d) and (e)represents the absorption spectra of EB-DNA complex in presence of MIL2 and DIL.

Fluorescence studies.

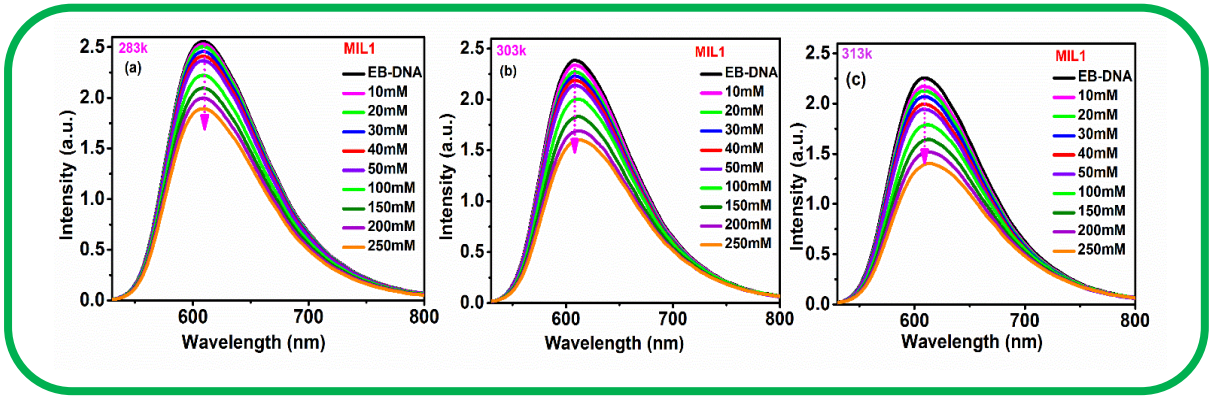

Figure APX5a.2. Fluorescence emission spectra of EB-DNA complex (λ_{ex} = 480 nm) in the absence and presence of gradual addition of MIL1 Br at (a) 283k, (b)303k and (C) 313k.

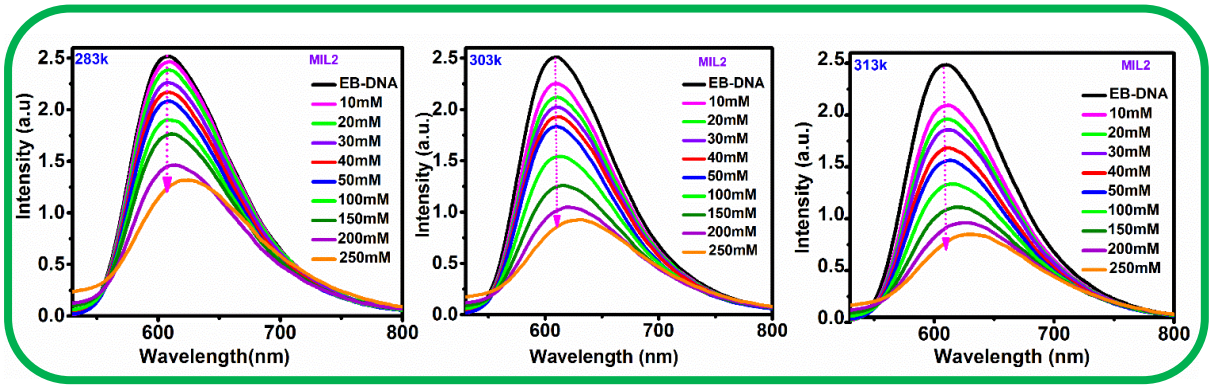

Figure APX5a.3. Fluorescence emission spectra of EB-DNA complex (λ_{ex} = 480 nm) in the absence and presence of gradual addition of MIL2 at (a) 283k, (b)303k and (C) 313k

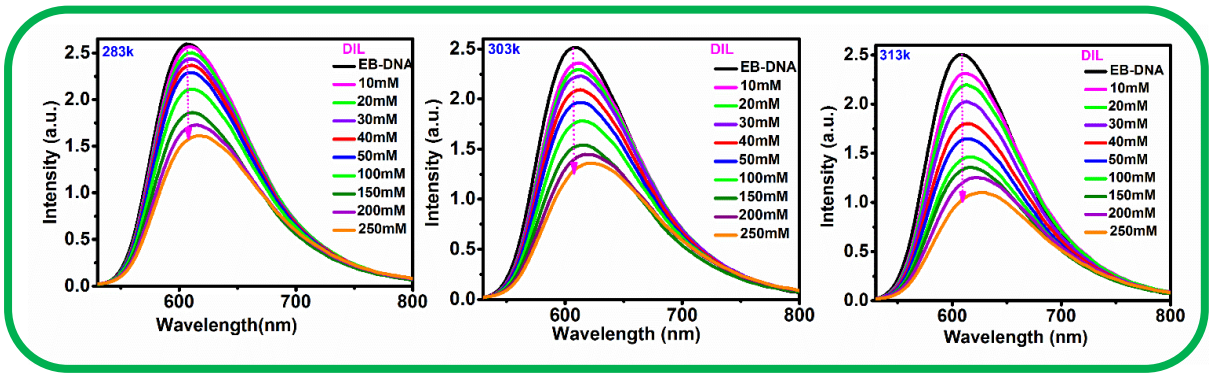

Figure APX5a.4. Fluorescence emission spectra of EB-DNA complex (λ_{ex} = 480 nm) in the absence and presence of gradual addition of DIL at (a) 283k, (b)303k and (C) 313k

Table APX5a.1. The stern-Volmer quenching constants at indicated temperatures for three IL systems.

systems	K_{SV} / (mM^{-1})		
	283k	303k	313
MIL1	0.00143	0.00196	0.00240
MIL2	0.00372	0.00705	0.00842
DIL	0.00257	0.00401	0.00546

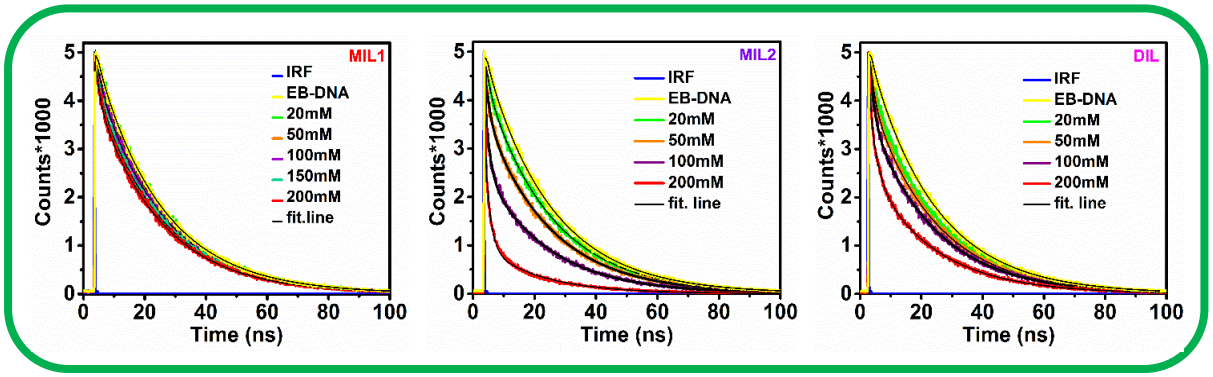

Figure APX5a.5. Fluorescence decay traces of EB-DNA complex in the absence and presence of gradual addition of ILs. The lifetime decreases gradually with the addition of ILs.

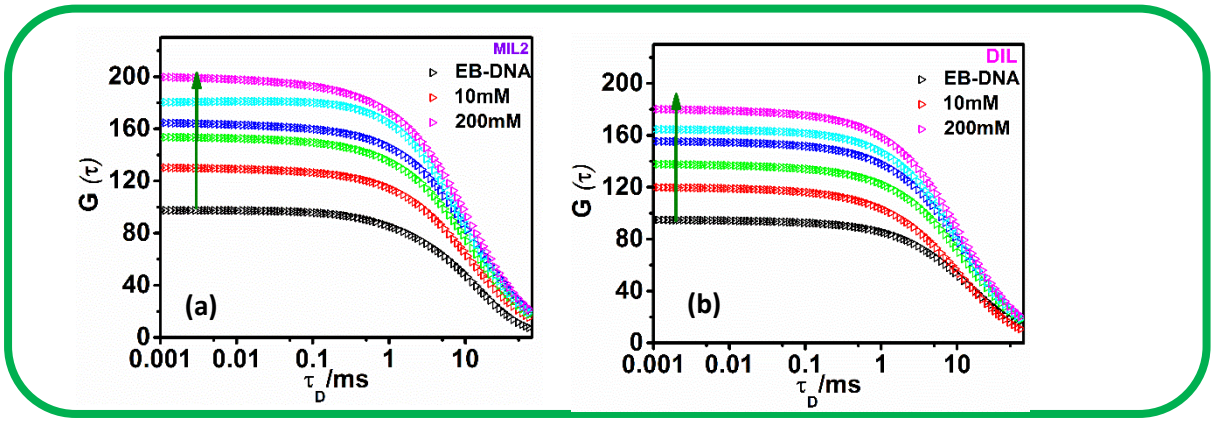

Figure APX5a.6. Fluorescence autocorrelation traces of EB-DNA complex in the absence and presence of gradual addition of (a)MIL2 and (b)DIL.

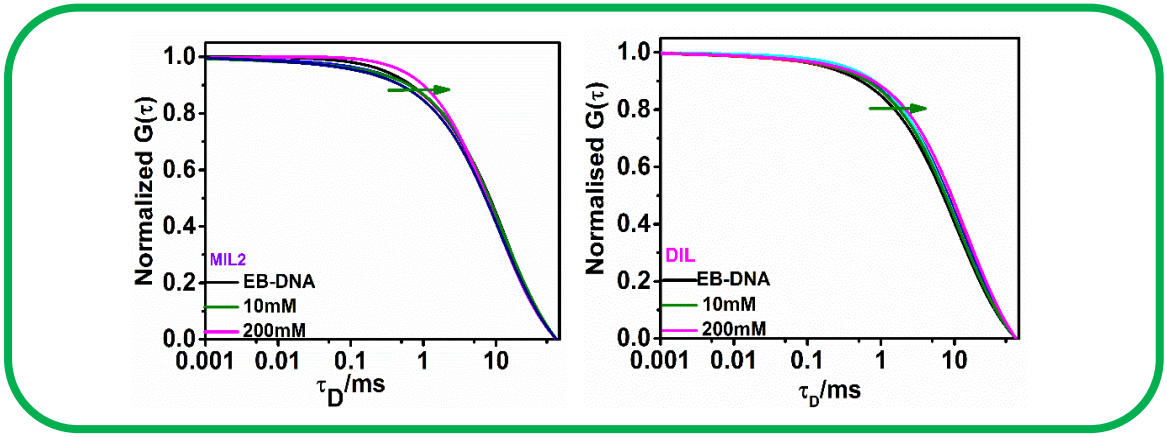

Figure APX5a.7. Normalised Fluorescence autocorrelation traces of EB-DNA complex in the absence and presence of gradual addition of MIL2 and DIL. The diffusion time has been increased gradually.

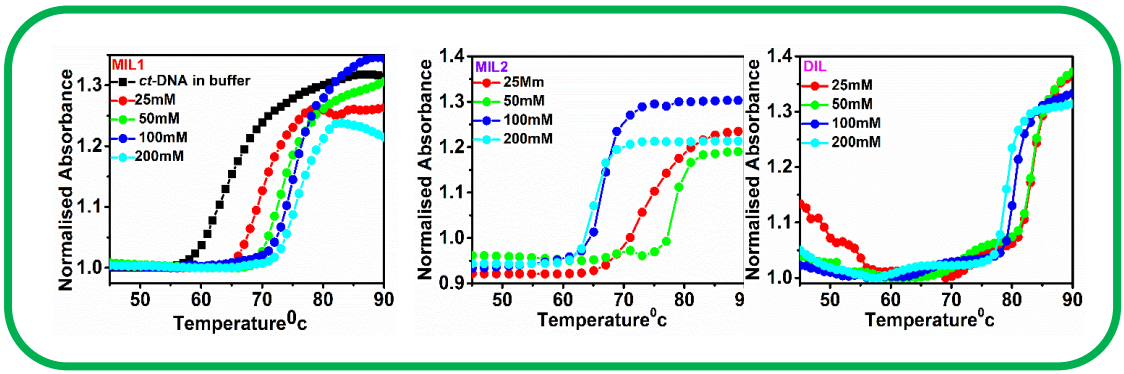

Figure APX.5a.8. UV melting profiles of *ct*-DNA in absence (black data points in figure APX5a.7a) and presence of ILs. As expected, *ct*-DNA in buffer shows a thermal transition temperature (Tm) at 69.5^0c

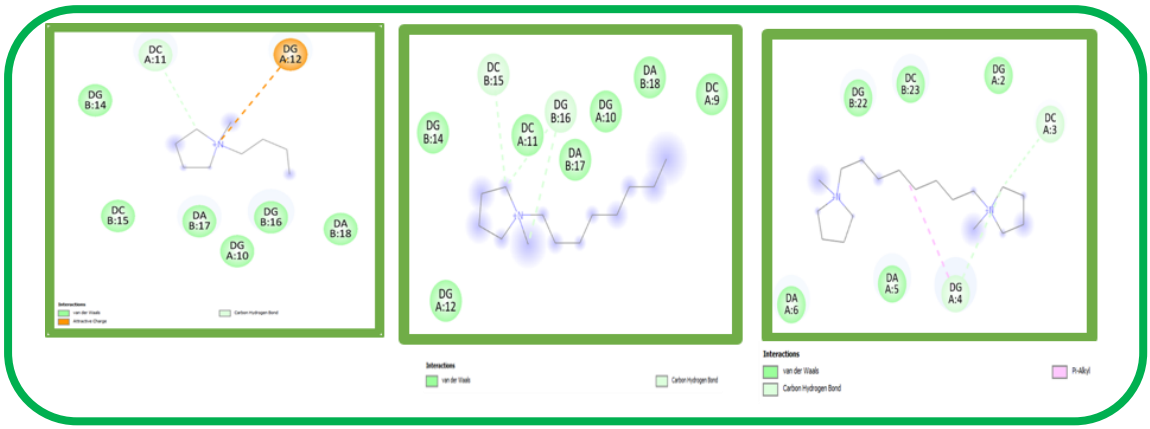

Figure APX5a.9. Diagram showing molecular interactions between ILs and DNA in 2-Dimension.

REFERENCES

1. Tateishi-Karimata, H.; Sugimoto, N., Structure, Stability and Behaviour of Nucleic Acids in Ionic Liquids. *Nucleic Acids Research* **2014**, *42*, 8831-8844.
2. Liu, H.; Liu, D., DNA Nanomachines and Their Functional Evolution. *Chemical Communications* **2009**, 2625-2636.
3. Krishnan, Y.; Simmel, F. C., Nucleic Acid Based Molecular Devices. *Angewandte Chemie International Edition* **2011**, *50*, 3124-3156.
4. Satpathi, S.; Sengupta, A.; Hridya, V. M.; Gavvala, K.; Koninti, R. K.; Roy, B.; Hazra, P., A Green Solvent Induced DNA Package. *Scientific Reports* **2015**, *5*, 9137.
5. Sequeira, R. A.; Bhatt, J.; Prasad, K., Recent Trends in Processing of Proteins and DNA in Alternative Solvents: A Sustainable Approach. *Sustainable Chemistry* **2020**, *1*, 116-137.
6. Pelta, J.; Livolant, F.; Sikorav, J.-L., DNA Aggregation Induced by Polyamines and Cobalthexamine (∗). *Journal of Biological Chemistry* **1996**, *271*, 5656-5662.
7. Samanta, D.; Iscen, A.; Laramy, C. R.; Ebrahimi, S. B.; Bujold, K. E.; Schatz, G. C.; Mirkin, C. A., Multivalent Cation-Induced Actuation of DNA-Mediated Colloidal Superlattices. *Journal of the American Chemical Society* **2019**, *141*, 19973-19977.
8. Grueso, E.; Cerrillos, C.; Hidalgo, J.; Lopez-Cornejo, P., Compaction and Decompaction of DNA Induced by the Cationic Surfactant Ctab. *Langmuir* **2012**, *28*, 10968-10979.
9. Benedetto, A.; Ballone, P., Room Temperature Ionic Liquids Meet Biomolecules: A Microscopic View of Structure and Dynamics. *ACS Sustainable Chemistry & Engineering* **2016**, *4*, 392-412.
10. Shukla, S. K.; Mikkola, J.-P., Use of Ionic Liquids in Protein and DNA Chemistry. *Frontiers in Chemistry* **2020**, *8*.
11. Wang, X.; Liu, M.; Ding, X., Guanidinium Hydrophobic Magnetic Ionic Liquid-Based Dispersive Droplet Extraction for the Selective Extraction of DNA. *Langmuir* **2021**, *37*, 11665-11675.
12. Xuan, S.; Meng, Z.; Wu, X.; Wong, J.-R.; Devi, G.; Yeow, E. K. L.; Shao, F., Efficient DNA-Mediated Electron Transport in Ionic Liquids. *ACS Sustainable Chemistry & Engineering* **2016**, *4*, 6703-6711.
13. Wang, J.-H.; Cheng, D.-H.; Chen, X.-W.; Du, Z.; Fang, Z.-L., Direct Extraction of Double-Stranded DNA into Ionic Liquid 1-Butyl-3-Methylimidazolium Hexafluorophosphate and Its Quantification. *Analytical Chemistry* **2007**, *79*, 620-625.
14. Singh, N.; Sharma, M.; Mondal, D.; Pereira, M. M.; Prasad, K., Very High Concentration Solubility and Long-Term Stability of DNA in an Ammonium-Based Ionic Liquid: A Suitable Medium for Nucleic Acid Packaging and Preservation. *ACS Sustainable Chemistry & Engineering* **2017**, *5*, 1998-2005.
15. Manojkumar, K.; Prabhu Charan, K. T.; Sivaramakrishna, A.; Jha, P. C.; Khedkar, V. M.; Siva, R.; Jayaraman, G.; Vijayakrishna, K., Biophysical Characterization and Molecular Docking Studies of Imidazolium Based Polyelectrolytes–DNA Complexes: Role of Hydrophobicity. *Biomacromolecules* **2015**, *16*, 894-903.
16. Gu, Z.; He, Z.; Chen, F.; Meng, L.; Feng, J.; Zhou, R., Ionic Liquid Decelerates Single-Stranded DNA Transport through Molybdenum Disulfide Nanopores. *ACS Applied Materials & Interfaces* **2022**, *14*, 32618-32624.
17. Soni, S. K.; Sarkar, S.; Mirzadeh, N.; Selvakannan, P. R.; Bhargava, S. K., Self-Assembled Functional Nanostructure of Plasmid DNA with Ionic Liquid [Bmim][Pf6]: Enhanced Efficiency in Bacterial Gene Transformation. *Langmuir* **2015**, *31*, 4722-4732.

18. Hayes, R.; Warr, G. G.; Atkin, R., Structure and Nanostructure in Ionic Liquids. *Chemical Reviews* **2015**, *115*, 6357-6426.
19. Anderson, J. L.; Ding, R.; Ellern, A.; Armstrong, D. W., Structure and Properties of High Stability Geminal Dicationic Ionic Liquids. *Journal of the American Chemical Society* **2005**, *127*, 593-604.
20. Shirota, H.; Mandai, T.; Fukazawa, H.; Kato, T., Comparison between Dicationic and Monocationic Ionic Liquids: Liquid Density, Thermal Properties, Surface Tension, and Shear Viscosity. *Journal of Chemical & Engineering Data* **2011**, *56*, 2453-2459.
21. Montalbán, M. G.; Víllora, G.; Licence, P., Synthesis and Characterization Data of Monocationic and Dicationic Ionic Liquids or Molten Salts. *Data in Brief* **2018**, *19*, 769-788.
22. Ding, Y.; Zhang, L.; Xie, J.; Guo, R., Binding Characteristics and Molecular Mechanism of Interaction between Ionic Liquid and DNA. *The Journal of Physical Chemistry B* **2010**, *114*, 2033-2043.
23. Wang, X.; Cui, F., Binding Characteristics of Imidazolium-Based Ionic Liquids with Calf Thymus DNA: Spectroscopy Studies. *Journal of Fluorine Chemistry* **2018**, *213*, 68-73.
24. Sharma, M.; Mondal, D.; Singh, N.; Trivedi, N.; Bhatt, J.; Prasad, K., High Concentration DNA Solubility in Bio-Ionic Liquids with Long-Lasting Chemical and Structural Stability at Room Temperature. *RSC Advances* **2015**, *5*, 40546-40551.
25. Sahoo, D. K.; Jena, S.; Dutta, J.; Chakrabarty, S.; Biswal, H. S., Critical Assessment of the Interaction between DNA and Choline Amino Acid Ionic Liquids: Evidences of Multimodal Binding and Stability Enhancement. *ACS Central Science* **2018**, *4*, 1642-1651.
26. Pabbathi, A.; Samanta, A., Spectroscopic and Molecular Docking Study of the Interaction of DNA with a Morpholinium Ionic Liquid. *The Journal of Physical Chemistry B* **2015**, *119*, 11099-11105.
27. Chandran, A.; Ghoshdastidar, D.; Senapati, S., Groove Binding Mechanism of Ionic Liquids: A Key Factor in Long-Term Stability of DNA in Hydrated Ionic Liquids? *Journal of the American Chemical Society* **2012**, *134*, 20330-20339.
28. Jumbri, K.; Ahmad, H.; Abdulmalek, E.; Abdul Rahman, M. B., Binding Energy and Biophysical Properties of Ionic Liquid-DNA Complex: Understanding the Role of Hydrophobic Interactions. *Journal of Molecular Liquids* **2016**, *223*, 1197-1203.
29. Vijayaraghavan, R.; Izgorodin, A.; Ganesh, V.; Surianarayanan, M.; MacFarlane, D. R., Long-Term Structural and Chemical Stability of DNA in Hydrated Ionic Liquids. *Angewandte Chemie International Edition* **2010**, *49*, 1631-1633.
30. Mishra, A.; Ekka, M. K.; Maiti, S., Influence of Ionic Liquids on Thermodynamics of Small Molecule–DNA Interaction: The Binding of Ethidium Bromide to Calf Thymus DNA. *The Journal of Physical Chemistry B* **2016**, *120*, 2691-2700.
31. Mahapatra, A.; Chakraborty, M.; Barik, S.; Sarkar, M., Comparison between Pyrrolidinium-Based and Imidazolium-Based Dicationic Ionic Liquids: Intermolecular Interaction, Structural Organization, and Solute Dynamics. *Physical Chemistry Chemical Physics* **2021**, *23*, 21029-21041.
32. Guglielmero, L.; Mezzetta, A.; Guazzelli, L.; Pomelli, C. S.; D'Andrea, F.; Chiappe, C., Systematic Synthesis and Properties Evaluation of Dicationic Ionic Liquids, and a Glance into a Potential New Field. *Frontiers in Chemistry* **2018**, *6*.
33. Montalbán, M. G.; Víllora, G.; Licence, P., Ecotoxicity Assessment of Dicationic Versus Monocationic Ionic Liquids as a More Environmentally Friendly Alternative. *Ecotoxicology and Environmental Safety* **2018**, *150*, 129-135.
34. Shimizu, Y.; Ohte, Y.; Yamamura, Y.; Tsuzuki, S.; Saito, K., Comparative Study of Imidazolium- and Pyrrolidinium-Based Ionic Liquids: Thermodynamic Properties. *The Journal of Physical Chemistry B* **2012**, *116*, 5406-5413.

35. Men, S.; Lovelock, K. R. J.; Licence, P., X-Ray Photoelectron Spectroscopy of Pyrrolidinium-Based Ionic Liquids: Cation–Anion Interactions and a Comparison to Imidazolium-Based Analogues. *Physical Chemistry Chemical Physics* **2011**, *13*, 15244-15255.
36. Chandra, D. Effect of Ionic Liquids on DNA-Ligands Interaction: Studied by Fluorescence. *Asian Journal of Science and Technology* **2015**, *06*, 2100– 2103.
37. Sen Mojumdar, S.; Chowdhury, R.; Chattoraj, S.; Bhattacharyya, K. Role of Ionic Liquid on the Conformational Dynamics in the Native, Molten Globule, and Unfolded States of Cytochrome C: A Fluorescence Correlation Spectroscopy Study. *The Journal of Physical Chemistry B* **2012**, *116*, 12189– 12198.
38. Kim, J.; Doose, S.; Neuweiler, H.; Sauer, M. The Initial Step of DNA Hairpin Folding: A Kinetic Analysis Using Fluorescence Correlation Spectroscopy. *Nucleic Acids Research* **2006**, *34*, 2516– 2527.
39. Wennmalm, S.; Edman, L.; Rigler, R. Conformational Fluctuations in Single Molecules. *Proc. Natl. Acad. Sci. U. S. A.* **1997**, *94*, 10641– 10646.
40. Bhadra, K.; Kumar, G. S. Interaction of Berberine, Palmatine, Coralyne, and Sanguinarine to Quadruplex DNA: A Comparative Spectroscopic and Calorimetric Study. *Biochimica et Biophysica Acta (BBA) - General Subjects* **2011**, *1810*, 485– 496.
41. Jumbri, K.; Kassim, M. A.; Yunus, N. M.; Abdul Rahman, M. B.; Ahmad, H.; Abdul Wahab, R. Fluorescence and Molecular Simulation Studies on the Interaction between Imidazolium-based Ionic Liquids and Calf Thymus DNA. *Processes* **2020**, *8*, 13.
42. Lakowicz, J. R. *Principles of Fluorescence Spectroscopy*; Springers, **2006**.
43. Heller, D. P.; Greenstock, C. L. Fluorescence Lifetime Analysis of DNA Intercalated Ethidium Bromide and Quenching by Free Dye. *Biophysical Chemistry* **1994**, *50*, 305– 312
44. Johnson, I. M.; Kumar, S. G.; Malathi, R., De-Intercalation of Ethidium Bromide and Acridine Orange by Xanthine Derivatives and Their Modulatory Effect on Anticancer Agents: A Study of DNA-Directed Toxicity Enlightened by Time Correlated Single Photon Counting. *Journal of Biomolcular Structure and Dynamics* **2003**, *20*, 677-86.
45. Islam, M. M.; Barik, S.; Preeyanka, N.; Sarkar, M., Interaction of Lysozyme with Monocationic and Dicationic Ionic Liquids: Toward Finding a Suitable Medium for Biomacromolecules. *The Journal of Physical Chemistry B* **2020**, *124*, 961-973.
46. Abou-Zied, O. K.; Al-Shihi, O. I. K., Characterization of Subdomain Iia Binding Site of Human Serum Albumin in Its Native, Unfolded, and Refolded States Using Small Molecular Probes. *Journal of the American Chemical Society* **2008**, *130*, 10793-10801.
47. Lasanta, T.; López-de-Luzuriaga, J. M.; Monge, M.; Olmos, M. E.; Pascual, D., Experimental and Theoretical Evidence of the Existence of Gold(I)···Mercury(II) Interactions in Solution through Fluorescence-Quenching Measurements. *Chemistry – A European Journal* **2013**, *19*, 4754-4766.
48. Paul, B. K.; Ray, D.; Guchhait, N., Spectral Deciphering of the Interaction between an Intramolecular Hydrogen Bonded Esipt Drug, 3,5-Dichlorosalicylic Acid, and a Model Transport Protein. *Physical Chemistry Chemical Physics* **2012**, *14*, 8892-8902.
49. Akhuli, A.; Chakraborty, D.; Agrawal, A. K.; Sarkar, M., Probing the Interaction of Bovine Serum Albumin with Copper Nanoclusters: Realization of Binding Pathway Different from Protein Corona. *Langmuir* **2021**, *37*, 1823-1837.
50. Tian, J.; Liu, J.; He, W.; Hu, Z.; Yao, X.; Chen, X., Probing the Binding of Scutellarin to Human Serum Albumin by Circular Dichroism, Fluorescence Spectroscopy, FTIR, and Molecular Modeling Method. *Biomacromolecules* **2004**, *5*, 1956-61.
51. Kumari, M.; Maurya, J. K.; Tasleem, M.; Singh, P.; Patel, R., Probing HSA-Ionic Liquid Interactions by Spectroscopic and Molecular Docking Methods. *Journal of Photochemistry and Photobiology B* **2014**, *138*, 27-35.

52. Ross, P. D.; Subramanian, S., Thermodynamics of Protein Association Reactions: Forces Contributing to Stability. *Biochemistry* **1981**, *20*, 3096-3102.
53. Zhang, X.; Poniewierski, A.; Sozański, K.; Zhou, Y.; Brzozowska-Elliott, A.; Holyst, R., Fluorescence Correlation Spectroscopy for Multiple-Site Equilibrium Binding: A Case of Doxorubicin–DNA Interaction. *Physical Chemistry Chemical Physics* **2019**, *21*, 1572-1577.
54. Kral, T.; Langner, M.; Benes, M.; Baczyńska, D.; Ugorski, M.; Hof, M., The Application of Fluorescence Correlation Spectroscopy in Detecting DNA Condensation. *Biophysical Chemistry* **2002**, *95*, 135-44.

55. Cheng, C.; Ran, S.-Y. Interaction between DNA and Trimethyl-Ammonium Bromides with Different Alkyl Chain Lengths. *The Scientific World Journal* **2014**, *2014*, 863049.

56. Majhi, D.; Seth, S.; Sarkar, M. Differences in the Behavior of Dicationic and Monocationic Ionic Liquids as Revealed by Time Resolved-Fluorescence, NMR and Fluorescence Correlation Spectroscopy. *Physical Chemistry Chemical Physics* ***2018****,20, 7844-7856.*

57. Li, S.; Feng, G.; Bañuelos, J. L.; Rother, G.; Fulvio, P. F.; Dai, S.; Cummings, P. T. Distinctive Nanoscale Organization of Dicationic Versus Monocationic Ionic Liquids. *The Journal of Physical Chemistry C* **2013**, *117*, 18251– 18257.

58. Shi, Y.; Liu, Y.-L.; Lai, P.-Y.; Tseng, M.-C.; Tseng, M.-J.; Li, Y.; Chu, Y.-H. Ionic Liquids Promote PCR Amplification of DNA. *Chemical Communications* **2012**, *48*, 5325– 5327.

59. Sindhu, A.; Bisht, M.; Bahadur, I.; Venkatesu, P. Assessing the Compatibility of Mono-, Di-, and Tri-Cholinium Citrate Ionic Liquids for the Stability and Activity of α-Chymotrypsin. *ACS Sustainable Chemistry & Engineering* **2021**, *9*, 4812– 4822.

60. Dasgupta, A.; Das, P. K.; Dias, R. S.; Miguel, M. G.; Lindman, B.; Jadhav, V. M.; Gnanamani, M.; Maiti, S. Effect of Headgroup on DNA–Cationic Surfactant Interactions. *The Journal of Physical Chemistry B* **2007**, *111*, 8502– 8508.

61. Roy, K. B.; Antony, T.; Saxena, A.; Bohidar, H. B. Ethanol-Induced Condensation of Calf Thymus DNA Studied by Laser Light Scattering *The Journal of Physical Chemistry B* **1999**, *103*, 5117– 5121.

Chapter 5b

Deciphering the Role of Anions of Ionic Liquids in Modulating the Structure and Stability of *ct*-DNA in Aqueous Solutions

---

Amita Mahapatra, Unmesh Dutta Chowdhury, Sahadev Barik, Subhakanta Parida, B. L. Bhargava, Moloy Sarkar. *Langmuir* **2023,** 39, 48, 17318–17332.

Abstract

While the role of cationic moiety of ILs in the IL-DNA interaction event has been thoroughly explored in chapter 5a, the importance of anionic moiety in ILs, if any, is rather poorly understood. Herein, we examine the function of anions of ILs in nucleic acid stabilization by examining the stability and structure of calf thymus-DNA (ct-DNA) in the presence of various ILs composed of a common 1-ethyl-3-methylimidazolium cations ($Emim^+$) and different anions, which includes Cl^-, Br^-, NO_3^-, Ac^-, HSO_4^- and BF_4^- by employing various spectroscopic techniques as well as Molecular dynamic (MD) simulation studies. Analysis of our data suggests that the chemical nature of anions including polarity, basicity and hydrophilicity become an important factor in the overall DNA-IL interaction event. At lower concentrations, the interplay of intermolecular interaction between the IL anions with their respective cations and the solvent molecules becomes a very crucial factor in inducing their stabilizing effect on ct-DNA. However, at higher concentrations of ILs, the *ct*-DNA stabilization is additionally governed by specific-ion effect. MD simulations studies have also provided valuable insights into molecular-level understanding on DNA-IL interaction event. Overall, the outcome of this study clearly demonstrated that along with cationic moiety of ILs, the anions of ILs can play a significant role in deciding the stability of duplex DNA in aqueous solution.

5b.1. Introduction

Recently, the utilization of ionic liquids (ILs) has emerged as a potential tool in the realm of nucleic-acid stabilization and preservation in aqueous solutions.[1-3] In this context, the cationic components of ILs are always believed to play a fundamental role as they are shown to preferentially interact with the phosphate backbone of DNA, thereby stabilizing the double helical structure.[4-5] Indeed, in the majority of research studies focusing on DNA-IL interactions, a significant emphasis has often been placed on understanding the role of cationic moiety of ILs. The importance of IL anions in the said event has often been overlooked, possibly due to their lower binding affinities for the DNA backbone. [6-8] However, ILs are known to display structural transitions from ion pairs to distinct ions based on their hydration characteristics, and these free ions and associated ion-pairs are considered to exhibit different behaviour in the interaction event with the biomolecules.[9-14] Therefore, IL anions can also contribute to nucleic acid stabilization not only directly through interactions with DNA bases but also indirectly by influencing the solvent structure surrounding DNA or by altering some physio-chemical parameters such as pH, ionic strength, and polarity of the medium.[15-17] Hence, understanding these interactions between anions of ILs and DNA, as well as their impact on the surrounding environment, is crucial for optimizing the composition and conditions of ILs for specific nucleic acid-based applications.

Till date, a few experimental and theoretical studies have been carried out to explore the influence of various IL anions on the binding characteristics of ILs with DNA. Notable contributions include the works by Senapati and co-workers,[18] Biswal and co-workers,[19] and Freire and co-workers.[15] However, the overall consensus from these studies is that anions of ILs have a weaker impact as compared to cations on DNA-IL interaction. Furthermore, the investigation led by Pegram et al. has explored the effects of the complete Hofmeister series of inorganic salt anions on DNA duplex structure.[20] The results of that study have revealed that

the majority of these salts cause denaturation of the DNA structure. Similarly, recent work by Singh and coworkers demonstrated that the hydrophobicity of anions plays a pivotal role in modulating the formation and stability of G-quadruplex DNA.[21] In a separate work, Hohng co-workers have also noticed that the z-DNA stabilization is mainly governed by the Hofmiester effect of anions.[22] It is evident from this discussion that while some information on the influence of anions on the structural integrity of DNA in aqueous solutions is available, the implications of the chemical structure of anions of ILs is rather poorly understood. It is important to mention that the Hofmeister series encompasses a diverse range of anions characterized by variations in charge, shape, size, and hydrophobicity.[23-25]These specific attributes of the anions can impact the interactions between ILs and DNA molecules.[23, 26-30] For instance, hydrophobic anions exhibit an inclination to interact with the hydrophobic regions of DNA bases, thereby establishing significant associations. Conversely, the hydrophilic anions can facilitate the electrostatic interactions that take place between ILs and DNA. Furthermore, the hydration characteristics of the anions can reorganize the surrounding solvent structure enveloping DNA, and this issue can further modify the interaction of ILs with DNA. Therefore, investigations that focus on all these specific features of IL anions, particularly their charge and hydration properties towards DNA-IL interaction event, are expected to provide valuable insight into the more mechanistic aspects of DNA-IL interaction.

Considering the above facts, this chapter aims to investigate the structural stability of ct-DNA in a series of imidazolium-based ILs comprising different anions spanning the Hofmeister series. The ILs that are examined in this work include 1-ethyl-3-methylimidazolium chloride (EmimCl), 1-ethyl-3-methylimidazolium bromide (EmimBr), 1-ethyl-3-methylimidazolium nitrate ($EmimNO_3$), 1-ethyl-3-methylimidazolium acetate (EmimAc), 1-ethyl-3-methylimidazolium hydrogen sulfate ($EmimHSO_4$), and 1-ethyl-3-methylimidazolium tetrafluoroborate (Emim BF_4). The chemical structure of the cation and anions of ILs has

provided in scheme 5b.1.The selection of IL anions was based on their solubility in buffer solutions and their different hydration properties. The binding characteristics and thermodynamics of IL-DNA interaction were investigated using various spectroscopic techniques such as UV-Vis absorption spectroscopy, steady-state, and time-resolved fluorescence spectroscopy. Furthermore, the conformational stability of ct-DNA was evaluated using circular dichroism (CD) spectroscopy. MD simulation study has also been employed to shed more light into the experimental observations. Unlike previous studies those are primarily focused on the interactions of cationic component of ILs with ct-DNA, the present work highlights the influence of IL anions on the structure and stability of *ct*-DNA in aqueous solutions. Quite interestingly, the findings of this study also underscore the significance of consideration of both the cation and anion of ILs in understanding the overall DNA-IL interaction event. Moreover, the fundamental knowledge gained from this study is expected to enhance our understanding for the judicious selection of appropriate ILs with suitable cation-anion combinations for various nucleic acid-based applications.

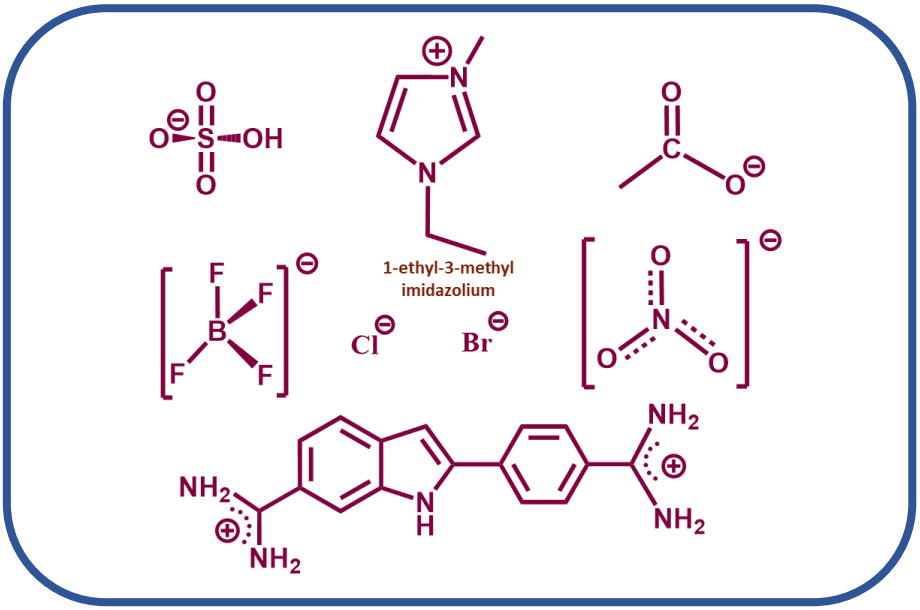

Scheme 5b.1. Chemical structure of cations and anions of ILs and the dye (DAPI) employed

5b.2. Materials, Experimental and Methods.

ct-DNA and DAPI (4′,6-diamidino-2-phenylindole) and tris-HCl buffer (1M) were obtained from Sigma-Aldrich. ILs 1-ethyl-3-methylimidazolium chloride (EmimCl), 1-ethyl-3-methylimidazolium bromide (EmimBr), 1-ethyl-3-methylimidazolium nitrate ($EmimNO_3$), 1-ethyl-3-methylimidazolium acetate (EmimAc), 1-ethyl-3-methylimidazolium hydrogen sulphate ($EmimHSO_4$), 1-ethyl-3-methylimidazolium tetrafluoroborate ($EmimBF_4$) were bought from TCI chemicals and have been used immediately after purchase.

5b.2.1. Sample preparation. A tris-HCl buffer solution of concentration 5mM and pH 7.2 was prepared by diluting a 1M buffer with Milli-Q water. The stock solutions of ct-DNA (100uM) and DAPI (200uM) were prepared in a 5mM buffer following the documented procedures.[5] The concentration of the ct-DNA solution in the buffer was determined by monitoring the molal extinction coefficient of ct-DNA at 260 nm, which was found to be 6600 cm^{-1}.[31] Each IL solution with a concentration of 2M was prepared in the buffer and kept in stock. In particular, the response of DAPI-bound ct-DNA complex (referred to as DAPI-DNA complex) was measured as a function of IL concentrations ranging from 0.05 M to 0.7 M using a solution containing 3uM DAPI and 60uM DNA in fluorescence measurements. The complete complexation of DAPI with *ct*-DNA under these conditions was confirmed through absorbance and fluorescence measurements. Additional details regarding the complexation of DAPI with DNA can be found in the Appendix 5b (Figure APX.5a.1). The methodology followed for various experiment has been described in chapter 2. Additionally, in the present study, the initial experiments are carried out in order to correct the presence of possible inner filter effect in fluorescence emission due to a minor absorption some investigated ILs at the DAPI-DNA complex excitation wavelength. The correction has been done by using a standard method with the help of equation 1 (eq.5b.1) and the corrected spectra have been used for further data analysis.[32]

$$F^{Corr}(\lambda_E, \lambda_F) = F(\lambda_E, \lambda_F) \frac{A(\lambda_E)}{A_{tot}(\lambda_E)} \quad \text{(eq.5b.1)}$$

Here $F^{Corr}(\lambda_E, \lambda_F)$ denotes the corrected fluorescence intensity at the excitation wavelength λ_E and emission wavelength λ_F, $F(\lambda_E,\lambda_F)$ is the observed fluorescence intensity at λ_E and λ_F , A represents the optical density of the EB-DNA complex, and A_{tot} represents the total optical density of the solution at the excitation wavelength λ_E.

5b.2.3. Molecular Dynamics (MD) Simulations: The starting configuration of the DNA molecule is taken from the RCSB pdb databank (ID-425D) having the nucleotide sequence 5'-ACCGGTACCGGT-3' (complementary strand 5'-TGGCCATGGCCA-3'). The atomistic simulations were carried out using GROMACS code (version-2019) with CHARMM-36 force field for the DNA molecule, charmm general force field (CGenFF) for the ILs components, and TIP3P for the water molecules.[34,35,36] Particle Mesh Ewald (PME) was used to treat the long ranged electrostatics with a cutoff value of 1.2 nm.[37] The DNA molecule, ILs with 1-ethyl-3-methylimidazolium (Emim) cation and one of the anions — chloride (Cl^-), tetra-fluoroborate (BF_4^-), acetate (Ac^-), hydrogen sulfate (HSO_4^-) and TIP3P water molecules were packed in a cubic box. 200 ion pairs were used in the simulations and nearly 12000 water molecules are used to pack the DNA molecule in the cubical box. Periodic boundary conditions (PBC) were employed in all directions. The temperature was kept at 298k with Nose-Hoover temperature coupling.[38] The pressure was maintained at 1 bar with isotropic Parrinello-Rahman pressure coupling with the coupling constant of 5 ps.[39] After the initial energy minimization of the systems and the subsequent equilibration in the NVT ensemble, the final production run was carried out for 200 ns in the NPT ensemble with a time step of 2 fs using the LINCS algorithm.[40] The simulations are replicated twice to increase the statistics. Simulation snapshots were rendered using VMD, the analysis scripts were written using the MD Analysis python library.[41,42] Hydrogen bonds are calculated using the geometric criteria of distance and angular

range between 0.2 – 0.3 nm and 90° – 180°, respectively. Watson-Crick hydrogen bonding between the opposite strands of nucleotides is calculated in accordance to the earlier reports.[43]

5b.3. Results and Discussion

5b.3.1. UV-visible absorption spectroscopy. UV-visible absorption spectroscopy is an effective technique that can be used to gather several valuable information on the fundamental aspects of DNA-IL interaction. Interaction between ILs and DNA can change the electronic environment surrounding the DNA bases. [19, 34] These changes can lead to shifts in the absorption maximum or intensity of the absorption spectra of DNA. By monitoring such changes, the coordination mode between a given IL and DNA can be interpreted.

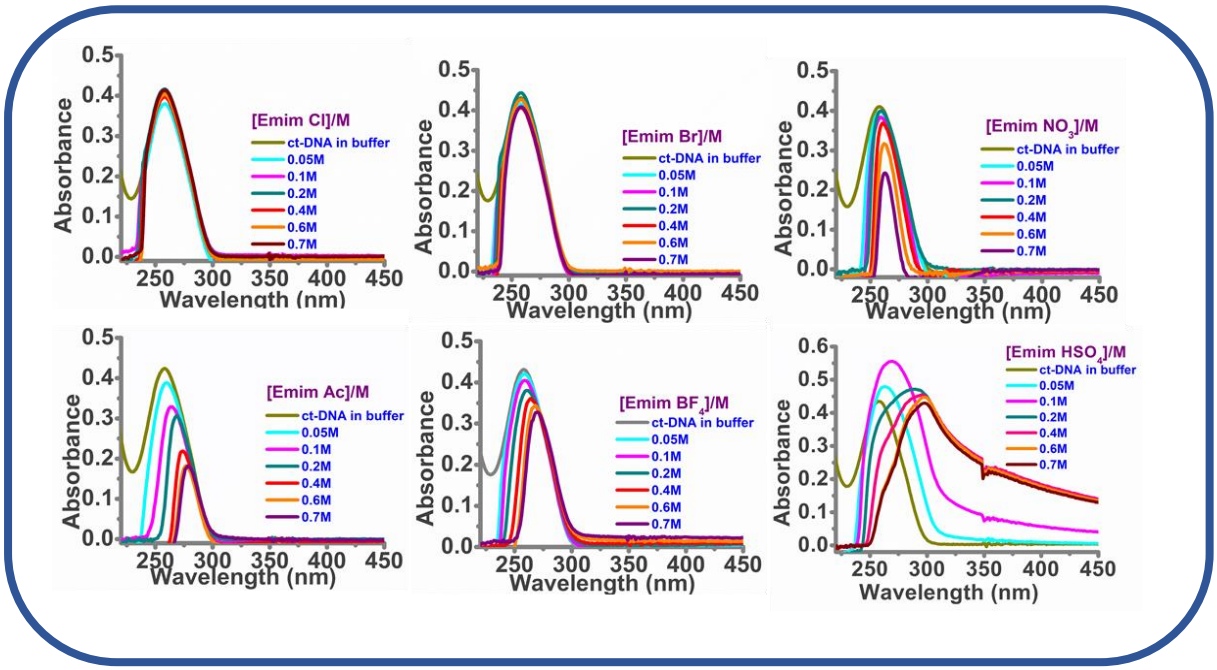

Figure 5b.1. Absorption spectra of free *ct*-DNA and DNA-IL system as indicated in the graph with varying the amount of ILs (0.05M to 0.7M) to a fixed concentration of DNA (60 μM)

Figure 5b.1 depicts the UV−vis absorption spectra of ct-DNA in the absence and presence of different ILs (in a concentration range of 0.05-0.7M). As can be seen from Figure 5b.1, the absorption spectrum of ct-DNA in buffer shows the characteristic peak maxima (λ_{max}) at 260

nm.[31] However, the intensity, as well as λ_{max} in the absorption spectrum of ct-DNA are observed to be altered with the gradual addition of selected ILs, and the spectral changes are found to be distinct for different ILs. DNA–IL interaction primarily involve covalent and noncovalent mode of binding.[19, 44] Covalent binding is identified by hyperchromism with a red shift in absorption maxima. In contrast, noncovalent binding is categorized into intercalative, electrostatic, and groove binding. Intercalative binding is indicated by hypochromism with a bathochromic shift, while electrostatic binding is characterized by lower hypochromicity without a bathochromic shift. Groove binding typically exhibits no or minor changes in UV–vis spectra. When both hyperchromic and hypochromic effects are observed with a moderate blue shift in the absorption band, it may suggest the involvement of more than one type of interaction, leading to the formation of DNA–ligand adducts. Table 5b.1 summarizes the changes in the spectral characteristics ct-DNA that has been induced by the addition of different ILs and their possible binding mode, which has been drawn from literature reports.[19] Moreover, from Figure 5b.1, it is clear that the local environment of the ct-DNA which has changed minimally in the presence of [EmimCl] and [EmimBr], changes considerably in the presence of [EmimNO_3], [EmimAc] and [EmimBF_4]. Moreover, prominent changes i.e., the absence of native-like spectra of ct-DNA in the presence of [Emim HSO_4] indicate that this IL has affected the native structure of the ct-DNA to a greater extent. It is pertinent to remember here that the cations of ILs are always considered as the dominant species to interact with ct-DNA via electrostatic attractions and H-bonds, while contributions of anions in the interactions event were often thought to be much less significant. In the present case, the only characteristic that separates the selected ILs from one another is the type of anions, and all the ILs share a common 1-ethyl-3-methyl imidazolium cation. Despite of the above fact, ct-DNA showed distinguishable spectral behavior in the presence of the individual ILs. This observation suggests that the interactions of ILs with DNA are not solely determined by the cations present

in the ILs. Instead, the anions that comprise up ILs also play a significant role in influencing their interactions with DNA.

Table 5b. 1. The spectral nature and binding mode of *ct*- DNA in presence of ILs

[EmimX], X denotes the anions of ILs	Spectral changes with respect to *ct*-DNA in buffer	Suggested mode of binding
X= $\mathbf{Cl^-}$, $\mathbf{Br^-}$	No or minor hyperchromic or hypochromic shift	May be electrostatic or groove binding.
X= $\mathbf{NO_3^-}$, $\mathbf{CH_3COO^-}$, $\mathbf{BF_4^-}$	Hypochromic with red shift	May be intercalative mode of binding.
X= $\mathbf{HSO_4^-}$	Hyperchromic and hypochromic effect with red shift	More than one type of interaction may exist.

5b.3.2 Steady-state and time-resolved fluorescence measurement. Based on the preliminary observations of the significant impact of the IL anions on the interaction process of ILs with *ct*-DNA, further investigations have been conducted to examine the binding strength, associated mechanism, and thermodynamics of interaction of these ILs with ct-DNA by exploiting the combination of steady-state and time-resolved fluorescence measurement. In order to do so, a temperature-dependent fluorescence indicator displacement (FID) assay has been carried out by titrating various ILs to a solution of DAPI-DNA complex, comprising of 3 μM DAPI and 60 μM DNA. It's important to note that the specific conditions required for the complete complexation of DAPI with ct-DNA may vary depending on the experimental setup and the specific goals of the study. DAPI is a small fluorescent molecule and is known to show enhanced fluorescence intensity when bound to the minor groove of DNA.[8] Any changes in the *ct*-DNA structure due to the interaction with ILs affect the DAPI micro-environment, which consequently hampers the emission of DAPI. The fluorescence emission spectra of the DAPI-DNA complex that are recorded as a function of IL concentration at 298k are provided in Figure 5b.2. Figure 5b.2 explicitly demonstrates a decrease in the fluorescence intensity of DAPI-DNA complex with gradual addition of different ILs at 298k. The reduction in fluorescence

intensity of DAPI-DNA complex indicates the displacement of DAPI from the minor groove of ct-DNA to the aqueous environment with the gradual addition ILs.

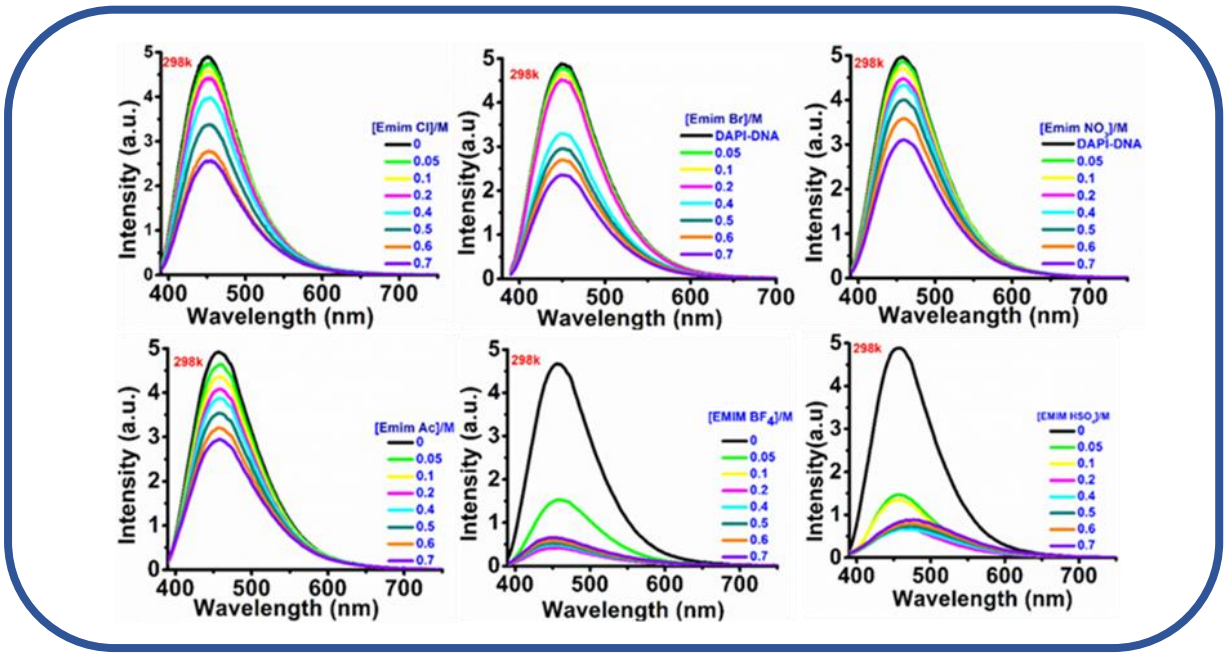

Figure 5b.2. Emission spectra of DAPI-DNA complex with varying the amount of different ILs (0.05M to 0. 7M) as indicated in the graph at 298k.

Similar spectra at three additional temperatures are provided in the appendix 5b. (Figures APX.5b.2, APX.5b.3, APX.5b.4 and APX.5b.5), and they exhibit similar quenching patterns. Notably, the ILs containing different anions are observed to induce varying degrees of quenching of the fluorescence of the DAPI-DNA complex. For example, while [Emim Cl] and [EmimBr] showed of approximately 55% reduction in in the fluorescence of DAPI-DNA complex, [EmimNO_3], [EmimAc] exhibited only a 45% reduction. More importantly, the spectral nature remained mostly unchanged in the presence of the four aforesaid anions-based ILs. In contrast, the decrease in the fluorescence intensities of the DAPI-DNA complex is observed to be much higher in presence of [EmimHSO_4] and [EmimBF_4]. For instance, the emission intensity has been reduced by almost 80 percent even in the presence of 0.1M of these ILs. This result suggests that the interaction of these two ILs is stronger with the ct-DNA

structure as compared to the rest of ILs. Furthermore, after addition of 0.2M of [Emim HSO_4], a red shift of 10nm has been observed in the emission maxima of DAPI-DNA complex. Conversely, the addition of 0.2M of [EmimBF_4] causes a blue shift of 10nm in the DAPI-DNA fluorescence. In this context, it is important to note here that among the anions considered, HSO_4^- is the most hydrophilic, while BF_4^- is the most hydrophobic.[24,29,25] These two anions occupy two opposite ends in the Hofmeister series of anions, which describes the relative effects of different ions on the properties of aqueous solutions.[29]The presence of these anions can lead to the creation of different polarities and pH levels in an aqueous solution. While HSO_4^- tends to interact with water molecules, potentially increasing the polarity of the media, BF_4^- is less likely to interact with water molecules and may lead to a decrease in the overall polarity of the solution.[45] Additionally, HSO_4^- anions being highly acidic may lead to changes in the pH levels of the solution. Some authors already associated acidic properties, along with the increase of the IL concentration, to a significant perturbation of the nucleic acids structure.[15] Such pH changes can alter the protonation states of DNA bases, affecting the overall DNA conformation. So, the shift observed in the emission spectrum of DAPI-DNA complex in the presence [EmimHSO_4] and [EmimBF_4] indicates the relocation of DAPI into different microenvironments in presence of these ILs. This observation further suggests that the IL-DNA interaction event is also susceptible to the change in polarity, pH of the medium, and in this regard the anions of ILs play a considerable role.

Quenching of the fluorescence of a fluorophore during its interaction with a fluorescence quencher can be attributed to various processes such as excited-state energy-transfer reactions or ground-state complex formation. These processes can be classified into two categories based on their mechanisms: dynamic fluorescence quenching and static fluorescence quenching. To understand the mechanistic pathway involved in the present case i.e., during the interaction of ILs with the DAPI-DNA complex and the resulting quenching of

fluorescence, we have utilized the classical Stern-Volmer equation (eq.5a.1). The Stern−Volmer plots (F_0/F vs [IL]) for [EmimCl], [EmimBr], [EmimNO$_3$], [EmimAc$^-$] obtained at four different temperatures are shown in Figure 5b.3.

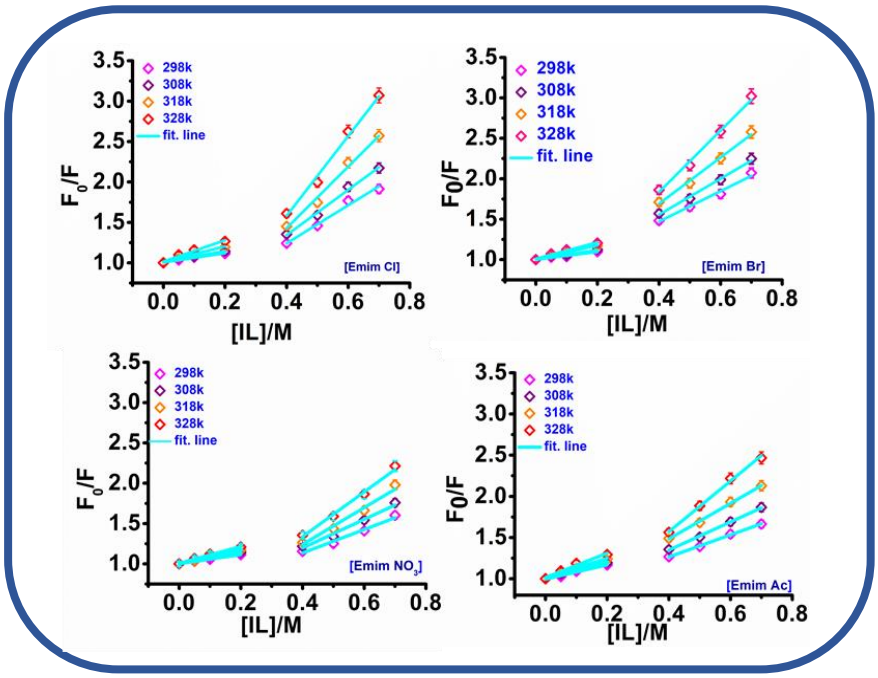

Figure 5b.3. Stern-Volmer plot for [EmimCl], [EmimBr], [EmimAc] and [EmimNO$_3$] showing two distinct binding region each following a straight line. The cyan line indicates fit to the data points.

It is pertinent to mention here that due to the existence of limited number of data points within the studied concentration range, the quenching due to [EmimHSO$_4$] and [Emim BF$_4$] ILs are not subjected for stern-Volmer analysis. The SV-analysis have revealed two distinct regions for each ILs in the Stern-Volmer plot, region I has been observed for lower concentration (0.05-0.2M) followed by region II which appeared at higher concentration (>0.2M). Each region exhibits a linear relationship with individual slope values, suggesting the involvement of either pure static or pure dynamic mechanisms in the quenching process. The K_{sv} values are estimated from the slope of the eq.5a.1 and are listed in Table APX5b.1.The obtained K_{sv} value at relevant temperatures are found to be in the range of $0.5M^{-1}$to $4.92M^{-1}$. The K_{sv} values obtained here

are comparable to those obtained in prior experimental studies for imidazolium-based ILs, where the interaction of imidazolium cation have been demonstrated to occur at the minor groove of ct-DNA.[7] Therefore, in the present case, it would be reasonable to assume a similar type of interaction for these ILs with DNA. Importantly, for each IL, higher (K_{sv}) values have been obtained at higher concentration regime (region II) than that has been observed for the lower concentration regime (region I). This observation signifies that at relatively higher concentration of ILs, there must be some changes either in the *ct*-DNA structure or in the micro-environment surrounding *ct*-DNA, which facilitates stronger interaction between ILs and *ct*-DNA. Interestingly, the K_{sv} value obtained at lower concentration regime different for different ILs are found to be in the order [EmimAc]> [EmimCl] >[EmimBr]> [EmimNO$_3$]. However, at higher concentration regime this sequence changes and falls in an order [EmimCl] >[EmimBr]> > [EmimNO$_3$]> [EmimAc] (Table APX5b.1). This observation clearly signifies that although cation binds preferentially with ct-DNA, the extent of interaction is significantly modified by the specific type of anion present. This might have happened due to the fact that, the anions of ILs exhibit varying degrees of association with the same $[Emim]^+$ cation. Consequently, they showcase distinct behaviours when introduced into an aqueous solution and as a result, their interactions with ct-DNA are not uniform. Additionally, the static or dynamic nature of the quenching mechanism can be distinguished by monitoring the temperature dependence of theK_{sv}.[5, 46] It is evident from the Table APX5b.1 that the K_{sv} value increases with the rise in temperatures in the presence of each IL. This observation indicates that the fluorescence quenching of the DAPI-DNA complex by ILs is dynamic in nature.

5b.3.2.1. Time-resolved fluorescence measurement. To verify further the nature of the quenching process, fluorescence lifetime measurements of the DAPI-DNA complex were conducted in the presence of each IL at concentrations similar to those used in the steady-state fluorescence measurements. The decay profiles of DAPI-DNA complex both in absence and

presence of concerned ILs can be found in Figure APX.5b.6 in the appendix 5b. It can be observed from decay the decay profiles that the lifetime of DAPI-DNA complex decreases with the gradual addition of ILs. The decay plots can be fitted to the exponential relation as described in the experimental section (eq. 2.8). The relevant decay parameters corresponding to DAPI-DNA complex with gradual addition of ILs are collected in Table APX5b.2. It has been observed that DAPI-DNA shows two decay components, the shorter component with a lifetime of ~1.27 ns, and the longer component of ~3.64 ns.[8, 47] These two lifetime components are often associated with free DAPI and DNA bound DAPI respectively. Interestingly, upon a careful look at the of the longer lifetime components, which is ascribed to the DAPI-DNA complex, decreases along with its contribution with the gradual addition of ILs. A short-lived third component also appear in the presence of higher concentration of each ILs indicating interaction of ILs with *ct*-DNA.[8] Moreover, steady decreases in the average lifetime, further supports the dynamic nature of the quenching process in ILs. [5]

5b.3.2.2. Thermodynamic parameters and nature of binding forces.

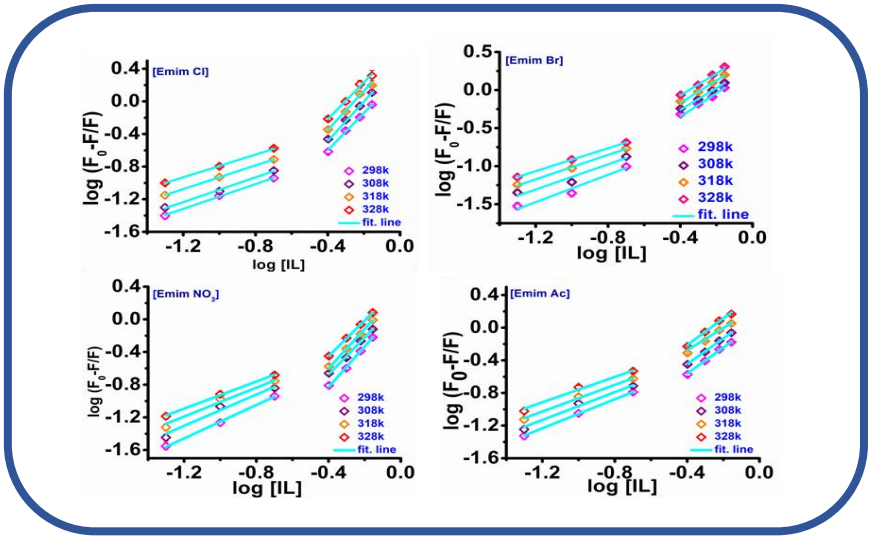

Figure 5b.4. The double logarithmic plots for DNA-IL systems as mentioned in the Figure. The solid cyan line indicates fit to the data points

To gain more insights into the influence of anions on the DNA-IL interaction event, the florescence quenching data has further been utilized to determine their binding equilibrium constants K_B and the number of binding site (n) for the DNA-IL interaction by employing the double logarithmic equation (eq.5a.2). The double logarithmic plot for each IL system at four different temperatures are displayed in Figure 5b.4. Two distinct binding regions have also been noticed in the double-logarithmic plots for all the IL systems at investigated temperature, where each region follows a straight line with separate slope value. The K_B value for each region are calculated from the intercept of the linear plots and are enlisted in Table 5b. 2. From Table 5b. 2 it can be noticed that the binding constant K_B for the second step is found to be higher than the first step in each case indicating stronger binding of ILs at higher concentration. This finding implies the binding strength of ILs with ct-DNA also varies depending on the concentration of ILs. Furthermore, the magnitude of the binding constant confirms that irrespective of the nature of anion to which imidazolium-ion is associated with, it interacts at the minor/major-grove of ct-DNA.[5, 7, 48]Interestingly, from Table 5b. 2, it can be revealed that at lower concentrations the binding strength between investigated ILs and ct-DNA follows an order [EmimAc]> [EmimCl]> [EmimBr]> [$EmimNO_3$]. As it is known that the more basic and hydrophilic anions in ILs tend to form their own hydration sphere and weakly associate with the imidazolium cation, these anions are expected to facilitate the interaction between the imidazolium cation and the DNA.[10] The binding trends of the DNA-IL complexes obtained at lower concentrations i.e. ([EmimAc]> [EmimCl]> [EmimBr]> [$EmimNO_3$]), convincingly demonstrate that the strength of interaction in between the cation and anions present in a given IL influences the extent of interaction between the IL cation and DNA. However, as the IL concentration increases, the lack of strong association of these hydrated anions with the imidazolium cation has led to a different behavior and subsequently changes and is observed to follow the order [EmimCl]> [EmimBr]> [$EmimNO_3$]> [EmimAc]. At higher concentration

of these ILs, both $[Emim]^+$cations and anions can penetrate the DNA duplex through the minor groove significantly and would tend to interact directly with nucleobases. [9]Upon entering the hydration layer of DNA, the extent of interaction changes considerably, depending on the nature of the anion present in the IL. This can further be understood by looking at the change in 'n' value (Table 5b. 2) which denotes the number of binding sites that DNA offer per ligand molecule for interaction.

Table 5b. 2. The binding constant and the thermodynamic parameters DNA-IL systems.

temp (k)	K_B (M^{-1})	*n*	$\Delta H/(kJmol^{-1})$	ΔS $/(Jmol^{-1}K^{-1})$	$\Delta G/(kJmol^{-1})$
			Region I (Lower concentration)/Emim Cl		
298	0.39	0.9	19.6	57.82	2.37
308	0.48	0.8			1.81
318	0.60	0.8			1.21
328	0.68	0.8			0.63
			Region II (Higher concentration)		
298	2.04	1.5	23.11	83.67	-1.80
308	3.01	1.4			-2.80
318	3.98	1.4			-3.50
328	4.78	1.3			-4.30
			Region I (Lower concentration) Emim Br		
298	0.37	0.8	15.36	43.27	2.46
308	0.44	0.8			2.03
318	0.56	0.8			1.60
328	0.64	0.7			1.17
			Region II (Higher concentration)		
298	1.69	1.4	18.30	67.20	-1.19
308	1.99	1.3			-1.86
318	2.57	1.3			-2.53
328	3.38	1.3			-3.21
			Region I (Lower concentration)/Emim NO_3		
298	0.16	0.9	7.90	22.40	1.23
308	0.24	0.9			1.00
318	0.35	0.9			0.78
328	0.42	0.8			0.56
			Region II (Higher concentration)		
298	1.44	2.4	16.94	59.69	0.46
308	1.69	2.2			-1.05
318	2.29	2.2			-1.63
328	2.63	2.1			-2.22
			Region I (Lower concentration) Emim Ac		
298	0.69	0.8	9.27	28.33	0.83
308	0.79	0.8			0.54
318	0.91	0.8			0.26
328	1.02	0.7			-0.01
			Region II (Higher concentration)		
298	1.17	1.6	10.74	38.48	-0.07
308	1.51	1.6			-1.10

318	1.81	1.6		-1.49
328	2.50	1.6		-1.87

It is worth noting that the native conformation of DNA in aqueous solutions is highly influenced by the nature of the surrounding aqueous environment and the presence of co-solutes or co-solvents. Various factors associated with a specific ion, including ionic size, shape and the interaction between polarizable ions and water molecules further may contribute to the complex interplay between ions, water, and DNA structure.[12, 14, 49] Therefore, it can be mentioned here that behavior and interactions of ILs with DNA are indeed a complex phenomenon and involve a combination of factors related to the cations, anions, and their relative concentration. To gain a deeper understanding of the observed binding trends at higher concentrations in the present study, we further have extended our investigation to explore the thermodynamics of the interaction using the Van't Hoff equation (eq.5a.3).

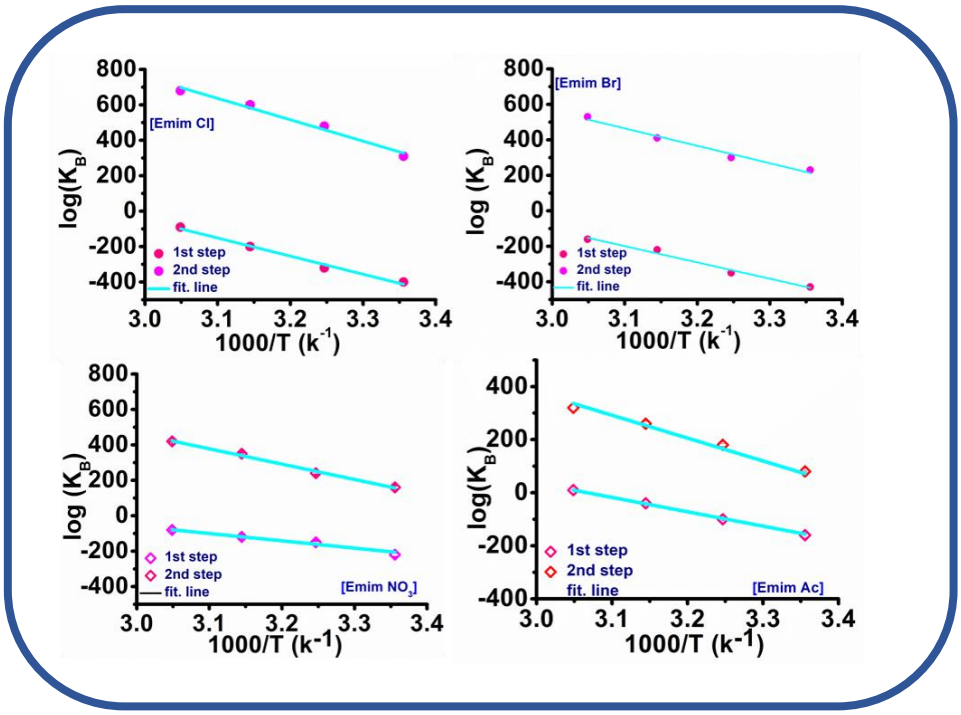

Figure 5b.5. Van't Hoff plot for the binding events of different IL as marked in the legend. Solid lines represent the fitting to the data points.

The Van't Hoff equation relates the equilibrium constant (K_B) of a reaction to the temperature (T) and the enthalpy change (ΔH) and entropy change (ΔS) of the reaction. By plotting the natural logarithm of the equilibrium constant ($\log K_B$) against the reciprocal of temperature (1/T), we can determine the values of ΔH and ΔS from the slope and intercept of the linear fit, respectively. The ΔH and ΔS values provide information about the enthalpic and entropic contributions to the IL-DNA binding process, shedding light on the driving forces and molecular interactions involved in the said event.[5] The Van't Hoff plot for each IL systems each region has been presented Figure 5b.5. The free energy (ΔG) associated with the interaction has been calculated using equation eq.5a.4. The thermodynamic parameters thus estimated are collected in Table 2. From the Table 5b.2, it can be noticed that the interaction of ILs with ct-DNA in the lower concentration regime is not favourable. This is because the interaction of ILs with *ct*-DNA at lower concentration requires breaking this hydration layer, which results in an unfavourable enthalpy change.[6, 8, 18] In other words, energy must be supplied to disrupt arrangement of water molecules and allow the ILs to approach *ct*-DNA. The unfavourable interaction between ILs and *ct*-DNA at lower concentrations is confirmed by the higher enthalpy value (Table 5b.2) indicating that breaking the hydration layer requires an input of energy. Furthermore, the lower entropy value in the first step suggests a limited degree of disorder, reflecting a relatively ordered arrangement of the system due to the stabilization provided by the surrounding water molecules in the hydration layer. But as the concentration of IL increases, the ruptured hydration layer makes the interaction favourably by exposing buried group of ct-DNA to the ILs thereby increasing the entropy of the system. This is reflected in the more favourable enthalpy and higher entropy values observed in Table 5b.2 for the second step of the interaction process at higher concentrations. However, the free energy value is found to be more negative in presence of [EmimCl] and [EmimBr] as compared to that for [EmimNO_3] and [EmimAc]. The negative values of ΔG is directly related to the

rearrangement in the water molecules in the presence of ionic solutes or destabilization of ct-DNA. To find out the exact reason of the high negative value of free energy for [EmimCl] and [EmimBr] as compared to [$EmimNo_3$] and [EmimAc], the circular dichroism (CD) measurements have been carried out.

5b.3.3.CD studies. CD spectroscopy is one of the most frequently used techniques to monitor the stability of the duplex structure of ct-DNA molecules in presence of various solute and solvent molecules.[50] Herein, CD spectroscopy has been utilized to examine the effect of various IL systems on the duplex structure of ct-DNA. Figure 5b.6 represents the CD spectra of ct-DNA in buffer as well as presence of individual ILs at different concentration. As can be seen from the figures, the CD spectra of ct-DNA in buffer (indicated as blue curve in each case) shows two characteristic peaks at 244nm and 275 nm. The positive maxima at 277 nm correspond to π–π base packing and the negative band at 244 nm corresponds to helicity for so-called of the native B-form of DNA.[4, 8] In the presence [EmimCl] and [EmimBr], no significant changes in either spectral shape or characteristics band position has been observed upto the highest concentration (0.6M), whereas in presence [$EmimNO_3$] and [EmimAc], a slight changes in the amplitude of both positive and negative band has been noticed, up to 0.2M and the changes become significant at higher concentration (beyond 0.2M) of these ILs. Furthermore, the absence of any noticeable induced signal in the DNA region of the CD spectra ensure that [$EmimNO_3$] and [EmimAc] do not intercalate as interpreted from the absorption measurement. [6]Therefore, the changes observed in the absorption spectrum in presence of [$EmimNO_3$] and [EmimAc] indicates some conformational changes in *ct*-DNA in presence of these two ILs. Moreover, both positive and negative band of ct-DNA disappeared in the presence [$EmimHSO_4$] and [$EmimBF_4$] ILs. This result suggests that the structure ct-DNA, which remains unaltered in the presence of [EmimCl] and [Emim Br] gets partially denatured in the presence of a higher concentration of [Emim NO_3] and [EmimAc]. In contrast, ct-DNA

gets completely denatured in presence of [EmimHSO$_4$] and [EmimBF$_4$]. Upon analysing the outcome of the present study investigation in conjunction with the result obtained from steady-state fluorescence data, it can further be suggested that the anions in ILs play a significant role in the DNA-IL interaction process. As CD spectra ruled out a change in the structure of *ct*-DNA in the presence of [EmimCl] and [EmimBr], the favourable interaction in such situation must have happened due to rearrangement in the solvent structure in the presence of those specific anions. The high entropy value (Table 5b.2) in the presence of such ILs further confirms this mechanism. However, for [EmimNO$_3$] and [EmimAc], the presence of these nitrate and acetate ions has led to the destabilisation of ct-DNA structure.

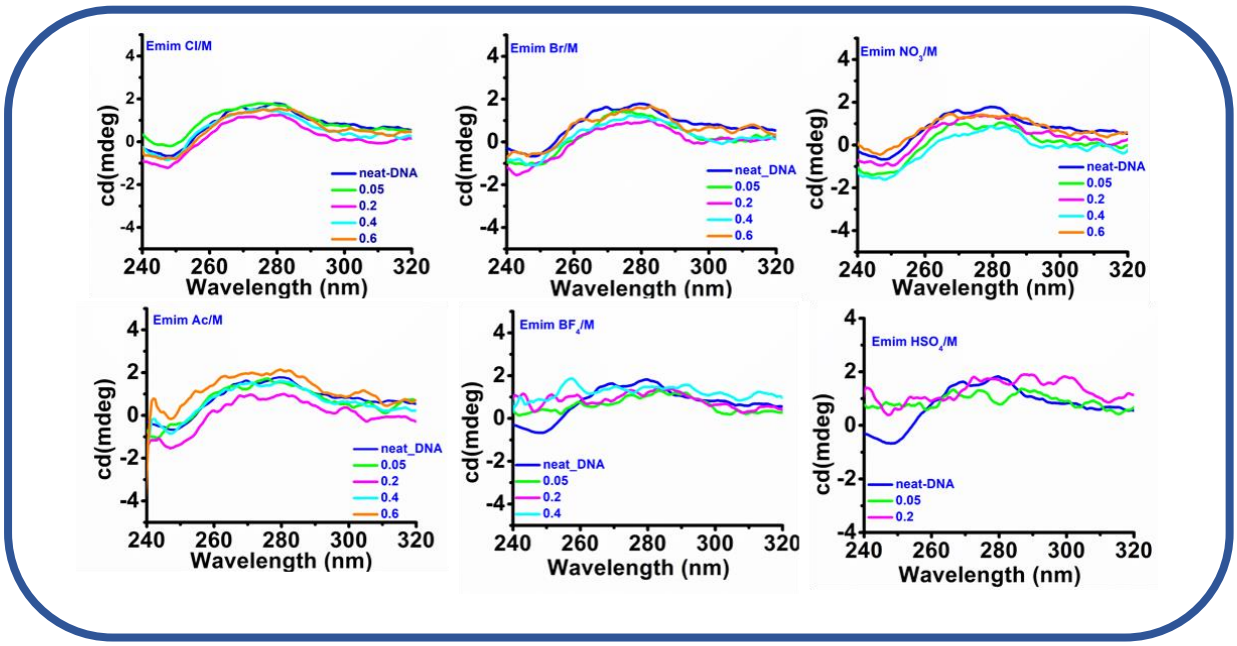

Figure 5b.6. CD spectra of *ct*-DNA in the presence of individual ILs at different concentrations as indicated in the figures.

5b.3.4. UV-melting studies. UV melting experiments on *ct*-DNA have been performed in the presence of all six IL systems, and representative melting profiles are provided in the Figure APX5b.7. Based on the representative melting profiles provided in Figure APX5b.7, it is evident that the presence of both [EmimHSO$_4$] and [EmimBF$_4$] drastically reduces the melting

temperature (T_m) of *ct*-DNA. Even at lower concentrations (0.1M) of these ILs, the T_m of *ct*-DNA falls below room temperature. However, T_m of *ct*-DNA has been observed to increase in presence of rest of the chosen ILs. Plots of melting temperature (T_m) of ct-DNA as a function of the concentration of [EmimAc], [Emim Cl], [EmimBr] and [$EmimNO_3$] are also provided in Figure 5b.7. From Figure 5b.7, it can be observed that native ct-DNA shows a thermal transition temperature (T_m) around 65.4^0C,[6] which is increased subsequently in presence of all the chosen ILs. Among the tested ILs, [EmimCl] and [$EmimNO_3$] leads to the highest Tm value of 80°C, followed by [EmimBr]. However, a slight decrease in the T_m Value has been observed at a relatively higher concentration of [EmimCl] and, [EmimBr] and, the estimated T_m values are still higher than that have been observed for the native DNA. However, one can also observe from Figure 5b. 7 that in the presence of [$EmimNO_3$] and [EmimAc], high concentration leads to partial denaturation of the ct-DNA (T_m less than 65^0).

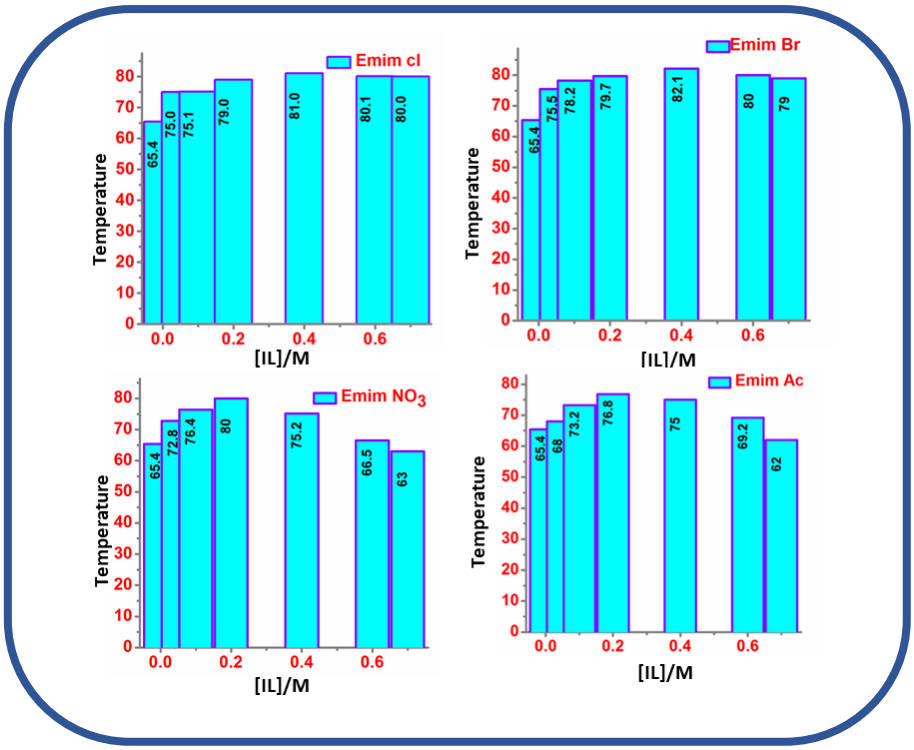

Figure 5b.7. Melting temperature of *ct*-DNA in the presence of individual ILs at different concentrations as indicated in the figure.

After carefully considering all the results, it can be suggested that the efficiency of ILs to stabilize the *ct*-DNA structure at the higher concentrations of ILs follows the order: [EmimCl] ≈[EmimBr]>[EmimNO$_3$]>[EmimAc]>[EmimBF$_4$]≈[EmimHSO$_4$]. Therefore, our investigations of the effect of the Hofmeister series of imidazolium-based ILs indicate that the *ct*-DNA stability does not strictly follow the Hofmeister anion series, as previously observed in the case of Z-DNA stability with higher salt concentrations.[22] The deviation from the Hofmeister order suggests that the stabilization of *ct*-DNA at higher IL concentrations may be attributed to ion-specific effects, where individual ions present in the ILs play a prominent role.[12, 14, 28, 49, 51] Specifically, at higher concentrations of [EmimCl], [EmimBr], [EmimAc], and [EmimNO$_3$], these individual ions can to penetrate the hydration layer at the groove. During this process, the Cl^- and Br^- ions exhibit specific interactions that contribute to stabilizing the *ct*-DNA structure. In contrast, Ac^- and NO_3^- ions appear to have a destabilizing effect on the *ct*-DNA structure. The findings from our study suggest that at higher concentrations of ILs, ion-specific effects play a crucial role in determining the stability of *ct*-DNA. During this process, the specific interactions between individual ions and *ct*-DNA become more pronounced, influencing the overall stability of the *ct*-DNA structure. Interestingly, our research reveals that the role of the anion in the ILs becomes more prominent at higher concentrations. This means that different anions, such as Cl^-, Br^-, NO_3^-, Ac^-, and others, exhibit varying effects on the stability of *ct*-DNA depending on their specific interactions with the *ct*-DNA molecules.

5b.3.5.MD simulation studies. To shed more light into our experimental observations, the radial distribution functions (RDF) of the DNA phosphate group with the cations and anions of the ILs are calculated from the MD simulations. The starting configuration of the simulation box showing the DNA molecule, water molecules, imidazolium cations and one of the counter ions (Cl^-) has been provided in Figure APX5b.8 (Appendix 5b). The RDF provides valuable

insights into the solvation preference of the IL components to the DNA phosphate groups providing valuable insight on the ion-specific interactions that mediate the DNA stabilization in the hydrated IL solvents. From the RDF in Figure 5b.8, it can be found that the interaction of cation with the phosphate group of DNA is nearly invariant with the choice of the counter anion involved. The RDF shows a peak at nearly 0.72 nm which describes the solvation of the $Emim^+$ cations within 0.72 nm of the DNA phosphate groups. The anions on the other hand interact less with the phosphate groups of DNA with the HSO_4^- anion showing the highest preference. The BF_4^- anion shows least preference of interaction with the phosphate groups of the DNA. This shows there is an exclusion of the anions within the solvation sphere of the IL components surrounded by the DNA. This is consistent with the earlier MD results which also had shown less preference of the counter anions of the IL to interact with the *ct*-DNA.[43]

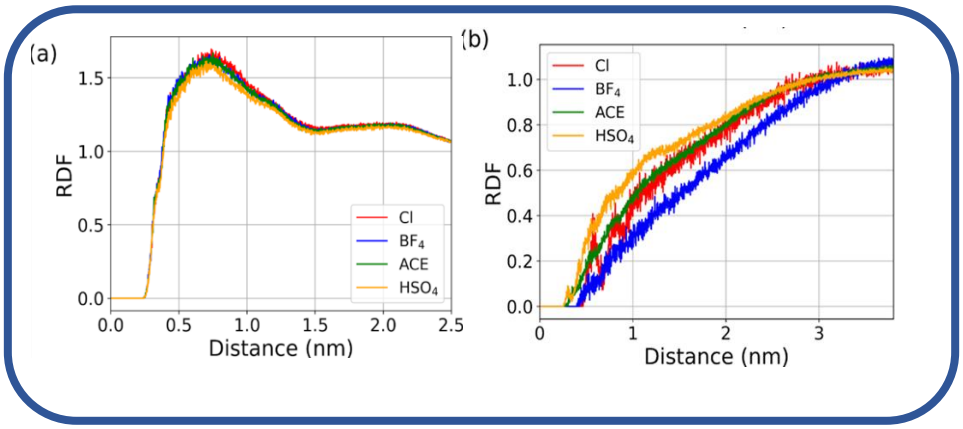

Figure 5b.8. The radial distribution function of the IL components around the phosphate groups of DNA (a) is the RDF of cations around the DNA and (b) is the RDF of anions around the DNA.

Figure 5b.9 shows the snapshots of the IL components interacting with the DNA molecules. The $Emim^+$ cations are seen to occupy the major groove of the DNA molecule. A few $Emim^+$ cations are also found to accumulate at the minor groove as well. The cations interact with the DNA bases through hydrophobic and electrostatic interactions, especially in the minor groove,

which is also proven experimentally (section 5b3.3). Previous MD studies have also shown the preference of the 1-butyl-3-methylimidazolium chloride $[Bmim]^+$ cations to accumulate both at the major and minor grooves of DNA.[18] This observation nicely corroborate with our experimental observation obtained from the fluorescence studies in a sense that irrespective of the nature of anions imidazolium cation in a given IL primarily interact at the minor groove of *ct*-DNA. In this context, we would like to also mention here that both CD spectra (the absence of any induced signals) as well the current simulation results rule out the possibility of intercalative binding of [$EmimNO_3$] and [EmimAc] with *ct*-DNA that was interpreted from the absorption measurements.

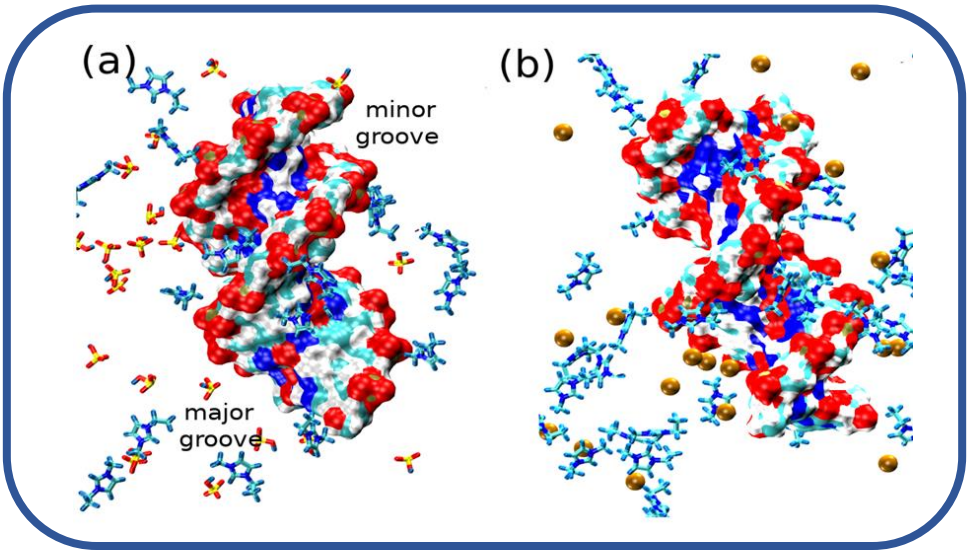

Figure 5b.9. The snapshots of the DNA interacting with the (a) [$EmimHSO_4$] and (b) [EmimCl]. The DNA is shown in surf representation, the ionic liquid components except chloride are shown in licorice representation, and chloride ions are shown as VDW spheres. The HSO_4^- anions are shown here in (a) illustrates both the major and minor groove binding, the chloride ions shown in (b) also shows major groove binding.

As the present study is mainly focused on examining the structural stability of ct-DNA in the aqueous environment of ILs, the root means square deviation (RMSD) values of ct-DNA (all

heavy atoms) when solvated in pure ILs in comparison to their initial positions in the crystal structure are further analysed and the results are presented in Figure 5b.10a. The pure water medium is taken as the control system. The RMSD of the replicate simulations are shown in the Figure APX5b.9. We have found that the ct-DNA molecule is stabilized within nearly 50 ns of the simulation time. The minimum RMSD of the DNA bases is in the bulk water medium (mean RMSD = 0.39 nm) as the control simulations and the maximum RMSD is in the presence of IL-containing HSO_4^- anion (mean RMSD = 0.41 nm). It is important to mention here that, the RMSD values denote the overall stability of the DNA in the IL medium. RMSD values are averaged over the entire *ct*-DNA and disruption in a small region may not be reflected in the RMSD values, especially if the disruption does not result in significant unfolding. For the replicate simulations we find that the RMSD of the systems (as shown Figure APX5b.9) containing BF_4^- and Ac^- ion did not converge within the simulation time. The root mean square fluctuation (RMSF) of the nucleotides determines the relative fluctuations of the nucleotides with respect to the control system. The RMSF for the ct-DNA in the IL solvents is shown in Figure 5b.10b. We found out that the relative fluctuations of the nucleobases are lower in the IL solvents compared to the water medium. The fluctuations are increased near the terminal bases of the DNA. The terminal nucleobases have fewer neighbouring nucleobases on one side, which can result in a reduced number of stabilizing interactions, such as hydrogen bonds and base stacking. These interactions contribute to restraining the movement of nucleobases in the internal regions of the DNA strand leading to higher fluctuations at the ends.

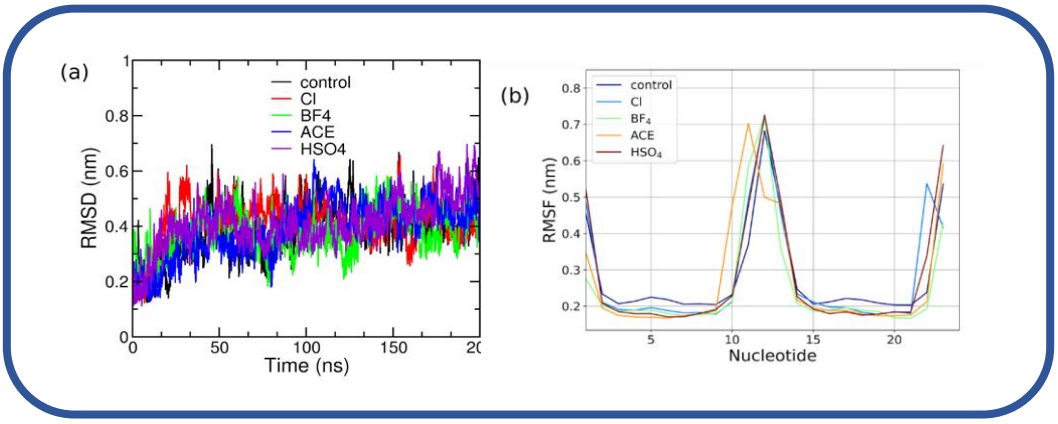

Figure 5b.10. (a) RMSD (nm) of ct-DNA (all heavy atoms) solvated by four hydrated ILs and the control simulation in water, (b) RMSF (nm) of the heavy atoms for the ct-DNA of nucleobases for the twelve pairs of nucleobases.

To gain more information on the structural stability of DNA in presence of IL containing different anions, from the MD simulation data, end-to-end distance (R_{ee}) of the DNA has been calculated. Studying the end-to-end distance of DNA through MD simulations offers valuable information about the conformational dynamics, flexibility, and interactions of the DNA molecule. A smaller end-to-end distance indicates a more compact and rigid conformation, while a larger end-to-end distance suggests increased flexibility and expansion of the DNA. The distribution of the end-to-end distances of the DNA is shown in Figure 5b.11. It has been observed that the DNA conformations are conserved, with end-to-end distances ranging between 3.5 - 4.4 nm. Hence, there is a minimal change in the overall shape of the DNA molecule in the presence of such IL solvents. The helical structure of DNA is retained in the hydrated IL solvents even with the change in the counter anions.

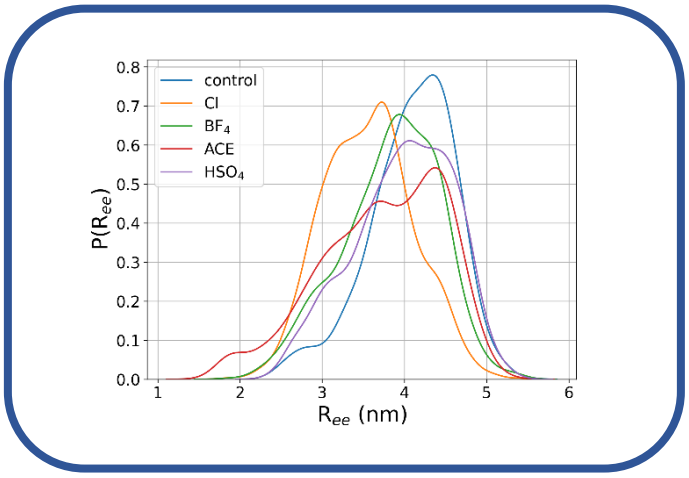

Figure 5b.11: The distribution of the end-to-end distance of the DNA in various IL solvents used in our study.

Though the globular structure of the DNA is mostly unaltered in the presence of the hydrated ILs, the base packing and helical structure of DNA are altered to a certain extent. Therefore, we have analysed the base stacking in various IL-DNA systems in the timescale of our simulations. The final snapshots of the simulation trajectories of 200 ns are shown in Figure 5b.12. We found that the base stacking is disrupted in the DNA structure for all the systems. Along with that, the Watson-Crick hydrogen bonding between the complementary pairs is disorganized. For example, in the IL solvent containing the HSO_4^- anion, the DNA undergoes the most disfigurement with the collapse of the inter-helical hydrogen bonding. Overall, the terminal nucleobases show the most disruption in all the systems as shown by RMSF earlier.

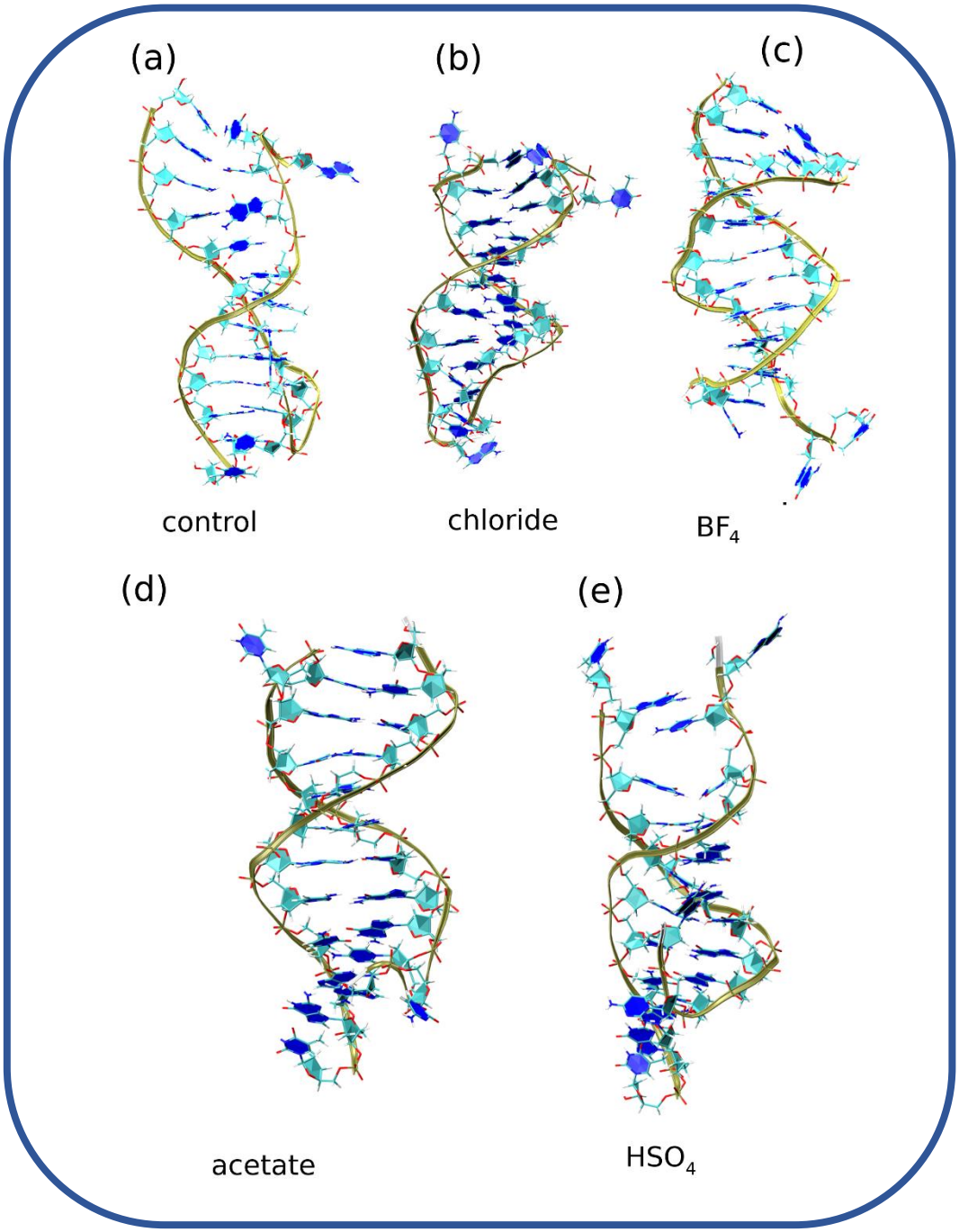

Figure 5b.12: The final structures of the *ct*-DNA derived from the 200 ns of simulations in control and the hydrated IL solvents comprising different anions.

To further corroborate the structural changes in the DNA, we have calculated the Watson–Crick hydrogen bonding distances and the glycosyl dihedral angle which is shown in Figure 5b.13 and Figure APX5b.10. We have considered the G5–C20 in the *ct*-DNA that shows significant stability with respect to the relative fluctuations. These hydrogen bonding distances are of

interest in studying the stability and conformational dynamics of DNA.[52,53] The distances are mostly conserved in the base pairs and the glycosylic dihedral shows negligible change. This shows the stability of the *ct*-DNA in the IL medium. The inner eight base pairs are mostly retaining their hydrogen bonding structure, whereas the terminal four base pairs, two from each end, disrupt their hydrogen bonding. This is illustrative of the MD simulation snapshots at the end of 200 ns simulations across both the runs (Figure 5b.12 and Figure APX5b.11). Earlier MD studies concerning the effect of IL on ct-DNA showed similar behavior with the disruption of the DNA base pairs in the head and the tail region of the DNA.[43] Even at the smaller simulation timescales (10 ns) they could find the disruption of the base pairs near the ends of the *ct*-DNA.[43] To further characterize the structural deformations in the DNA, we calculated the Watson-Crick hydrogen bonds for the DNA structure. The Watson-Crick hydrogen bonds for the systems are shown in Figure APX5b.12. The crystal structure of the DNA has 32 hydrogen bonds between the helices as the Watson-Crick hydrogen bonds.[4] The DNA structure with the hydrated IL systems having HSO_4^- anion has the least number of hydrogen bonds. The IL solvents with BF_4^- are found to have a higher number of Watson-Crick hydrogen bonds compared to the HSO_4^- system. Thus, the lowest number of Watson-Crick hydrogen bonds are observed in the system with HSO_4^- anion. The BF_4^- anion helps to maintain the Watson–Crick hydrogen bonds and prevent the opening of base pairs. The differences observed in the hydrogen bond interactions of these two ILs with *ct*-DNA further illustrate that anions of ILs also play a crucial role in determining the extent of DNA-IL interactions. Hence MD simulation results clearly reflects the role of anions in deciding the stability of the *ct*-DNA in aqueous IL solutions. The binding modes of the anions with the DNA grove is also observed from the simulation trajectories. Yet, further studies need to be performed taking longer simulation time and using different force-fields, or employing advanced sampling methods to obtain the complete information.[52-55]

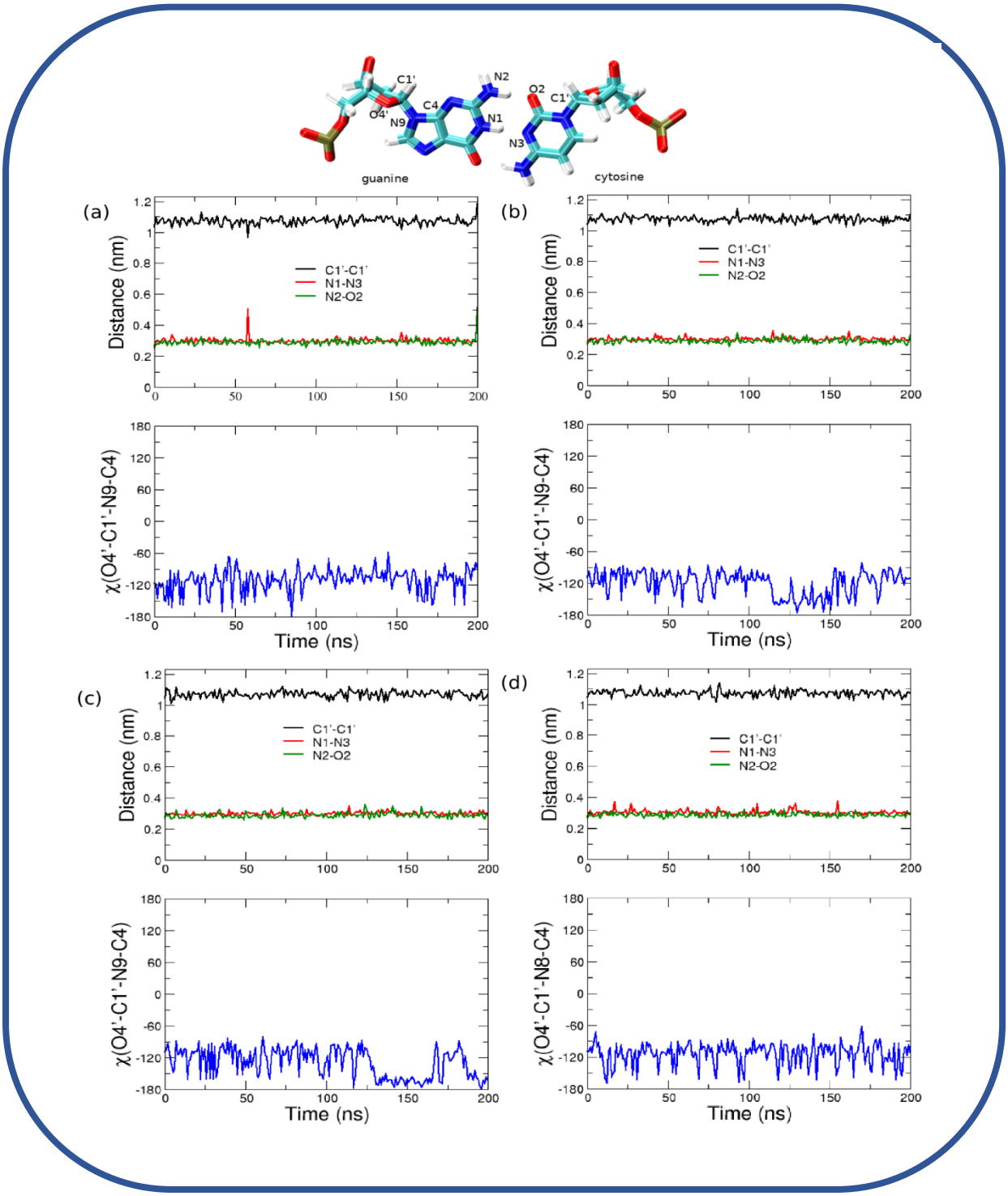

Figure 5b.13. Watson–Crick pairing modes of G5:C20 in *ct*-DNA. The time evolution of the glycosyl torsion angle [χ (O4′-C1′–N9-C4), shown in ball-and-stick representation], C1′–C1′ distance ($d_{C1'–C1'}$), and hydrogen-bond distances ($d_{N1–N3}$, $d_{N2–O4}$) during the 200 ns unbiased MD simulations is shown. The distances and the glycosyl torsional angle are shown for the (a) control, (b) [EmimCl] (c) [EmimBF$_4$], (d) [EmimAc].

5b.4.Conclusions

In the midst of several studies that focus on the role of the cationic moiety of ILs in stabilizing duplex structure of *ct*-DNA in an aqueous solution, the present study has been undertaken with the objective to find out the influence of anionic moieties of IL, if any, in the said event. For this purpose, the interaction of a series of ILs based on a common 1-ethyl-3-methyl imidazolium cation and different anions that include Cl^-, Br^-, Ac^-, $HSO_4^-$and BF_4^- with *ct*-DNA have been monitored by employing several spectroscopic techniques and MD simulations studies. These studies have demonstrated that the stability of *ct*-DNA in aqueous solution of ILs is significantly influenced by various factors such as pH, polarity, and concentration of ILs, and since the chemical nature of anions of ILs can influence these parameters in an appreciable manner, the role of anions become extremely crucial in the said process. The analysis of all the data obtained from this study has suggested that at lower concentrations of ILs, the extent of DNA-IL interaction is primarily mediated by the interactions between the cations and anions within the ILs, and the, structure of *ct*-DNA remains mostly stable under these conditions. However, at higher concentrations of ILs, the role of anions becomes prominent as specific ions (IL)-*ct*-DNA interaction takes place. Moreover, it has also been observed that depending on the nature of anions, these interactions can stabilize or destabilize *ct*-DNA structure. Overall, the outcome of this study has revealed that the role of the anionic moieties of ILs can play an extremely crucial role in determining the stability of *ct*-DNA in the aqueous solution of ILs. Therefore, while considering the stability of *ct*-DNA in presence of aqueous solution of ILs, the contribution from anion should be taken seriously along with the effect of cationic moieties of ILs. Additionally, the knowledge obtained on the DNA-IL interaction through the present investigation is expected to be helpful in choosing suitable IL systems for various nucleic acid-based applications.

5b.5. Appendix 5b.

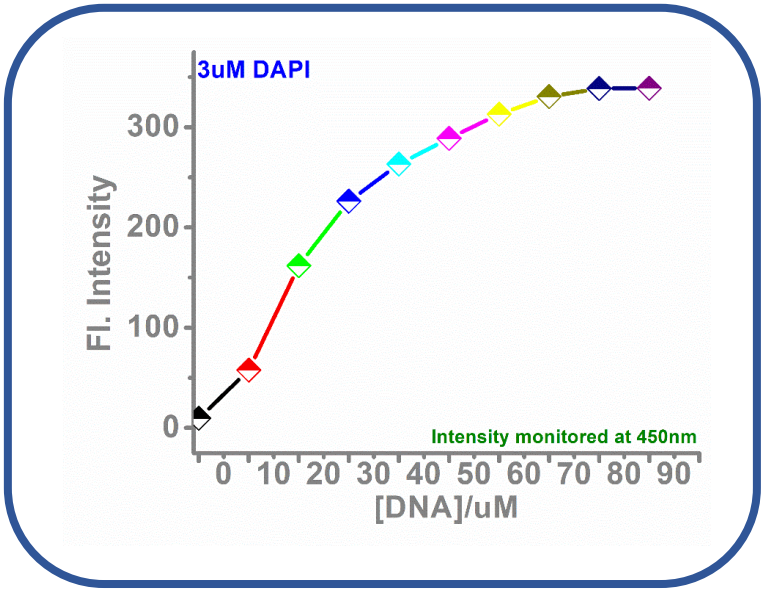

Figure APX5b.1. Represents the variation in fluorescence intensity of $3uM$ DAPI ($\lambda_{max} = 450nm$) when excited at $375nm$ with gradual addition of *ct*-DNA. The emission intensity of DAPI has been increased gradually with the subsequent addition of *ct*-DNA as marked in the x-axis. No more increase emission intensity has been observed when the concentration after the addition of $60uM$ *ct*-DNA. This indicates that at this concentration maximum DAPI is present in the bound form with *ct*-DNA.

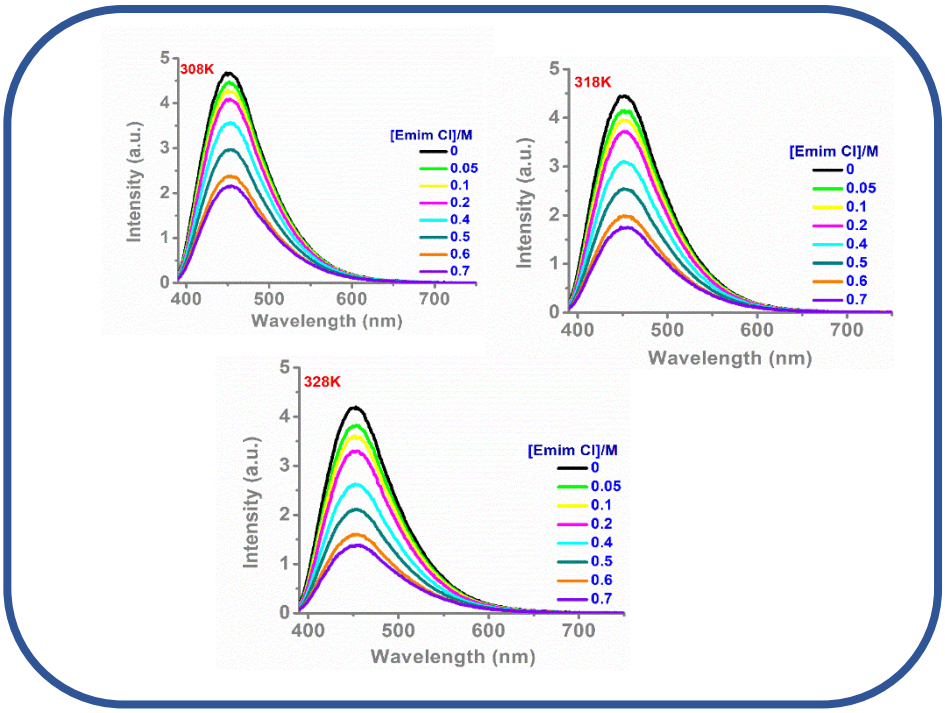

Figure APX5b.2. Fluorescence emission spectra of DAPI-DNA complex (λ_{ex} = 375 nm) in the absence and presence of gradual addition of [EmimCl] at (a) 308k, (b)318kand (C) 328k.

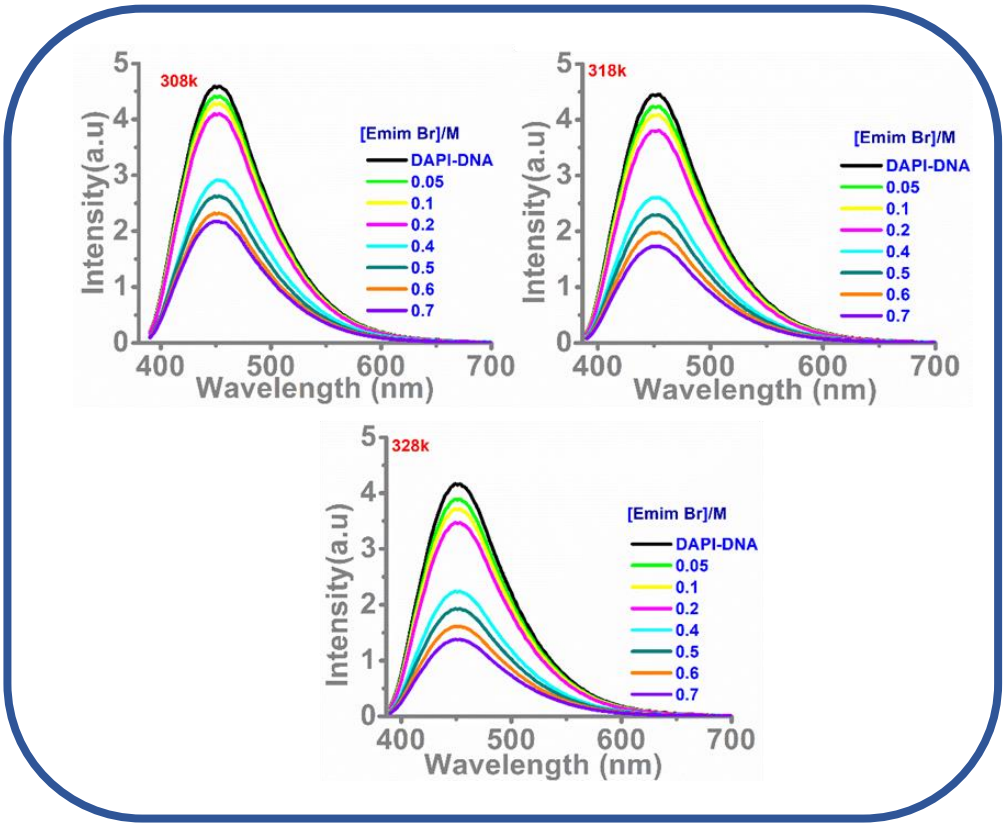

Figure APX5b.3. Fluorescence emission spectra of DAPI-DNA complex (λ_{ex} = 375 nm) in the absence and presence of gradual addition of [EmimBr] at (a) 308k, (b)318k and (C) 328k.

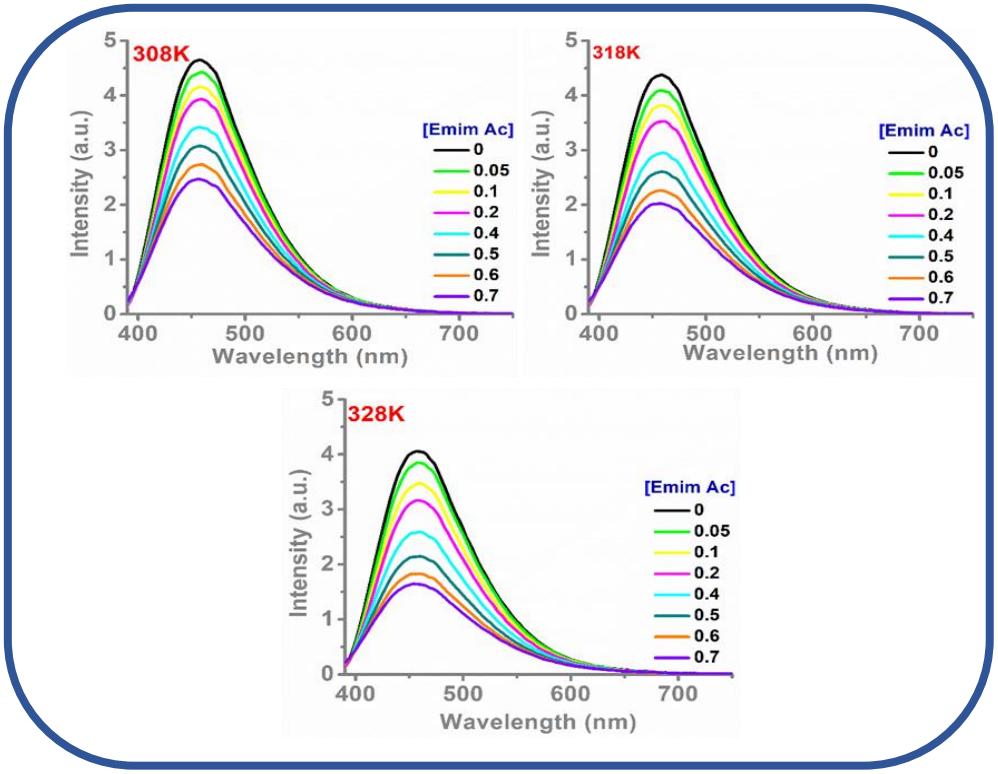

Figure APX5b.4. Fluorescence emission spectra of DAPI-DNA complex (λ_{ex} = 375 nm) in the absence and presence of gradual addition of [EmimNO_3] at (a) 308k, (b)318k and (C) 328k.

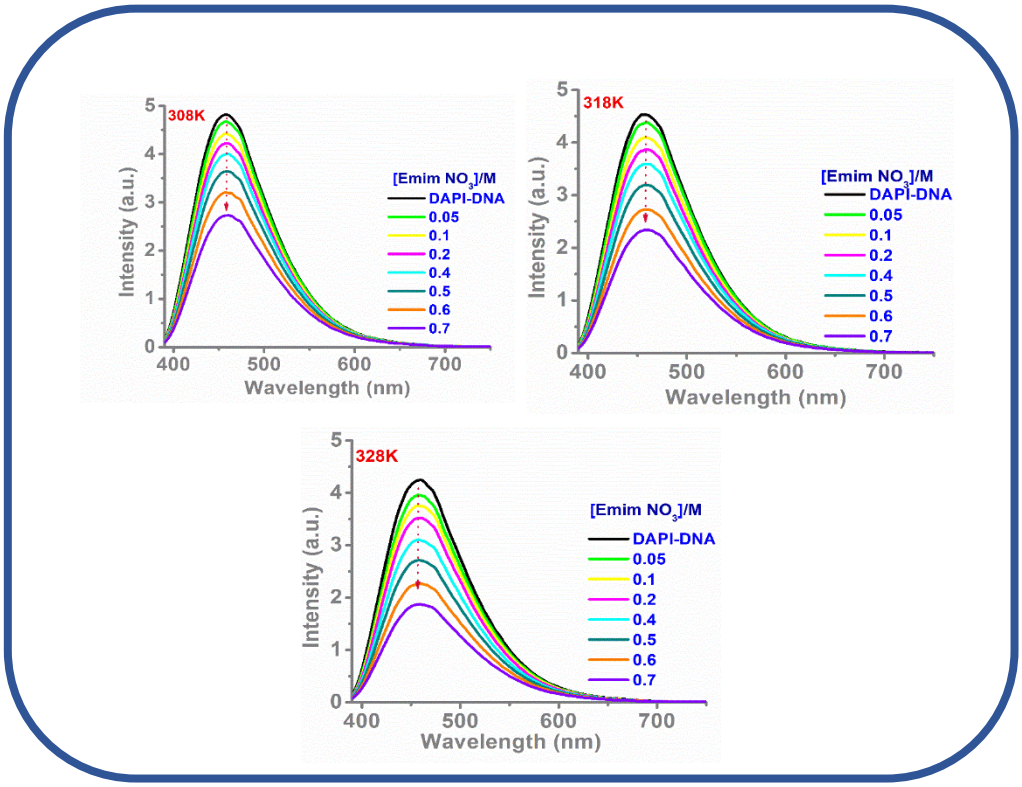

Figure APX5b.5. Fluorescence emission spectra of DAPI-DNA complex (λ_{ex} = 375 nm) in the absence and presence of gradual addition of [EmimNO$_3$] at (a) 308k, (b)318k and (C) 328k.

Table APX5b.1. The stern-Volmer quenching constants at indicated temperatures for IL systems

Temperature (k)	Region I	Region II
298	0.57	2.35
308	0.67	2.79
318	0.96	3.80
328	1.01	4.92
	K_{SV}/ [Emim Br]	
Temperature (k)	Region I	Region II
298	0.47	1.92
308	0.57	2.26
318	0.83	2.90
328	0.99	3.81
	K_{SV}/Emim Ac	
Temperature (k)	Region I	Region II
298	0.86	1.34
308	0.98	1.70
318	1.19	2.16
328	1.48	2.50
	K_{SV}/Emim NO$_3$	
Temperature (k)	Region I	Region II
298	0.56	1.45
308	0.74	1.77
318	0.90	2.28
328	1.04	2.77

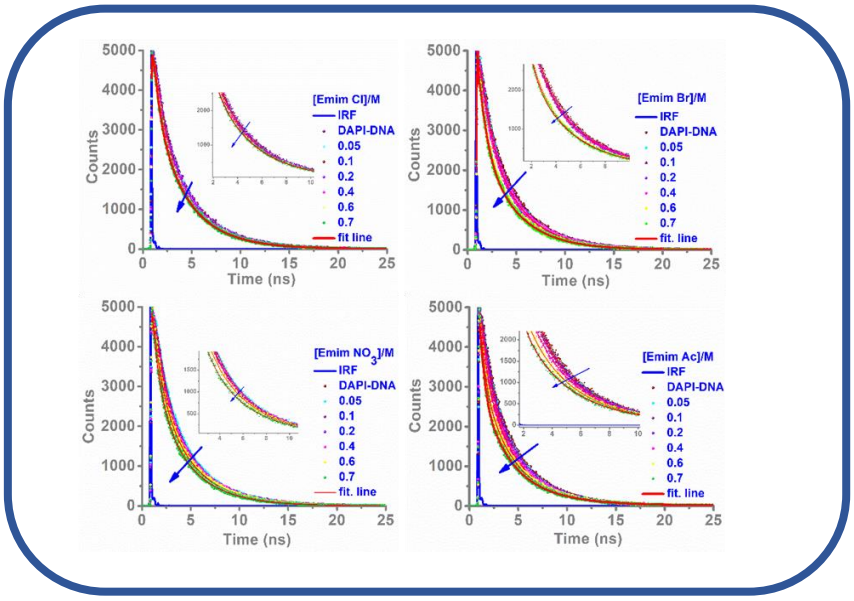

Figure APX5b.6. Life time decay-plots of DAPI-DNA complex in presence of ILs

Table APX5b.2. Decay parameters of DAPI-DNA complex with gradual addition of ILs.

[Emim Cl]/M	$\tau_1\ (B_1)$	$\tau_2\ (B_2)$	$\tau_3\ (B_3)$	τ_{avg} /ns
0	1.27(0.33)	3.64(0.67)		2.86
0.05	1.28(0.37)	3.64(0.63)		2.76
0.1	1.17(0.36)	3.59(0.64)		2.71
0.2	1.13(0.37)	3.57(0.63)		2.67
0.4	1.16(0.26)	3.54(0.56)	0.35(0.18)	2.35
0.6	1.10(0.26)	3.51(0.56)	0.43(0.18)	2.33
[Emim Br]/M	$\tau_1\ (B_1)$	$\tau_2\ (B_2)$	$\tau_3\ (B_3)$	τ_{avg} /ns
0.05	1.20(0.38)	3.64(0.62)		2.71
0.1	1.09(0.36)	3.61(0.64)		2.7
0.2	1.21(0.38)	3.58(0.62)		2.67
0.4	1.05(0.37)	3.55(0.63)		2.62
0.6	1.24(0.12)	3.50(0.54)	0.5(0.34)	2.20
[Emim Ac]/M	$\tau_1\ (B_1)$	$\tau_2\ (B_2)$	$\tau_3\ (B_3)$	τ_{avg} /ns
0.05	1.33(0.37)	3.65(0.63)		2.79
0.1	1.26(0.38)	3.64(0.62)		2.73
0.2	1.16(0.37)	3.60(0.58)	0.35(0.15)	2.57
0.4	1.12(0.2)	3.57(0.58)	0.43(0.22)	2.39
0.6	1.25(0.18)	3.55(0.49)	0.46(0.33)	2.12
[Emim NO_3]/M	$\tau_1\ (B_1)$	$\tau_2\ (B_2)$	$\tau_3\ (B_3)$	τ_{avg} /ns
0.05	1.11(0.33)	3.64(0.67)		2.80
0.1	1.12(0.33)	3.62(0.67)		2.79
0.2	1.1(0.33)	3.57(0.67)		2.75
0.4	1.11(0.25)	3.52(0.59)	0.21(0.16)	2.39
0.6	1.11(0.30)	3.47(0.57)	0.23(0.13)	2.34

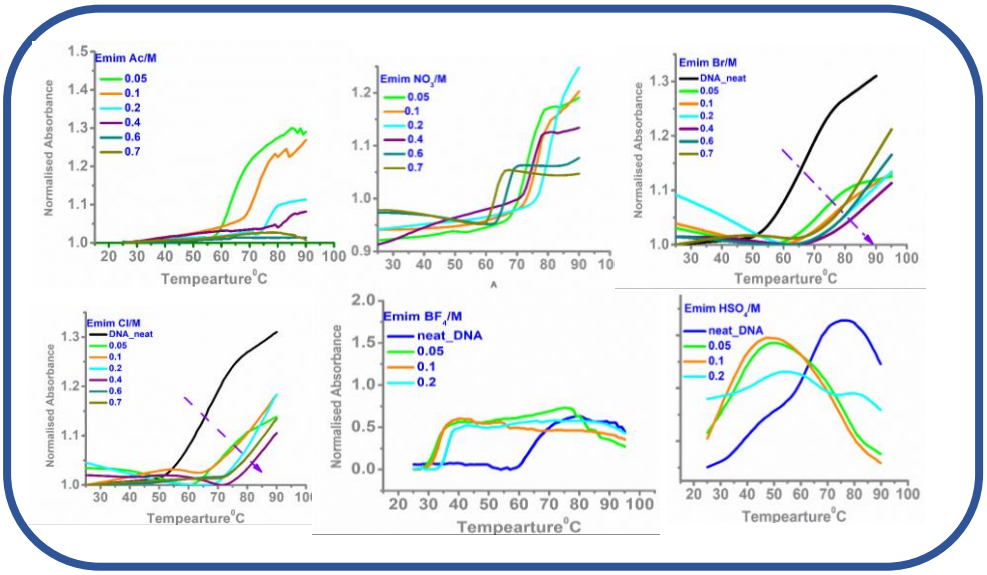

Figure APX5b.7. UV-melting profiles *ct*-DNA in the presence of different ILs.

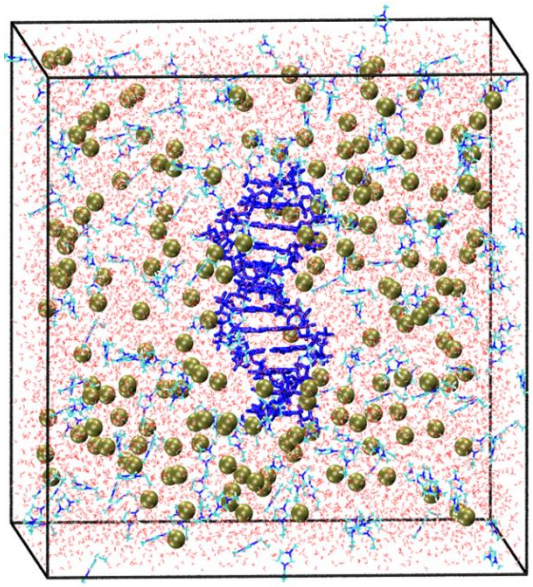

Figure APX5b.8. The starting configuration of the simulation box showing the DNA molecule, water molecules, ionic liquid cations and chloride counter ions

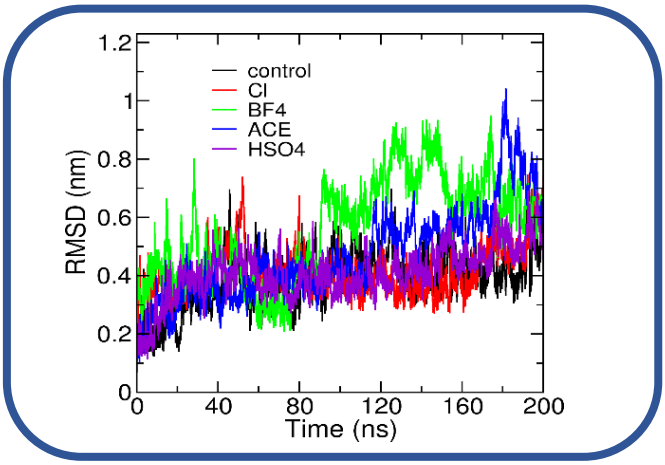

Figure APX5b.9. The RMSD of the heavy atoms of the *ct*-DNA derived from the replicate simulations.

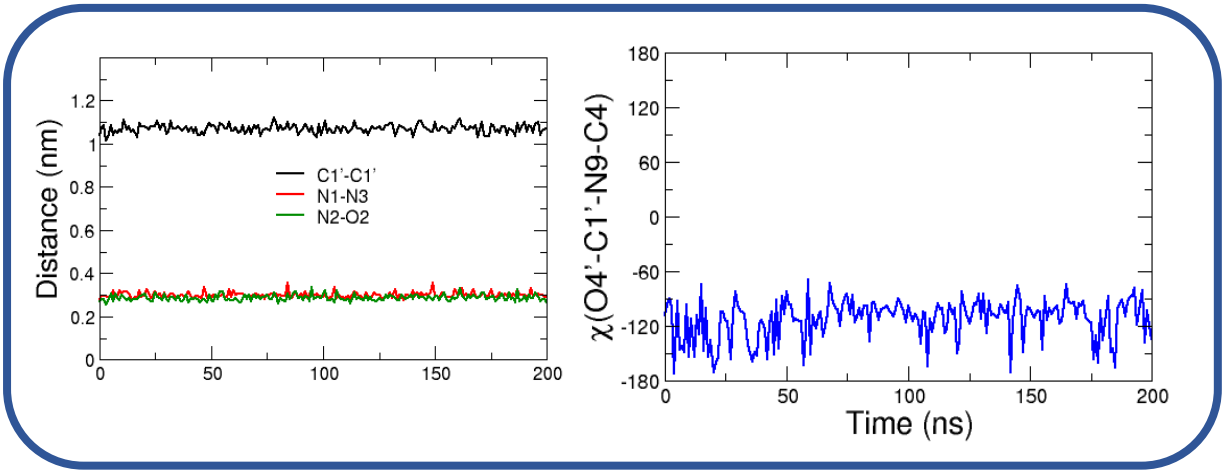

Figure APX5b.10. The distance between the nucleotides and the dihedral for the guanine and cytosine pair in the [EmimHSO$_4$] system. The definitions for the atom types are shown in the main text.

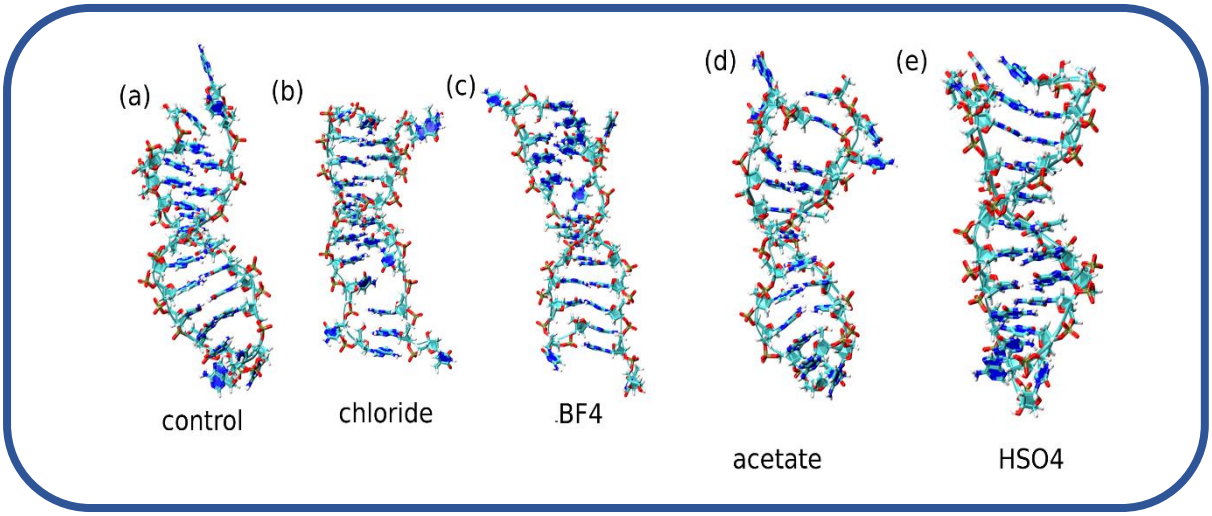

Figure APX.5b.11. The final snapshot of the *ct*-DNA structures derived from the replicate simulations for 200 ns.

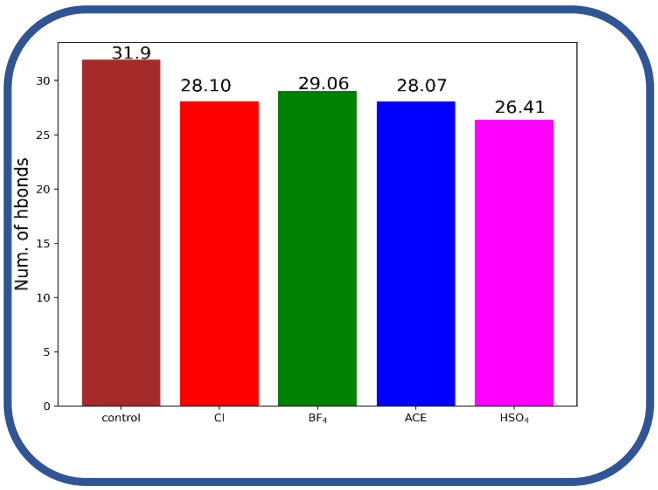

Figure APX5b.12. Bar plots of the number of Watson-crick hydrogen bonding.

REFERENCES

1. Benedetto, A.; Ballone, P., Room Temperature Ionic Liquids Meet Biomolecules: A Microscopic View of Structure and Dynamics. *ACS Sustainable Chemistry & Engineering* **2016**, *4*, 392-412.
2. Manojkumar, K.; Prabhu Charan, K. T.; Sivaramakrishna, A.; Jha, P. C.; Khedkar, V. M.; Siva, R.; Jayaraman, G.; Vijayakrishna, K., Biophysical Characterization and Molecular Docking Studies of Imidazolium Based Polyelectrolytes–DNA Complexes: Role of Hydrophobicity. *Biomacromolecules* **2015**, *16*, 894-903.
3. Shukla, S. K.; Mikkola, J.-P., Use of Ionic Liquids in Protein and DNA Chemistry. *Frontiers in Chemistry* **2020**, *8*, 598662.
4. Ding, Y.; Zhang, L.; Xie, J.; Guo, R., Binding Characteristics and Molecular Mechanism of Interaction between Ionic Liquid and DNA. *The Journal of Physical Chemistry B* **2010**, *114*, 2033-2043.
5. Mahapatra, A.; Barik, S.; Satish, L.; Chakraborty, M.; Sarkar, M., Assessing the Suitability of a Dicationic Ionic Liquid as a Stabilizing Material for the Storage of DNA in Aqueous Medium. *Langmuir* **2022**, *38*, 14857-14868.
6. Mishra, A.; Ekka, M. K.; Maiti, S., Influence of Ionic Liquids on Thermodynamics of Small Molecule–DNA Interaction: The Binding of Ethidium Bromide to Calf Thymus DNA. *The Journal of Physical Chemistry B* **2016**, *120*, 2691-2700.
7. Wang, X.; Cui, F., Binding Characteristics of Imidazolium-Based Ionic Liquids with Calf Thymus DNA: Spectroscopy Studies. *Journal of Fluorine Chemistry* **2018**, *213*, 68-73.
8. Pabbathi, A.; Samanta, A., Spectroscopic and Molecular Docking Study of the Interaction of DNA with a Morpholinium Ionic Liquid. *The Journal of Physical Chemistry B* **2015**, *119*, 11099-11105.
9. Xuan, S.; Meng, Z.; Wu, X.; Wong, J.-R.; Devi, G.; Yeow, E. K. L.; Shao, F., Efficient DNA-Mediated Electron Transport in Ionic Liquids. *ACS Sustainable Chemistry & Engineering* **2016**, *4*, 6703-6711.
10. Yee, P.; Shah, J. K.; Maginn, E. J., State of Hydrophobic and Hydrophilic Ionic Liquids in Aqueous Solutions: Are the Ions Fully Dissociated? *The Journal of Physical Chemistry B* **2013**, *117*, 12556-12566.

11. Voroshylova, I. V.; Ferreira, E. S.; Malček, M.; Costa, R.; Pereira, C. M.; Cordeiro, M. N. D., Influence of the Anion on the Properties of Ionic Liquid Mixtures: A Molecular Dynamics Study. *Physical Chemistry Chemical Physics* **2018**, *20*, 14899-14918.
12. Kumar, A.; Venkatesu, P., A Comparative Study of Myoglobin Stability in the Presence of Hofmeister Anions of Ionic Liquids and Ionic Salts. *Process Biochemistry* **2014**, *49*, 2158-2169.
13. Zhou, Y.; Zhan, J.; Gao, X.; Li, C.; Chingin, K.; Le, Z., The Cation− Anion Interaction in Ionic Liquids Studied by Extractive Electrospray Ionization Mass Spectrometry. *Canadian Journal of Chemistry* **2014**, *92*, 611-615.
14. Kumar, A.; Rani, A.; Venkatesu, P., A Comparative Study of the Effects of the Hofmeister Series Anions of the Ionic Salts and Ionic Liquids on the Stability of A-Chymotrypsin. *New Journal of Chemistry* **2015**, *39*, 938-952.
15. Dinis, T. B.; Sousa, F.; Freire, M. G., Insights on the DNA Stability in Aqueous Solutions of Ionic Liquids. *Frontiers in Bioengineering and Biotechnology* **2020**, 1207.
16. Sarkar, S.; Chandra Singh, P., Anions of Ionic Liquids Are Important Players in the Rescue of DNA Damage. *The Journal of Physical Chemistry Letters* **2020**, *11*, 10150-10156.
17. Hettige, J. J.; Kashyap, H. K.; Annapureddy, H. V.; Margulis, C. J., Anions, the Reporters of Structure in Ionic Liquids. *The journal of physical chemistry letters* **2013**, *4*, 105-110.
18. Chandran, A.; Ghoshdastidar, D.; Senapati, S., Groove Binding Mechanism of Ionic Liquids: A Key Factor in Long-Term Stability of DNA in Hydrated Ionic Liquids? *Journal of the American Chemical Society* **2012**, *134*, 20330-20339.
19. Sahoo, D. K.; Jena, S.; Dutta, J.; Chakrabarty, S.; Biswal, H. S., Critical Assessment of the Interaction between DNA and Choline Amino Acid Ionic Liquids: Evidences of Multimodal Binding and Stability Enhancement. *ACS Central Science* **2018**, *4*, 1642-1651.
20. Pegram, L. M.; Wendorff, T.; Erdmann, R.; Shkel, I.; Bellissimo, D.; Felitsky, D. J.; Record Jr, M. T., Why Hofmeister Effects of Many Salts Favor Protein Folding but Not DNA Helix Formation. *Proceedings of the National Academy of Sciences* **2010**, *107*, 7716-7721.
21. Sarkar, S.; Singh, P. C., The Combined Action of Cations and Anions of Ionic Liquids Modulates the Formation and Stability of G-Quadruplex DNA. *Physical Chemistry Chemical Physics* **2021**, *23*, 24497-24504.
22. Bae, S.; Son, H.; Kim, Y.-G.; Hohng, S., Z-DNA Stabilization Is Dominated by the Hofmeister Effect. *Physical Chemistry Chemical Physics* **2013**, *15*, 15829-15832.
23. Moghaddam, S. Z.; Thormann, E., The Hofmeister Series: Specific Ion Effects in Aqueous Polymer Solutions. *Journal of colloid and interface science* **2019**, *555*, 615-635.
24. Lu, L.; Hu, Y.; Huang, X.; Qu, Y., A Bioelectrochemical Method for the Quantitative Description of the Hofmeister Effect of Ionic Liquids in Aqueous Solution. *The Journal of Physical Chemistry B* **2012**, *116*, 11075-11080.
25. Kang, B.; Tang, H.; Zhao, Z.; Song, S., Hofmeister Series: Insights of Ion Specificity from Amphiphilic Assembly and Interface Property. *ACS omega* **2020**, *5*, 6229-6239.
26. He.X.; Ewing.A.G., Hofmeister Series: From Aqueous Solution of Biomolecules to Single Cells and Nanovesicle. *ChemBioChem* **2023**, 24, e2022006
27. Lezin, G.; Kuehn, M. R.; Brunelli, L., Hofmeister Series Salts Enhance Purification of Plasmid DNA by Non-Ionic Detergents. *Biotechnology and Bioengineering* **2011**, *108*, 1872-1882.

28. Kumar, A.; Venkatesu, P., Does the Stability of Proteins in Ionic Liquids Obey the Hofmeister Series? *International journal of biological macromolecules* **2014**, *63*, 244-253.
29. Gregory, K. P.; Elliott, G. R.; Robertson, H.; Kumar, A.; Wanless, E. J.; Webber, G. B.; Craig, V. S.; Andersson, G. G.; Page, A. J., Understanding Specific Ion Effects and the Hofmeister Series. *Physical Chemistry Chemical Physics* **2022**, *24*, 12682-12718.
30. Cebasek, S.; Serucnik, M.; Vlachy, V., Presence of Hydrophobic Groups May Modify the Specific Ion Effect in Aqueous Polyelectrolyte Solutions. *The Journal of Physical Chemistry B* **2013**, *117*, 3682-3688.
31. Chandra, D., Effect of Ionic Liquids on DNA-Ligands Interaction: Studied by Fluorescence. *Asian Journal of Science and Technology* **2015**, *6*, 2100-2103.
32. Islam, M. M.; Barik, S.; Preeyanka, N.; Sarkar, M., Interaction of Lysozyme with Monocationic and Dicationic Ionic Liquids: Toward Finding a Suitable Medium for Biomacromolecules. *The Journal of Physical Chemistry B* **2020**, *124*, 961-973.
33. Das, A.; Biswas, R., Dynamic Solvent Control of a Reaction in Ionic Deep Eutectic Solvents: Time-Resolved Fluorescence Measurements of Reactive and Nonreactive Dynamics in (Choline Chloride+ Urea) Melts. *The Journal of Physical Chemistry B* **2015**, *119*, 10102-10113.
34. Berendsen, H.J.C.; van der Spoel, D. and van Drunen, R. GROMACS: A message-passing parallel molecular dynamics implementation, *Computer Physics Communication* **1995***, 91*, 43–56.
35. Vanommeslaeghe, K.; Hatcher, E.; Acharya, C.; Kundu, S.; Zhong, S.; Shim, J., ... and Mackerell Jr, A. D., CHARMM general force field: A force field for drug-like molecules compatible with the CHARMM all-atom additive biological force fields. *Journal of computational chemistry* **2010**, *31*, 671-690.
36. Huang, J., & MacKerell Jr, A. D., CHARMM36 all-atom additive protein force field: Validation based on comparison to NMR data. *Journal of computational chemistry* **2013**, *34*, 2135-2145.
37. Darden, T.; York, D.; Pedersen, L., Particle Mesh Ewald: An N·log (N) Method for Ewald Sums in Large Systems. *The Journal of Chemical Physics* **1993**, 98, 10089–10092.
38. Evans, D. J., & Holian, B. L., The nose–hoover thermostat. *The Journal of Chemical Physics* **1985**, 83, 4069-4074.
39. Parrinello, M. and Rahman, A., Polymorphic Transitions in Single Crystals: A New Molecular Dynamics Method. *Journal of Applied Physics* **1981**, 52, 7182-7190.
40. Hess, B.; Bekker, H.; Berendsen, H. J.; Fraaije, J. G., LINCS: a Linear Constraint Solver for Molecular Simulations. *Journal of Computational Chemistry* **1997**, 18, 1463–1472.
41. Humphrey, W.; Dalke, A. and Schulten, K., VMD - Visual Molecular Dynamics. *Journal of Molecular Graphics* **1996**, 14, 33-38.
42. Michaud-Agrawal, N.; Denning, E. J.; Woolf, T. B.; Beckstein, O. MDAnalysis: a toolkit for the analysis of molecular dynamics simulations. *Journal of Computational Chemistry* **2011**, 32, 2319–2327.
43. Jumbri, K.; Rahman, M. A.; Abdulmalek, E.; Ahmad, H., & Micaelo, N. M., An insight into structure and stability of DNA in ionic liquids from molecular dynamics simulation and experimental studies. *Physical Chemistry Chemical Physics* **2014**, 16(27), 14036-14046.
44. Biver, T., Use of Uv-Vis Spectrometry to Gain Information on the Mode of Binding of Small Molecules to Dnas and Rnas. *Applied Spectroscopy Reviews* **2012**, *47*, 272-325.
45. Fedunova, D.; Antosova, A.; Marek, J.; Vanik, V.; Demjen, E.; Bednarikova, Z.; Gazova, Z., Effect of 1-Ethyl-3-Methylimidazolium Tetrafluoroborate and Acetate

Ionic Liquids on Stability and Amyloid Aggregation of Lysozyme. *International Journal of Molecular Sciences* **2022**, *23*, 783.

46. Barik, S.; Mahapatra, A.; Preeyanka, N.; Sarkar, M., Assessing the Impact of Choline Chloride and Benzyltrimethylammonium Chloride-Based Deep Eutectic Solvents on the Structure and Conformational Dynamics of Bovine Serum Albumin: A Combined Steady-State, Time-Resolved Fluorescence and Fluorescence Correlation Spectroscopic Study. *Physical Chemistry Chemical Physics* **2023**, *25*.
47. Barcellona, M. L.; Gratton, E., The Fluorescence Properties of a DNA Probe. *European Biophysics Journal* **1990**, *17*, 315-323.
48. Liu, H.; Dong, Y.; Wu, J.; Chen, C.; Liu, D.; Zhang, Q.; Du, S., Evaluation of Interaction between Imidazolium-Based Chloride Ionic Liquids and Calf Thymus DNA. *Science of The Total Environment* **2016**, *566-567*, 1-7.
49. Čebašek, S.; Seručnik, M.; Vlachy, V., Presence of Hydrophobic Groups May Modify the Specific Ion Effect in Aqueous Polyelectrolyte Solutions. *The Journal of Physical Chemistry B* **2013**, *117*, 3682-3688.
50. Mallick, T.; Karmakar, A.; Batuta, S.; Ahamed, G.; Das, S.; Alam, M. N.; Mukherjee, M.; Das, N.; Mandal, D.; Begum, N. A., Fluorescent Small Molecules Are Big Enough to Sense Biomacromolecule: Synthesis of Aromatic Thioesters and Understanding Their Interactions with Ctdna. *ACS Omega* **2018**, *3*, 334-348.
51. Gregory, K. P.; Elliott, G. R.; Robertson, H.; Kumar, A.; Wanless, E. J.; Webber, G. B.; Craig, V. S. J.; Andersson, G. G.; Page, A. J., Understanding Specific Ion Effects and the Hofmeister Series. *Physical Chemistry Chemical Physics* **2022**, *24*, 12682-12718.
52. Geronimo, I., & De Vivo, M., Alchemical Free-Energy Calculations of Watson–Crick and Hoogsteen Base Pairing Interconversion in DNA. *Journal of Chemical Theory and Computation* **2022**, 18, 6966-6973.
53. Stone, S. E., Ray, D., & Andricioaei, I., Force-Field-Dependent DNA Breathing Dynamics: A Case Study of Hoogsteen Base Pairing in A6-DNA. *Journal of Chemical Information and Modeling* **2022** , 62, 6749-6761.
54. Lemkul, J. A.; MacKerell Jr, A. D. Polarizable force field for DNA based on the classical Drude oscillator: II. Microsecond molecular dynamics simulations of duplex DNA. *Journal of Chemical Theory and Computation* **2017,** 13, 2072-2085.
55. Bevan, D. R.; Li, L.; Pedersen, L. G.; Darden, T. A. Molecular dynamics simulations of the d (CCAACGTTGG) 2 decamer: influence of the crystal environment. *Biophysical Journal* **2000,** 78, 668-682.

Chapter 6

Insight into the Structure and Transport Properties of Pyrrolidinium-based Geminal Dicationic-Organic Ionic Crystals: Unravelling the Role of Alkyl-Chain Length

---

Amita Mahapatra, Aneeya K. Samantara, Sahadev Barik, Malaya K. Sahoo, Dr. J. N. Behera and Dr. Moloy Sarkar. *Soft Matter* **2023**, 19, 3510-3518

CHAPTER 6

Abstract

In a recent breakthrough, organic ionic crystals have emerged as exceptionally efficient candidates for advancing the field of all solid-state electrolytes. This innovative development holds the promise of addressing leakage-issue inherent to conventional room temperature ionic liquid-based electrolytes. In this work, a series of geminal di-cationic Organic Ionic Crystals (OICs), based on C_3-, C_6-, C_8- and C_9-alkylbridged bis-(methylpyrrolidinium)bromide are synthesized, and the structural features, thermal properties and phase behaviours of as synthesized OICs have been investigated. Additionally, a number of electro-analytical techniques have been employed to assess their suitability as an efficient electrolyte composite (OIC: I_2: TBAI) for all solid-state dye sensitised solar cells (DSSC). The structural analysis has revealed that along with excellent thermal stability and well- defined surface morphology, OICs exhibit a well-ordered three-dimensional network of cations and anions that can serve as a conducting channel for the diffusion of iodide ions. Electrochemical investigations have shown that OICs with an intermediate length of alkyl bridge (C_6- and C_8-alkyl bridged) show better electrolytic performance than that are based on OICs with a relatively shorter (C_3-) or longer (C_9-) alkyl-bridged OICs. A careful analysis of the data has essentially demonstrated that the length of the alkyl bridge chain plays a significant role in determining the structural organisation, morphology and eventually the ionic conductivity of OICs.

CHAPTER 6

6.1. Introduction

Ionic liquids (ILs) are typically organic salts with melting point below or near room temperature.[1-4] They possess structural features reminiscent of molten salts as well as molecular liquid.[5-6] In recent times, majority of the research works on ILs are devoted to the study of structure, properties and application of ionic liquids in their liquid state.[7-16]However, studies on organic ionic crystal (OICs) which are solid state analogue of RTILs are rather limited. Interestingly, these organic ionic crystals have shown great promise to replace liquid-based electrolyte in the energy related applications such as in dye sensitized solar cell, Li-ion battery etc. [17-18] Interestingly, these systems also show comparable conductivity and diffusion efficiency like usually employed liquid- based electrolyte.[19,20]More importantly, these OIC-based electrolytes are exempted from the leakage problem that are commonly associated with the liquid-based electrolyte.[21-22] While some OICs based on mono-cationic ionic liquids (MILs) as well as dicationic ionic liquids (DILs) have been synthesized and have been used as electrolyte matrices for various electrochemical devices, design and development of OIC-based electrolyte with high thermal stability and high conductivity has remained as a formidable challenge.[19, 23-27] One of the possible ways through which this particular challenge can be tackled is by tuning the thermal and electrochemical properties of the OICs by introducing various combination of cation and anion in their structure. However, the judicious selection of cations and anions for a suitable OIC invariably demands proper understanding of the solid-state structure and various intermolecular interaction associated with them. In this context, we also note that OICs, which can be developed based on dications are expected to be more interesting than those are based on monocations due to the fact that former possess superior physiochemical properties than that of later.[16, 28-30] Therefore, proper information on the structure and inter-constituent interactions of OICs that are based on dications are expected to

be helpful in designing highly efficient solid-state electrolyte for various energy related applications.

OICs are a kind of crystalline compound consisting of anions and cations whose properties are different than those of the conventional crystals.[31] The microstructure with three-dimensional ionic channels in this kind of ionic crystals are responsible for their excellent electrochemical property. [32] Besides that, few other parameters such as crystallinity, morphology and size of OICs are shown to significantly influence the electrolytic properties of the OICs.[33-34]Till date, majority of the research on OICs is confined to the imidazolium-based compounds, such as 1-methyl-3-acetylimidazolium iodide (MA-II), [35] N-propargyl imidazolium carbazole-imidazolium iodide,[36] and ester-functionalized imidazolium iodide salts.[37] It is to be mentioned in this context that Yan and co-workers have observed improved efficiency of DSSCs by employing cyanobiphenyl-functionalized imidazolium ionic crystals.[32]Although, Pyrrolidinium-based OICs possess better electrochemical stability than that of imidazolium-based OICs due to its non-aromatic character, only a handful of pyrrolidinium-based OICs have been synthesized and studied. All the above discussions have demonstrated while most of the studies on OICs are devote to their application in various electrochemical devices, not much quantitative and comprehensive information which demonstrates the correlation between structure and electrochemical properties of pyrrolidinium based OICs are available in the existing literatures. Since the impact of the structure and inter-constituent interaction are expected to influence the physical, chemical and transport properties of pyrrolidinium-based geminal OICs, understanding the structure and ion transport behaviour of OICs would be a worthwhile objective to pursue.

Keeping these in mind, in this work, a series geminal di-cationic OICs based on 1-methyl pyrrolidinium, 1,3-bis(1-methylpyrrolidinium-1-yl)propane bromide [PMPYBr] 1,6-bis(1-methylpyrrolidinium-1-yl)hexane bromide [HMPYBr], 1,8-bis(1-methylpyrrolidinium-1-

yl)octane bromide [OMPYBr] and 1,9-bis(1-methylpyrrolidinium-1-yl)nonane bromide [NMPYBr] has been synthesized and their structure, physiochemical properties and electro-chemical properties of composite electrolyte OIC: I_2: TBAI (Tetra-butyl ammonium iodide), are analysed by employing various analytical methods such as X-ray diffraction, Differential Scanning Calorimetry (DSC), Scanning Electron Microscopy (SEM), Electrochemical Impedance Spectroscopy (EIS) and Cyclic-Voltammetry and Linear-Sweep Voltammetry (LSV). This study is intended to show how the structural arrangement and subsequently the electrochemical properties can be influenced by the composition of longer-chained geminal dicationic OICs. This has been achieved by correlating the single crystal structure and morphology of these OICs with their observed electrochemical properties. Several interesting aspects in terms of understanding structural organisation, interionic interaction and ion-transport behaviour have been extracted from the current study.

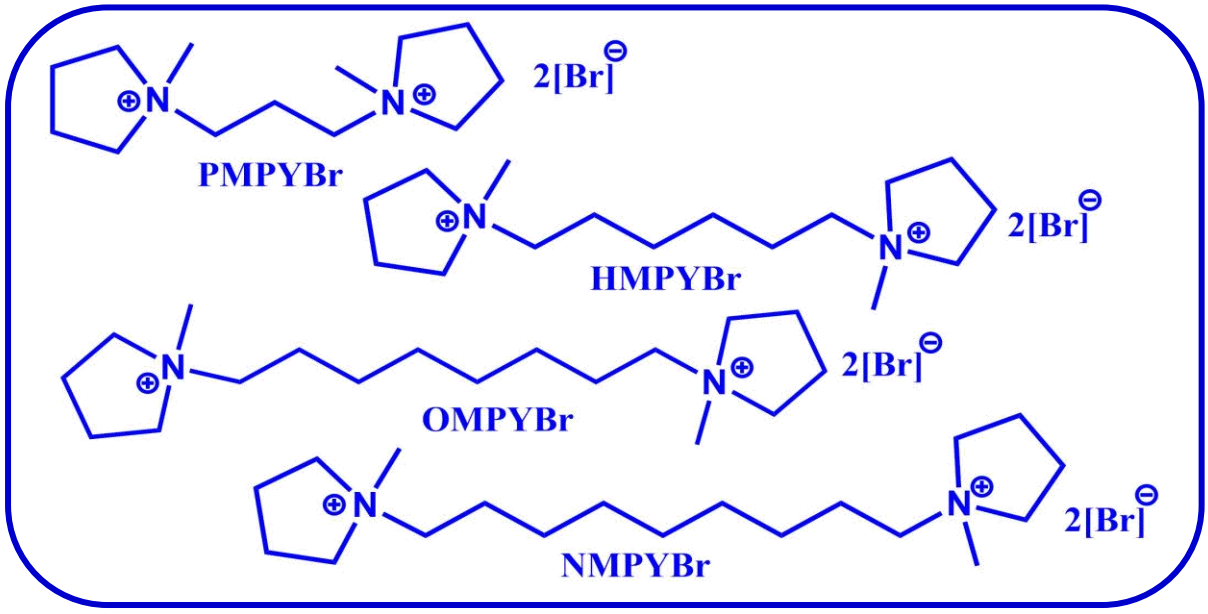

[PMPYBr]: 1,3-bis(1-methylpyrrolidinium-1-yl) propane bromide

[HMPYBr]:1,6-bis(1-methylpyrrolidinium-1-yl) hexane bromide

[OMPYBr]: 1,8-bis(1-methylpyrrolidinium-1-yl) octane bromide

[NMPYBr]:1,9-bis(1-methylpyrrolidinium-1-yl) nonane bromide

Scheme 6.1. Chemical structure and Abbreviation of the chemical species used in the study

6.2. Experimental techniques and methods

6.2.1 Synthesis of Organic Ionic Crystals The organic ionic crystals were prepared according to the reported procedures as described in chapter 2.[38-40] ^{1}H NMR of all the dicationic crystals thus synthesized are subsequently characterised by NMR spectroscopy and the spectra can be found in Appendix 6 (Figure APX6.1).

6.2.2. Preparation of Electrolyte

The formation of triiodide/iodide redox couple is an essential for the DSSC operation. The photovoltaic performance of a DSSC is not only dependent on the concentration of these salts but also depends on the size and charge density of the cations.[41] To the best of our knowledge, even though a range of Lithium iodides and imidazolium IL- based iodides are known to show high I^- and I_3^- transport in OICs matrices, the diffusion of tetra-butyl ammonium iodide (TBAI) in these OICs-doped electrolyte have not been reported till yet. [22, 37, 42-43]The current study employs electrolytes made up of three parts: ionic crystal matrix or OIC, I^- source (TBAI) and iodine (I_2). All components were mixed in the relevant molar proportion and uniformly ground. We found better conductivity with molar proportion of electrolytic additives in the ratio 0.1:0.1:0.02 (OIC: I^- :TBAI) which is found to be similar to the proportion that have been taken by Zeng and co-workers for similar experiment.[42]The solid-state electrolytes thus obtained are subsequently characterised using different electroanalytical methods. All the electrolytes were dried under vacuum at room temperature for 24 h before the characterization.

6.3. Results and discussion

6.3.1. X-ray Crystal Structure. It has been reported in several literatures that the length of the alkyl chain has a significant influence on the cation geometry of this type of compound.[8] Thus determining the X-ray crystal structure and nature of crystalline packing of as synthesized OICs consisting of different alkyl bridge can help us to predict the structural organisation of

the crystalline phase of OICs. Single crystals HMPYBr,OMPYBr and NMPYBr are grown from slow evaporation of their methanol solution at room temperature and the crystallographic informations obtained are summarized in Table 6.1.The crystal data of PMPYBr are collected from previous literature report and can be found in Table APX6.1.[39]

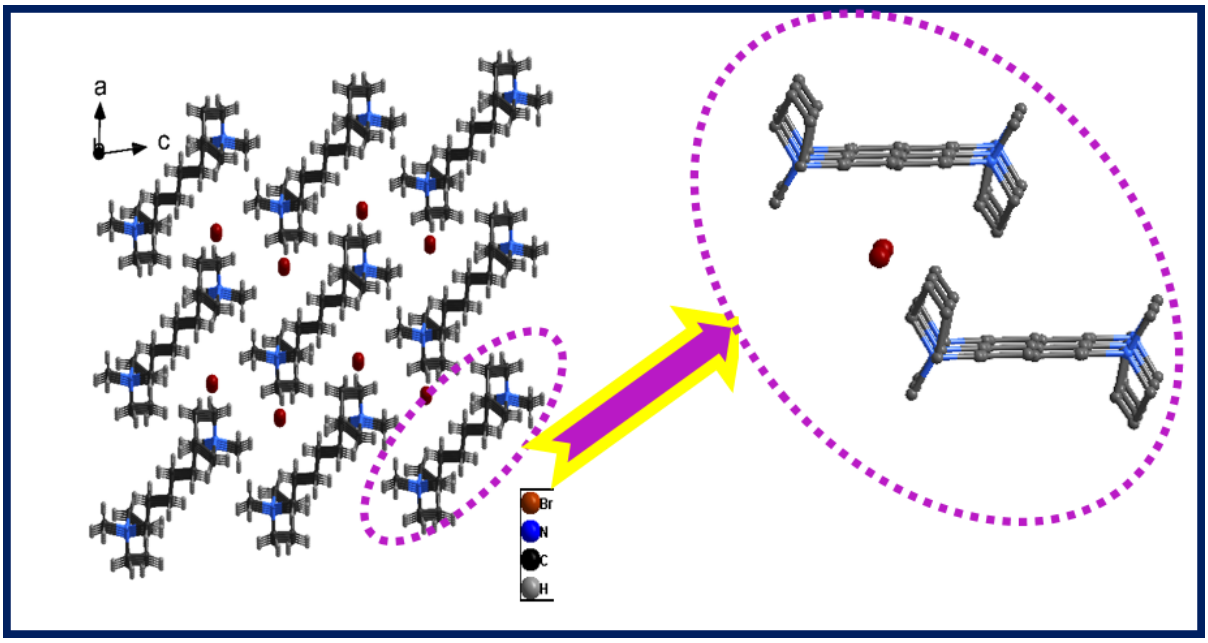

Figure 6. 1 Packing diagram of HMPYBr showing molecular arrangement within the crystal lattice.

As can be seen from Figure 6.1, the crystal structure of HMPYBr consists of zigzag bands of molecules along the crystallographic-b axes of a triclinic unit cell. Two pyrrolidinium cations of one molecule are exactly parallel to each other and lie trans to each other and two pyrrolidinium rings of two different molecules are joined together by electrostatic interactions. The crystal structure of OMPYBr and NMPYBr also show similar packing pattern and can be found in Appendix 6 (Figures APX6.2 and Figure APX6.3).

Table 6. 1. Crystallographic Information

Crystal Data	HMPYBr	OMPYBr	NMPYBr
Empirical formula	$C_8H_{19}BrNO$	$C_9H_{21}BrNO$	$C_{19}H_{29}Br_2N_2$
Formula weight	225.15	239.18	445.26
Temperature/K	294.6(5)	293(2)	293(2)
Crystal system	triclinic	triclinic	orthorhombic
Space group	P-1	P-1	Pbcn
a/Å	8.2705(3)	8.7747(6)	15.6157(17)
b/Å	8.3119(4)	8.8458(6)	13.7323(16)
c/Å	8.6304(4)	8.9862(5)	10.4556(10)
α/°	81.434(4)	94.525(5)	90
β/°	78.227(4)	105.831(5)	90
γ/°	66.545(4)	117.457(7)	90
Volume/$Å^3$	531.30(4)	578.09(7)	2242.1(4)
Z	2	2	4
$\rho_{calc}g/cm^3$	1.407	1.374	1.319
μ/mm^{-1}	3.823	3.518	3.617
F(000)	234.0	250.0	908.0
Crystal size/mm^3	0.05 × 0.03 × 0.01	0.5 × 0.3 × 0.28	0.6 × 0.3 × 0.3
Radiation	MoKα (λ =0.71073)	MoKα (λ =0.71073)	MoKα (λ =0.71073)
Independent reflections	2191 [R_{int} = 0.0669, R_{sigma} = 0.0266]	2438 [R_{int} = 0.1104, R_{sigma} = 0.0544]	2472 [R_{int} = 0.0441, R_{sigma} = 0.0364]
Data/restraints/parameters	2191/0/109	2438/0/118	2472/75/106
Goodness-of-fit on F^2	1.060	1.029	1.050
CCDC Crystal deposition Number	2219093	2219098	2219101

Interestingly, the crystal structure of NMPYBr shows a slightly different structure (Figure APX.3) where the longer alky bridge chain is found to be in bent conformation indicating dense packing of the molecules with the aids of hydrophobic interaction among the alkyl chains. This observation indicates that structural organisation of these type of geminal dication also depends on the length of the alkyl bridge. However, perspective view of the structural organisation

confirms the presence of ordered three-dimensional ionic channels in all these OICs which is the basic requirement for using these OICs to serve as electrolyte matrices.

6.3.2. Thermal and Phase Behaviour:

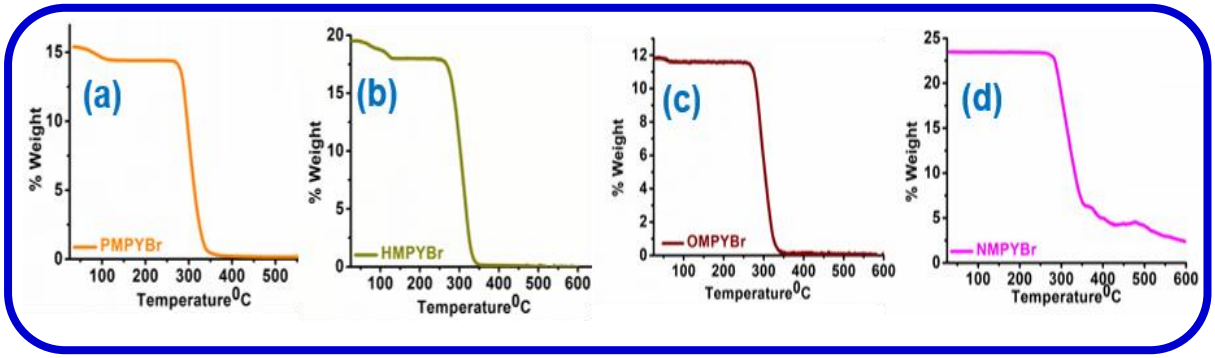

Figure 6.2 Thermogravimetric analysis curve of as synthesised OICs.

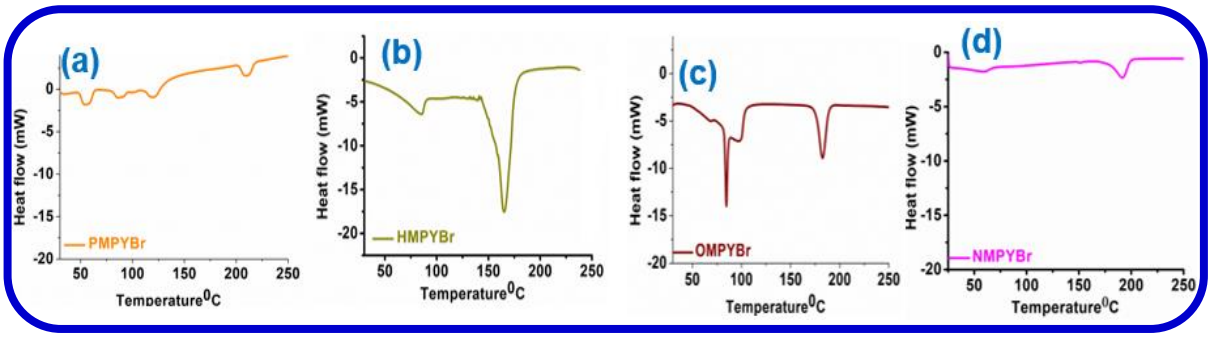

Figure 6.3. Differential scanning thermograms of as synthesised OICs. The y-axis for each thermogram has been kept constant for the comparative view of enthalpy of phase transitions.

Determining the thermal stabilities of OICs is essential for application of these as electrolyte in various optoelectronic devices. The thermal stability of OICs is tested using TGA method. Figure 6.2 represents thermogram of the OICs ramped from room temperature to 600^{0}C. From the Figure 6.2 it can be noticed that all the OICs, irrespective of the length of the alkyl-bridge chain they contain, are thermally stable up to 250^{0}C. This excellent thermal stability of OICs ensure that, these OICs can be considered as good candidate for high temperature outdoor applications. Furthermore, the phase behaviour of these OICs is examined using DSC method. Figure 6.3 represents differential scanning thermogram of OICs in a temperature range 25^{0}C to 250°C. Interestingly, it can be noticed that all these ionic crystals do exhibit multiple solid-

solid phase transition behaviour before their decomposition. In this context we would like to mention here that several monocation-based organic ionic plastic crystal such as 1- butyl-1-methylpyrrolidinium bromide (BMPYBr) as well as several bis-imidazolium salts also show multiple phase transition before their melting temperature. These phases are called as plastic crystalline phase and these characteristics feature is highly beneficial for these material as these allow the redox couple to show high ionic conductivity by facilitating better electrode-electrolyte interfacial contact.[19-20] Therefore, in the present case also the good thermal stability and phase behaviour of the OICs made us to consider them as an ideal electrolytic component to form all solid-state electrolytes for various electrochemical applications. Furthermore, it can also be noticed from the DSC curves presented in Figure 6.3, that the enthalpy of phase transitions is relatively lower for the PMPYBr and NMPYBr than that has been observed for HMPYB and OMPYBr. This observation can be rationalized by considering the higher flexibility or disorderness within the crystal lattice of PMPYBr and NMPYBr .[19]

3.3. PXRD measurements

Figure 6.4a and Figure 6.4b and show the observed PXRD patterns in an angle (2θ) range between 10° and 50° of the pure OICs without any electrolytic additives as well as electrolyte composite (OIC: I_2: TBAI) respectively. In order to avoid the exposure of the samples to air, the samples were sandwiched in between two thin glass slide and mounted on the X-ray diffractometer. The major diffraction peaks of the pure OICs are detected within the angle (2θ) from 20^0 to 30^0. The present diffraction pattern of OICs is found to match with the diffraction pattern obtained for a similar compound reported by Zeng and co-workers.[42] Of all the OICs relatively sharper peaks are observed for PMPYBr, HMPYBr and OMPYBr indicating their higher crystallinity. However, relatively boarder diffraction peaks are observed for NMPYBr which is consistent with the data obtained from single crystal structure. The position of some major peaks as marked in the figure (pink numerical) are found to be at similar diffraction angle

for all the OICs containing different alkyl bridge indicating the presence of similar type crystal plane these OICs. Interestingly, sharp diffraction peaks at the same angle with relatively lower intensity are also observed in Figure 6.4b for respective electrolyte composite which indicates that the crystallinity of OICs remains intact in the electrolyte composite.[33, 44] Additionally, this also indicates that the dopant i.e. the (TBAI and Iodine) are compatible with the OICs to form an electrolytic a mixture. [45]

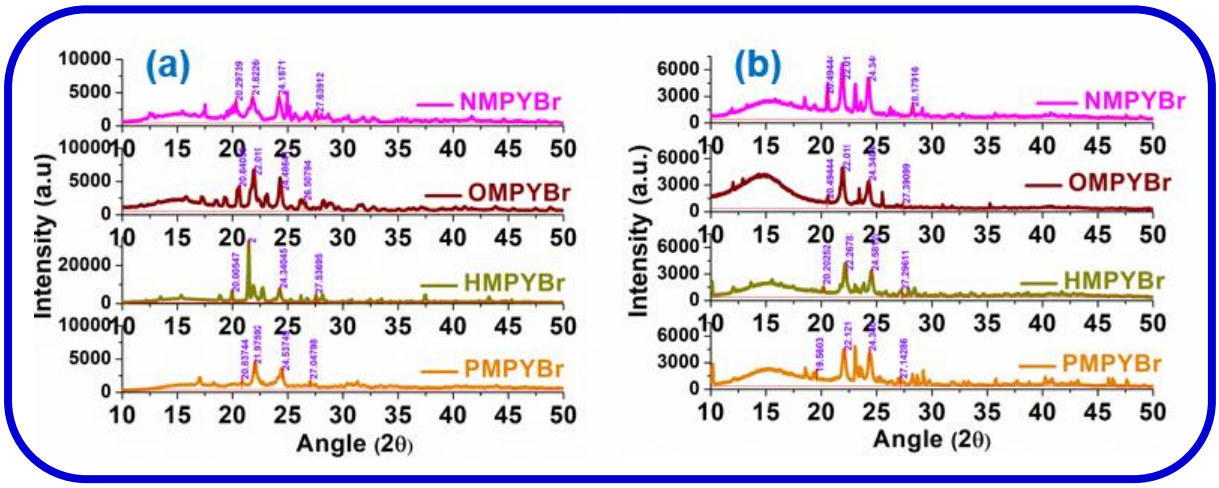

Figure 6.4 (a) X-ray diffraction patterns of pure OICs; (b) electrolyte composite (OIC: I_2: TBAI)

3.4. Morphological features of OICs.

The detailed morphological features of as synthesized OICs were observed using a Scanning Electron Microscope (SEM). The surface micrographs of the OICs are displayed in Figures 6.5 (a-d) which show grey/white coloured crystalline structure with highly textured surfaces of the sample which further conveyed the crystalline nature of these materials. However, it can also be noticed from the SEM images that PMPYBr, HMPYBr and OMPYBr showed a homogeneous distribution of particle with void spaces. On contrary to that to that NMPYBr doesn't show any well-defined morphology. PMPYB showed rod shaped crystals with sharp edges. On the other hand, HMPYBr and OMPYBr showed a partially rectangular sheet like morphology in micrometre range. The micrographs of NMPYBr shows scattered powder like

morphology that can be attributed to a result of segregation of the particles due to the hydrophobic interaction among the longer alkyl chain. The broader X-ray diffraction peaks as well as bent crystal structure highly corroborate the observed morphological feature of NMPYBr revealing their relatively lower crystallinity. This result essentially suggests that the length of the alkyl bridge promotes different crystalline structure which also affect the surface morphology of OICs.

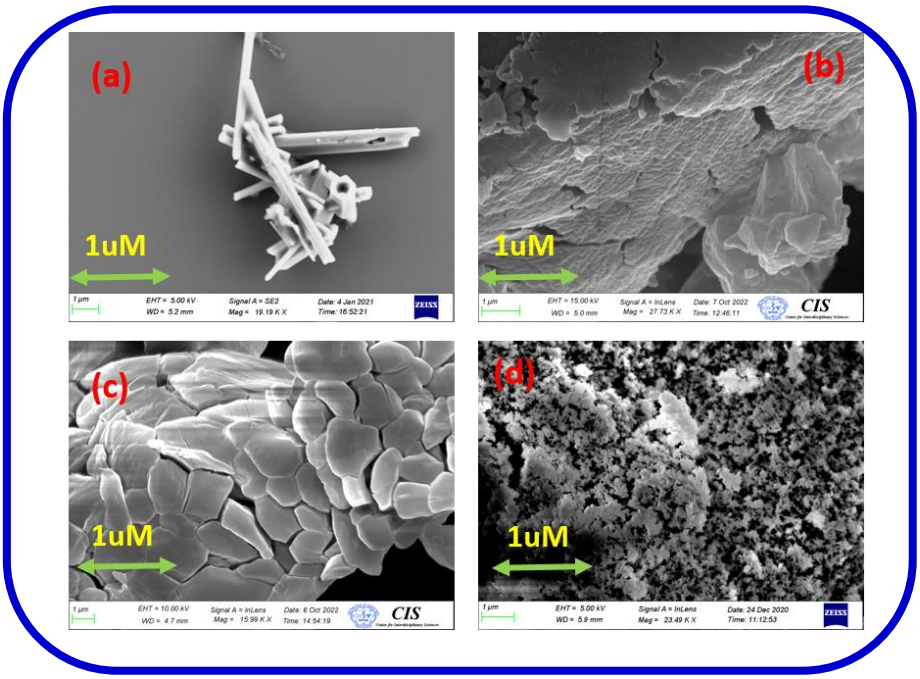

Figure 6.5. SEM micrographs of pure OICs.

3.5. Electrochemical measurements

The efficiency of a DSSC is majorly dependent on the ion conductivity and stable potential window of electrolyte used in the cell. Therefore, the optimization and analysis of electrochemical stable potential window of a particular electrolyte is a vital task for the energy researchers. Here, after successful characterization, the electrochemical stable potential window of the as prepared electrolytes (OIC: I_2: TBAI) were optimised using the linear sweep voltammograms. This was performed by applying an anodic voltage with a scan rate of 10 mV/s to a two electrode Swagelok cell consisting of solid powdered electrolyte sandwiched

between two stainless steel electrodes. The voltage was swept from 0V to higher anodic potential (up to 3.0V) until a sharp rise in current was observed. As can be seen in Figure 6.6a, more rise in anodic current was noticed in case of PMPYBr and NMPYBr indicating the decomposition of the electrolyte. However, in case of HMPYBr and OMPYBr, no such increase in current was found with applied potential even up to 3V, demonstrating an optimised operating potential window of 3V. Further in comparison to OMPYBr, the HMPYBr observed to be more stable resisting the decomposition under similar electrochemical conditions. Figure 6.6b represents the cyclic voltammetry for the conductive HMPYBr electrolyte recorded at 100 mV/s sweep rate. A minimal value of 0.05±0.001 mA/cm^2 current density (~5×10 -5 mA/cm^2 per cycle) was found to be changed after 1000th cycle demonstrating the excellent stability of the HMPYBr electrolyte.

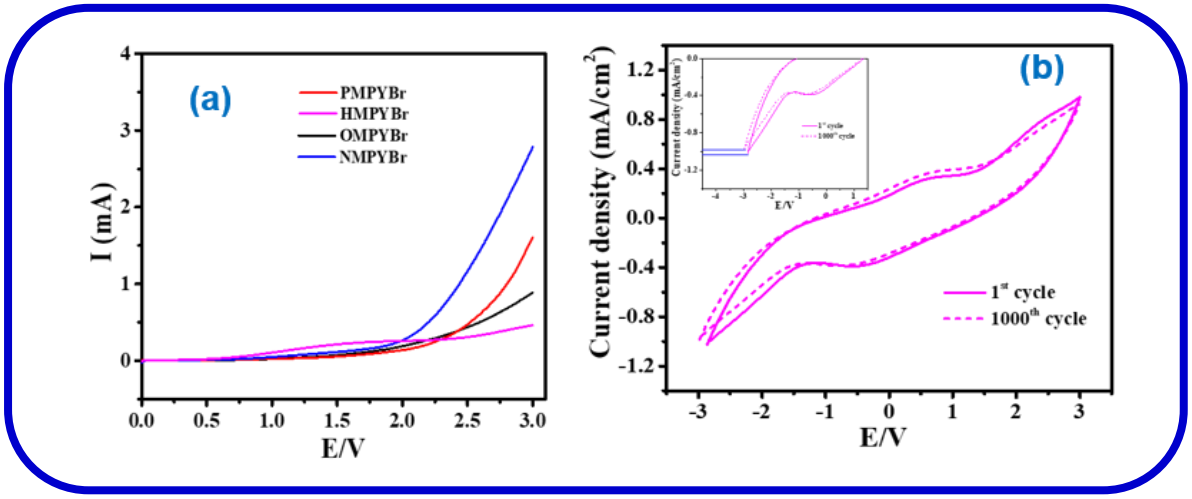

Figure 6.6. Linear sweep voltammograms at 10 mV/s showing the potential window optimisation of OMPYBr, PMPYBr, NMPYBr and HMPYBr electrolytes and (b) cyclic stability at a sweep rate of 100 mV/s of HMPYB in a Swagelok type two electrode system.

Further the exchange current density (J_0) has been calculated from the Tafel plot (logarithmic Current-Voltage Tafel polarization plot) derived from the recorded linear sweep voltammogram. The J_0 value defines the intrinsic rates of electron transfer among the electrolyte and electrode surface at zero over potential. As presented in Figure 6.7, the Tafel

curve is divided into three zones as (1) polarization region, (2) Tafel and (3) diffusion zone respectively. The J_0 obtained from the cross point of the extrapolation of the Tafel zones of cathodic and anodic curves at zero over potential. The values of J_0 observed to be increases on increasing the chain length of the cationic part of the electrolyte. At an optimum condition, OMPYBr shows highest value of J_0 (3.52±0.01 mA/cm^2) demonstrating the excellency in the current and charge transfer capability at minimum over potential among all other electrolytes studied here. On further increasing the chain length, in case of NMPYBr, the J_0 decreased. The magnitude of exchange current density is -2.2±0.02 mA/cm^2 for PMPYBr, 2.96±0.012 mA/cm^2 for HMPYBr and for NMPYBr it is 2.72±0.015 mA/cm^2.

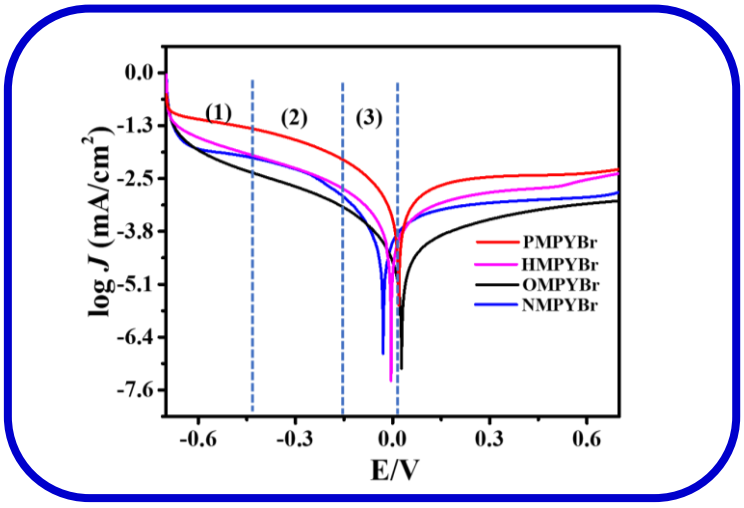

Figure 6.7. Tafel polarization curve for the electrolyte with different cationic chain length.

The ionic conductivity (σ, S/cm) is an important parameter of an electrolyte which need to be evaluated prior to use in dye sensitize solar cells (DSSCs). Therefore, the electrochemical impedance spectroscopy (EIS) measurement has been performed to evaluate the conductivity of the electrolytes containing cationic counter ions with variable chain lengths.

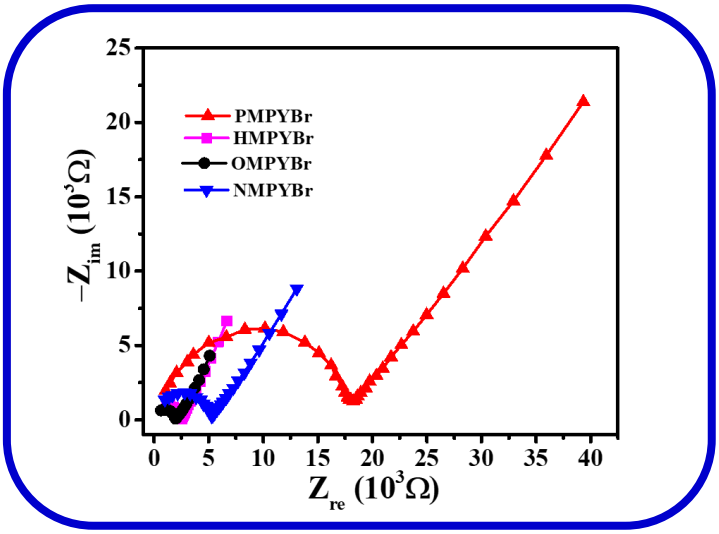

Figure 6.8. The Nyquist plot for the PMPYBr, HMPYBr, OMPYBr and NMPYBr electrolytes.

The Figure 6.8 shows the plot of imaginary versus real impedance of all the electrolytes with variable cationic chain length taken in a Swagelok electrode as discussed in the above section. All the plots show similar pattern with a semi-circular arc in the higher frequency region and a spike in the lower frequency region. Then the ionic conductivity was calculated using the following equation,

$$\sigma = \frac{l}{R \times S} \qquad \text{eq 6.1}$$

Here, l and S are length and area of cross section of the electrode and R is the recorded resistance of the material.[31]

All the electrolytes show average performance with ionic conductivity in the range of 1×10^{-5} S/cm range. In this context it is worth to mention here that the conductivity and diffusion coefficient of I^- ion (where TBAI is the source of iodide ion) is found to be somehow lower than previously reported values with IL-based iodide additives. [19, 33, 42] However, the results obtained above also suggests that the ionic conductivity also depends on the source of iodide ion. Moreover, the ionic conductivities have also been found to vary depending on the alkyl

chain lengths i.e., on increasing the chain length from PMPYBr to OMPYBr, the value increases and decreased on further increasing the carbon chain as in case of NMPYB. Specifically, the PMPYBr, HMPYBr, OMPYBr and NMPYBr shows the specific conductivities of 0.73×10^{-5} S/cm, 5.08×10^{-5} S/cm, 6.68×10^{-5} S/cm and 2.50×10^{-5} S/cm respectively. More concretely the ionic conductivity of electrolyte composite based on C_n-alkyl bridged OICs are found to be in the order 3<9<6<8. The observed trends of ionic conductivity can be explained by taking into consideration of the number of ionic conducting channel per unit length. [31,46]It is supposed that the increase in conductivity of electrolyte with increase in the length of the alkyl bridge is due to the formation of well-ordered ion-conductive network in the electrolytes by longer saturated carbon linkage chains.[46] However, lower conductivity of NMPYBr doped electrolyte despite of the presence of longest saturated hydrocarbon linkage is quite surprising. In this context we would like to note here that Xu et.al have also reported a sharp decrease in conductivity of 1-alkyl-3-methylimidazolium fluoro-hydrogenate salts ($C_xMIm(FH)_2F$, (x=8, 10, 12, 14, 16, and 18) with increasing alkyl chain length due to the breaking of layered structures.[46] Several experimental reports suggest that conductivity of solid-state electrolyte composite is highly dependent on the structural organization of the crystalline phase as well as the morphology of the crystal matrix.[44] In the current study we have explained the observed trends of conductivity on the basis of the microstructure of the OICs which forms the conducting matrices. The rod-shaped microstructures of the PMPYBr (Figure 6.5a) with high surface area perhaps provide only few voids that significantly reduces the paths for iodide ion conduction.[47] However, the partially rectangular sheet like structure that HMPYBr and OMPYBr shows (Figures 6.5b & Figure 6.5c), provide smaller interfacial contact with the electro-active active material thereby facilitates ionic conduction.[34] Moreover, NMPYBr due to highly dense packing exhibit few voids due to formation of larger aggregates as a result of hydrophobic interaction among alkyl chains (See the crystal structure of

NMPYBr, Figure APX6.3). Moreover, these larger sized particles formed result in disconnected iodide-ion motion pathways which significantly lower the conductivity.[43,47] The present study essentially highlights that both the structural organisation and morphology of OICs have a crucial influence on the rate conductivity of the electrolyte.

6.4. Conclusions

In summary, we have synthesized a series geminal organic ionic crystals (OICs) with increasing length of the alkyl bridged chain C_n (n= 3, 6, 8, 9) and investigated their structure, thermal and electrochemical behaviours by employing different spectroscopic and analytical methods. Analysis of the DSC thermogram has indicated that these OICs are thermally stable and show multiple phase transition prior to their decomposition temperature. Structural analysis studies have indicated that all of these OICs form matrices like structure that allow conducting channels for diffusion of iodide ions. However, the surface morphology of these OICs is found to be a function of length of the alkyl bridge chain. Electrochemical measurements have collectively revealed that compared to C_3- and C_9-alkyl bridged-based OICs, C_6- and C_8 -alkyl bridged OICs exhibit the highest conductivity and widest potential coverage. Analysis of the above results in conjunction with X-ray crystal structure and morphology of the corresponding moieties lead us to conclude that the better conductivity of C_6-, C_8 -alkyl bridged OICs is because of the good crystallinity and ordered morphology that offers better conducting channel for electrochemical transport. However, presence of lesser number of conducting channel, due to difference in the crystal structure of C_3-, C_9 -alkyl bridged OICs, limits their conductivity. The results of the current study are exciting and are expected to drive the designing of various geminal OICs that can be used in various energy related applications.

6.5.Appendix 6

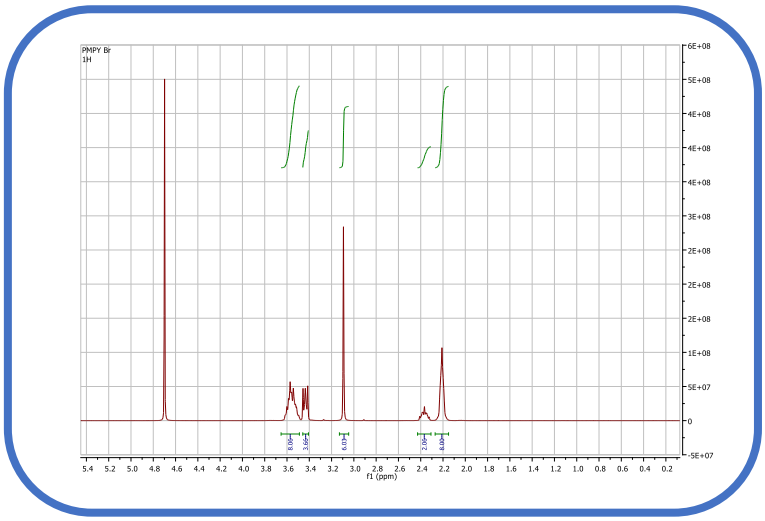

Figure APX6.1a [1]HNMR Spectra of PMPYBr

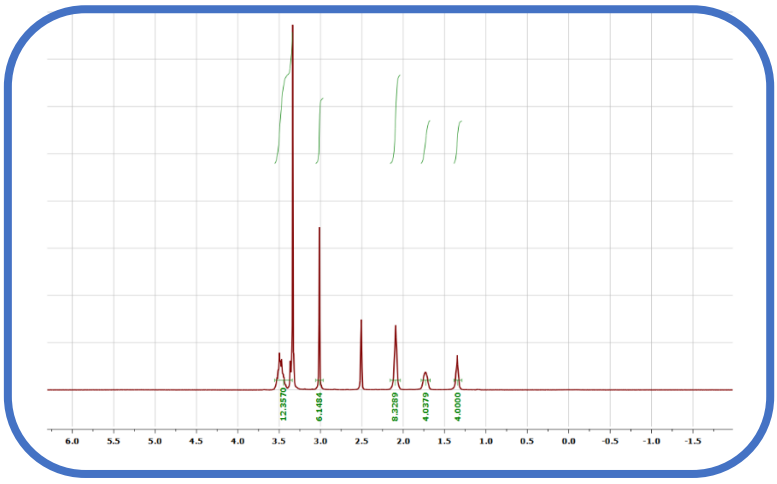

Figure APX6.1b [1]HNMR Spectra of HMPYBr

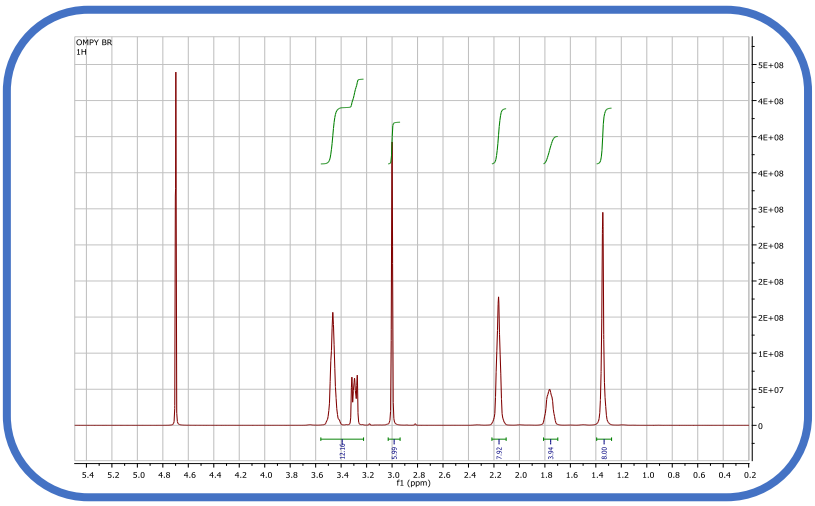

Figure APX6.1c [1]HNMR Spectra of OMPYBr

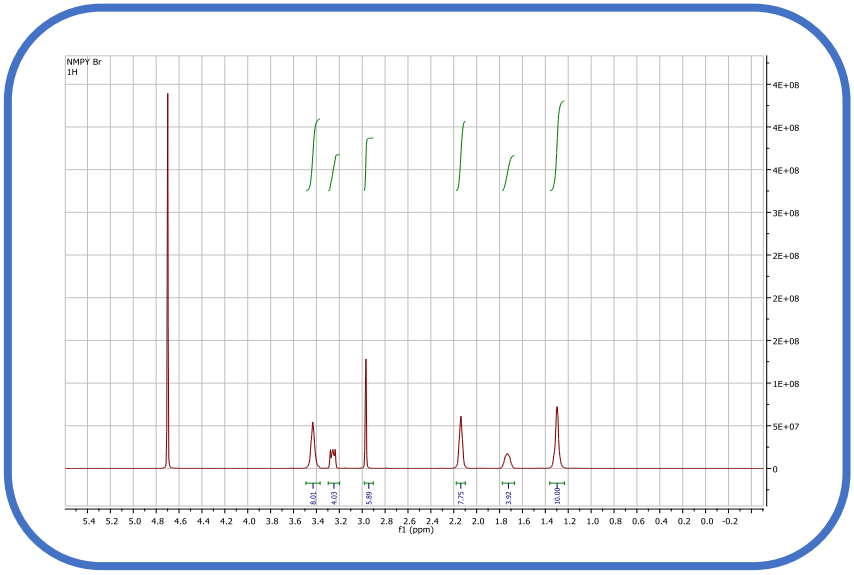

Figure APX6.1d [1]HNMR Spectra of NMPYBr

Table APX6.1. Crystallographic information on PMPYBr.[39]

Formula	$C_{13}H_{28}Br_2N2$
fw (g)	372.19
T (K)	193(2)
Lattice cell	orthorhombic
space group	Pbca
a (Å)	21.367(6)
b (Å)	19.888(5)
c (Å)	23.787(6)
α (deg)	90
β (deg)	90
γ (deg)	90
V (Å3)	10108(5)
Z	24
d (calc d) (Mg/m^3)	1.467
abs coeff. (mm^{-1})	4.798
F(000)	4560
θ range (deg)	1.64-20.82
Reflections collected	45036
R1,[a] wR2[b] [I > 2σ(I)]	0.0702, 0.1628

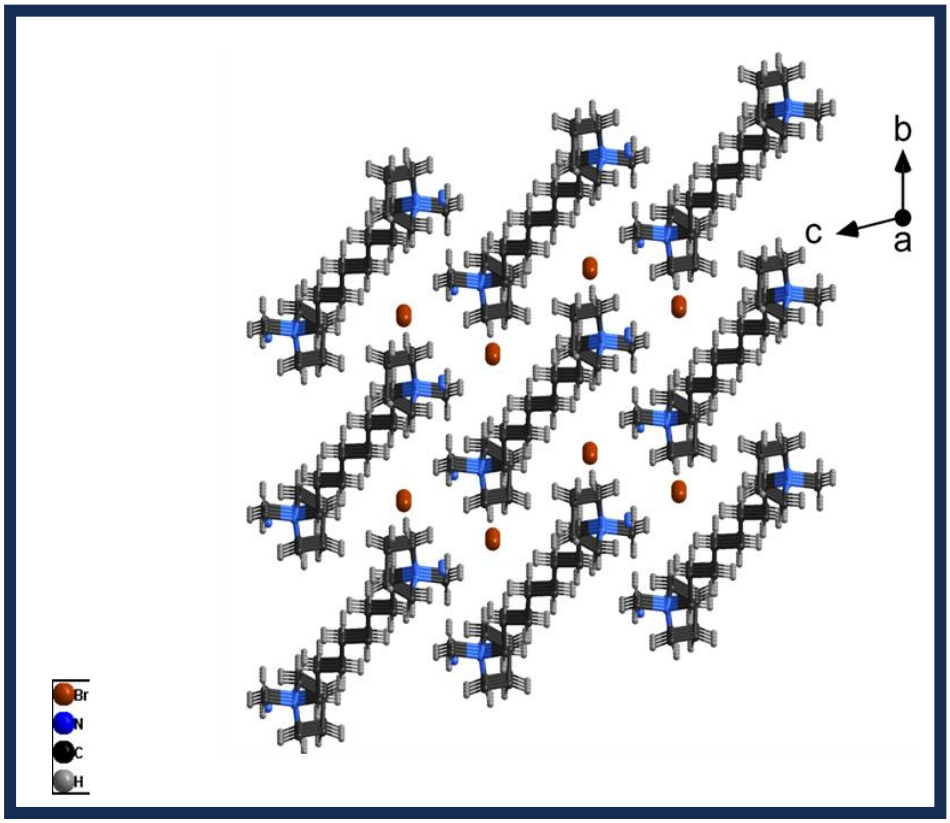

Figure APX6.2 Crystal packing of OMPYBr along the crystallographic a-axes.

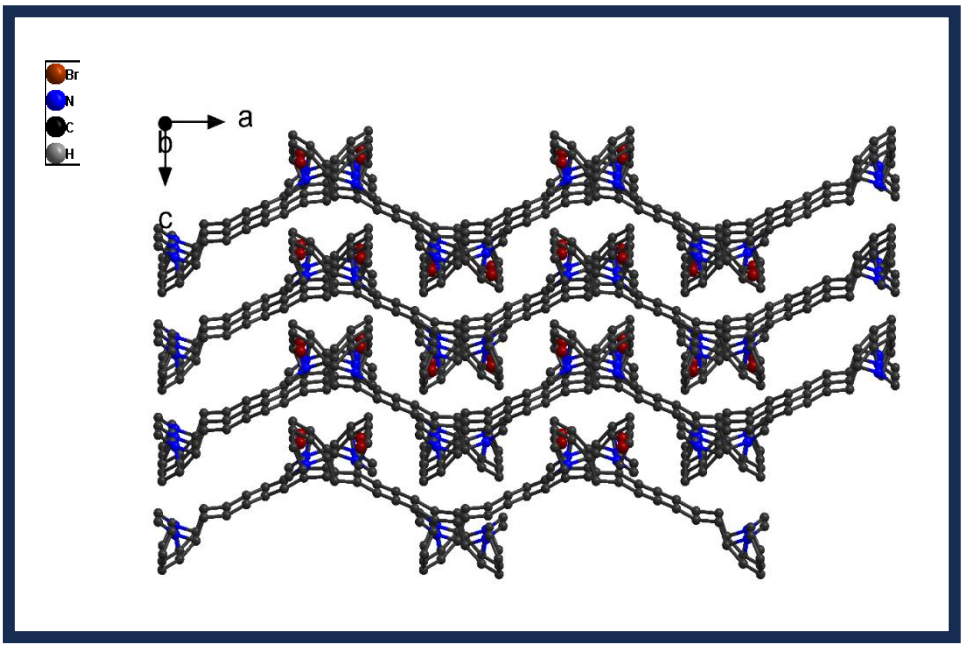

Figure APX6.3 Crystal packing of NMPYBr along the crystallographic a-axes.

REFERENCES

1. Lei, Z.; Chen. B.; Koo.Y.M. Macfarlane.D.R.; Introduction: Ionic Liquids. *Chemical Reviews* **2017**, *117*, 6633-6635.
2. Ratti, R., Ionic Liquids: Synthesis and Applications in Catalysis. *Advances in Chemistry* **2014**, *2014*, 729842.
3. Liu, Q.-P.; Hou, X.-D.; Li, N.; Zong, M.-H., Ionic Liquids from Renewable Biomaterials: Synthesis, Characterization and Application in the Pretreatment of Biomass. *Green Chemistry* **2012**, *14*, 304-307.
4. Hallett, J. P.; Welton, T., Room-Temperature Ionic Liquids: Solvents for Synthesis and Catalysis. 2. *Chemical Reviews* **2011**, *111*, 3508-3576.
5. Angell, C. A.; Ansari, Y.; Zhao, Z., Ionic Liquids: Past, Present and Future. *Faraday discussions* **2012**, *154*, 9-27.
6. Wilkes, J. S., A Short History of Ionic Liquids—from Molten Salts to Neoteric Solvents. *Green Chemistry* **2002**, *4*, 73-80.
7. Silva, W.; Zanatta, M.; Ferreira, A. S.; Corvo, M. C.; Cabrita, E. J., Revisiting Ionic Liquid Structure-Property Relationship: A Critical Analysis. *International Journal of Molecular Sciences* **2020**, *21*.
8. Hayes, R.; Warr, G. G.; Atkin, R., Structure and Nanostructure in Ionic Liquids. *Chemical Reviews* **2015**, *115*, 6357-6426.
9. Galiński, M.; Lewandowski, A.; Stępniak, I., Ionic Liquids as Electrolytes. *Electrochimica Acta* **2006**, *51*, 5567-5580.
10. Karuppasamy, K.; Theerthagiri, J.; Vikraman, D.; Yim, C. J.; Hussain, S.; Sharma, R.; Maiyalagan, T.; Qin, J.; Kim, H. S., Ionic Liquid-Based Electrolytes for Energy Storage Devices: A Brief Review on Their Limits and Applications. *Polymers (Basel)* **2020**, *12*.
11. Ingram, J. A.; Moog, R. S.; Ito, N.; Biswas, R.; Maroncelli, M., Solute Rotation and Solvation Dynamics in a Room-Temperature Ionic Liquid. *The Journal of Physical Chemistry B* **2003**, *107*, 5926-5932.
12. Nirmale, T. C.; Khupse, N. D.; Kalubarme, R. S.; Kulkarni, M. V.; Varma, A. J.; Kale, B. B., Imidazolium-Based Dicationic Ionic Liquid Electrolyte: Strategy toward Safer Lithium-Ion Batteries. *ACS Sustainable Chemistry & Engineering* **2022**, *10*, 8297-8304.
13. De, C. K.; Ghosh, A.; Mandal, P. K., Hydrophobicity-Dependent Heterogeneous Nanoaggregates and Fluorescence Dynamics in Room-Temperature Ionic Liquids. *The Journal of Physical Chemistry B* **2022**, *126*, 1551-1557.
14. García-Garabal, S.; Vila, J.; Rilo, E.; Domínguez-Pérez, M.; Segade, L.; Tojo, E.; Verdía, P.; Varela, L. M.; Cabeza, O., Transport Properties for 1-Ethyl-3-Methylimidazolium N-Alkyl Sulfates: Possible Evidence of Grotthuss Mechanism. *Electrochimica Acta* **2017**, *231*, 94-102.
15. Biswas, R.; Bagchi, B., Limiting Ionic Conductance of Symmetrical, Rigid Ions in Aqueous Solutions: Temperature Dependence and Solvent Isotope Effects. *Journal of the American Chemical Society* **1997**, *119*, 5946-5953.
16. Ishida, T.; Shirota, H., Dicationic Versus Monocationic Ionic Liquids: Distinctive Ionic Dynamics and Dynamical Heterogeneity. *The Journal of Physical Chemistry B* **2013**, *117*, 1136-1150.
17. Pringle, J. M.; Howlett, P. C.; MacFarlane, D. R.; Forsyth, M., Organic Ionic Plastic Crystals: Recent Advances. *Journal of Materials Chemistry* **2010**, *20*, 2056-2062.
18. Chuan-Pei, L.; Te-Chun, C.; Ling-Yu, C.; Jiang-Jen, L.; Kuo-Chuan, H., Solid-State Ionic Liquid Based Electrolytes for Dye-Sensitized Solar Cells. *Ionic Liquids*, Jun-ichi, K., Ed. IntechOpen: Rijeka, 2013; p Ch. 10.

19. Li, Q.; Chen, X.; Zhao, J.; Qiu, L.; Zhang, Y.; Sun, B.; Yan, F., Organic Ionic Plastic Crystal-Based Electrolytes for Solid-State Dye-Sensitized Solar Cells. *Journal of Materials Chemistry* **2012**, *22*, 6674-6679.
20. MacFarlane, D. R.; Meakin, P.; Sun, J.; Amini, N.; Forsyth, M., Pyrrolidinium Imides: A New Family of Molten Salts and Conductive Plastic Crystal Phases. *Journal of Physical Chemistry B* **1999**, *103*, 4164-4170.
21. Iftikhar, H.; Sonai, G. G.; Hashmi, S. G.; Nogueira, A. F.; Lund, P. D. Progress on Electrolytes Development in Dye-Sensitized Solar Cells *Materials* **2019**, DOI: 10.3390/ma12121998.
22. Chowdhury, F. I.; Buraidah, M. H.; Arof, A. K.; Mellander, B. E.; Noor, I. M., Impact of Tetrabutylammonium, Iodide and Triiodide Ions Conductivity in Polyacrylonitrile Based Electrolyte on Dssc Performance. *Solar Energy* **2020**, *196*, 379-388.
23. Luo, J., et al., 1,2,4-Triazolium Perfluorobutanesulfonate as an Archetypal Pure Protic Organic Ionic Plastic Crystal Electrolyte for All-Solid-State Fuel Cells. *Energy & Environmental Science* **2015**, *8*, 1276-1291.
24. Armel, V.; Velayutham, D.; Sun, J.; Howlett, P. C.; Forsyth, M.; MacFarlane, D. R.; Pringle, J. M., Ionic Liquids and Organic Ionic Plastic Crystals Utilizing Small Phosphonium Cations *Journal of Materials Chemistry* **2011**, *21*, 7640-7650.
25. Janikowski, J.; Forsyth, C.; MacFarlane, D. R.; Pringle, J. M., Novel Ionic Liquids and Plastic Crystals Utilizing the Cyanate Anion. *Journal of Materials Chemistry* **2011**, *21*, 19219-19225.
26. Pringle, J.; Howlett, P.; MacFarlane, D.; Forsyth, M., Organic Ionic Plastic Crystals: Recent Advances. *Journal of Materials Chemistry* **2010**, *20*.
27. Yang, B.; Li, C.; Zhou, J.; Liu, J.; Zhang, Q., Pyrrolidinium-Based Ionic Liquid Electrolyte with Organic Additive and Litfsi for High-Safety Lithium-Ion Batteries. *Electrochimica Acta* **2014**, *148*, 39-45.
28. Majhi, D.; Dvinskikh, S. V., Ion Conformation and Orientational Order in a Dicationic Ionic Liquid Crystal Studied by Solid-State Nuclear Magnetic Resonance Spectroscopy. *Scientific Report* **2021**, *11*, 5985.
29. Tadesse, H.; Blake, A. J.; Champness, N. R.; Warren, J. E.; Rizkallah, P. J.; Licence, P., Supramolecular Architectures of Symmetrical Dicationic Ionic Liquid Based Systems. *CrystEngComm* **2012**, *14*, 4886-4893.
30. Bhowmik, P. K.; Koh, J. J.; King, D.; Han, H.; Heinrich, B.; Donnio, B.; Zaton, D.; Martinez-Felipe, A., Dicationic Stilbazolium Salts: Structural, Thermal, Optical, and Ionic Conduction Properties. *Journal of Molecular Liquid* **2021**, *341*, 117311.
31. Han, L.; Wang, Y. F.; Zeng, J. H., Effective Solid Electrolyte Based on Benzothiazolium for Dye-Sensitized Solar Cells. *ACS Applied Materials & Interfaces* **2014**, *6*, 22088-22095.
32. Cao-Cen, H.; Zhao, J.; Qiu, L.; Xu, D.; Li, Q.; Chen, X.; Yan, F., High Performance All-Solid-State Dye-Sensitized Solar Cells Based on Cyanobiphenyl-Functionalized Imidazolium-Type Ionic Crystals. *Journal of Materials Chemistry* **2012**, *22*, 12842-12850.
33. Yamada, H.; Miyachi, Y.; Takeoka, Y.; Rikukawa, M.; Yoshizawa-Fujita, M., Pyrrolidinium-Based Organic Ionic Plastic Crystals: Relationship between Side Chain Length and Properties. *Electrochimica Acta* **2019**, *303*, 293-298.
34. Gorrasi, G.; Bugatti, V.; Milone, C.; Mastronardo, E.; Piperopoulos, E.; Iemmo, L.; Di Bartolomeo, A., Effect of Temperature and Morphology on the Electrical Properties of Pet/Conductive Nanofillers Composites. *Composites Part B: Engineering* **2018**, *135*, 149-154.
35. Zhao, Y.; Zhai, J.; He, J.; Chen, X.; Chen, L.; Zhang, L.; Tian, Y.; Jiang, L.; Zhu, D., High-Performance All-Solid-State Dye-Sensitized Solar Cells Utilizing Imidazolium-Type Ionic Crystal as Charge Transfer Layer. *Chemistry of Materials* **2008**, *20*, 6022-6028.

36. Wang, H.; Li, J.; Gong, F.; Zhou, G.; Wang, Z. S., Ionic Conductor with High Conductivity as Single-Component Electrolyte for Efficient Solid-State Dye-Sensitized Solar Cells. *Journal of the American Chemical Society* **2013**, *135*, 12627-33.
37. Xu, X.; Wang, H.; Gong, F.; Zhou, G.; Wang, Z.-S., Performance Enhancement of Dye-Sensitized Solar Cells Using an Ester-Functionalized Imidazolium Iodide as the Solid State Electrolyte. *ACS Applied Materials & Interfaces* **2013**, *5*, 3219-3223.
38. Chang, J.-C.; Ho, W.-Y.; Sun, I. W.; Tung, Y.-L.; Tsui, M.-C.; Wu, T.-Y.; Liang, S.-S., Synthesis and Characterization of Dicationic Ionic Liquids That Contain Both Hydrophilic and Hydrophobic Anions. *Tetrahedron* **2010**, *66*, 6150-6155.
39. Anderson, J. L.; Ding, R.; Ellern, A.; Armstrong, D. W., Structure and Properties of High Stability Geminal Dicationic Ionic Liquids. *Journal of the American Chemical Society* **2005**, *127*, 593-604.
40. Montalbán, M. G.; Víllora, G.; Licence, P., Synthesis and Characterization Data of Monocationic and Dicationic Ionic Liquids or Molten Salts. *Data in Brief* **2018**, *19*, 769-788.
41. Chowdhury, F. I.; Khalil, I.; Khandaker, M. U.; Rabbani, M. M.; Uddin, J.; Arof, A. K., Electrochemical and Structural Characterization of Polyacrylonitrile (Pan)–Based Gel Polymer Electrolytes Blended with Tetrabutylammonium Iodide for Possible Application in Dye-Sensitized Solar Cells. *Ionics* **2020**, *26*, 4737-4746.
42. He, T.; Wang, Y. F.; Zeng, J. H., Stable, High-Efficiency Pyrrolidinium-Based Electrolyte for Solid-State Dye-Sensitized Solar Cells. *ACS Applied Materials & Interfaces* **2015**, *7*, 21381-90.
43. Wang, Y. F.; Zhang, J. M.; Cui, X. R.; Yang, P. C.; Zeng, J. H., A Novel Organic Ionic Plastic Crystal Electrolyte for Solid-State Dye-Sensitized Solar Cells. *Electrochimica Acta* **2013**, *112*, 247-251.
44. Dey, A.; Karan, S.; Dey, A.; De, S. K., Structure, Morphology and Ionic Conductivity of Solid Polymer Electrolyte. *Materials Research Bulletin* **2011**, *46*, 2009-2015.

45. Choi, S.; Ann, J.; Do, J.; Lim, S.; Park, C.; Shin, D., Application of Rod-Like Li6ps5cl Directly Synthesized by a Liquid Phase Process to Sheet-Type Electrodes for All-Solid-State Lithium Batteries. *Journal of The Electrochemical Society* **2019**, *166*, A5193.

46. Xu, F.; Matsumoto. K.; and Hagiwara , R.; Effects of alkyl chain length on properties of 1-alkyl-3-methylimidazolium fluorohydrogenate ionic liquid crystals. *Chemmistry A-Europian Journal* **2010**, *16* , 12970 —12976.

47. Dey, A.; Karan, S.; Structure, morphology and ionic conductivity of solid polymer electrolyte. *Materials Research Bulletin* **2011**, *46* , 2009-2015.

Summary and Future Prospects

The current thesis work provides several new and interesting physical insights about RTILs, aqueous solutions of ILs and Organic ionic crystals (OICs). Moreover, this thesis mainly tries to understand the difference in the behavior of dicationic category of ILs than that of monocationic variant. The knowledgeobtained from the current thesis work is expected to be useful in understanding the structural organization, intermolecular interaction and dynamics of RTILs as well as OICs in better fashion. The thesis work also illustrates the implications of microscopic structural attributes of these material in various applications. The outcome of the present thesis work is expected to advance ourexisting understanding of behavior ILs both at fundamental and application level. Understanding and exploring different cation based polycationic ILs is in the future is expected to open up new direction for the potential use of these complex material system in various applications.